Планета Земля

Earth Planet / Planet Erde

Dorman L.I.*, Pustil'nik L.A., Yom Din G.***, Applbaum D.Sh.******


Lev I. Dorman


Lev A. Pustil'nik


Gregory Yom Din


David Sh. Applbaum

Cosmic rays and other space weather factors influenced on satellite operation and technology, people health, climate change, and agriculture production

*Prof. Lev I. Dorman, Head of Israel Cosmic Ray and Space Weather Center, Institute of Advanced Study of Tel Aviv University and Israel Space Agency, Chief Scientist of Cosmic Ray Department of N.V. Pushkov IZMIRAN, Russian Academy of Science (Troitsk, Russia)
E-mail: lid@physics.technion.ac.il

**Lev A. Pustil'nik, Israel Cosmic Ray and Space Weather Centre with Emilio Segré Israel-Italian Observatory, affiliated to Tel Aviv University and Israel Space Agency (Israel)
E-mail: levpust2149@gmail.com

***Gregory Yom Din, Open University, Raanana (Israel)

****David Sh. Applbaum, Israel Cosmic Ray and Space Weather Center, Institute of Advanced Study of Tel Aviv University and Israel Space Agency, Tel Aviv University (Israel)

This paper is an example how fundamental research in Cosmic Ray (CR) Astrophysics and Geophysics can be applied to very important modern practical problem: monitoring by cosmic rays space weather and prediction by using on-line cosmic ray data space phenomena dangerous for satellites electronics and astronauts health in the space, for crew and passengers health on commercial jets in atmosphere, and in some rare cases for technology and people on the ground, role of CR and other space weather factors in climate change and influence on agriculture production.

It is well known that in periods of great SEP (Solar Energetic Particle) events, the fluxes can be so big that memory of computers and other electronics in space may be destroyed, satellites and spacecrafts became dead (each year insurance companies paid more than 500,000,000 dollars for these failures; if will be event as February 23, 1956 will be destroyed about all satellites in 1—2 hours, the price of this will be more than 10—20 Billion dollars, total destroying satellite communications and a lot of other problems). In these periods is necessary to switch off some part of electronics for short time to protect computer memories. These periods are also dangerous for astronauts on space-ships, and passengers with crew in commercial jets (especially during S5—S7 radiation storms). The problem is how to forecast exactly these dangerous phenomena. We show that exact forecast can be made by using high-energy particles (about 2—10 GeV/nucleon and higher) which transportation from the Sun is characterized by much bigger diffusion coefficient than for small and middle energy particles. Therefore high energy particles came from the Sun much more early (8—20 minutes after acceleration and escaping into solar wind) than main part of smaller energy particles caused dangerous situation for electronics and people health (about 30—60 minutes later).

We describe here principles and experience of automatically working programs "SEP-Search-1 min", "SEP-Search-2 min","SEP-Search-5 min", developed and checked in the Emilio Segre' Observatory of Israel Cosmic Ray and Space Weather Center (Mt. Hermon, 2050 m above sea level). The second step is automatically determination of flare energetic particle spectrum, and then automatically determination of diffusion coefficient in the interplanetary space, time of ejection and energy spectrum of SEP in the source, and then — forecasting of expected SEP flux and radiation hazard for space-probes in space, satellites in the magnetosphere, jets and various objects in the atmosphere and on the ground.

We will describe also the theory and experience of high energy cosmic ray data using for forecasting of major geomagnetic storms accompanied by Forbush-effects (what influenced very much on satellites, on communications, navigation systems, people health, and high-level technology systems in space, in the atmosphere, and on the ground).

Keywords: cosmic rays, space weather, Sun, solar wind, Earth's climat, Forbush-effect, agricultural goods, wheat prices.

1. Introduction

CR is one of important factors of space weather because namely CR of galactic and solar origin determined radiation storms and radiation hazard for people and technology, computer and memory upsets and failures, solar cell damage, radio wave propagation disturbances, failures in communication and navigation systems. Beside this CR can be used as effective instrument for space weather monitoring and forecasting dangerous phenomena, especially, great magnetic storms. In **Fig. 1** are shown CR and other space weather factors influenced on satellites, communication, navigation systems, people health, and others.

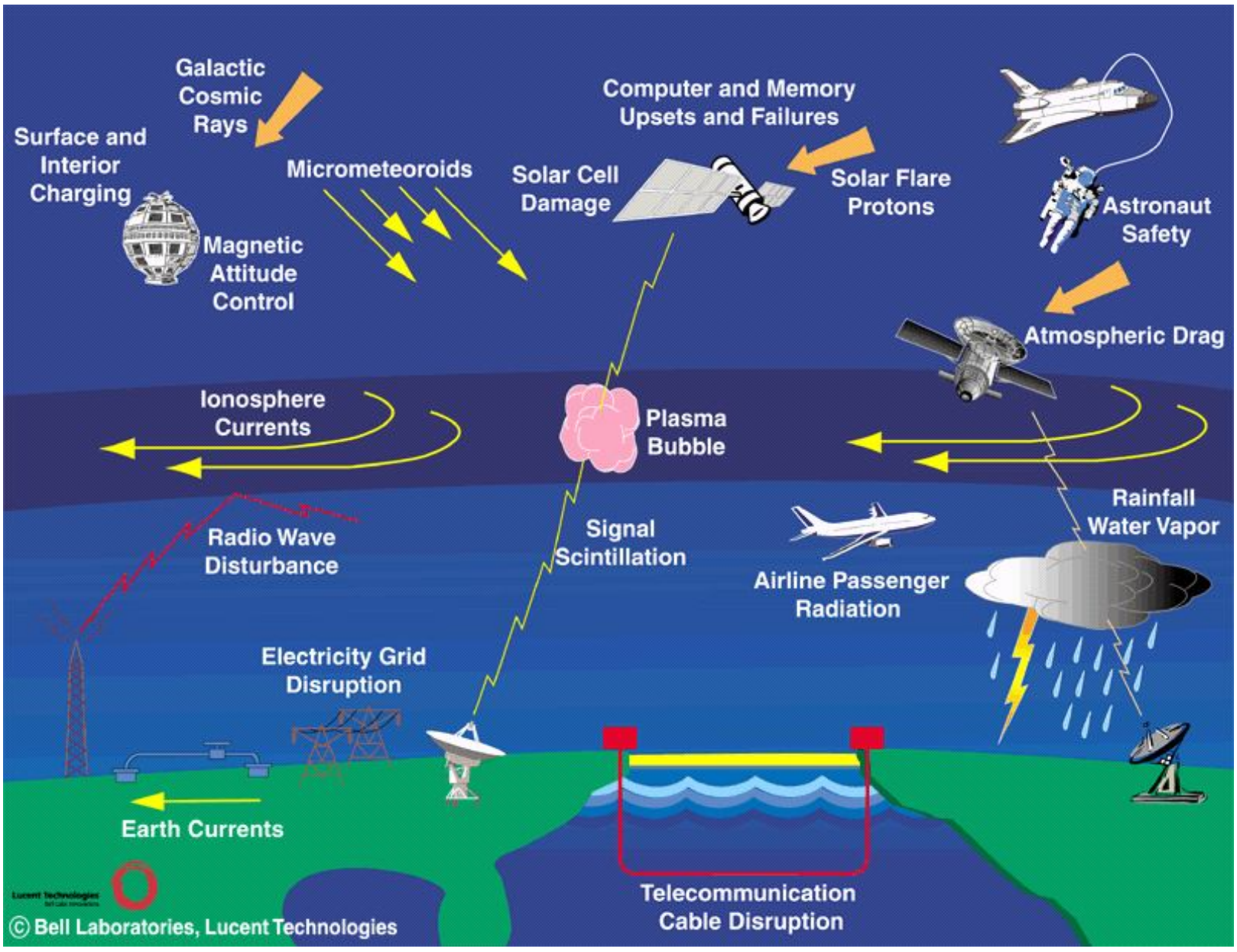

Fig. 1. Space weather effects (from Bell Laboratories web-site in Internet).

2. Satellite anomalies in connection with CR and other space weather factors

2.1. The matter of problem

Satellite anomalies (or malfunctions), including total distortion of electronics and loose of some satellites cost for Insurance Companies billions dollars per year. During especially active periods the probability of big satellite anomalies and their loosing increased very much. Now, when a great number of civil and military satellites are continuously worked for our practice life, the problem of satellite anomalies became very important. Many years ago about half of satellite anomalies were caused by technical reasons (for example, for Russian satellites Kosmos), but with time with increasing of production quality, this part became smaller and smaller. The other part, which now is dominated, caused by different space weather effects.

2.2. Formation of database on satellite anomalies

The main contribution was from NGDC satellite anomaly database, created by J. Allen and D. Wilkinson *[Allen, Wilkinson 1993]* + "Kosmos" data (circular orbit at 800 km altitude and 74º inclination) + 1994 year anomalies — W. Thomas report *[Thomas 1994]* + The satellites characteristics — from: *http://spacescience.nasa.gov/missions/index.htm; http://www.skyrocket.de/space/index2.htm; http://hea-www.harvard.edu/QEDT/jcm/space/jsr/jsr.html; http://www.astronautix.com/index.htm*

2.3. Time variations of satellite number and its anomaly total numbers

Results are shown in **Fig. 2.**

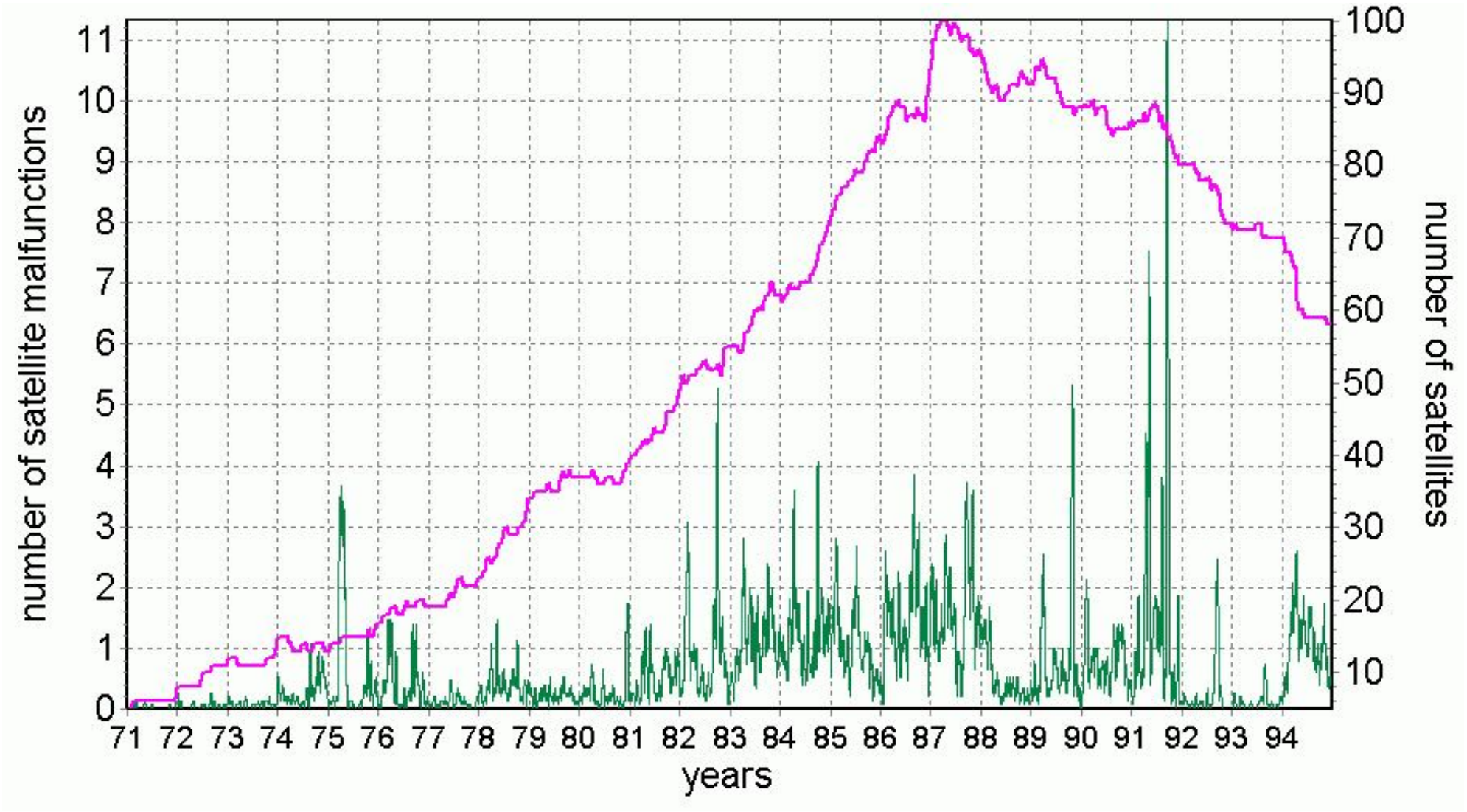

Fig. 2. Time variations of monthly data for ~ 300 satellites and ~ 6000 anomalies.

2.4. Three groups of satellites

In **Fig. 3** are shown the separation of satellites on three groups in dependence of altitude and inclination of their orbits (as it will be shown below, space weather effects sufficiently depend from satellite orbit). The biggest group of satellites — GEO (135 satellites) — **high altitude — low inclination** (in **Fig. 3** this group is shown as **green**). In the group **low altitude — high inclination** (in **Fig. 3** is shown as **blue**) are 68 satellites (mostly Russian satellites Kosmos). In the group **high altitude — high inclination** (in **Fig. 3** is shown as **red**) are only 14 satellites (mostly MEO satellites), but they informed on about 1000 anomalies. There is also fourth group **low altitude — low inclination** (in **Fig. 3** is not shown) with only 5 satellites and very low number of anomalies (not considered in this paper).

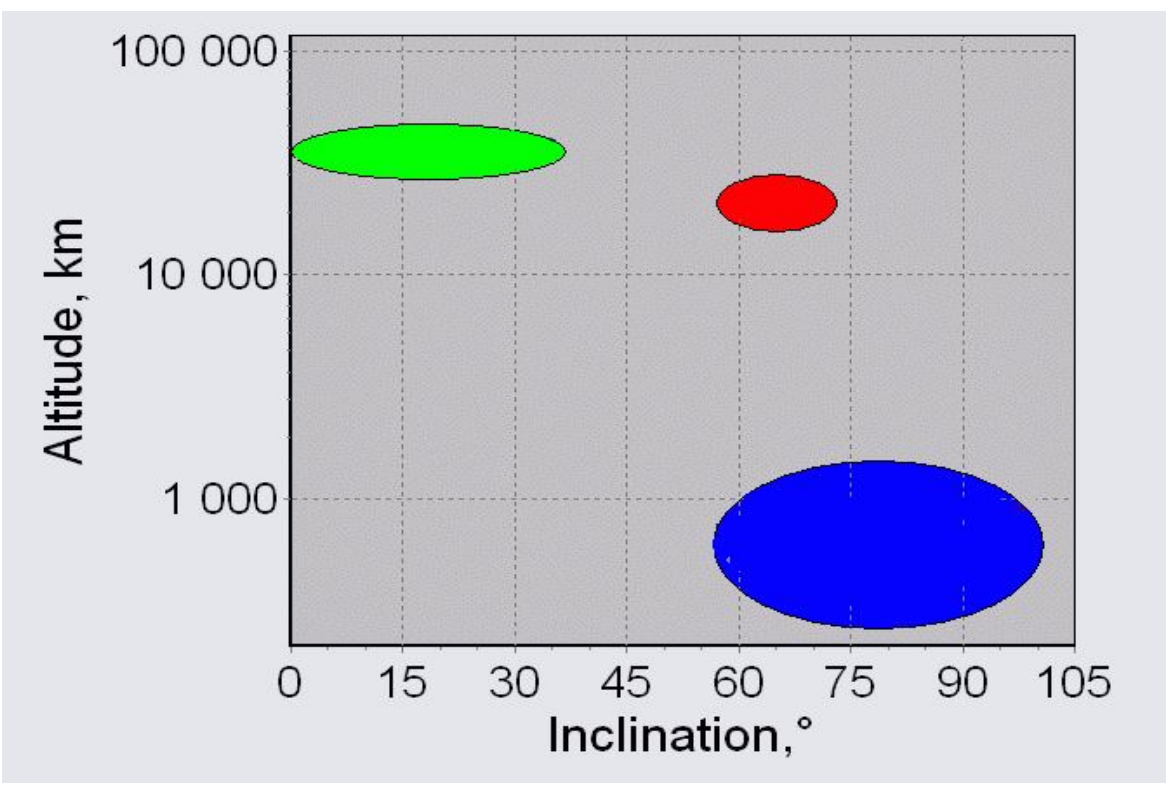

Fig. 3. The separation of satellites on three groups.

2.5. Periods with big numbers of satellite anomalies

Two examples are shown in **Figs. 4** and **5**.

Fig. 4. Period in October 1989. Upper panel: vertical arrows — moments of satellite anomalies, CR variations at 10 GV, solar protons (> 10 MeV and >60 MeV) fluxes. Lower panel: Kp- and Dst-indices.

In **Fig. 4** is shown the well known period — October 1989, characterized with very bad space weather. We see here three big solar proton events and very strong magnetic storm. We have three clusters of satellite anomalies and they coincide with maximal solar proton fluxes.

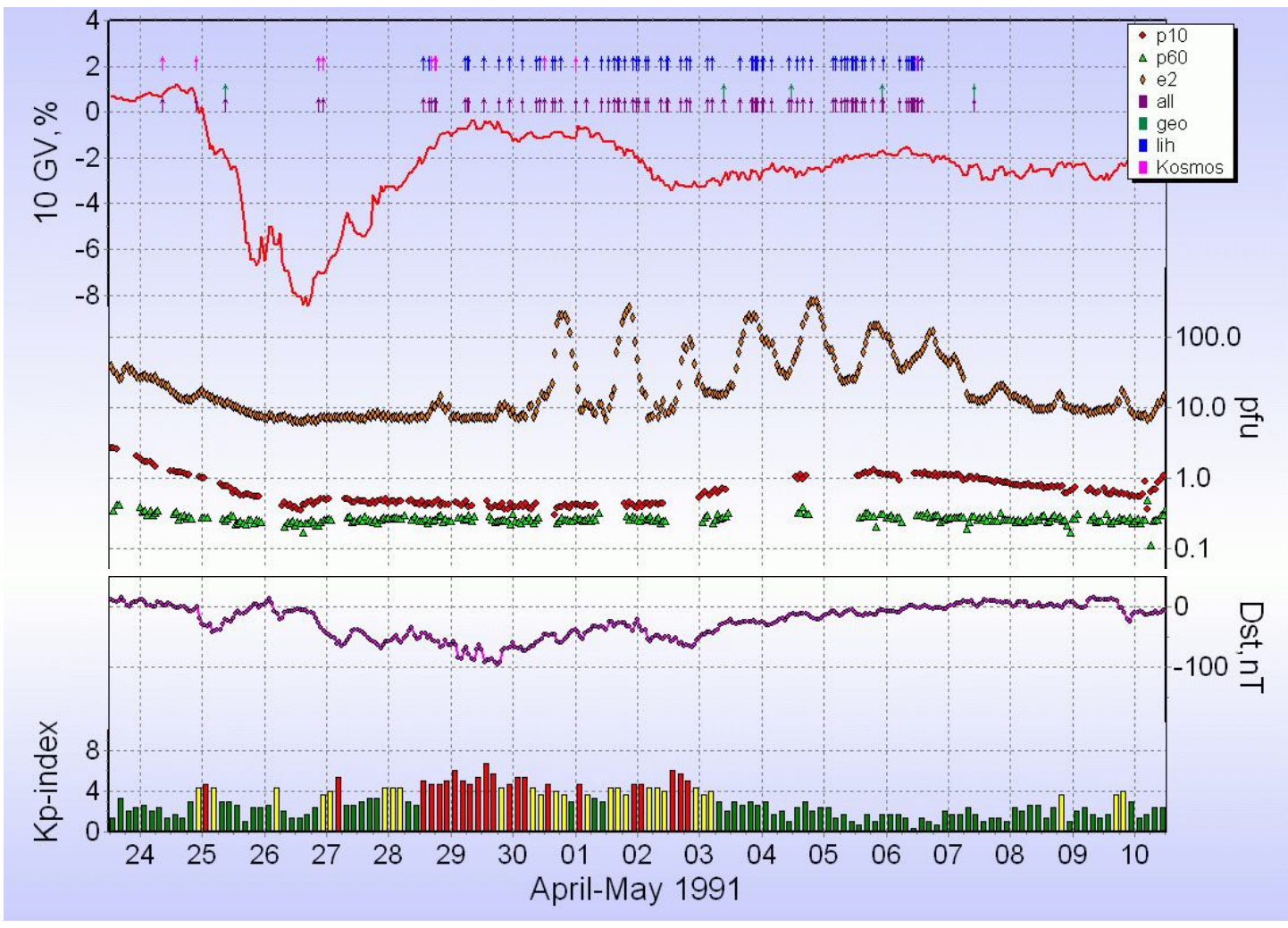

Fig. 5. The same as in **Fig. 4**, but for the period in April-May 1991 and in upper panel are added fluxes of electrons with energy > 2 MeV.

In **Fig. 5** the majority of anomalies coincide with magnetic storm and enhancements of electron fluxes from radiation belts. The anomalies are absent entirely in the high altitude — high inclination group, which played the main role in preceding example. Only a few anomalies were in GEO group and huge majority — in blue group (low altitude — high inclination).

2.6. Seasonal variations of anomalies of all satellites in comparison with Ap index

Results are shown in **Fig. 6.**

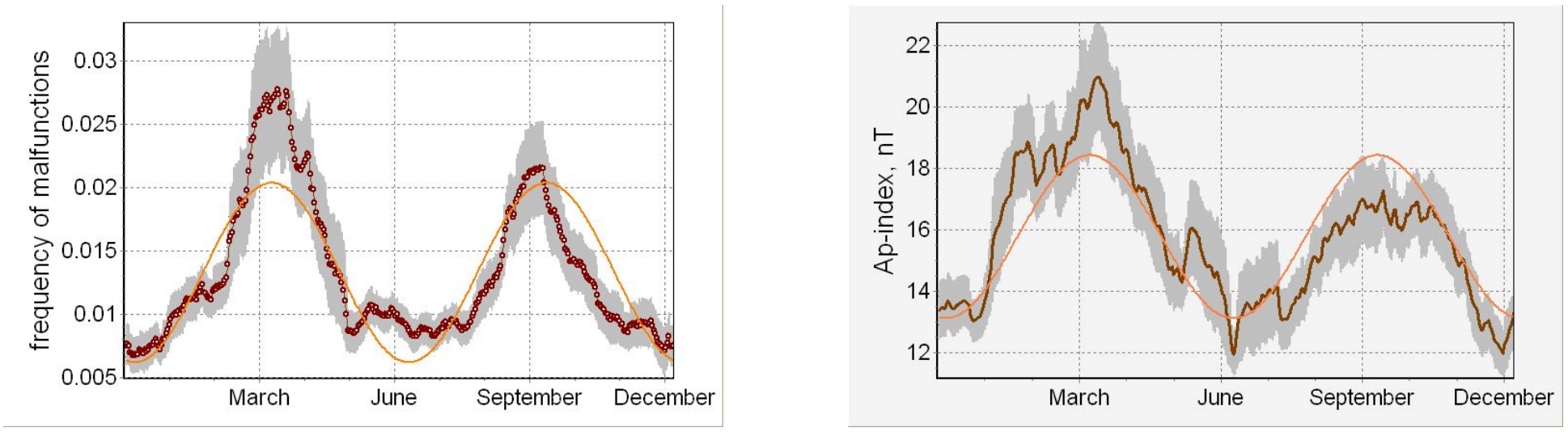

Fig. 6. Satellite anomalies frequency (per day and per one satellite) and Ap-index averaged over the period 1975—1994. The curve with points is the 27-day running mean values; the grey band corresponds to the 95% confidence interval. The sinusoidal curve is a semiannual wave with maxima in equinoxes best fitting the frequency data.

2.7. Seasonal variations of anomalies for different satellite orbits

Results are shown in **Figs. 7—9**.

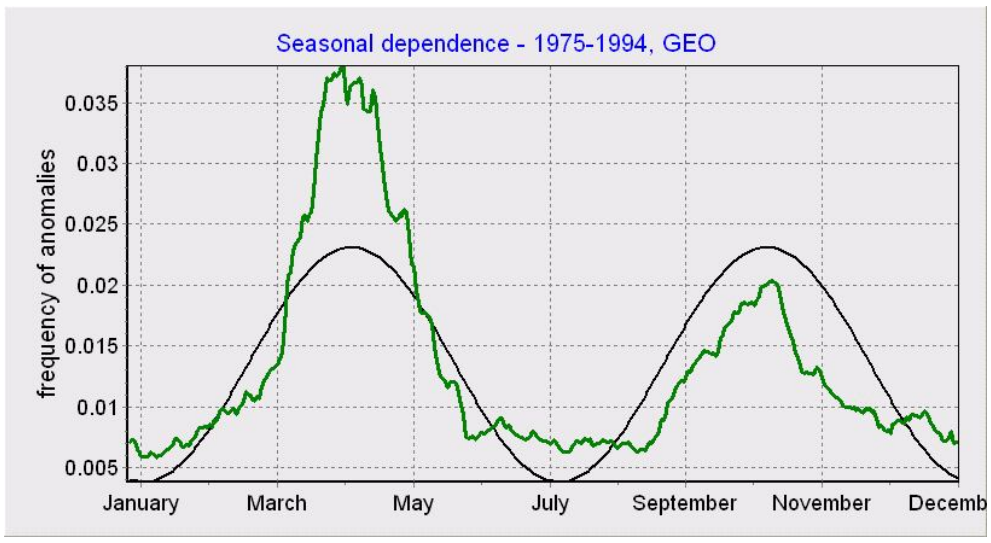

Fig. 7. 27-day averaged anomaly frequencies (per day and per one satellite) and corresponding half year wave for high altitude — low inclination (green) group.

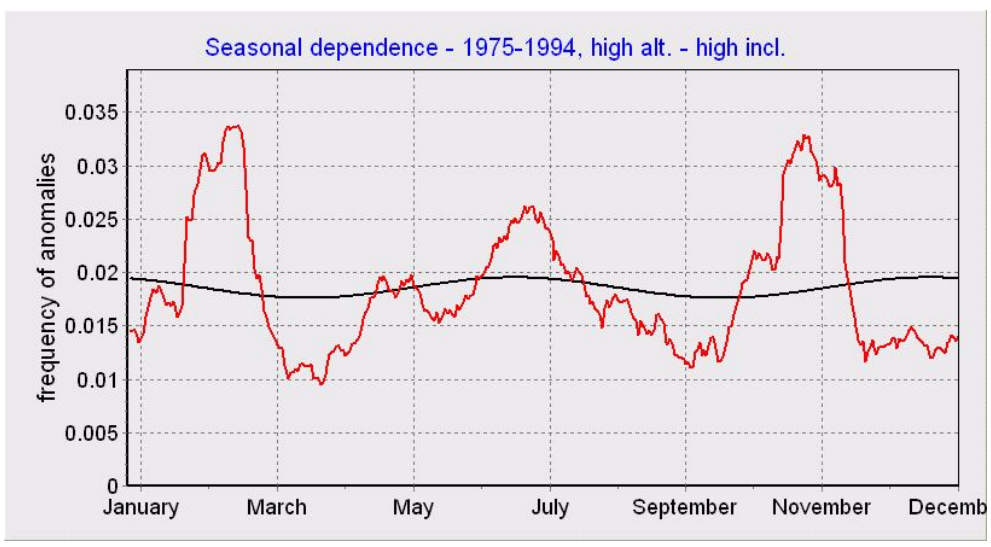

Fig. 8. The same as in Fig. 7, but for high altitude — high inclination satellite (red) group.

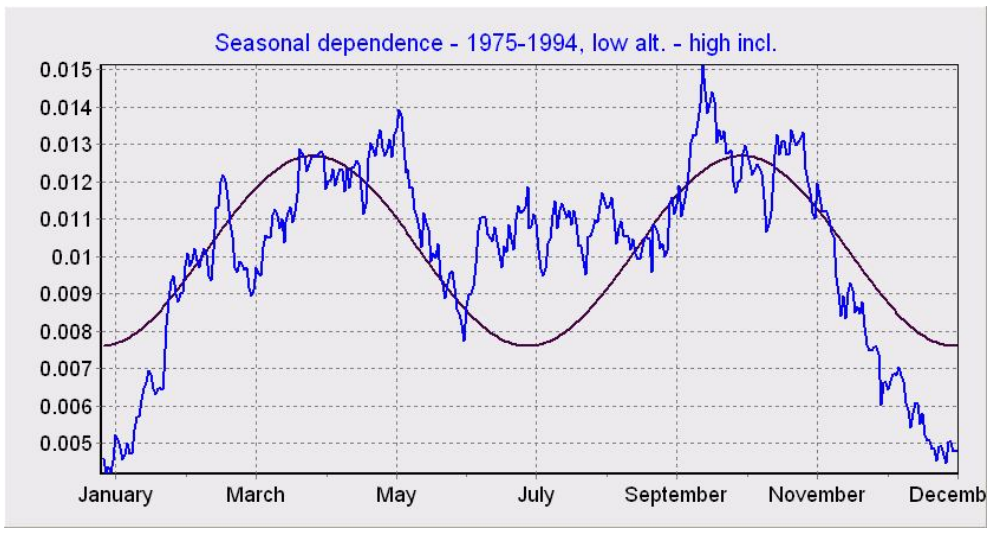

Fig. 9. The same as in Fig. 7, but for low altitude – high inclination satellite (blue) group.

From **Figs. 7—9** can be seen that the biggest season variation is in GEO green group (high altitude — low inclination, **Fig. 7**). The red group (high altitude — high inclination, **Fig. 8**) is not demonstrated visible spring – autumn preference. The blue group (low altitude — high inclination, **Fig. 9**) demonstrated some spring – autumn preference, but not so clear as green group (compare with **Fig. 7**).

2.8. Clustering of satellite anomalies

Fig. 10 shows that satellite anomalies have a tendency to clustering in small groups of few days.

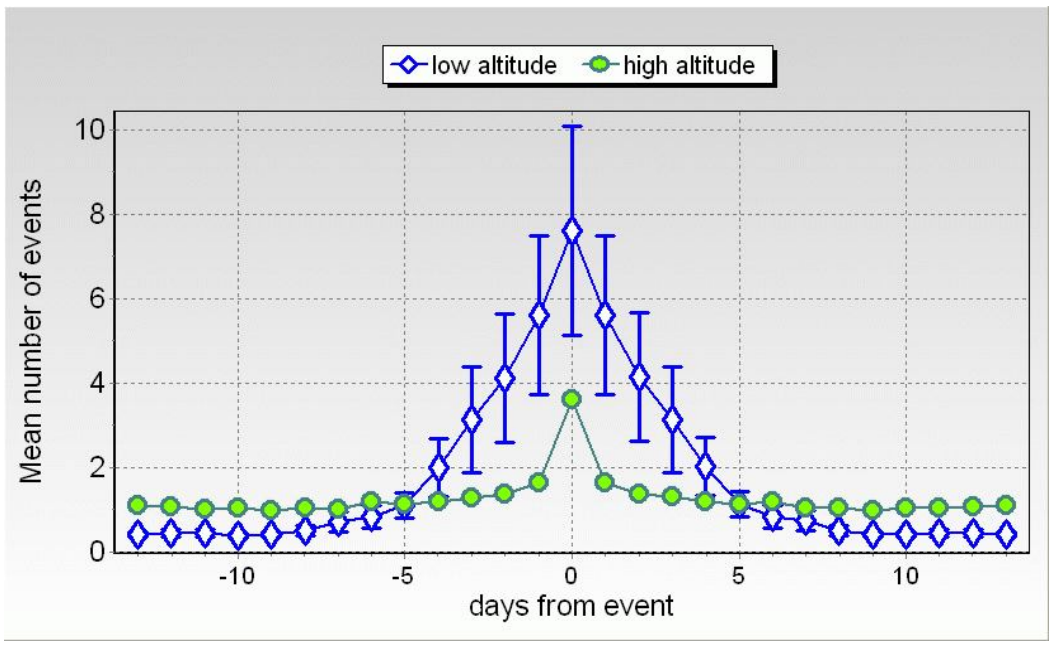

Fig. 10. The tendency to clustering of satellite anomalies in small groups of few days for low altitude (blue) and high altitude (green) satellites.

2.9. Influence of geomagnetic storms on satellite anomalies

In **Figs. 11** and **12** are shown connection of geomagnetic storms SSC with satellite anomalies.

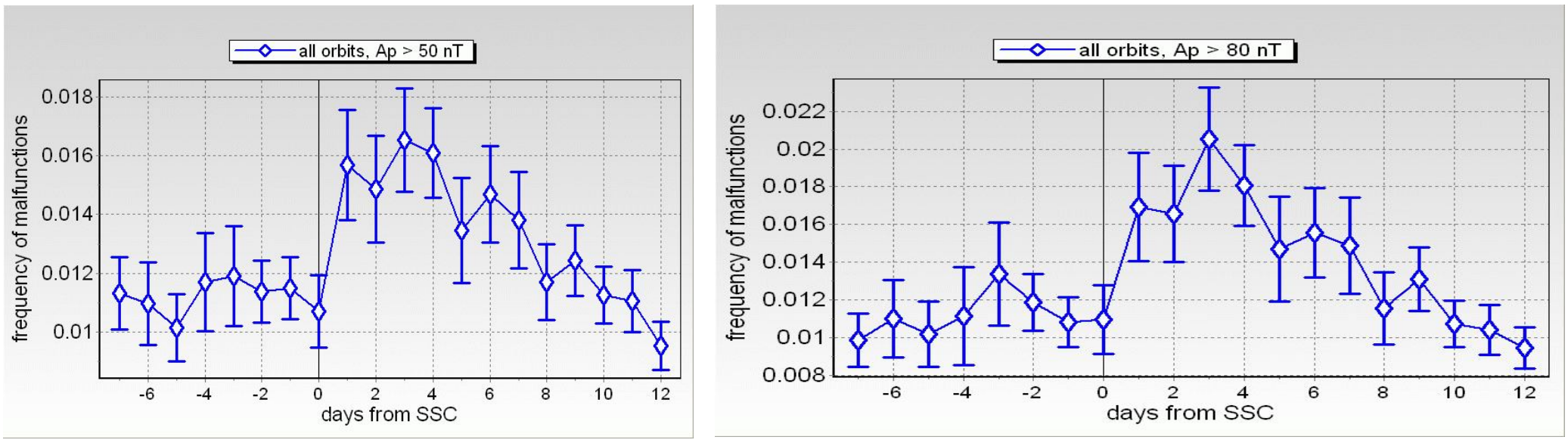

Fig. 11. SSC and satellite anomalies for all orbits and for Ap > 50 nT and > 80 nT (left and right panels).

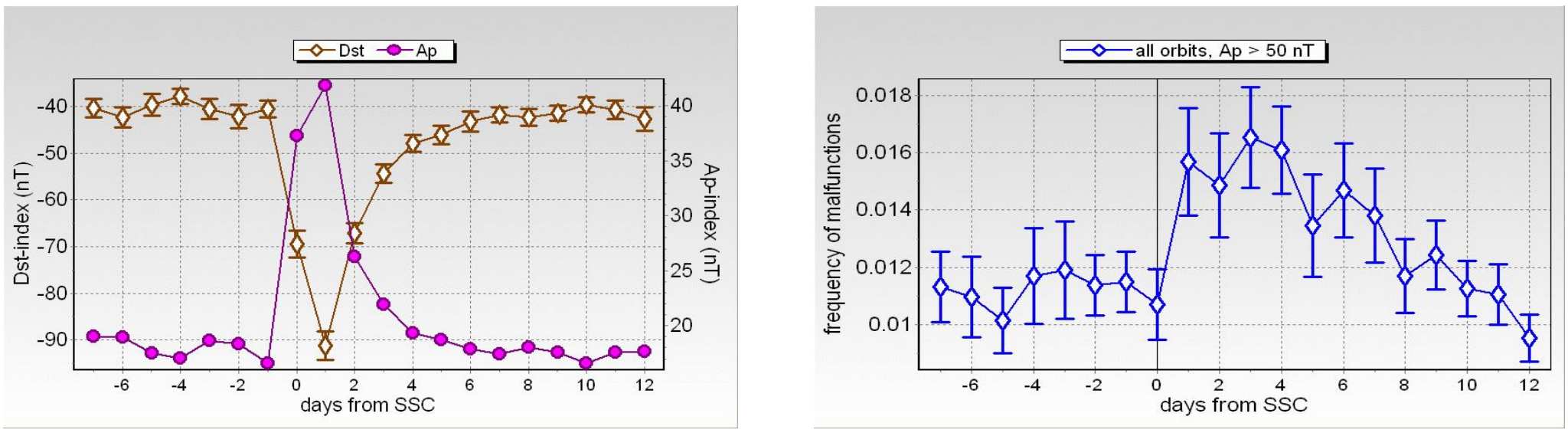

Fig. 12. Variations of Ap and Dst indexes (left panel) in comparison with satellite anomalies (right panel).

Fig. 11 shows that there are effective connection between magnetic storms and satellite anomalies (probability of anomaly increases in about 1.5 times), and from **Fig. 12** can be seen that in average anomalies start later and lasted longer than magnetic storms.

2.10. Solar cosmic ray events and satellite anomalies

Results are shown in **Figs. 13—15**.

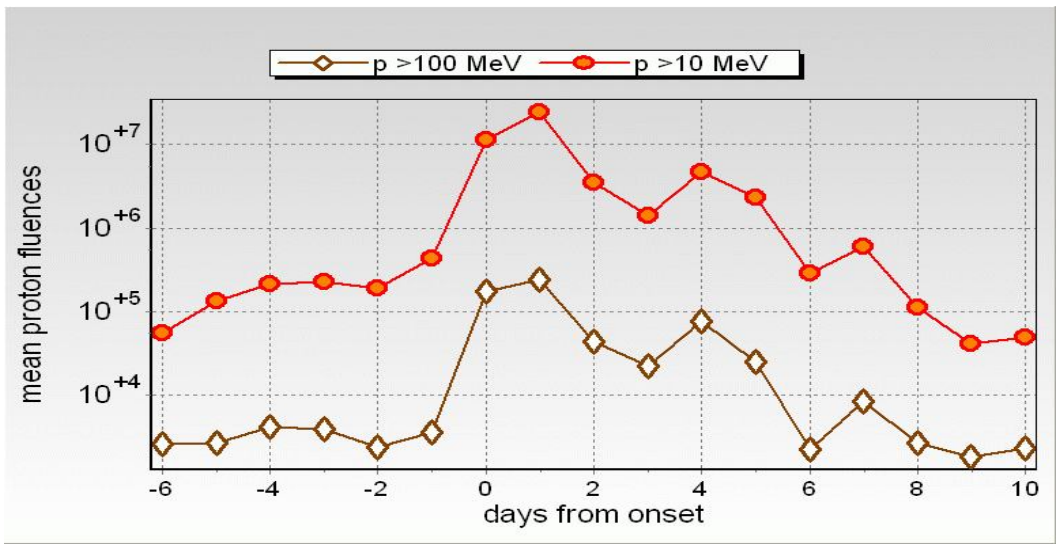

Fig. 13. Solar proton events and satellite anomalies.

In **Fig. 13** the 0-day is proton event onset day. Hear we used only enhancements in which average hour flux was bigger than 300 pfu. We see increasing of satellite anomalies in the 0-day and in 1-day. The increasing is bigger on high altitudes than at low altitudes.

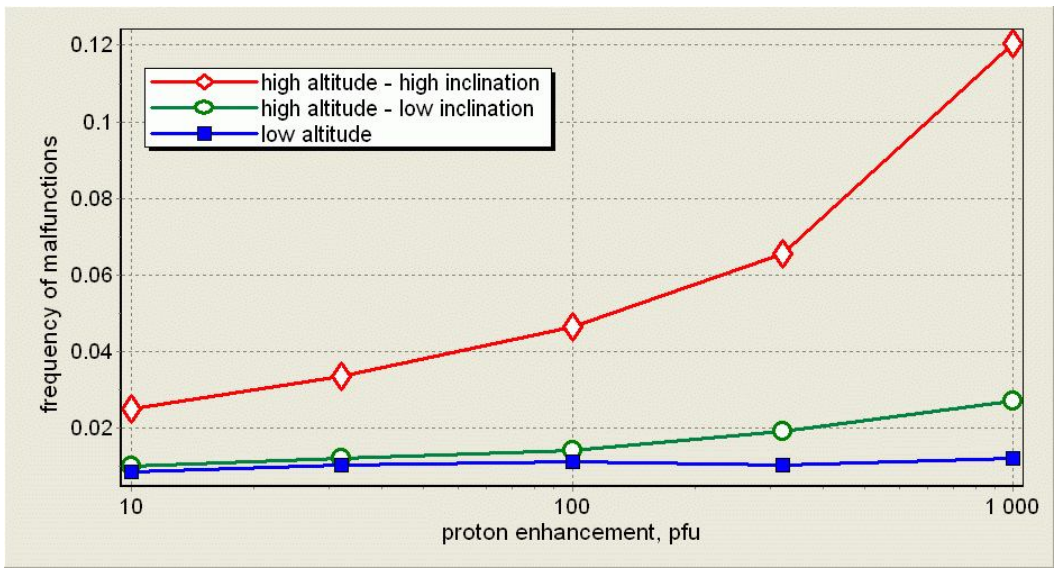

Fig. 14. Dependence of the frequency of satellite anomaly (per day and per one satellite) from the flux of protons with energy ≥ 10 MeV for different groups of satellites.

From **Fig. 14** can be seen that the biggest effect is in the red group (high altitude, high inclination). The smaller effect is in green group (high altitude, low inclination), and nothing for blue group (low altitudes). The differences between satellite groups are visible.

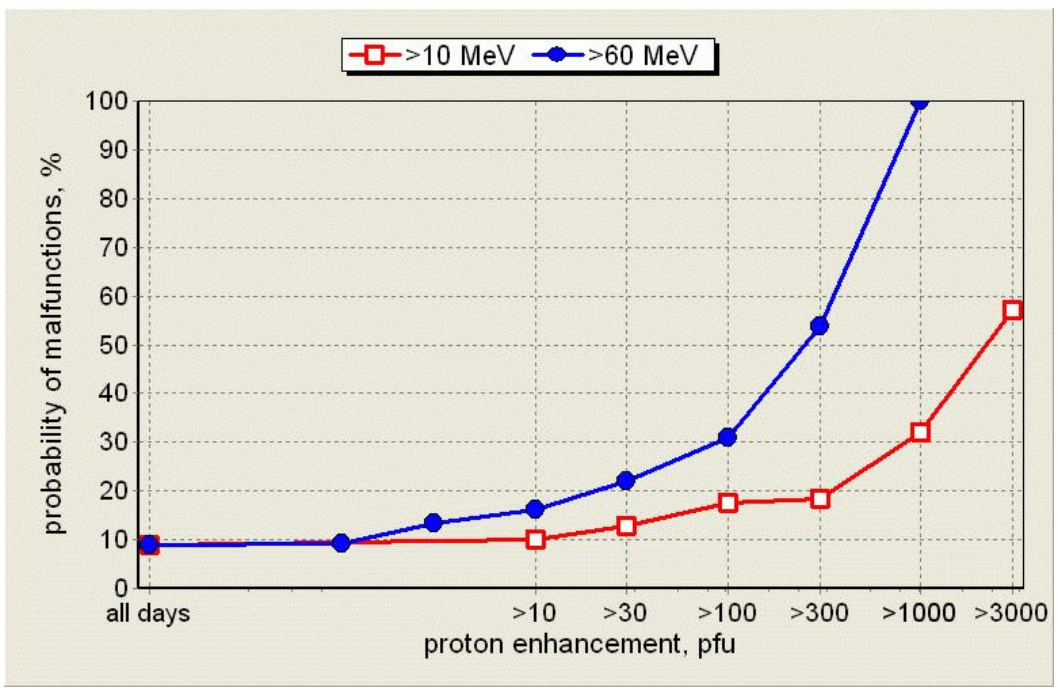

Fig. 15. Dependence of the probability of satellite anomaly (per one day) from the flux of protons with energies > 10 MeV and > 60 MeV for high altitude — high inclination group of satellites.

From **Fig. 15** can be seen that usually we have 10% probability of anomaly, but in special solar proton days this probability rises up to 100%. If we consider only data when in the group high altitude – high inclination was > 6 satellites, correlation coefficient between fluence of solar protons with energy > 10 MeV and frequency of anomalies increased up to 0.83.

2.11. Hazards of energetic protons from solar flares and relativistic electrons from radiation belts for satellites on different orbits

Results of statistical analysis are shown in **Fig. 16**.

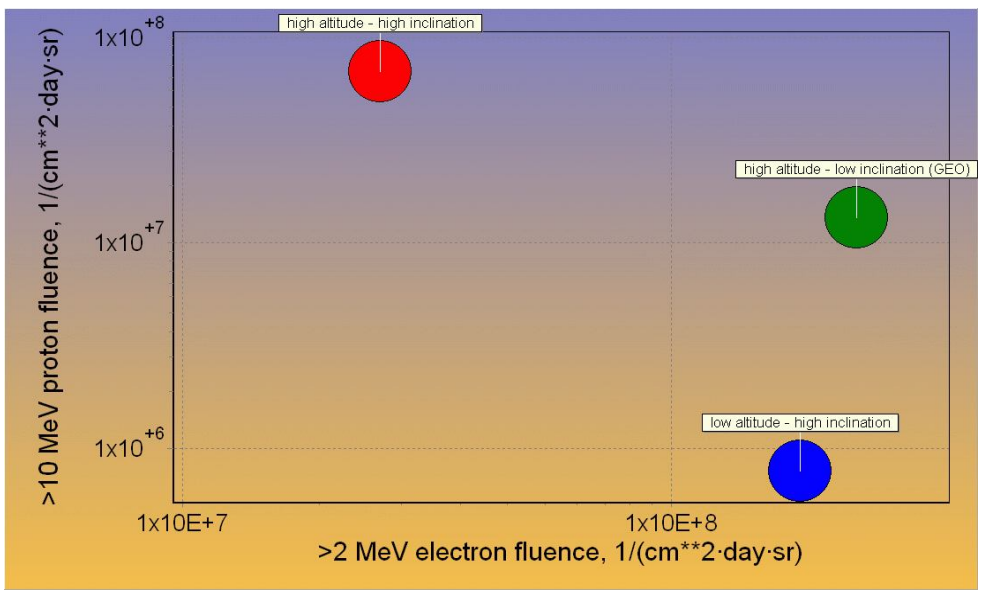

Fig. 16. Mean proton and electron fluencies on the anomaly day for the different satellite groups.

From **Fig. 16** can be seen that anomalies in the red group (high altitude — high inclination) are caused mostly by energetic protons from solar flares. Blue group (low altitude — high inclination) — caused mostly by energetic electrons from radiation belts, and green group (high altitude — low inclination) is mixed — caused by both energetic protons and electrons.

2.12. Possible precursors for satellite anomalies

We found interesting behavior of some parameters of space weather related to satellite anomalies.

2.12.1. Ap index

Results of statistical analysis for Ap index are shown in Fig. 17.

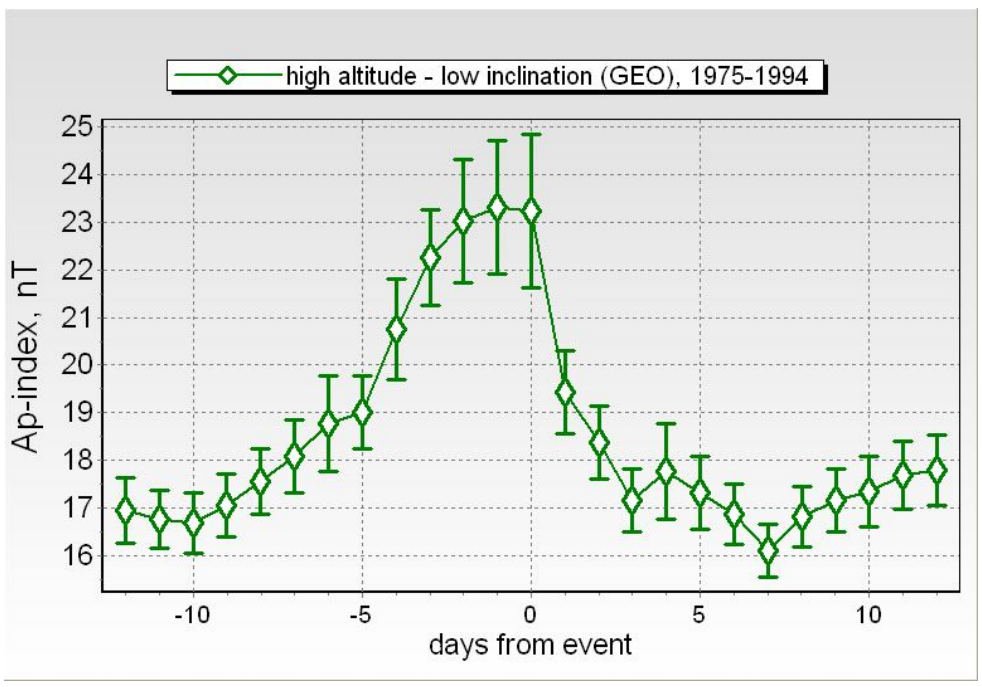

Fig. 17. Mean behavior of Ap-index in anomaly periods for high altitude — low inclination group (GEO satellites).

From **Fig. 17** we see the enhanced geomagnetic activity not only in day of satellite anomaly (zero-day) but also several days before.

2.12.2. Fluencies of electrons from radiation belts with energy > 2 MeV

From **Fig. 18** can be seen that >2 MeV electron fluence also may be used as for several days precursor for high altitude — low inclination satellite anomalies.

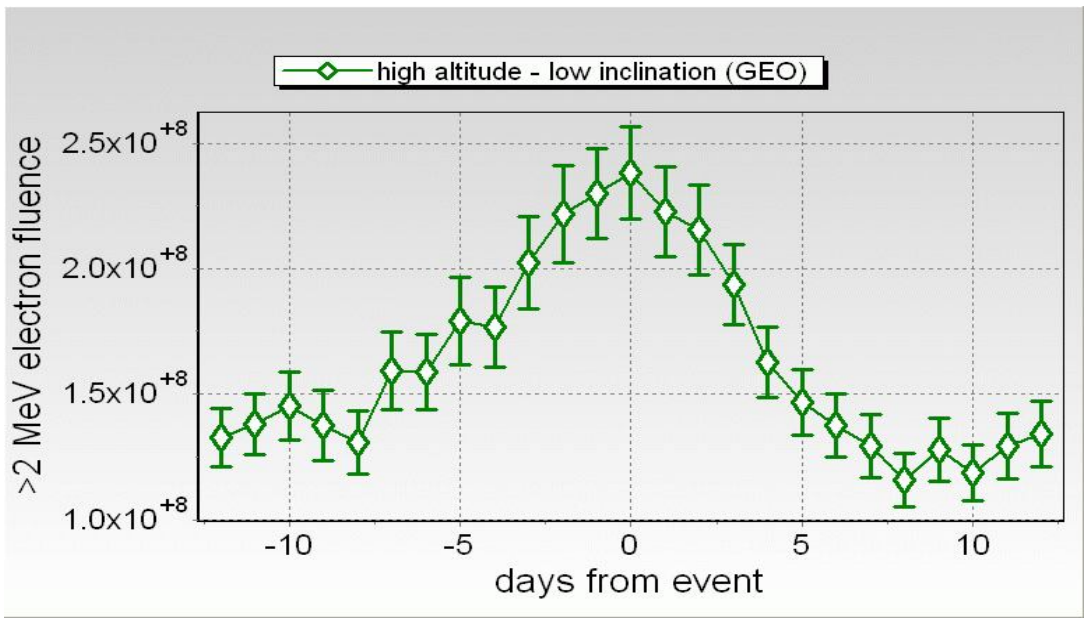

Fig. 18. The mean behavior of >2 MeV electron fluence in anomaly periods for high altitude — low inclination group (GEO satellites).

2.12.3. Velocity of solar wind

Results are shown in **Fig. 19.**

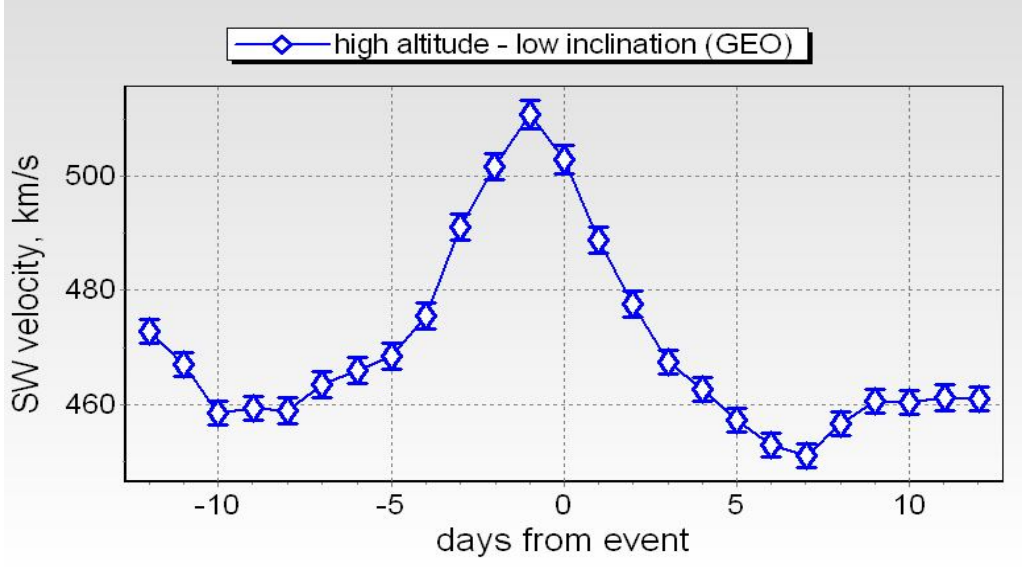

Fig. 19. The mean behavior of solar wind velocity in anomaly periods for high altitude — low inclination group (GEO satellites).

From **Fig. 19** can be seen that solar wind velocity also may be used as for several days precursor for high altitude — low inclination satellite anomalies. In principle, all three considered in this Section factors may be used as combined precursor for anomalies in the high altitude — low inclination satellite group.

2.13. Models for satellite anomaly probabilities and forecasting

Results schematically are shown in **Fig. 20**.

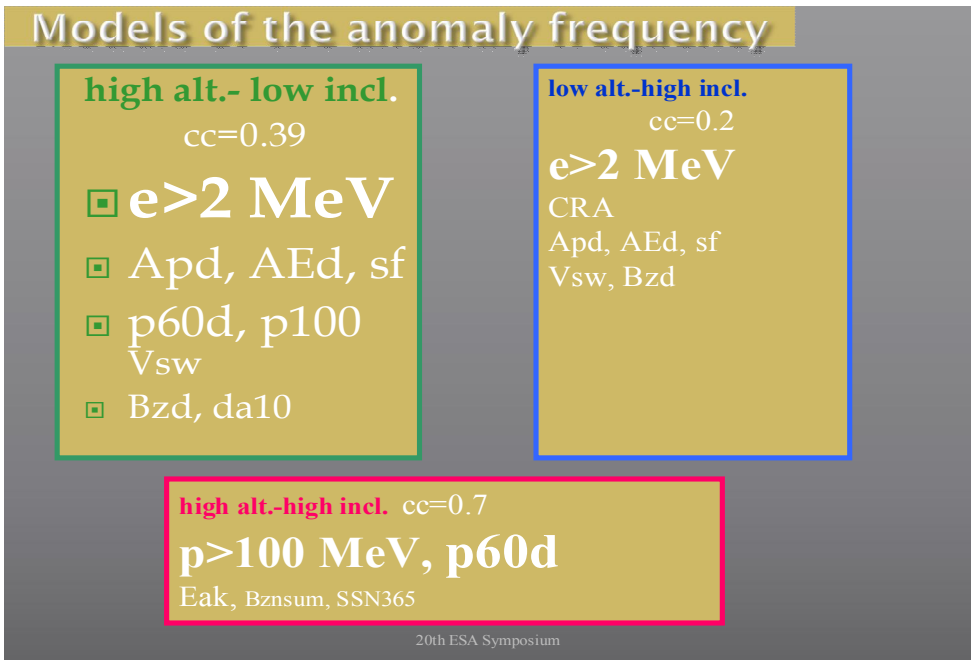

Fig. 20. Results for three groups of satellites. Bigger symbols correspond bigger regression coefficients.

From **Fig. 20** can be seen that main role in formation anomalies play energetic electrons (generated mostly in the Earth's magnetosphere during magnetic storms) in green and blue groups of satellites (especially — in green group), but in red group solar energetic protons are much more important than other indices. Therefore, for forecasting satellite anomalies are important forecasting of SEP events (see below Sections 4—6) and magnetic storms.

3. Data from the past and classification of Space Weather dangerous phenomena (NOAA classification and its modernization)

As it well known, NOAA Space Weather Scale establishes 5 gradations of SEP events, what are called Solar Radiation Storms: from S5 (the highest level of radiation, corresponded to the flux of solar protons with energy >10 MeV about 10^5 proton.cm^{-2}.s^{-1}) up to S1 (the lowest level, the flux about 10 proton.cm^{-2}.s^{-1} for protons with energy >10 MeV). From our opinion, by ground level CR neutron monitors and muon telescopes it is possible monitoring and forecast (by using much higher energy particles than smaller energy particles caused the main radiation hazard) SEP events of levels S5, S4 and S3. With increasing of SEP event level of radiation will increase the accuracy of forecasting. Let us note that from our opinion, for satellite damage and influence on people health and technology, on communications by HF radio-waves more important is the total fluence of SEP during the event than the protons flux what is used now in NOAA Space Weather Scale. The second note is, that the level S5 (corresponds to the flux 10^5 proton.cm^{-2}.s^{-1}, or fluency F ~ 10^9 proton.cm^{-2} for protons with $E_k \geq 10$ MeV) is not maximal (as it is supposed by NOAA Solar Radiation Storms Scale), but can be much higher and with much smaller probability than S5 *[Dorman et al. 1993; Dorman and Venkatesan 1993; Dorman and Pustil'nik 1995, 1999]*. As it was shown by *[McCracken et al. 2001]*, the dependence of event probability from fluence can be prolonged at least up to $F = 2 \times 10^{10}$ proton.cm^{-2} for protons with

$E_k \geq 30$ MeV, what was observed in SEP of September 1859 according to data of nitrate contents in polar ice and on other SEP events (see **Figs. 21—23**).

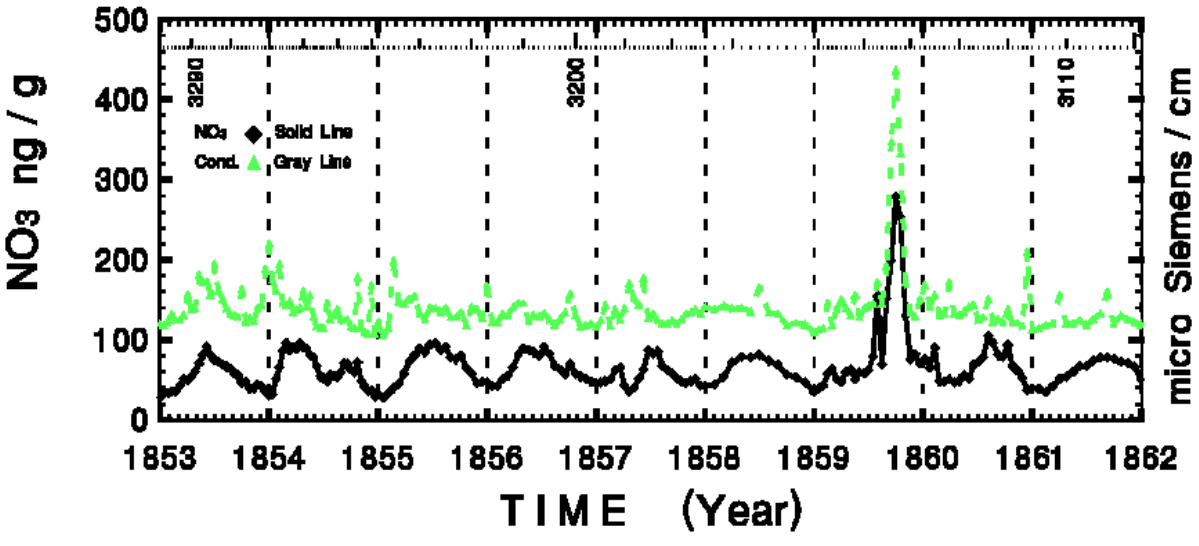

Fig. 21. Example on a great SEP event in September 1859 with fluency $F = 2\times10^{10}$ proton. cm^{-1} for protons with $E_k \geq 30$ MeV. According to *[McCracken et al. 2001]*.

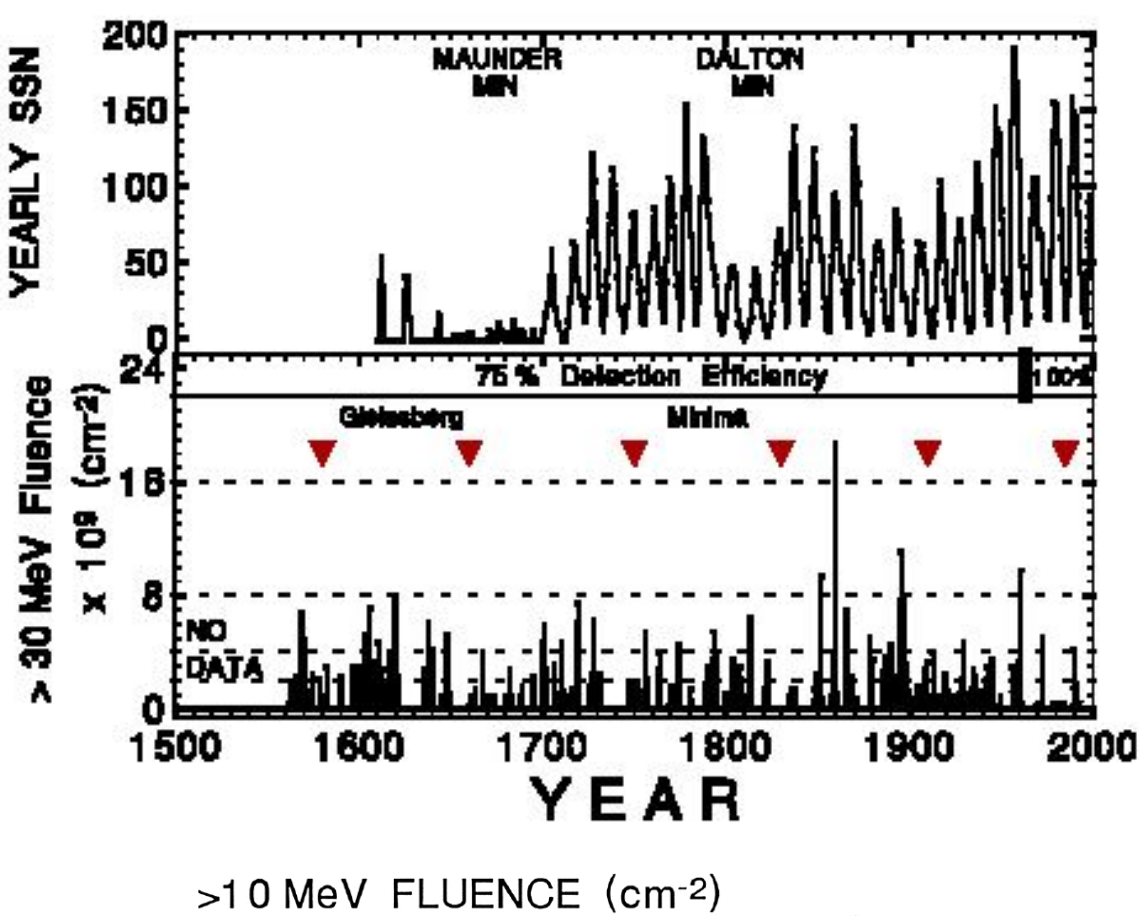

Fig. 22. Great SEP events in the last 450 years according to nitrate data *[McCracken et al. 2001]*.

Fig. 23. The dependence of SEP events probability (number of events per year) from the value of fluence according to direct satellite and NM data, nitrate in polar ice data and cosmogenic nuclide data on the moon *[McCracken et al. 2001]*.

This type of great dangerous events is very rarely (about one in few hundred years). According to Fig 23 it is not excluded that in principle can occurred very great SEP events with fluency in 10 and even in 100 times bigger (correspondingly one in few thousand and one in several ten thousand years). So, we suppose to correct the very important classification, developed by NOAA, in two directions: to use fluency F of SEP during all event (in units proton.cm^{-2}) instead of flux I, and to extend levels of radiation hazard. As result, the modernized classification of SEP events is shown in **Table 1**.

Table 1

Extended SEP events radiation hazard scale (based on NOAA Space Weather Scale for Solar Radiation Storms)

SEP events radiation hazard			Fluence level ≤ 30 MeV protons	Number of events per one year
S7	**Especially extreme**	**Biological:** Lethal doze for astronauts, for passengers and crew on commercial jets; great influence on people health and gene mutations on the ground **Satellite operations:** very big damages of satellites electronics and computers memory, damage to solar panels, loosing of many satellites **Other systems**: complete blackout of HF (high frequency) communications through polar and middle-latitude regions, big position errors make navigation operations extremely difficult.	**$10^{(11-12)}$**	**One in few thousand years**
S6	**Very extreme**	**Biological:** About lethal doze for astronauts, serious influence on passengers and crew health on commercial jets; possible influence on people health and genes mutations on the ground **Satellite operations:** a big damages of satellites electronics and computers memory, damage to solar panels, loosing of several satellites **Other systems**: complete blackout of HF communications through polar regions, some position errors make navigation operations very difficult.	**$10^{(10-11)}$**	**One in few hundred years**
S5	**Extreme**	**Biological:** unavoidable high radiation hazard to astronauts on EVA (extra-vehicular activity); high radiation exposure to passengers and crew in commercial jets at high latitudes (approximately 100 chest X-rays) is possible. **Satellite operations:** satellites may be rendered useless, memory impacts can cause loss of control, may cause serious noise in image data, star-trackers may be unable to locate sources; permanent damage to solar panels possible. **Other systems:** complete blackout of HF (high frequency) communications possible through the polar regions, and position errors make navigation operations extremely difficult.	**10^{9}**	**One in 20-50 years**
S4	**Severe**	**Biological:** unavoidable radiation hazard to astronauts on EVA; elevated radiation exposure to passengers and crew in commercial jets at high latitudes (approximately 10 chest X-rays) is possible. **Satellite operations:** may experience memory device problems and noise on imaging systems; star-tracker problems may cause orientation problems, and solar panel efficiency can be degraded. **Other systems:** blackout of HF radio communications through the polar regions and increased navigation errors over several days are likely.	**10^{8}**	**One in 3-4 years**
S3	**Strong**	**Biological**: radiation hazard avoidance recommended for astronauts on EVA; passengers and crew in commercial jets at high latitudes may receive low-level radiation exposure (approximately 1 chest X-ray). **Satellite** operations: single-event upsets, noise in imaging systems, and slight reduction of efficiency in so/lar panel are likely. **Other systems**: degraded HF radio propagation through the polar regions and navigation position errors likely.	**10^{7}**	**One per year**

Let us note, that the expected frequency of SEP events in the last column of Table 1 is averaged over solar cycle. Really, this frequency is much higher in periods of high solar activity than in periods of low solar activity *[Dorman et al. 1993; Dorman and Pustil'nik, 1995, 1999]*.

4. On-line search of the start of great SEP events, automatically formation Alerts, estimation of probability of false Alerts and probability of missing Alerts (realized in the Emilio Segré Observatory at Mt. Hermon)

4.1. Why we need to use solar high energetic particles for SEP forecasting and determine the time of their arriving?

It is well known that in periods of great solar energetic particle (SEP) ground events, fluxes of energetic particles can be so big that memory of computers and other electronics in space may be damaged, and satellite and spacecraft operations can be seriously degraded. In these periods it is necessary to switch off some part of electronics for a few hours to protect computer memories. The problem is how to forecast exactly these dangerous phenomena. We show that exact forecasts can be made by using high-energy particles (few GeV/nucleon and higher) whose transportation from the Sun is characterized by much bigger

diffusion coefficients than lower energy particles. High-energy particles arrive from the Sun much earlier (8—20 minutes after acceleration and escaping into solar wind) than the lower energy particles that damage electronics (about 30-60 minutes later). We describe here the principles and operation of automated programs "SEP-Search-1 min", "SEP-Search-2 min",and "SEP-Search-5 min", developed and checked in the Emilio Segre' Observatory (ESO) of the Israel Cosmic Ray Center (2025 m above sea level, R_c =10.8 GV). The determination of increasing flux is made by comparison with the intensity, averaged from 120 to 61 minutes, prior to the current one-minute data. For each minute of data the program "SEP-Search-1 min" is run. If the result is negative (no simultaneous increase in both channels of total intensity ≥ $2.5\sigma_1$, where σ_1 is the standard deviation for one minute of observation in one channel [for ESO σ_1=1.4 %]), start the program "SEP-Search-2 min", using two minute averages with $\sigma_2 = \sigma_1/\sqrt{2}$, and so on. If any positive result is obtained, the "SEP-Search" programs check the next minute of data. If the result is again positive, automatically run the on-line the programs "SEP-Collect" and "SEP-Research" that determine the expected flux and spectrum and generate automatic alerts. These programs are described in *[Dorman and Zukerman 2001]*.

4.2. Short description of ICR&SWC and Emilio Segre' Observatory

The Israel Cosmic Ray & Space Weather Center (ICR&SWC) and Israel-Italian Emilio Segre' Observatory (ESO) were established in 1998, with affiliation to Tel Aviv University, to the Technion (Israel Institute of Technology, Haifa) and to the Israel Space Agency (under the aegis of the Ministry of Science). The Mobile Cosmic Ray Neutron Monitor of the Emilio Segre' Observatory, was prepared in collaboration with scientists of the Italian group in Rome, and transferred in June 1998 to the site selected for the Emilio Segre' Observatory (33°18'N, 35°47.2'E, 2050 m above sea level, vertical cut-off rigidity R_c = 10.8 GV). The results of measurements (data taken at one-minute intervals of cosmic ray neutron total intensities from two separate 3NM-64, as well as similar one-minute data about the intensities relating to neutron multiplicities m ≥1, ≥2, ≥3, ≥4, ≥5, ≥6, ≥7 and ≥8) have been computer-stored. Similar one-minute data relating to the atmospheric electric field, wind speed, air temperature outside, and humidity and temperature inside the Cosmic Ray Observatory have also been recorded and archived. Each month one-hour data of the Emilio Segre' Observatory (short title ESO) are sending to the World Data Center in Boulder (USA, Colorado), to the WDC C-2 for cosmic rays (Japan) and to many Cosmic Ray Observatories in the world as well as are putting to our website. We established the automatic system of electric power supply using a diesel generator for providing continuous power for the Emilio Segre' Observatory. We finished the foundation of direct radio-connection in real time scale of the Emilio Segre' Observatory with our Laboratory in Qazrin, and with the Internet. In Fig. 24 we show a block-scheme of the main components of the Emilio Segré Observatory (ESO) and their connection with the Central Laboratory of Israel Cosmic Ray & Space Weather Center in Qazrin and with the Internet.

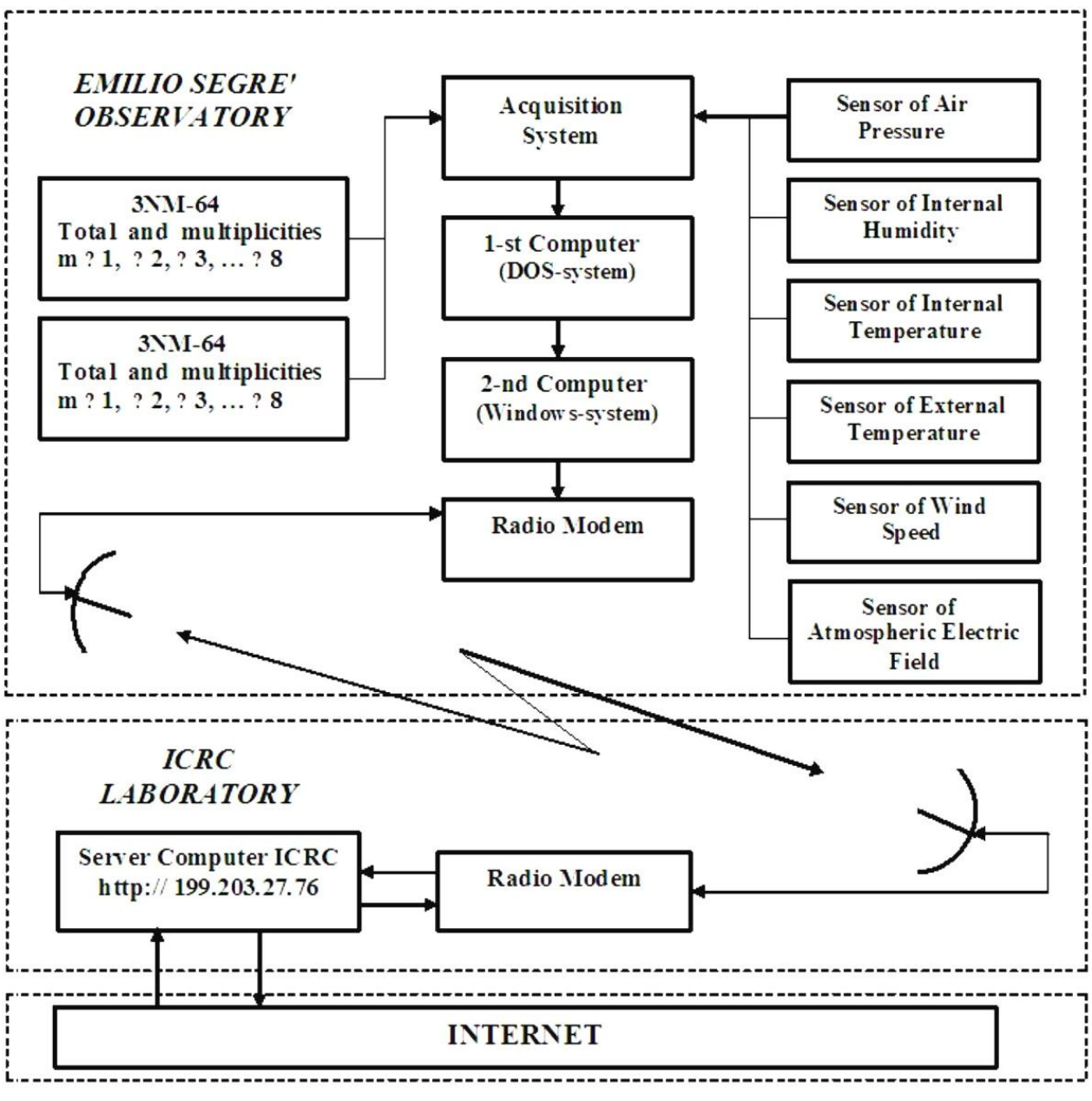

Fig. 24. Schematic of the main components of the Emilio Segre' Observatory (ESO) and their connection with the Central Laboratory of Israel Cosmic Ray Center (ICRC) in Qazrin and with INTERNET.

4.3. The method of automatically search of the start of ground SEP events

Let us consider the problem of automatically searching for the start of ground SEP events. Of course, the patrol of the Sun and forecast of great solar flares are very important, but not enough: only very small part of great solar flares produce dangerous SEP events. In principal this exact forecast can be made by using high-energy particles (few *GeV/nucleon* and higher) whose transportation from the Sun is characterized by much bigger diffusion coefficient than for small and middle energy particles. Therefore high-energy particles arrive from the Sun much earlier (8—20 minutes after acceleration and escaping into solar wind) than the lower energy particles that cause a dangerous situation for electronics (at least about 30—60 minutes later). The flux of high-energy particles is very small and cannot be dangerous for people and electronics.

The problem is that this very small flux cannot be measured with enough accuracy on satellites to use for forecast (it needs very large effective surfaces of detectors and thus large weight). High-energy particles of galactic or solar origin are measured continuously by ground-based neutron monitors, ionization chambers and muon telescopes with very large effective surface areas (many square meters) that provide very small statistical errors. It was shown on the basis of data in periods of great historical SEP events (as the greatest of February 23, 1956 and many tens of others), that one-minute on-line data of high energy particles could be used for forecasting of incoming dangerous fluxes of particles with much smaller energy. The method of coupling (response) functions *[Dorman 1957; Dorman et al., 2000; Clem and Dorman 2000; Dorman 2004]* allows us to calculate the expected flux above the atmosphere and out of the Earth's magnetosphere from ground based data. Let us describe the principles and on-line operation of programs "SEP-Search-1 min", "SEP-Search-2 min","SEP-Search-5 min", developed and checked in the Emilio Segre' Observatory of ICRC.

The determination of increasing flux is made by comparison with intensity averaged from 120 to 61 minutes before the present Z-th one-minute data. For each Z minute data, start the program "SEP-Search-1 min" (see **Figure 25**).

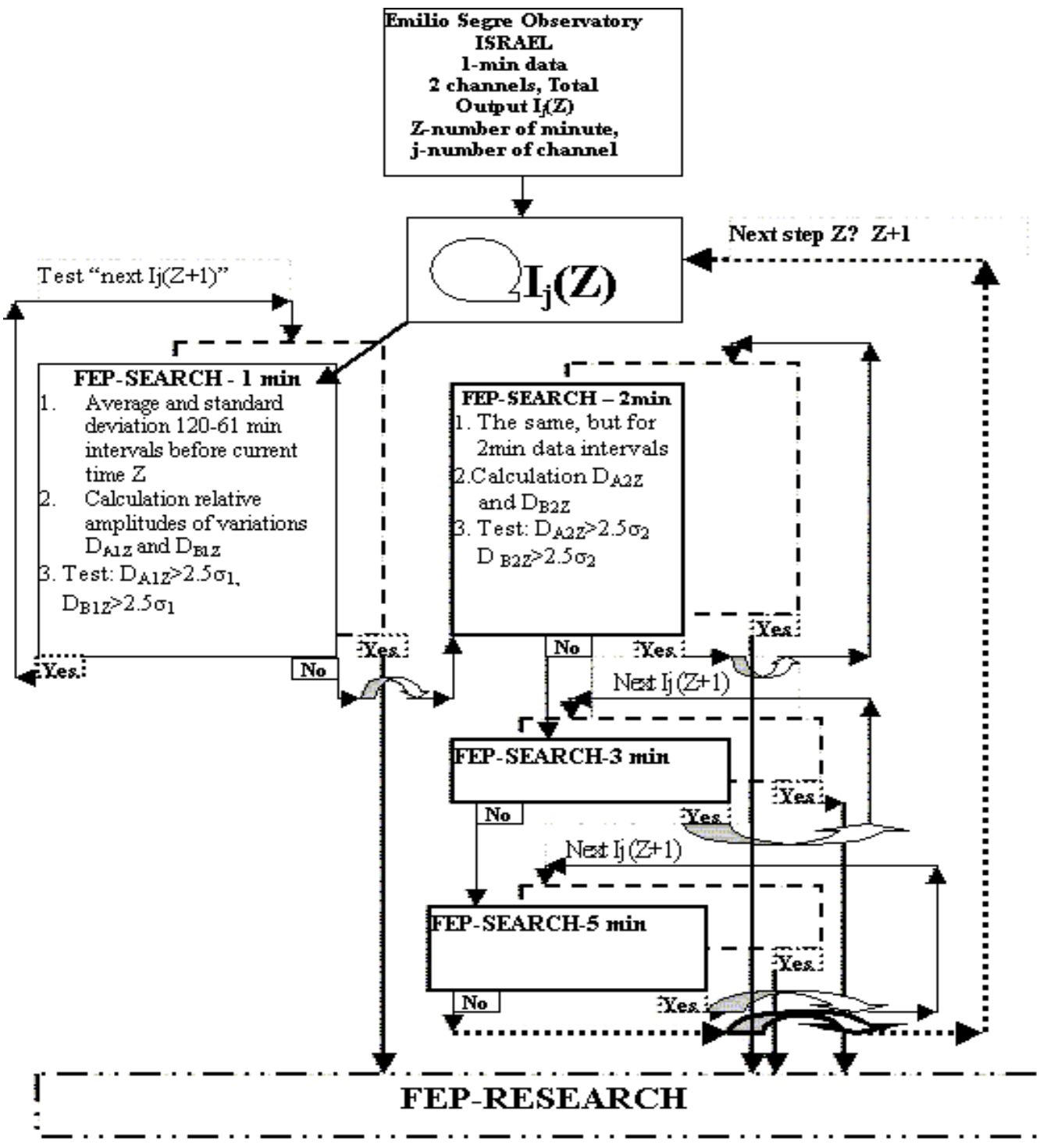

Fig. 25. Schematic of programs "SEP-Search".

The program for each Z-th minute determines the values

$$D_{A1Z} = \left[\ln(I_{AZ}) - \sum_{k=Z-120}^{k=Z-60} \ln(I_{Ak})/60 \right] \Big/ \sigma_1 , \qquad (1)$$

$$D_{B1Z} = \left[\ln(I_{BZ}) - \sum_{k=Z-120}^{k=Z-60} \ln(I_{Bk})/60 \right] \Big/ \sigma_1 , \quad \textbf{(2)}$$

where I_{Ak} and I_{Bk} are one-minute total intensities in the sections of neutron super-monitor *A* and *B*. If simultaneously

$$D_{A1Z} \geq 2.5,\ D_{B1Z} \geq 2.5, \quad \textbf{(3)}$$

the program "SEP-Search-1 min" repeat the calculation for the next Z+1-th minute and if **Eq. (3)** is satisfied again, the onset of great SEP is determined and programs "SEP-Collect" and "SEP-Re-search" described in the next section, are started.

If **Eq. (3)** is not satisfied, the program "SEP-Search-2 min" starts by using two-min data characterized by $\sigma_2 = \sigma_1 / \sqrt{2}$. In this case, the program "SEP-Search-2 min" will calculate values

$$D_{A2Z} = \left[\left(\ln(I_{AZ}) + \ln(I_{A,Z-1}) \right) \Big/ 2 - \sum_{k=Z-120}^{k=Z-60} \ln(I_{Ak}) \Big/ 60 \right] \Big/ \sigma_2 , \quad \textbf{(4)}$$

$$D_{B2Z} = \left[\left(\ln(I_{BZ}) + \ln(I_{B,Z-1}) \right) \Big/ 2 - \sum_{k=Z-120}^{k=Z-60} \ln(I_{Bk}) \Big/ 60 \right] \Big/ \sigma_2 , \quad \textbf{(5)}$$

If the result is negative (no simultaneous increase in both channels of total intensity ≥ $2.5\sigma_2$, i.e. the condition $D_{A2Z} \geq 2.5$, $D_{B2Z} \geq 2.5$ fails), then "SEP-Search-3 min" uses the average of three minutes Z-2, Z-1 and Z with $\sigma_3 = \sigma_1 / \sqrt{3}$. If this program also gives a negative result, then the program "SEP-Search-5 min" uses the average of five minutes Z-4, Z-3, Z-2, Z-1 and Z with $\sigma_5 = \sigma_1 / \sqrt{5}$. If this program also gives negative result, i.e. all programs "SEP-Search-*K* min"(where *K* = 1, 2, 3, 5) give negative result for the Z-th minute, it means that in the next 30—60 minutes there will be no radiation hazard (this information can be also very useful). After obtaining this negative result, the procedure repeats for the next, Z +1-th minute, and so on. If any positive result is obtained for some Z = Z', the "SEP-Search" programs checked the next Z' +1-th minute data. If the result obtained is again positive, then the programs, described in Section 4, are started to determine the expected flux and spectrum and to send automated alerts.

4.4. Monitoring and preliminary Alert for starting of great SEP events on the web-site of ICR&SWC and ESO

Fig. 26 shows an example of the image in the website of ICR&SWC and ESO for the moment 20:27:03 UT at 13 May 2001 (it was obtained 3 seconds after registration by NM in ESO, at 20:27:00 UT). On this image are shown on-line one-minute data of total neutron intensity for the last 6 hours (360 circles in the upper part) and one-hour data during the last 6 days (144 circles in the down part). One minute data are upgraded each minute in ASCII form. In the bottom of image is given information on variations in the A and B channels on the basis of one-, two-, and three-minute data (A1, A2, A3, B1, B2 and B3 in units of standard deviations).

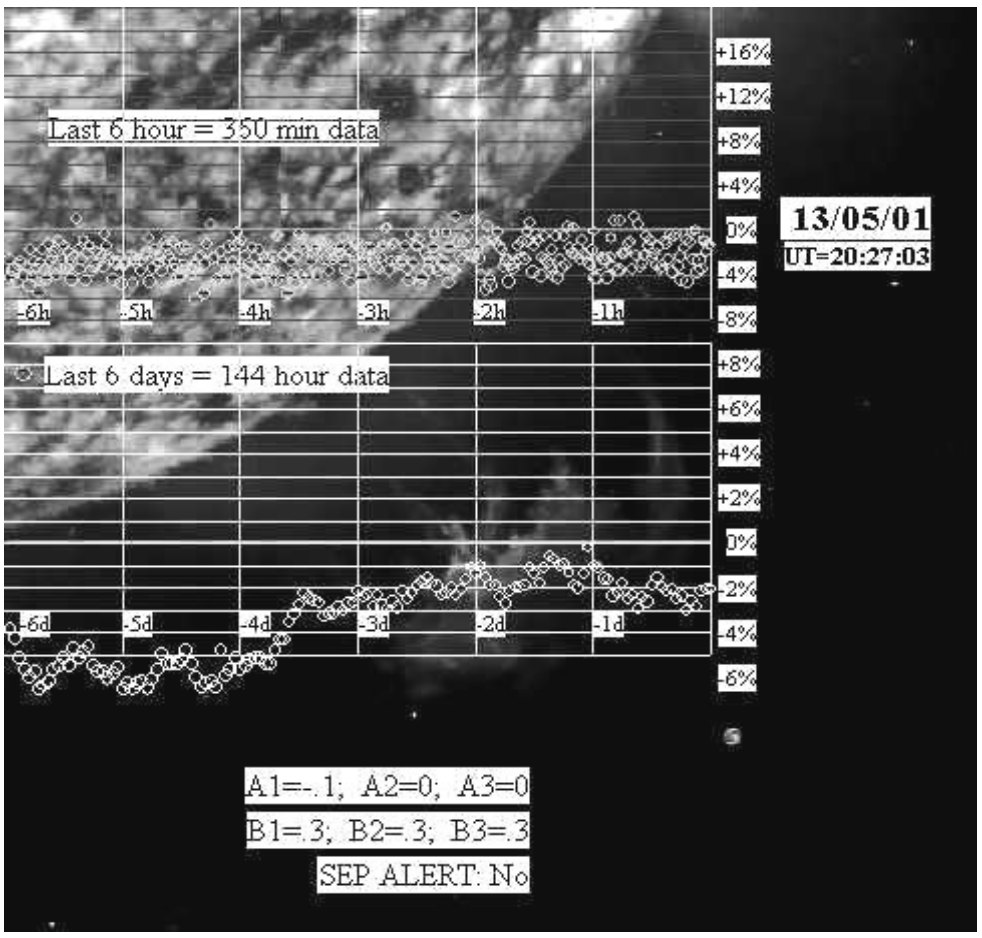

Fig. 26. Monitoring and preliminary alert for starting of great SEP events on the website of ICR&SWC.

In the last line in **Fig.26** is shown the Alert for starting of great SEP (based on data of both channels and checked by situation in the previous minute). It can be seen that in the considered moment of time there is the following situation, SEP ALERT: No. It means that at least during one hour will be no dangerous radiation hazard.

4.5. The probability of false alarms

Because the probability function $\Phi(2.5) = 0.9876$, that the probability of an accidental increase with amplitude more than 2.5σ in one channel will be $(1 - \Phi(2.5))/2 = 0.0062$ min^{-1}, that means one in 161.3 minutes (in one day we expect 8.93 accidental increases in one channel). The probability of accidental increases simultaneously in both channels will be $((1 - \Phi(2.5))/2)^2 = 3.845 \times 10^{-5}$ min^{-1} that means one in 26007 minutes ≈ 18 days. The probability that the increases of 2.5σ will be accidental in both channels in two successive minutes is equal to $((1 - \Phi(2.5))/2)^4 = 1..478 \times 10^{-9}$ min^{-1} that means one in 6.76×10^8 minutes ≈1286 years. If this false alarm (one in about 1300 years) is sent it is not dangerous, because the first alarm is preliminary and can be cancelled if in the third successive minute is no increase in both channels bigger than 2.5σ (it is not excluded that in the third minute there will be also an accidental increase, but the probability of this false alarm is negligible: $((1 - \Phi(2.5))/2)^6 = 5.685 \times 10^{-14}$ min^{-1} that means one in 3.34×10^7 years). Let us note that the false alarm can be sent in the case of solar neutron event (which really is not dangerous for electronics in spacecrafts or for astronauts health), but this event usually is very short (only few minutes) and this alarm will be automatically canceled in the successive minute after the end of a solar neutron event.

4.6. The probability of missed triggers

The probability of missed triggers depends very strongly on the amplitude of the increase. Let us suppose for example that we have a real increase of 7σ (that for ESO corresponds to an increase of about 9.8%). The trigger will be missed if in any of both channels and in any of both successive minutes if as a result of statistical fluctuations the increase of intensity is less than 2.5σ. For this the statistical fluctuation must be negative with amplitude more than 4.5σ. The probability of this negative fluctuation in one channel in one minute is equal $(1 - \Phi(2.5))/2 = 3.39 \times 10^{-6}$ min^{-1}, and the probability of missed trigger for two successive minutes of observation simultaneously in two channels is 4 times larger: 1.36×10^{-5}. It means that missed trigger is expected only one per about 70000 events. In Table 2 are listed probabilities P_{mt} of missed triggers for ESO (where standard deviation for one channel for one minute $\sigma = 1.4\%$) as a function of the amplitude of increase A.

Table 2

Probabilities P_{mt} of missed triggers as a function of amplitude of increase A (in % and in σ)

***A*, %**	5.6	6.3	7.0	7.7	8.4	9.1	9.8	10.5
***A*, σ**	4.0	4.5	5.0	5.5	6.0	6.5	7.0	7.5
P_{mt}	2.7×10^{-1}	9.1×10^{-2}	2.5×10^{-2}	5.4×10^{-3}	9.3×10^{-4}	1.3×10^{-4}	1.4×10^{-5}	1.1×10^{-6}

4.7. Discussion on the supposed method

Obtained results show that the considered method of automatically searching for the onset of great, dangerous SEP on the basis of one-minute NM data practically does not give false alarms (the probability of false preliminary alarm is one in about 1300 years, and for false final alarm one in 3.34×10^{-7} years). None dangerous solar neutron events also can be separated automatically. We estimated also the probability of missed triggers; it was shown that for events with amplitude of increase more than 10% the probability of a missed trigger for successive two minutes NM data is smaller than 1.35×10^{-5} (this probability decreases sufficiently with increased amplitude A of the SEP increase, as shown in **Table 2**). Historical ground SEP events show very fast increase of amplitude in the start of event *[Dorman 1957; Carmichael 1962; Dorman and Miroshnichenko 1968; Duggal 1979; Dorman and Venkatesan 1993; Stoker 1995]*. For example, in great SEP event of February 23, 1956 amplitudes of increase in the Chicago NM were at 3.51 UT — 1%, at 3.52 UT — 35%, at 3.53 UT — 180%, at 3.54 UT — 280 %. In this case the missed trigger can be only for the first minute at 3.51 UT. The described method can be used in many Cosmic Ray Observatories where one-minute data are detected. Since the frequency of ground SEP events increases with decreasing cutoff rigidity, it will be important to introduce described method in high latitude Observatories. For low latitude Cosmic Ray Observatories the SEP increase starts earlier and the increase is much faster; this is very important for forecasting of dangerous situation caused by great SEP events.

5. On-line determination of SEP spectrum by the method of coupling functions

5.1. Principles of SEP radiation hazard forecasting

The problem is that the time-profiles of solar cosmic ray increases are very different for different great SEP events. It depends on the situation in the interplanetary space. If the mean free path of high-energy particles is large enough, the initial increase will be sharp, very short, only a few minutes, and in this case one or two-minute data will be useful. Conversely when the mean free path of high energy particles is much smaller, the increase will be gradual, possibly prolonged for 30-60

minutes, and in this case 2-, 3- or 5-minute data will be useful. Moreover, for some very anisotropic events (as February 23, 1956) the character of increase on different stations can be very different (sharp or gradual depending on the station location and anisotropy). *[Dorman et al. 2001]* described the operation of programs "SEP Search-*K* min" (where *K* = 1, 2, 3, and 5). If any of the "SEP Search-*K* min" programs gives a positive result for any Cosmic Ray Observatory the on-line program "SEP Collect" is started and collects all available data on the SEP event from Cosmic Ray Observatories and satellites. The many "SEP Research" programs then analyze these data. The real-time research method consists of:

1. Determination of the energy spectrum above the atmosphere from the start of the SEP-event (programs "SEP Research-Spectrum");
2. Determination of the anisotropy and its energy dependence (program "SEP Research-Anisotropy");
3. Determination of the propagation parameters, time of SEP injection into the solar wind and total source flux of SEP as a function of energy (programs "SEP Research-Propagation", "SEP Research-Time Ejection", "SEP Research-Source");
4. Forecasting the expected fluxes and the spectrum in space, in the magnetosphere and in the atmosphere (based on the results obtained from steps 1—3 above) using programs "SEP Research-Forecast in Space", "SEP Research-Forecast in Magnetosphere", and "SEP Research-Forecast in Atmosphere";
5. Issuing of preliminary alerts if the forecast fluxes are at dangerous levels (space radiation storms **S5**, **S4** or **S3** according to the classification of NOAA. These preliminary alerts are from the programs "SEP Research-Alert 1 for Space", "SEP Research-Alert 1 for Magnetosphere", and "SEP Research-Alert 1 for Atmosphere".

Then, based on further on-line data collection, more accurate Alert 2, Alert 3 and so on are sent. Here we will consider three modes of the research method:

1. a single station with continuous measurements and at least two or three cosmic ray components with different coupling functions for magnetically quiet and disturbed periods;
2. two stations with continuous measurements at each station and at least two cosmic ray components with different coupling functions; and
3. an International Cosmic Ray Service (ICRS), as described in *[Dorman et al. 1993]*, that could be organized in the near future based on the already existing world-wide network of cosmic ray observatories (especially important for anisotropic SEP events).

These programs can be used with real-time data from a single observatory (very roughly), with real-time data from two observatories (roughly), with real-time data from several observatories (more exactly), and with an International Cosmic Ray Service (much more exactly). Here we consider how to determine the spectrum of SEP and with a simple model of SEP propagation in the interplanetary space, and how to determine the time of injection, diffusion coefficient, and flux in the source. Using this simple model we can calculate expected fluxes in space at 1/2, 1, 3/2, 2 and more hours after injection. The accuracy of the programs can be checked and developed through comparison with data from the historical large ground SEP events described in detail in numerous publications (see for example: *[Elliot 1952; Dorman 1957;, Carmichael 1962; Dorman and Miroshnichenko 1968; Duggal 1979; Dorman and Venkatesan 1993k Stoker 1995]*).

5.2. Main properties of on-line CR data used for determining SEP spectrum in space; available data for determining the SEP energy spectrum

Let us suppose that we have on-line one-minute data from a single observatory with least 3 cosmic ray components with different coupling functions (if the period is magnetically disturbed) or at least 2 components (in a magnetically quiet period). For example, our Emilio Segre' Observatory (ESO) at 2020 m altitude, with cut-off rigidity 10.8 GV currently has the following different components *[Dorman et al. 2001]*: total and multiplicities *m* = 1, 2, 3, 4, 5, 6, 7, and ≥8. We started to construct a new multidirectional muon telescope that includes 1441 single telescopes in vertical and many inclined directions with different zenith and azimuth angles. From this multidirectional muon telescope we will have more than a hundred components with different coupling functions. Now many cosmic ray stations have data of several components with different coupling functions, where the method described below for determining on-line energy spectrum can be used. Also available are real-time satellite data, what are very useful for determining the SEP energy spectrum (especially at energies lower than detected by surface cosmic ray detectors).

5.3. Analytical approximation of coupling functions

Based on the latitude survey data of *[Aleksanyan et al. 1985; Moraal et al. 1989; Dorman et al. 2000]* the polar normalized coupling functions for total counting rate and different multiplicities *m* can he approximated by the function *[Dorman 1969]*:

$$W_{om}(R) = a_m k_m R^{-(k_m+1)} \exp\left(-a_m R^{-k_m}\right), \qquad \textbf{(6)}$$

where *m* = tot, 1, 2, 3, 4, 5, 6, 7, ≥ 8. Polar coupling functions for muon telescopes with different zenith angles *θ* can be approximated by the same type of functions **(6)** determined only by two parameters $a_m(\theta)$ and $k_m(\theta)$. Let us note that functions **(6)** are normalized: $\int_0^\infty W_{om}(R)\,dR = 1$ at any values of a_m and k_m.

The normalized coupling functions for point with cut-off rigidity R_c, will be

$$W_m(R_c,R)=a_m k_m R^{-(k_m+1)}\left(1-a_m R_c^{-k_m}\right)^{-1}\exp\left(-a_m R^{-k_m}\right),\ \text{if}\ R\ge R_c,\quad W_m(R_c,R)=0,\ \text{if}\ R<R_c \qquad (7)$$

5.4. The first approximation of the SEP energy spectrum

In the first approximation the spectrum of primary variation of SEP event can be described by the function

$$\Delta D(R)/D_o(R)=bR^{-\gamma}, \qquad (8)$$

where $\Delta D(R) = D(R,t) - D_o(R)$, $D_o(R)$ is the differential spectrum of galactic cosmic rays before the SEP event and $D(R,t)$ is the spectrum at a later time t. In **Eq. 8** parameters b and γ depend on t. Approximation **(8)** can be used for describing a limited interval of energies in the sensitivity range detected by the various components. Historical SEP data show that, in the broad energy interval, the SEP spectrum has a maximum, and the parameter γ in **Eq. 8** depends on particle rigidity R (usually γincreases with increasing R) that can be described by the second approximation.

5.5. The second approximations of the SEP energy spectrum

The second approximation of the SEP spectrum can be determined if it will be possible to use on-line 4 or 5 components with different coupling functions. In this case the form of the spectrum will be

$$\Delta D(R)/D_o(R)=bR^{-\gamma_o-\gamma_1\ln(R/R_o)}, \qquad (9)$$

with 4 unknown parameters b, γ_o, γ, R_o. The position of the maximum in the SEP spectrum will be at

$$R_{\max}=R_o\exp(-\gamma_o/\gamma_1), \qquad (10)$$

which varies significantly from one event to another and changes very much with time: in the beginning of the SEP event it is great (many GV), but, with time during the development of the event, R_{max} decreases very much.

5.6. On-line determining of the SEP spectrum from data of single observatory

5.6.1. The case of magnetically quiet periods ($\Delta R_c = 0$); Energy spectrum in the first approximation

In this case the observed variation $\delta I_m(R_c)\equiv\Delta I_m(R_c)/I_{mo}(R_c)$ in some component m can be described in the first approximation by function $F_m(R_c, \gamma)$:

$$\delta I_m(R_c)=bF_m(R_c,\gamma) \qquad (11)$$

where m = tot, 1, 2, 3, 4, 5, 6, 7, ≥ 8 for neutron monitor data (but can denote also the data obtained by muon telescopes at different zenith angles and data from satellites), and

$$F_m(R_c,\gamma)=a_m k_m\left(1-\exp\left(-a_m R_c^{-k_m}\right)\right)^{-1}\int_{R_c}^{\infty}R^{-(k_m+1+\gamma)}\exp\left(-a_m R^{-k_m}\right)dR \qquad (12)$$

is a known function. Let us compare data for two components m and n. According to Eq. 11 we obtain

$$\delta I_m(R_c)/\delta I_n(R_c)=\Psi_{mn}(R_c,\gamma),\ \text{where}\ \Psi_{mn}(R_c,\gamma)=F_m(R_c,\gamma)/F_n(R_c,\gamma) \qquad (13)$$

as calculated using **Eq. 12**. Comparison of experimental results with function $\Psi_{mn}(R_c, \gamma)$ according to **Eq. 13** gives the value of γ, and then from **Eq. 11** the value of the parameter b. The observed SEP increase for different components allows the determination of parameters b and $\gamma$for the SEP event beyond the Earth's magnetosphere.

5.6.2. The case of magnetically quiet periods ($\Delta R_c = 0$); Energy spectrum in the second approximation

Let us suppose that on-line are available for, at least, 4 components $i = k, l, m, n$ with different coupling functions. Then for the second approximation taking into account **Eq. 9**, we obtain

$$\delta I_i(R_c)=b\Phi_i(R_c,\gamma_o,\gamma_1,R_o), \qquad (14)$$

where $I = k, l, m, n$ and

$$\Phi_i(R_c,\gamma_o,\gamma_1,R_o)=a_i k_i\left(1-\exp\left(-a_i R_c^{-k_i}\right)\right)^{-1}\int_{R_c}^{\infty}R^{-(k_i+1+\gamma_o+\gamma_1\ln(R/R_o))}\exp\left(-a_i R^{-k_i}\right)dR \qquad (15)$$

By comparison data of different components we obtain

$$\frac{\delta I_k(R_c)}{\delta I_l(R_c)}=Y_{kl}(R_c,\gamma_o,\gamma_1,R_o),\quad \frac{\delta I_l(R_c)}{\delta I_m(R_c)}=Y_{lm}(R_c,\gamma_o,\gamma_1,R_o),\quad \frac{\delta I_m(R_c)}{\delta I_n(R_c)}=Y_{mn}(R_c,\gamma_o,\gamma_1,R_o), \qquad (16)$$

where ($i, j = k, l, m, n$)

$$Y_{ij}(R_c,\gamma_o,\gamma_1,R_o)=\Phi_i(R_c,\gamma_o,\gamma_1,R_o)/\Phi_j(R_c,\gamma_o,\gamma_1,R_o) \quad \textbf{(17)}$$

is calculated using **Eq. 15**. The solving of the system of **Eq. 16** gives the values of γ_o, γ_1, R_o, and then parameter b can be determined by **Eq. 14**: $b = \delta I_i(R_c)/\Phi_i(R_c, \gamma_o, \gamma_1, R_o)$ for any $i = k, l, m, n$.

5.6.3. The case of magnetically disturbed periods ($\Delta R_c \neq 0$); Energy spectrum in the first approximation

For magnetically disturbed periods the observed cosmic ray variation instead of **Eq. 11** will be described by

$$\delta I_k(R_c)=-\Delta R_c W_k(R_c,R_c)+bF_k(R_c,\gamma), \quad \textbf{(18)}$$

where ΔR_c is the change of cut-off rigidity due to change of the Earth's magnetic field, and $W_k(R_c.R_c)$ is determined by **Eq. 7** at $R = R_c$. Now for the first approximation of the SEP energy spectrum we have unknown variables γ, b, ΔR_c, and for their determination we need data from at least 3 different components $k = l, m, n$ in **Eq. 18**. In accordance with the spectrographic method *[Dorman 1975]* let us introduce the function

$$\Psi_{lmn}(R_c,\gamma)=\frac{W_l F_m(R_c,\gamma)-W_m F_l(R_c,\gamma)}{W_m F_n(R_c,\gamma)-W_n F_m(R_c,\gamma)}, \quad \textbf{(19)}$$

where

$$W_l \equiv W_l(R_c,R_c),\ W_m \equiv W_m(R_c,R_c),\ W_n \equiv W_n(R_c,R_c). \quad \textbf{(20)}$$

Then from

$$\Psi_{lmn}(R_c,\gamma)=\frac{W_l \delta I_m(R_c)-W_m \delta I_l(R_c)}{W_m \delta I_n(R_c)-W_n \delta I_m(R_c)}, \quad \textbf{(21)}$$

the value of γ can be determined. Using this value of γ, for each time t, we determine

$$\Delta R_c=\frac{F_l(R_c,\gamma)\delta I_m(R_c)-F_m(R_c,\gamma)\delta I_l(R_c)}{F_m(R_c,\gamma)\delta I_n(R_c)-F_n(R_c,\gamma)\delta I_m(R_c)},\quad b=\frac{W_l \delta I_m(R_c)-W_m \delta I_l(R_c)}{W_l F_m(R_c,\gamma)-W_m F_l(R_c,\gamma)}, \quad \textbf{(22)}$$

In magnetically disturbed periods, the observed SEP increase for different components again allows the determination of parameters γ and b, for the SEP event beyond the Earth's magnetosphere, and ΔR_c, giving information on the magnetospheric ring currents.

5.6.4. The case of magnetically disturbed periods ($\Delta R_c \neq 0$); Energy spectrum in the second approximation

In this case, for magnetically disturbed periods we need at least 5 different components, and the observed cosmic ray variation, instead of **Eq. 18**, will be described by

$$\delta I_i(R_c)=-\Delta R_c W_i(R_c,R_c)+b\Phi_i(R_c,\gamma_o,\gamma_1,R_o), \quad \textbf{(23)}$$

where $i = j, k, l, m, n$. Here $W_i(R_c,R_c)$ are determined by **Eq. 7** at $R = R_c$ and $\Phi_i(R_c, \gamma_o, \gamma_1, R_o)$ are determined by **Eq. 15**. By excluding from the system of **Eq. 23** linear unknown variables ΔR_c and b we obtain three equations for determining three unknown parameters γ_o, γ_1, R_o of SEP energy spectrum of the type

$$\frac{W_l \delta I_m(R_c)-W_m \delta I_l(R_c)}{W_m \delta I_n(R_c)-W_n \delta I_m(R_c)} = Y_{lmn}(R_c,\gamma_o,\gamma_1,R_o), \quad \textbf{(24)}$$

where

$$Y_{lmn}(R_c,\gamma_o,\gamma_1,R_o)=\frac{W_l \Phi_m(R_c,\gamma_o,\gamma_1,R_o)-W_m \Phi_l(R_c,\gamma_o,\gamma_1,R_o)}{W_m \Phi_n(R_c,\gamma_o,\gamma_1,R_o)-W_n \Phi_m(R_c,\gamma_o,\gamma_1,R_o)}. \quad \textbf{(25)}$$

In **Eq. 24** the left side is known from experimental data for each moment of time t, and the right side are known functions from γ_o, γ_1, R_o, what is calculated by taking into account **Eq. 15** and **Eq. 7** (at $R = R_c$). From the system of three equations of the type of **Eq. 24** we determine on-line γ_o, γ_1, R_o, and then parameters b and ΔR_c:

$$b=\frac{W_l \delta I_m(R_c)-W_m \delta I_l(R_c)}{W_l \Phi_m(R_c,\gamma_o,\gamma_1,R_o)-W_m \Phi_l(R_c,\gamma_o,\gamma_1,R_o)}, \quad \textbf{(26)}$$

$$\Delta R_c=\frac{\Phi_l(R_c,\gamma_o,\gamma_1,R_o)\delta I_m(R_c)-\Phi_m(R_c,\gamma_o,\gamma_1,R_o)\delta I_l(R_c)}{\Phi_m(R_c,\gamma_o,\gamma_1,R_o)\delta I_n(R_c)-\Phi_n(R_c,\gamma_o,\gamma_1,R_o)\delta I_m(R_c)}. \quad \textbf{(27)}$$

5.7. Using real-time cosmic ray data from two observatories

For determining the on-line SEP energy spectrum in the first and in the second approximations (**Eqs. 8** and **9**, correspondingly) it is necessary to use data from pairs of observatories in the same impact zone (to exclude the influence of the anisotropy distribution of the SEP ground increase), but with different cut-off rigidities R_{c1} and R_{c2}.

5.7.1. Magnetically quiet periods ($\Delta R_c = 0$)**; The SEP energy spectrum in the interval** $R_{c1} \div R_{c2}$

If it is the same component *m* for both observatories (e.g., total neutron component on about the same level of average air pressure h_o), the energy spectrum in the interval $R_{c1} \div R_{c2}$ can be determined directly for any moment of time *t* (here $W_{om}(R)$ is determined by **Eq. 6**):

$$\frac{\Delta D}{D_o}(R_{c1} \div R_{c2}) = \left(\delta I_m(R_{c1})\left(1 - a_m R_{c1}^{-k_m}\right) - \delta I_m(R_{c2})\left(1 - a_m R_{c2}^{-k_m}\right)\right) \Big/ \int_{R_{c1}}^{R_{c2}} W_{om}(R)\,dR, \quad \textbf{(28)}$$

5.7.2. Magnetically quiet periods ($\Delta R_c = 0$)**; the SEP energy spectrum in the first approximation**

In this case for determining *b* and γ in **Eq. 8** we need on line data at least of one component on each Observatory. If it is the same component *m* on both Observatories, parameter γ will be found from equation

$$\delta I_m(R_{c1}) / \delta I_m(R_{c2}) = \Psi_{mm}(R_{c1}, R_{c2}, \gamma), \text{ where } \Psi_{mm}(R_{c1}, R_{c2}, \gamma) = F_m(R_{c1}, \gamma) / F_m(R_{c2}, \gamma), \quad \textbf{(29)}$$

and then can be determined

$$b = \delta I_m(R_{c1}) / F_m(R_{c1}, \gamma) = \delta I_m(R_{c2}) / F_m(R_{c2}, \gamma) \quad \textbf{(30)}$$

If there are different components *m* and *n,* the solution will be determined by equations:

$$\delta I_m(R_{c1}) / \delta I_n(R_{c2}) = \Psi_{mn}(R_{c1}, R_{c2}, \gamma), \text{ where } \Psi_{mn}(R_{c1}, R_{c2}, \gamma) = F_m(R_{c1}, \gamma) / F_n(R_{c2}, \gamma), \quad \textbf{(31)}$$

$$b = \delta I_m(R_{c1}) / F_m(R_{c1}, \gamma) = \delta I_n(R_{c2}) / F_n(R_{c2}, \gamma). \quad \textbf{(32)}$$

5.7.3. Magnetically quiet periods ($\Delta R_c = 0$)**; the SEP energy spectrum in the second approximation**

In this case we need at least 4 components: it can be 1 and 3 or 2 and 2 different components in both observatories with cut-off rigidities R_{c1} and R_{c2}. If there are 1 and 3 components, parameters γ_o, γ_1, R_o will be determined by the solution of the system of equations

$$\frac{\delta I_k(R_{c1})}{\delta I_l(R_{c2})} = \frac{\Phi_k(R_{c1}, \gamma_o, \gamma_1, R_o)}{\Phi_l(R_{c2}, \gamma_o, \gamma_1, R_o)}, \quad \frac{\delta I_l(R_{c2})}{\delta I_m(R_{c2})} = Y_{lm}(R_{c2}, \gamma_o, \gamma_1, R_o), \quad \frac{\delta I_m(R_{c2})}{\delta I_n(R_{c2})} = Y_{mn}(R_{c2}, \gamma_o, \gamma_1, R_o), \quad \textbf{(33)}$$

and then we determine

$$b = \frac{\delta I_k(R_{c1})}{\Phi_k(R_{c1}, \gamma_o, \gamma_1, R_o)} = \frac{\delta I_l(R_{c2})}{\Phi_l(R_{c2}, \gamma_o, \gamma_1, R_o)} = \frac{\delta I_m(R_{c2})}{\Phi_m(R_{c2}, \gamma_o, \gamma_1, R_o)} = \frac{\delta I_n(R_{c2})}{\Phi_n(R_{c2}, \gamma_o, \gamma_1, R_o)}. \quad \textbf{(34)}$$

If there are two and two components in both observatories with cut-off rigidities R_{c1} and R_{c2}, the system of equations for determining parameters γ_o, γ_1, R_o will be

$$\frac{\delta I_k(R_{c1})}{\delta I_l(R_{c1})} = Y_{kl}(R_{c1}, \gamma_o, \gamma_1, R_o), \quad \frac{\delta I_l(R_{c1})}{\delta I_m(R_{c2})} = \frac{\Phi_l(R_{c1}, \gamma_o, \gamma_1, R_o)}{\Phi_m(R_{c2}, \gamma_o, \gamma_1, R_o)}, \quad \frac{\delta I_m(R_{c2})}{\delta I_n(R_{c2})} = Y_{mn}(R_{c2}, \gamma_o, \gamma_1, R_o) \quad \textbf{(35)}$$

and then we determine

$$b = \frac{\delta I_k(R_{c1})}{\Phi_k(R_{c1}, \gamma_o, \gamma_1, R_o)} = \frac{\delta I_l(R_{c1})}{\Phi_l(R_{c1}, \gamma_o, \gamma_1, R_o)} = \frac{\delta I_m(R_{c2})}{\Phi_m(R_{c2}, \gamma_o, \gamma_1, R_o)} = \frac{\delta I_n(R_{c2})}{\Phi_n(R_{c2}, \gamma_o, \gamma_1, R_o)}. \quad \textbf{(36)}$$

5.7.4. Magnetically disturbed periods ($\Delta R_c \neq 0$)**; The SEP energy spectrum in the first approximation**

In this case we have 4 unknown variables: ΔR_{c1}, ΔR_{c2}, b, γ. If there are 1 and 3 components in both observatories with cut-off rigidities R_{c1}, R_{c2}, the system of equations for determining ΔR_{c1}, ΔR_{c2}, b, γ is

$$\delta I_k(R_{c1}) = -\Delta R_{c1} W_k(R_{c1}, R_{c1}) + b F_k(R_{c1}, \gamma), \quad \textbf{(37)}$$

$$\delta I_l(R_{c2}) = -\Delta R_{c2} W_l(R_{c2}, R_{c2}) + b F_l(R_{c2}, \gamma), \quad \textbf{(38)}$$

$$\delta I_m(R_{c2}) = -\Delta R_{c2} W_m(R_{c2}, R_{c2}) + b F_m(R_{c2}, \gamma), \quad \textbf{(39)}$$

$$\delta I_n(R_{c2}) = -\Delta R_{c2} W_n(R_{c2}, R_{c2}) + b F_n(R_{c2}, \gamma). \quad \textbf{(40)}$$

In this case we determine, from **Eqs. 38—40**, γ, b, and ΔR_{c2} as it was described above by **Eqs. 19—22**. From **Eq. 37** we then determine

$$\Delta R_{c1} = \left(b F_k(R_{c1}, \gamma) - \delta I_k(R_{c1})\right) / W_k(R_{c1}, R_{c1}). \quad \textbf{(41)}$$

If there are two and two components in both observatories, we will have the same system as **Eqs. 37—40**; however, **Eq. 38** is replaced by

$$\delta I_l(R_{c1}) = -\Delta R_{c1} W_l(R_{c1}, R_{c1}) + b F_l(R_{c1}, \gamma). \quad \textbf{(42)}$$

From the system of **Eqs. 37, 39, 40,** and **42**, we exclude linear unknown variables b, ΔR_{c1}, ΔR_{c2} and finally obtain a non-linear equation for determining γ:

$$\frac{W_k \delta I_l(R_{c1}) - W_l \delta I_k(R_{c1})}{W_m \delta I_n(R_{c2}) - W_n \delta I_m(R_{c2})} = \Psi_{klmn}(R_{c1}, R_{c2}, \gamma) \quad \textbf{(43)}$$

Where

$$\Psi_{klmn}(R_{c1}, R_{c2}, \gamma) = \frac{W_k(R_{c1}, R_{c1}) F_l(R_{c1}, \gamma) - W_l(R_{c1}, R_{c1}) F_k(R_{c1}, \gamma)}{W_m(R_{c2}, R_{c2}) F_n(R_{c2}, \gamma) - W_n(R_{c2}, R_{c2}) F_m(R_{c2}, \gamma)} \quad \textbf{(44)}$$

can be calculated for any pair of stations using known functions $F_k(R_{c1},\gamma)$, $F_m(R_{c2},\gamma)$, $F_n(R_{c2},\gamma)$ (calculated from **Eq. 12**), and known values $W_k(R_{c1},R_{c1})$, $Wi(R_{c1},R_{c1})$, $W_m(R_{c2},R_{c2})$ and $W_n(R_{c2},R_{c2})$ (calculated from **Eq. 7**). After determining γ we can determine the other 3 unknown variables:

$$\Delta R_{c1} = \frac{F_k(R_{c1}, \gamma) \delta I_l(R_{c1}) - F_l(R_{c1}, \gamma) \delta I_k(R_{c1})}{W_k F_l(R_{c1}, \gamma) - W_l F_k(R_{c1}, \gamma)} \quad \textbf{(45)}$$

$$\Delta R_{c2} = \frac{F_m(R_{c2}, \gamma) \delta I_n(R_{c2}) - F_n(R_{c2}, \gamma) \delta I_m(R_{c2})}{W_m F_n(R_{c2}, \gamma) - W_n F_m(R_{c2}, \gamma)} \quad \textbf{(46)}$$

$$b = \frac{W_k \delta I_l(R_{c1}) - W_l \delta I_k(R_{c1})}{W_k F_l(R_{c1}, \gamma) - W_l F_k(R_{c1}, \gamma)} = \frac{W_m \delta I_n(R_{c2}) - W_n \delta I_m(R_{c2})}{W_m F_n(R_{c2}, \gamma) - W_n F_m(R_{c2}, \gamma)} \quad \textbf{(47)}$$

5.7.5. Magnetically disturbed periods ($\Delta R_c \neq 0$)**; Energy spectrum in the second approximation**

In this case we have 6 unknown variables ΔR_{c1}, ΔR_{c2},b,γ_o,γ_1,R_o, thus from both observatories we need a total of at least 6 components in any combination. This problem also can be solved by the method described above, only instead of functions F and Ψ the functions Φ and γ will be used. Here we have not enough space to describe these results; it will be done in other paper.

5.8. Using real-time cosmic ray data from many observatories (ICRS)

Using the International Cosmic Ray Service (ICRS) proposed by Dorman et al. *[Dorman et al. 1993]* and the above technique, much more accurate information on the distribution of the increased cosmic ray flux near the Earth can be found. We hope that for large SEP events it will be possible to use the global-spectrographic method (reviewed by Dorman, *[Dorma M1974]*) to determine, in real-time, the temporal changes in the anisotropy and its dependence on particle rigidity. It will allow a better determination of SEP propagation parameters in interplanetary space, and of the total flux and energy spectrum of particles accelerated in the solar flare, in turn improving detailed forecasts of dangerous large SEP events.

5.9. Determining of coupling functions by latitude survey data

The coefficients a_m and k_m for the coupling functions in **Eqs. 6** and **7** were determined from a latitude survey by *[Aleksanyan et al. 1985]* and they are in good agreement with theoretical calculations of *[Dorman and Yanke 1981; Dorman et al. 1981]*. Improved coefficients were determined on the basis of the recent Italian expedition to Antarctica *[Dorman et al. 2000]*. The dependence of a_m and k_m on the average station pressure h (in bar) and solar activity level is characterized by the logarithm of CR intensity (we used here monthly averaged intensities from the Climax, USA neutron monitor as $\ln(I_{Cl})$; however, the monthly averages of the Rome NM or monthly averages of the ESO NM (with some recalculation coefficients) can be approximated by the functions:

$$a_{tot} = \left(-2.9150h^2 - 2.2368h - 8.6538\right)\ln(I_{Cl}) + \left(24.5842h^2 + 19.4600h + 81.2299\right) \quad \textbf{(48)}$$

$$k_{tot} = \left(0.1798h^2 - 0.8487h + 0.7496\right)\ln(I_{Cl}) + \left(-1.4402h^2 + 6.4034h - 3.6975\right) \quad \textbf{(49)}$$

$$a_m = [\left(-2.915h^2 - 2.237h - 8.638\right)\ln(I_{Cl}) + \left(24.584h^2 + 19.46h + 81.23\right)] \times \left(0.987m^2 + 0.2246m + 6.913\right)/9.781 \quad \textbf{(50)}$$

$$k_m = [\left(0.1798h^2 - 0.8487h + 0.7496\right)\ln(I_{Cl}) + \left(-1.4402h^2 + 6.4034h - 3.6975\right)] \times \left(0.0808m + 1.8186\right)/1.9399. \quad \textbf{(51)}$$

Instead of Climax, other stations can be used in **Eqs. 48—51** with the appropriate coefficients.

5.10. Calculation of integrals $F_m(R_c,\gamma)$ and $\Phi_m(R_c,\gamma_o,\gamma_1,R_o)$

The integrals $F_m(R_c,\gamma)$ of **Eq. 12** are calculated for values of γ from **-**1 to +7, for different average station air pressure, h, cut-off rigidities, R_c, and different levels of solar activity characterized by the value $\ln(I_{Cl})$ according to

$$F_m(R_c,\gamma) = a_m k_m \left(1 - \exp\left(-a_m R_c^{-k_m}\right)\right)^{-1} R_c^{-k_m-\gamma} \sum_{n=0}^{\infty} (-1)^n a_m^n R_c^{-nk_m} \left(n!\left((n+1)k_m + \gamma\right)\right)^{-1} \quad \textbf{(52)}$$

Results of calculations of **Eq. 52** at different values of γ from **-**1 to +7 show that integrals $F_m(R_c,\gamma)$ can be approximated, with correlation coefficients between 0.993 and 0.996, by the function

$$F_m(R_c,\gamma,h,\ln(I_{Cl})) = A_m(R_c,h,\ln(I_{Cl}))\exp(-\gamma B_m(R_c,h,\ln(I_{Cl}))) \quad \textbf{(53)}$$

Results of calculations of functions $\Phi_m(R_c,\gamma_o,\gamma_1,R_o)$ (for the second approximation of the SEP energy spectrum) will be present in another paper.

5.11. Calculation of functions $\Psi_{mn}(R_c,\gamma)$, $\Psi_{lmn}(R_c,\gamma)$, and $\Psi_{klmn}(R_c,\gamma)$

Functions $\Psi_{mn}(R_c,\gamma)$ determined by **Eq. 13** now by using **Eq. 53** becomes

$$\Psi_{mn}(R_c,\gamma) = F_m(R_c,\gamma)/F_n(R_c,\gamma) = (A_m/A_n)\exp(-\gamma(B_m - B_n)), \quad \textbf{(54)}$$

Eq. 19 becomes

$$\Psi_{lmn}(R_c,\gamma) = \frac{W_l(R_c,R_c)A_m\exp(-B_m\gamma) - W_m(R_c,R_c)A_l\exp(-B_l\gamma)}{W_m(R_c,R_c)A_n\exp(-B_n\gamma) - W_n(R_c,R_c)A_m\exp(-B_m\gamma)}, \quad \textbf{(55)}$$

and **Eq. 44** becomes

$$\Psi_{klmn}(R_{c1},R_{c2},\gamma) = \frac{W_k(R_{c1},R_{c1})A_l\exp(-B_l\gamma) - W_l(R_{c1},R_{c1})A_k\exp(-B_k\gamma)}{W_m(R_{c2},R_{c2})A_n\exp(-B_n\gamma) - W_n(R_{c2},R_{c2})A_m\exp(-B_m\gamma)} \quad \textbf{(56)}$$

5.12. Examples of determination of the SEP energy spectrum

For example let us compare **Eq. 54** and **Eq. 13**: the spectral index is

$$\gamma = (\ln(A_m/A_n) - \ln(\delta I_m(R_c)/\delta I_n(R_c)))/(B_m - B_n) \quad \textbf{(57)}$$

Then from Eq. 11 we determine

$$b = \delta I_m(R_c)[A_m\exp(-B_m((\ln(A_m/A_n) - \ln(\delta I_m(R_c)/\delta I_n(R_c)))/(B_m - B_n)))]^{-1} \quad \textbf{(58)}$$

So for magnetically quite times the inverse problem can be solved on-line for each one-minute data interval during the rising phase. For magnetically disturbed times the inverse problem can also be solved automatically in real-time, using the special function described in **Eq. 55** (for observations by at least three components at one observatory), or by using the function described in **Eq. 56** (for observations by two observatories). Note that for the first approximation we have assumed a two-parameter form of the energy spectrum. In reality the SEP energy spectrum could be more complicated; γ may also change with energy. If the spectrum can only be described by three or four-parameters (considered in the second approximation given previously) then observations from a range of neutron monitors (including those with low cut-off rigidities) and from satellites will be needed. We conclude that in these cases solutions can also be obtained for the energy spectrum, its change with time and the change of cut-off rigidities. The details of these solutions will be reported in another paper.

5.13. Special program for on-line determining of energy spectrum for each minute after SEP starting (for the case of single observatory)

Let us consider data from neutron monitor with independent registration of total flux and 7 multiplicities as input flux of data as vector $I_m(i)$, where i — is number of time registration index, m — number of channel (m = 0 — total flux, m = 1÷7 — different multiplicities). For estimation of the statistical properties of input flux we calculate mean and standard deviation for each channel $\langle I_m(i)\rangle$ and $\sigma_m(i)$ on the 1-hour interval, preceded to i-time moment on 1-hour. During next step we calculate vector of relative deviations:

$$\delta I_m(i) = (I_m(i) - \langle I_m(i)\rangle)/\langle I_m(i)\rangle \quad \textbf{(59)}$$

and correspondent standard deviation $\sigma(\delta I_m(i))$. On the basis of deviation's vector $\delta I_m(i)$ we calculate matrix

$$R_{mn}(i) = \delta I_m(i)/\delta I_n(i) \quad \textbf{(60)}$$

of ratios deviations for different energetic channels m, n at the time moment i and its standard deviation $\sigma(R_{mn}(i))$. On the basis of **Eq. 5.52** and **Eq. 5.53** by using **Eq. 5.54** we calculate matrix of the spectral slope $\gamma_{mn}(i)$, matrix of amplitude $b_{mn}(i)$ and estimations of correspondent standard deviations $\sigma(\gamma_{mn}(i))$ and $\sigma(b_{mn}(i))$.

For conversation of matrix output of estimated slope $\gamma_{mn}(i)$ to the scalar's form $\gamma(i)$ we use estimation of the average values taking into account the correspondent weights W of the individual values $\gamma_{mn}(i)$ determined by the correspondent standard deviations

$$W(\gamma_{mn}(i)) = (\sigma(\gamma_{mn}(i)))^{-2}\left(\sum_{m,n}(\sigma(\gamma_{mn}(i)))^{-2}\right)^{-1}, \quad \textbf{(61)}$$

that

$$\gamma(i) = \sum_{m,n}\gamma_{mn}(i)\times W(\gamma_{mn}(i)) \quad \textbf{(62)}$$

The same we made for parameter *b(i)*:

$$b(i) = \sum_{m,n} b_{mn}(i) \times W(b_{mn}(i)), \quad \textbf{(63)}$$

where

$$W(b_{mn}(i)) = (\sigma(b_{mn}(i)))^{-2} \left(\sum_{m,n} (\sigma(b_{mn}(i)))^{-2} \right)^{-1} \quad \textbf{(64)}$$

By founding values of $\gamma(i)$ and *b(i)* can be determined SEP energy spectrum by using **Eq. 8** for each moment of time:

$$\Delta D(R,i) = b(i) R^{-\gamma(i)} \times D_o(R) \quad \textbf{(65)}$$

We checked this procedure on the basis of neutron monitor data on the Mt. Gran-Sasso in Italy for the event September 29, 1989. We used one minute data of total intensity and multiplicities from 1 to 7. The number of minutes is start from 10.00 UT at September 29, 1989. Upper limit of indexes *m*, *n* we choose about 3÷4, since for higher multiplicities accuracy level decreases fast and we may decrease confidence of the estimation.

6. On-line determination of diffusion coefficient in the interplanetary space, time of ejection and energy spectrum of SEP in source by NM data (the case, when diffusion coefficient depends only from the particles rigidity)

6.1. On-line determination of SEP spectrum in source when diffusion coefficient in the interplanetary space and time of ejection are known

According to observation data of many events for about 60 years the time change of SEP flux and energy spectrum can be described in the first approximation by the solution of isotropic diffusion from the pointing instantaneous source described by function

$$Q(R,r',t') = N_o(R)\delta(r')\delta(t'). \quad \textbf{(66)}$$

Let us suppose that the time of ejection and diffusion coefficient are known. In this case the expected SEP rigidity spectrum on the distance *r* from the Sun in the time *t* after ejection will be

$$N(R,r,t) = N_o(R) \times \left[2\pi^{1/2} (K(R)t)^{3/2} \right]^{-1} \times \exp\left(-\frac{r^2}{4K(R)t} \right), \quad \textbf{(67)}$$

where *No(R)* is the rigidity spectrum of total number of SEP in the source, *t* is the time relative to the time of ejection and *K(R)* is the known diffusion coefficient in the interplanetary space in the period of SEP event. At $r = r_1 = 1$ AU and at some moment r_1 the spectrum determined in Section 4, will be described by the function

$$N(R,r_1,t_1) = b(t_1) R^{-\gamma(t_1)} D_o(R), \quad \textbf{(68)}$$

where $b(t_1)$ and $\gamma(t_1)$ are parameters determined the observed rigidity spectrum in the moment t_1, and $D_o(R)$ is the spectrum of galactic cosmic rays before event (see Section 5). From other side, the SEP spectrum will be determined at $r = r_1$, $t = t_1$. according to **Eq. 66**. That we obtain equation

$$b(t_1) R^{-\gamma(t_1)} D_o(R) = N_o(R) \left[2\pi^{1/2} (K(R)t_1)^{3/2} \right]^{-1} \times \exp\left(-r_1^2 / (4K(R)t_1) \right). \quad \textbf{(69)}$$

If the diffusion coefficient *K(R)* and time of ejection (i.e., time t_1 relative to the time of ejection) are known, that from **Eq. 69** we obtain

$$N_o(R) = 2\pi^{1/2} b(t_1) R^{-\gamma(t_1)} D_o(R) \times \left(K(R) t_1 \right)^{3/2} \exp\left(r_1^2 / (4K(R)t_1) \right). \quad \textbf{(70)}$$

6.2. On-line determination of diffusion coefficient in the interplanetary space when SEP spectrum in source and time of ejection are known

Let us consider the case when SEP spectrum in source and time of ejection may be known (e.g. from direct solar gamma-ray and solar neutron measurements what gave information on the time of acceleration and spectrum of accelerated particles, see detail review in *[Dorman M2010]*. In this case, from **Eq. 69** we obtain the following iteration solution

$$K(R) = \frac{r_1^2}{4t_1} \left(\ln(N_o(R)) - \ln\left(b(t_1) R^{-\gamma(t_1)} D_o(R) \right) - \ln\left(2\pi^{1/2} \right) - \frac{3}{2} \ln(K(R)t_1) \right)^{-1}. \quad \textbf{(71)}$$

As the first approximation in the right hand of **Eq. 71** can be used *K(R)* for galactic cosmic rays obtained from investigation of hysteresis phenomenon *[Dorman 2001; Dorman et al. 2001 a,b]*. The iteration process in **Eq. 71** is very fast and only few approximations are necessary.

6.3. On-line determination of the time of ejection when diffusion coefficient in the interplanetary space and SEP spectrum in source are known

In this case we obtain from **Eq. 69**

$$t_1 = \frac{r_1^2}{4K(R)}\left(\ln(N_o(R)) - \ln\left(b(t_1)R^{-\gamma(t_1)}D_o(R)\right) - \ln\left(2\pi^{1/2}\right) - \frac{3}{2}\ln(K(R)t_1)\right)^{-1} \quad \textbf{(72)}$$

As the first approximation in the right hand of **Eq. 72** can be used t_1 obtained from measurements of the start of increase in very high energy region where the time of propagation from the Sun is about the same as for light. The iteration process in **Eq. 72** is very fast and only few approximations are necessary.

6.4. On-line determination simultaneously of SEP diffusion coefficient and SEP spectrum in source, if the time of ejection is known

Let us suppose that $K(R)$ and $N_o(R)$ are unknown functions, but the time of ejection is known. In this case we need to use data at least for two moments of time t_1 and t_2 relative to the time of ejection (what is supposed as known value). In this case we will have system from two equations:

$$b(t_1)R^{-\gamma(t_1)}D_o(R) = N_o(R)\times\left[2\pi^{1/2}(K(R)t_1)^{3/2}\right]^{-1}\times\exp\left(-r_1^2/(4K(R)t_1)\right), \quad \textbf{(73)}$$

$$b(t_2)R^{-\gamma(t_2)}D_o(R) = N_o(R)\times\left[2\pi^{1/2}(K(R)t_2)^{3/2}\right]^{-1}\times\exp\left(-r_1^2/(4K(R)t_2)\right) \quad \textbf{(74)}$$

By dividing **Eq. 73** on **Eq. 74**, we obtain

$$\frac{b(t_1)}{b(t_2)}(t_1/t_2)^{3/2}R^{-[\gamma(t_1)-\gamma(t_2)]} = \exp\left(-\frac{r_1^2}{4K(R)}\left(\frac{1}{t_1}-\frac{1}{t_2}\right)\right), \quad \textbf{(75)}$$

from what follows

$$K(R) = \left(-\frac{r_1^2}{4}\left(\frac{1}{t_1}-\frac{1}{t_2}\right)\right)\times\left(\ln\left(\frac{b(t_1)}{b(t_2)}(t_1/t_2)^{3/2}R^{-[\gamma(t_1)-\gamma(t_2)]}\right)\right)^{-1} \quad \textbf{(76)}$$

The found result for $K(R)$ will be controlled and made more exactly on the basis of **Eq. 76** by using the next data in moments t_2 and t_3, as well as for moments t_1 and t_3, then by data in moments t_3, and t_4, and so on. By introducing result of determining of diffusion coefficient $K(R)$ on the basis of **Eq. 76** in **Eq. 69** we determine immediately the expected flux and spectrum SEP in the source:

$$\begin{aligned} N_o(R) &= 2\pi^{1/2}b(t_1)R^{-\gamma(t_1)}D_o(R)\times(K(R)t_1)^{3/2}\exp\left(r_1^2/(4K(R)t_1)\right) \\ &= 2\pi^{1/2}b(t_2)R^{-\gamma(t_2)}D_o(R)\times(K(R)t_2)^{3/2}\exp\left(r_1^2/(4K(R)t_2)\right), \end{aligned} \quad \textbf{(77)}$$

where $K(R)$ is determined by **Eq. 76**.

6.5. On-line determination simultaneously time of ejection and SEP spectrumin source if the diffusion coefficient is known

Let us suppose that diffusion coefficient $K(R)$ is known, but the time of ejection T_e is unknown. In this case we need measurements of SEP energy spectrum at least in two moments of time. Let us suppose that in two moments T_1 and T_2 were made measurements of energetic spectrum as it was described in Section 4. Here times T_e, T_1 and T_2 are in UT scale. Let us suppose that

$$t_1 = T_1 - T_e = x, \quad t_2 = T_2 - T_e = T_2 - T_1 + x, \quad \textbf{(78)}$$

where t_1 and t_2 are times relative to the moment of SEP ejection into solar wind, and T_1 and T_2 are known UT and $T_e = T_1 - x$ is unknown value what can be determined from the following system of equations:

$$b(T_1)R^{-\gamma(T_1)}D_o(R) = N_o(R)\times\left[2\pi^{1/2}(K(R)x)^{3/2}\right]^{-1}\times\exp\left(-r_1^2/(4K(R)x)\right), \quad \textbf{(79)}$$

$$b(T_2)R^{-\gamma(T_2)}D_o(R) = N_o(R)\times\left[2\pi^{1/2}(K(R)(T_2-T_1+x))^{3/2}\right]^{-1}\times\exp\left(-r_1^2/(4K(R)(T_2-T_1+x))\right). \quad \textbf{(80)}$$

By dividing of **Eq. 79** on **Eq. 80**, we obtain

$$\frac{b(T_1)}{b(T_2)}(x/(T_2-T_1+x))^{3/2}R^{-[\gamma(T_1)-\gamma(T_2)]} = \exp\left(-\frac{r_1^2}{4K(R)}\left(\frac{1}{x}-\frac{1}{T_2-T_1+x}\right)\right), \quad \textbf{(81)}$$

From **Eq. 81** unknown value x can be found by iteration:

$$t_1 = x = \Omega^{2/3}(T_2-T_1)\left(1-\Omega^{2/3}\right)^{-1}, \quad \textbf{(82)}$$

where

$$\Omega(x)=\frac{b(T_2)}{b(T_1)}R^{[\gamma(T_1)-\gamma(T_2)]}\times\exp\left(-\frac{r_1^2}{4K(R)}\left(\frac{1}{x}-\frac{1}{T_2-T_1+x}\right)\right) \quad \textbf{(83)}$$

As the first approximation we can use $x_1 = T_1 - T_e \approx 500$ sec what is a minimum time of relativistic particles propagation from the Sun to the Earth's orbit. Then by **Eq. 83** we determine $\Omega(x_1)$ and by **Eq. 82** determine the second approximation x_2. To put x_2 in **Eq. 83** we compute $\Omega(x_2)$, and then by **Eq. 82** determine the third approximation x_3, and so on. After determining $x = t_1$ and UT time of ejection $T_e = T_1 - x$ we can determine the SEP spectrum in the source:

$$\begin{aligned} N_o(R) &= 2\pi^{1/2}\left(K(R)(T_1-T_e)\right)^{3/2} b(T_1)R^{-\gamma(T_1)} D_o(R)\exp\left(r_1^2/(4K(R)(T_1-T_e))\right)= \\ &= 2\pi^{1/2}\left(K(R)(T_2-T_e)\right)^{3/2} b(T_2)R^{-\gamma(T_2)} D_o(R)\exp\left(r_1^2/(4K(R)(T_2-T_e))\right) \end{aligned} \quad \textbf{(84)}$$

6.6. On-line determination simultaneously time of ejection, diffusion coefficient and SEP spectrum in the source

Let us suppose that the time of ejection T_e, diffusion coefficient $K(R)$ and SEP spectrum in the source $N_o(R)$ are unknown. In this case for determining on-line simultaneously time of ejection T_e, diffusion coefficient $K(R)$ and SEP spectrum in the source $N_o(R)$ we need information on SEP spectrum at least in three moments of time T_1, T_2 and T_3 (all times T are in UT scale). In this case instead of **Eq. 6.13** we will have for times after SEP ejection into solar wind:

$$t_1 = T_1 - T_e = x,\ t_2 = T_2 - T_1 + x,\ t_3 = T_3 - T_1 + x, \quad \textbf{(85)}$$

where $T_2 - T_1$ and $T_3 - T_1$ are known values, and x is unknown value what we need to determine by solution of the system of equations

$$b(T_1)R^{-\gamma(T_1)} D_o(R) = N_o(R)\times\left[2\pi^{1/2}\left(K(R)x\right)^{3/2}\right]^{-1}\times\exp\left(-r_1^2/(4K(R)x)\right), \quad \textbf{(86)}$$

$$b(T_2)R^{-\gamma(T_2)} D_o(R) = N_o(R)\times\left[2\pi^{1/2}\left(K(R)(T_2-T_1+x)\right)^{3/2}\right]^{-1}\times\exp\left(-r_1^2/(4K(R)(T_2-T_1+x))\right), \quad \textbf{(87)}$$

$$b(T_3)R^{-\gamma(T_3)} D_o(R) = N_o(R)\times\left[2\pi^{1/2}\left(K(R)(T_3-T_1+x)\right)^{3/2}\right]^{-1}\times\exp\left(-r_1^2/(4K(R)(T_3-T_1+x))\right). \quad \textbf{(88)}$$

From this system of **Eqs. 86—88** by dividing one equation on other (to exclude $N_o(R)$) we obtain

$$\frac{T_2-T_1}{x(T_2-T_1+x)} = -\frac{4K(R)}{r_1^2}\times\ln\left\{\frac{b(T_1)}{b(T_2)}\left(x/(T_2-T_1+x)\right)^{3/2} R^{-[\gamma(T_1)-\gamma(T_2)]}\right\}, \quad \textbf{(89)}$$

$$\frac{T_3-T_1}{x(T_3-T_1+x)} = -\frac{4K(R)}{r_1^2}\times\ln\left\{\frac{b(T_1)}{b(T_3)}\left(x/(T_3-T_1+x)\right)^{3/2} R^{-[\gamma(T_1)-\gamma(T_3)]}\right\}. \quad \textbf{(90)}$$

By dividing **Eq. 89** on **Eq. 90** (to exclude $K(R)$) we obtain

$$x = \left[(T_2-T_1)\Psi(x)-(T_3-T_1)\right]/(1-\Psi(x)), \quad \textbf{(91)}$$

where $\Psi(x)$ is function very weekly depended from x:

$$\Psi(x) = \frac{T_3-T_1}{T_2-T_1}\times\frac{\ln\left\{\frac{b(T_1)}{b(T_2)}\left(\frac{x}{T_2-T_1+x}\right)^{3/2} R^{\gamma(T_2)-\gamma(T_1)}\right\}}{\ln\left\{\frac{b(T_1)}{b(T_3)}\left(\frac{x}{T_3-T_1+x}\right)^{3/2} R^{\gamma(T_3)-\gamma(T_1)}\right\}}. \quad \textbf{(92)}$$

Eq, 91 can be solved by iteration method: as the first approximation we can use, as in Section 6.5, $x_1 = T_1 - T_e \approx 500$ sec what is a minimum time of relativistic particles propagation from the Sun to the Earth's orbit. Then by **Eq. 92** we determine $\Psi(x_1)$ and by **Eq. 91** determine the second approximation x_2. To put x_2 in **Eq. 92** we compute $\Psi(x_2)$, and then by **Eq. 91** determine the third approximation x_3, and so on:

$$x_k = \left[(T_2-T_1)\Psi(x_{k-1})-(T_3-T_1)\right]/(1-\Psi(x_{k-1})), \quad \textbf{(93)}$$

After solving **Eq. 91** and determining the time of ejection $T_e = T_1 - x$, we can compute diffusion coefficient from **Eq. 89** or **Eq. 90**:

$$K(R) = -\frac{\frac{r_1^2(T_2-T_1)}{4(T_1-T_e)(T_2-T_e)}}{\ln\left\{\frac{b(T_1)}{b(T_2)}\left(\frac{T_1-T_e}{T_2-T_e}\right)^{3/2} R^{\gamma(T_2)-\gamma(T_1)}\right\}} = -\frac{\frac{r_1^2(T_3-T_1)}{4(T_1-T_e)(T_3-T_e)}}{\ln\left\{\frac{b(T_1)}{b(T_3)}\left(\frac{T_1-T_e}{T_3-T_e}\right)^{3/2} R^{\gamma(T_3)-\gamma(T_1)}\right\}}. \quad \textbf{(94)}$$

After determining time of ejection and diffusion coefficient we can determine the total flux and energy spectrum in source from any of **Eqs. 86—88**:

$$N_o(R) = 2\pi^{1/2} b(T_1) R^{-\gamma(T_1)} D_o(R) \left(K(R)(T_1 - T_e)\right)^{3/2} \exp\left(r_1^2 / (4K(R)(T_1 - T_e))\right) =$$
$$= 2\pi^{1/2} b(T_2) R^{-\gamma(T_2)} D_o(R) \left(K(R)(T_2 - T_e)\right)^{3/2} \exp\left(r_1^2 / (4K(R)(T_2 - T_e))\right) = \quad \textbf{(95)}$$
$$= 2\pi^{1/2} b(T_3) R^{-\gamma(T_3)} D_o(R) \left(K(R)(T_3 - T_e)\right)^{3/2} \exp\left(r_1^2 / (4K(R)(T_3 - T_e))\right),$$

where $T_e = T_1 - x$ was determined by **Eq. 91**, and $K(R)$ by **Eq. 94**.

6.7. Controlling on-line of the used model of SEP generation and propagation

The on-line controlling of using model can be made by data obtained in the next minutes T_4, T_5, T_6, and others. For example, we can determine the time of ejection T_e, diffusion coefficient $K(R)$ and SEP spectrum in the source $N_o(R)$ on the basis of data obtained in moments T_2, T_3, T_4, then in moments T_3, T_4, T_5, then in moments T_4, T_5, T_6, or for any other combinations of time moments, for example, at T_1, T_3, T_5, and so on. Obtained values of T_e, $K(R)$ and $N_o(R)$ in the frame of errors must be the same what obtained on the basis of data in time moments T_1, T_2, T_3. If this condition will be satisfied for any combinations of T_i, T_j, T_k, it will be meant that the used model of SEP generation and propagation in the interplanetary space is correct and it can be used also for prediction of expected SEP fluxes in space, in the magnetosphere, and in the Earth's atmosphere. If this condition will be not satisfied, it will be meant that the real model of SEP generation and propagation in the interplanetary space is more complicated. In this case, the using of data from only one observatory is not enough, it is necessary to use data from many cosmic ray observatories to determine anisotropy of SEP fluxes on the Earth and parameters of more complicated model. On the basis of consideration of many SEP events we expect that after some short time $T_{min} - T_e$ SEP distribution became isotropic and considered above simple model of SEP generation and propagation in the interplanetary space became correct. This moment $T_{min} - T_e$ can be determined automatically by the described above method of estimation of T_e, $K(R)$ and $N_o(R)$ for different combinations T_i, T_j, T_k.

6.8. On-line forecasting of expected SEP flux and radiation hazard for space-probes in space, satellites in the magnetosphere, jets and various objects in the atmosphere, and on the ground in dependence of cut-off rigidity

If the controlling described in the Section 6.7 will give positive result, we can predict the expected SEP rigidity spectrum in the space at any moment T and at any distance r from the Sun:

$$D_S(R, r, T) = N_o(R) \times \left[2\pi^{1/2} \left(K(R)(T - T_e)\right)^{3/2}\right]^{-1} \times \exp\left(-r^2 / (4K(R)(T - T_e))\right) \quad \textbf{(96)}$$

The expected flux inside any space-probe at distance r from the Sun with the threshold energy $E_{k\,min}$ will be

$$I_S(r, T, E_{k\min}) = \int_{E_{k\min}}^{\infty} N_o(R(E_k)) \times \left[2\pi^{1/2} \left(K(R(E_k))(T - T_e)\right)^{3/2}\right]^{-1} \times \exp\left(-r^2 / (4K(R(E_k))(T - T_e))\right) dE_k \quad \textbf{(97)}$$

and the fluency what will receive a space-probe during all time of event (determined the radiation doze) will be

$$Y_S(r, E_{k\min}) = \int_{T_e}^{\infty} dT \int_{E_{k\min}}^{\infty} N_o(R(E_k)) \times \left[2\pi^{1/2} \left(K(R(E_k))(T - T_e)\right)^{3/2}\right]^{-1} \times \exp\left(-r^2 / (4K(R(E_k))(T - T_e))\right) dE_k \quad \textbf{(98)}$$

6.9. Prediction of expected SEP energy spectrum, SEP flux and SEP fluency (radiation doze) for satellites at different cut-off rigidities inside the Earth's magnetosphere

Inside the Earth's magnetosphere the expected SEP energy spectrum will be determined by **Eq. 96** at $r = r_1 = 1AU$. For satellites at different cut-off rigidities $R_c(T)$ inside the Earth's magnetosphere the expected SEP flux will be

$$I_S(T, R_c(T)) = \int_{R_c(T)}^{\infty} N_o(R) \times \left[2\pi^{1/2} \left(K(R)(T - T_e)\right)^{3/2}\right]^{-1} \times \exp\left(-r_1^2 / (4K(R)(T - T_e))\right) dR \quad \textbf{(99)}$$

where $R_c(T)$ is determined by the orbit of satellite. The expected fluency what will receive a satellite with orbit $R_c(T)$ during all time of event (proportional to the radiation doze) will be

$$Y_S(R_c(T)) = \int_{T_e}^{\infty} dT \int_{R_c(T)}^{\infty} N_o(R) \times \left[2\pi^{1/2} \left(K(R)(T - T_e)\right)^{3/2}\right]^{-1} \times \exp\left(-r_1^2 / (4K(R)(T - T_e))\right) dR \quad \textbf{(100)}$$

6.10. Prediction of expected intensity of secondary components generated by SEP in the Earth's atmosphere and expected radiation doze for planes and ground objects on different altitudes at different cut-off rigidities

The expected intensity of secondary component of type *i* (electron-photon, nucleon, muon and others) generated in the Earth's atmosphere by SEP at moment of time *T* will be in the some point characterized by pressure level h_o and cut-off rigidity R_c as following

$$I_{Si}(T,R_c,h_o)=\int_{R_c}^{\infty}N_o(R)\times\left[2\pi^{1/2}\left(K(R)(T-T_e)\right)^{3/2}\right]^{-1}\times\exp\left(-r_1^2/\left(4K(R)(T-T_e)\right)\right)W_i(R,h_o)dR \qquad \textbf{(101)}$$

,

where $W_i(R,h_o)$ is the coupling function. The expected total fluency (proportional to the radiation doze) for planes and ground objects on different altitudes at different cut-off rigidities will be determined by integration of **Eq. 7.6** over all time of event and summarizing over all secondary components:

$$Y_S(R_c,h_o)=\sum_i\int_{T_e}^{\infty}dT\int_{R_c}^{\infty}N_o(R)\times\left[2\pi^{1/2}\left(K(R)(T-T_e)\right)^{3/2}\right]^{-1}\times\exp\left(-r_1^2/\left(4K(R)(T-T_e)\right)\right)W_i(R,h_o)dR \qquad \textbf{(102)}$$

6.11. Alerts in cases if the radiation dozes are expected to be dangerous

If the described in Sections 7.1—7.3 forecasted radiation dozes are expected to be dangerous, will be send in the first few minutes of event preliminary "SEP-Alert_1/Space", "SEP-Alert_1/ Magnetosphere", "SEP-Alert_1/ Atmosphere", "SEP-Alert_1 /Ground", and then by obtaining on-line more exact results on the basis of for coming new data will be automatically send more exact Alert_2, Alert_3 and so on. These Alerts will give information on the expected time and level of dangerous; experts must operative decide what to do: for example, for space-probes in space and satellites in the magnetosphere to switch-off the electric power for 1—2 hours to save the memory of computers and high level electronics, for jets to decrease their altitudes from 10—20 km to 4—5 km to protect crew and passengers from great radiation hazard, and so on.

6.12. The checking of the model when diffusion coefficient does not depend from the distance from the Sun by the real data during SEP event in September 1989

We will use the data obtained during the great SEP event in September 1989 by NM on the top of Gran-Sasso in Italy *[Dorman et al. 2005 a,b]*. This NM detects one-minute data not only of total neutron intensity, but also many of neutron multiplicities (≥ 1, ≥ 2, ≥ 3, up to ≥ 8), what gave possibility by using method of coupling functions to determine the energy spectrum in high energy range (≥ 6 GV) for each minute. On the basis of these data we determine at first the values of diffusion coefficient *K(R)*. These calculations have been done according to the procedure described above, by supposing that *K(R)* does not depend on the distance to the Sun. Results are shown in **Fig. 27**.

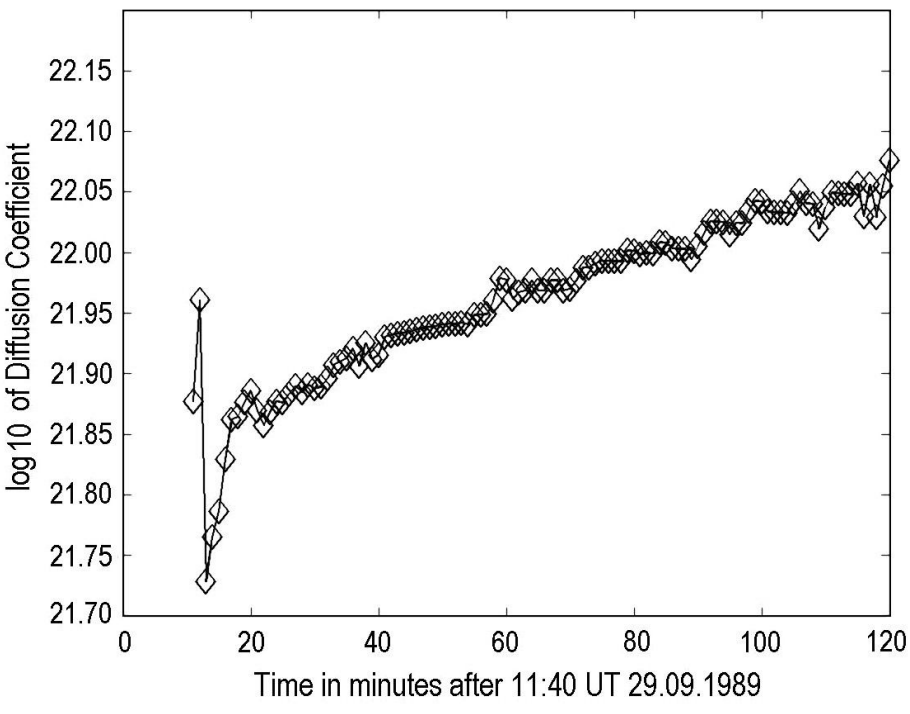

Fig. 27. The time behavior of *K(R)* for *R* ~ 10 GV for the SEP event 29 September, 1989. From *[Dorman et al. 2005 a, b]*.

From **Fig. 27** can be seen that at the beginning of the event the obtained results are not stable, due to large relative statistical errors. After several minutes the amplitude of CR intensity increase becomes many times bigger than statistical error for one minute data σ (about 1%), and we can see a systematical increase of the diffusion coefficient *K(R)* with time. This result contradicts the conditions at which was solved the inverse problem in Section 6. Really the systematical increase of the diffusion coefficient with time reflects the increasing of *K(R)* with the diffusion propagation of solar CR from the Sun, i.e. reflects the increasing of *K(R)* with the distance from the Sun. It means that for the considered SEP event we need to apply the inverse problem, where it will be assumed increasing of diffusion coefficient with the distance from the Sun.

7. Determination of diffusion coefficient in the interplanetary space, time of ejection and energy spectrum of SEP in source by NM and satellite data (the case, when diffusion coefficient depends from particles rigidity and distance from the Sun)

7.1. The inverse problem for the case when diffusion coefficient depends from particle rigidity and from the distance to the Sun

Let us suppose, according to *[Parker M1963]*, that the diffusion coefficient

$$\kappa(R,r) = \kappa_1(R) \times (r/r_1)^{\beta} . \quad \textbf{(103)}$$

In this case the solution of diffusion equation will be

$$N(R,r,t) = \frac{N_o(R) \times r_1^{3\beta/(2-\beta)} (\kappa_1(R) t)^{-3/(2-\beta)}}{(2-\beta)^{(4+\beta)/(2-\beta)} \Gamma(3/(2-\beta))} \times \exp\left(-\frac{r_1^{\beta} r^{2-\beta}}{(2-\beta)^2 \kappa_1(R) t}\right), \quad \textbf{(104)}$$

where t is the time after SEP ejection into solar wind. So now we have four unknown parameters: time of SEP ejection into solar wind T_e, β, $\kappa_1(R)$, and $N_o(R)$. Let us assume that according tN1o ground and satellite measurements at the distance $r = r_1 =$ *1AU* from the Sun we know $N_1(R)$ $N_2(R)$, $N_3(R)$ at UT times T_1, T_2,T_3, T_4. In this case

$$t_1 = T_1 - T_e = x, \;\; t_2 = T_2 - T_1 + x, \;\; t_3 = T_3 - T_1 + x, \;\; t_4 = T_4 - T_1 + x , \quad \textbf{(105)}$$

For each $N_i(R,r = r_1,T_i)$ we obtain from **Eq. 104** and **Eq. 105**:

$$N_i(R, r = r_1, T_i) = \frac{N_o(R) \times r_1^{3\beta/(2-\beta)} (\kappa_1(R)(T_i - T_1 + x))^{-3/(2-\beta)}}{(2-\beta)^{(4+\beta)/(2-\beta)} \Gamma(3/(2-\beta))} \times \exp\left(-\frac{r_1^2 (2-\beta)^{-2}}{\kappa_1(R)(T_i - T_1 + x)}\right), \quad \textbf{(106)}$$

where i = 1, 2, 3, and 4. To determine x let us step by step exclude unknown parameters $N_o(R)$, $\kappa_1(R)$, and thenβ. In the first we exclude $N_o(R)$ by forming from four **Eq. 106** for different i three equations for ratios

$$\frac{N_1(R, r = r_1, T_1)}{N_i(R, r = r_1, T_i)} = \left(\frac{x}{T_i - T_1 + x}\right)^{-3/(2-\beta)} \times \exp\left(-\frac{r_1^2}{(2-\beta)^2 \kappa_1(R)} \left(\frac{1}{x} - \frac{1}{T_i - T_1 + x}\right)\right), \quad \textbf{(107)}$$

where i = 2, 3, and 4. To exclude $\kappa_1(R)$ let us take logarithm from both parts of **Eq. 107** and then divide one equation on another; as result we obtain following two equations:

$$\frac{\ln(N_1/N_2) + (3/(2-\beta))\ln(x/(T_2 - T_1 + x))}{\ln(N_1/N_3) + (3/(2-\beta))\ln(x/(T_3 - T_1 + x))} = \frac{(1/x) - (1/(T_2 - T_1 + x))}{(1/x) - (1/(T_3 - T_1 + x))} , \quad \textbf{(108)}$$

$$\frac{\ln(N_1/N_2) + (3/(2-\beta))\ln(x/(T_2 - T_1 + x))}{\ln(N_1/N_4) + (3/(2-\beta))\ln(x/(T_4 - T_1 + x))} = \frac{(1/x) - (1/(T_2 - T_1 + x))}{(1/x) - (1/(T_4 - T_1 + x))} . \quad \textbf{(109)}$$

After excluding from **Eq. 108** and **Eq. 109** unknown parameter β, we obtain equation for determining x:

$$x^2(a_1a_2 - a_3a_4) + xd(a_1b_2 + b_1a_2 - a_3b_4 - b_3a_4) + d^2(b_1b_2 - b_3b_4) = 0 , \quad \textbf{(110)}$$

where

$$d = (T_2 - T_1)(T_3 - T_1)(T_4 - T_1), \quad \textbf{(111)}$$

$$a_1 = (T_2 - T_1)(T_4 - T_1)\ln(N_1/N_3) - (T_3 - T_1)(T_4 - T_1)\ln(N_1/N_2), \quad \textbf{(112)}$$

$$a_2 = (T_3 - T_1)(T_4 - T_1)\ln(x/(T_2 - T_1 + x)) - (T_2 - T_1)(T_3 - T_1)\ln(x/(T_4 - T_1 + x)), \quad \textbf{(113)}$$

$$a_3 = (T_2 - T_1)(T_3 - T_1)\ln(N_1/N_4) - (T_3 - T_1)(T_4 - T_1)\ln(N_1/N_2), \quad \textbf{(114)}$$

$$a_4 = (T_3 - T_1)(T_4 - T_1)\ln(x/(T_2 - T_1 + x)) - (T_2 - T_1)(T_4 - T_1)\ln(x/(T_3 - T_1 + x)), \quad \textbf{(115)}$$

$$b_1 = \ln(N_1/N_3) - \ln(N_1/N_2), \;\; b_2 = \ln(x/(T_2 - T_1 + x)) - \ln(x/(T_4 - T_1 + x)), \quad \textbf{(116)}$$

$$b_3 = \ln(N_1/N_4) - \ln(N_1/N_2), \;\; b_4 = \ln(x/(T_2 - T_1 + x)) - \ln(x/(T_3 - T_1 + x)). \quad \textbf{(117)}$$

As it can be seen from **Eq. 110** and **Eqs. 111—117**, coefficients a_2, a_4, b_2, b_4 very weekly (as logarithm) depend from x. Therefore, **Eq. 110** we solve by iteration method, as above we solved **Eq. 99**: as a first approximation, we use $x_1 = T_1 - Te \approx 500$ sec (which is the minimum time propagation of relativistic particles from the Sun to the Earth's orbit). Then by **Eq. 113** and **Eq. 115—117** we determine $a_2(x_1)$, $a_4(x_1)$, $b_2(x_1)$, $b_4(x_1)$ and by **Eq. 110** we determine the second approximation x_2, and so on. After determining x, i.e. according **Eq. 105** determining t_1, t_2, t_3, t_4, the final solutions for β, $x_1(R)$, and $N_o(R)$ can be found. Unknown parameter β in **Eq. 103** we determine from **Eq. 108** and **Eq. 109**:

$$\beta = 2 - 3\left[(\ln(t_2/t_1)) - \frac{t_3(t_2 - t_1)}{t_2(t_3 - t_1)}\ln(t_3/t_1)\right] \times \left[(\ln(N_1/N_2)) - \frac{t_3(t_2 - t_1)}{t_2(t_3 - t_1)}\ln(N_1/N_3)\right]^{-1} . \quad \textbf{(118)}$$

Then we determine unknown parameter $\kappa_1(R)$ in **Eq. 103** from **Eq. 107**:

$$\kappa_1(R) = \frac{r_1^2\left(t_1^{-1} - t_2^{-1}\right)}{3(2-\beta)\ln(t_2/t_1) - (2-\beta)^2\ln(N_1/N_2)} = \frac{r_1^2\left(t_1^{-1} - t_3^{-1}\right)}{3(2-\beta)\ln(t_3/t_1) - (2-\beta)^2\ln(N_1/N_3)}. \quad \textbf{(119)}$$

After determining parameters β and $\kappa_1(R)$ we can determine the last parameter $N_o(R)$ from **Eq. 106**:

$$N_o(R) = N_i(2-\beta)^{(4+\beta)/(2-\beta)}\Gamma\left(3/(2-\beta)\right)r_1^{-3\beta/(2-\beta)}\left(\kappa_1(R)t_i\right)^{3/(2-\beta)}\exp\left(\frac{r_1^2}{(2-\beta)^2\kappa_1(R)t_i}\right), \quad \textbf{(120)}$$

where index i = 1, 2 or 3.

Above we show that for some simple model of SEP propagation is possible to solve inverse problem on the basis of ground and satellite measurements at the beginning of the event. Obtained results we used in the method of great radiation hazard forecasting based on on-line CR one-minute ground and satellite data *[Dorman et al. 2005 b]*.

7.2. The checking of the model when diffusion coefficient depends from the distance to the Sun

On the basis of the inverse problem solution described in Section 7.1, by using the first few minutes NM data of the SEP event we can determine the effective parameters β by **Eq. 118**, $\kappa_1(R)$ by **Eq. 119**, and $N_o(R)$ by **Eq. 120**, corresponding to high rigidity, about 10 GV. In **Fig. 28** the values of parameter $\kappa_1(R)$ are shown for event in September 1989.

From **Fig. 28** can be seen that at the very beginning of event (the first point) the result is unstable: in this period the amplitude of increase is relatively small, so the relative accuracy is too low, and we obtain very big diffusion coefficient. Let us note, that at the very beginning of the event the diffusion model can be very hardly applied (more correct would be the application of kinetic model of SEP propagation). After the first point we have about stable result with accuracy ± 20 % (let us compare with **Fig. 27**, where the diffusion coefficient was found as effectively increasing with time). In **Fig. 29** are shown values of parameter β.

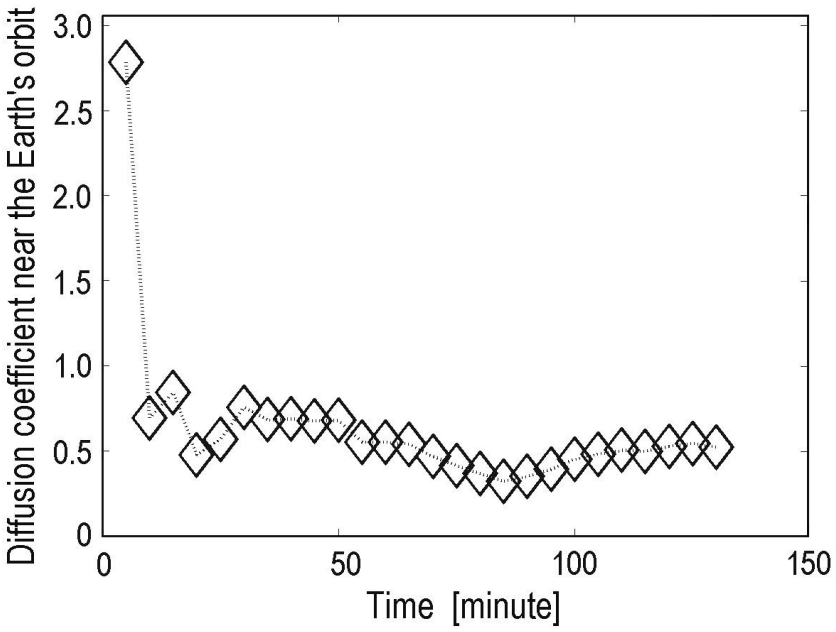

Fig. 28. Diffusion coefficient $\kappa_1(R)$ near the Earth's orbit (in units 10^{23} cm^2sec^{-1}) in dependence of time (in minutes after 11.40 UT of September 29, 1989).

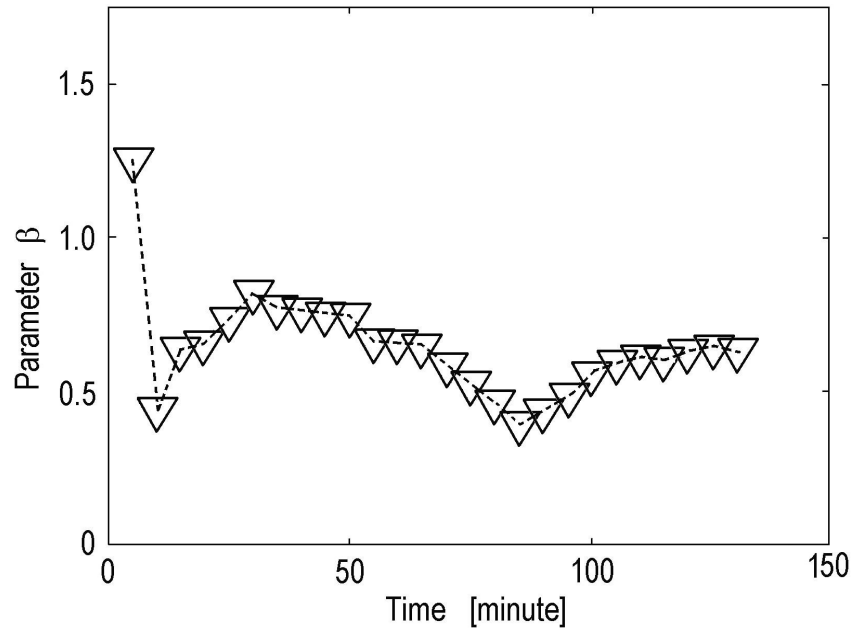

Fig. 29. Values of parameter β in dependence of time (in minutes after 11.40 UT of September 29, 1989).

It can be seen from **Fig. 29** that again the first point is anomalously big, but after the first point the result become almost stable with average value $\beta \approx 0.6$ (with accuracy about ± 20%). Therefore, we can hope that the model of the inverse problem solution, described in Section 7.1 (the set of **Eqs. 103—120**) reflects adequately SEP propagation in the interplanetary space.

7.3. The checking of the model by comparison of predicted SEP intensity time variation with NM observations

More accurate and exact checking of the solution of the inverse problem can be made by comparison of predicted SEP intensity time variation with NM observations. For this aim after determining of the effective parameters β, $\kappa_1(R)$, and $N_o(R)$ we may determine by **Eq. 104** the forecasting curve of expected SEP flux behavior for total neutron intensity. With each new minute of observations we can determine parameters β, $\kappa_1(R)$, and $N_o(R)$more and more exactly. It means that with each new minute of observations we can determine more and more exactly the forecasting curve of expected SEP flux behavior. We compare this forecasting curve with time variation of observed total neutron intensity (see **Fig. 30** which contains 8 panels for time moments t = 10 min up to t = 120 min after 11.40 UT of 29 September, 1989).

From Fig. 30 it can be seen that it is not enough to use only the first few minutes of NM data (t = 10 min): the obtained curve forecasts too low intensity. For t = 15 min the forecast shows some bigger intensity, but also not enough. Only for t = 20 min (15 minutes of increase after beginning) and later (up to t = 40 min and more) we obtain about stable forecast with good agreement with observed CR intensity.

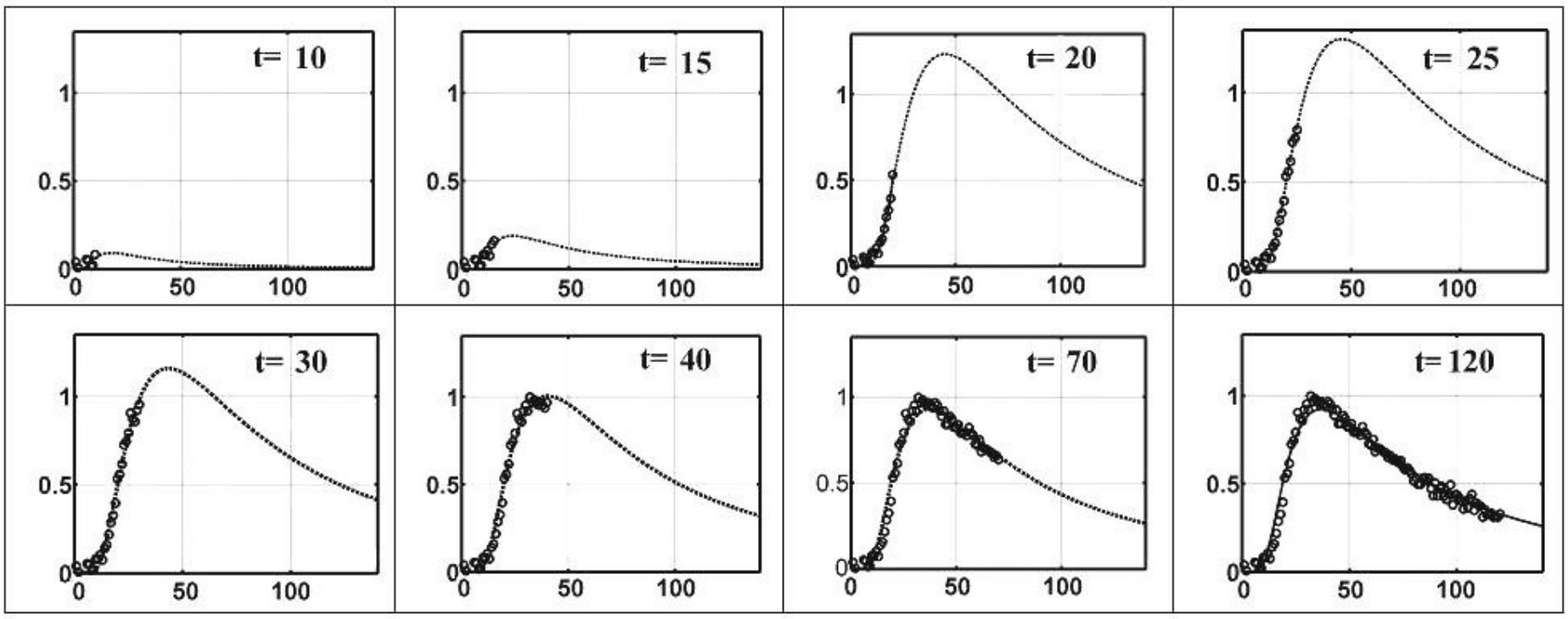

Fig. 30. Calculation for each new minute of SEP intensity observations parametersβ, $\kappa_1(R)$, $N_o(R)$ and forecasting of total neutron intensity (time t is in minutes after 11.40 UT of September 29, 1989; curves — forecasting, circles — observed total neutron intensity). From *[Dorman et al. 2005 a,b]*.

7.4. The checking of the model by comparison of predicted SEP intensity time variation with NM and satellite observations

The results described above, based only on NM data, reflect the situation in SEP behavior in the high energy (more than 6 GeV) region. For extrapolation of these results to the low energy interval (dangerous for space-probes and satellites), we use satellite on-line data available through the Internet. The problem is how to extrapolate the SEP energy spectrum from high NM energies to very low energies detected by GOES satellite. The main idea of this extrapolation is the following: 1) the time of ejection for high and small energy ranges (detected by NM and by satellite) is the same, so it can be determined by using only NM data; 2) the source function relative to time is a δ–function, and relative to energy is a power function with an energy-dependent index $\gamma = \gamma_o + \ln(E_k/E_{ko})$ with maximum at $E_{k\,max} = E_{ko}exp(-\gamma_o)$:

$$N_o(R,T) = N_o\delta(T - T_e)R^{-(\gamma_o + \ln(E_k/E_{ko}))} \quad \textbf{(121)}$$

Fig. 31 shows results based on the NM and satellite data of forecasting of expected SEP fluxes also in small energy intervals and comparison with observation satellite data.

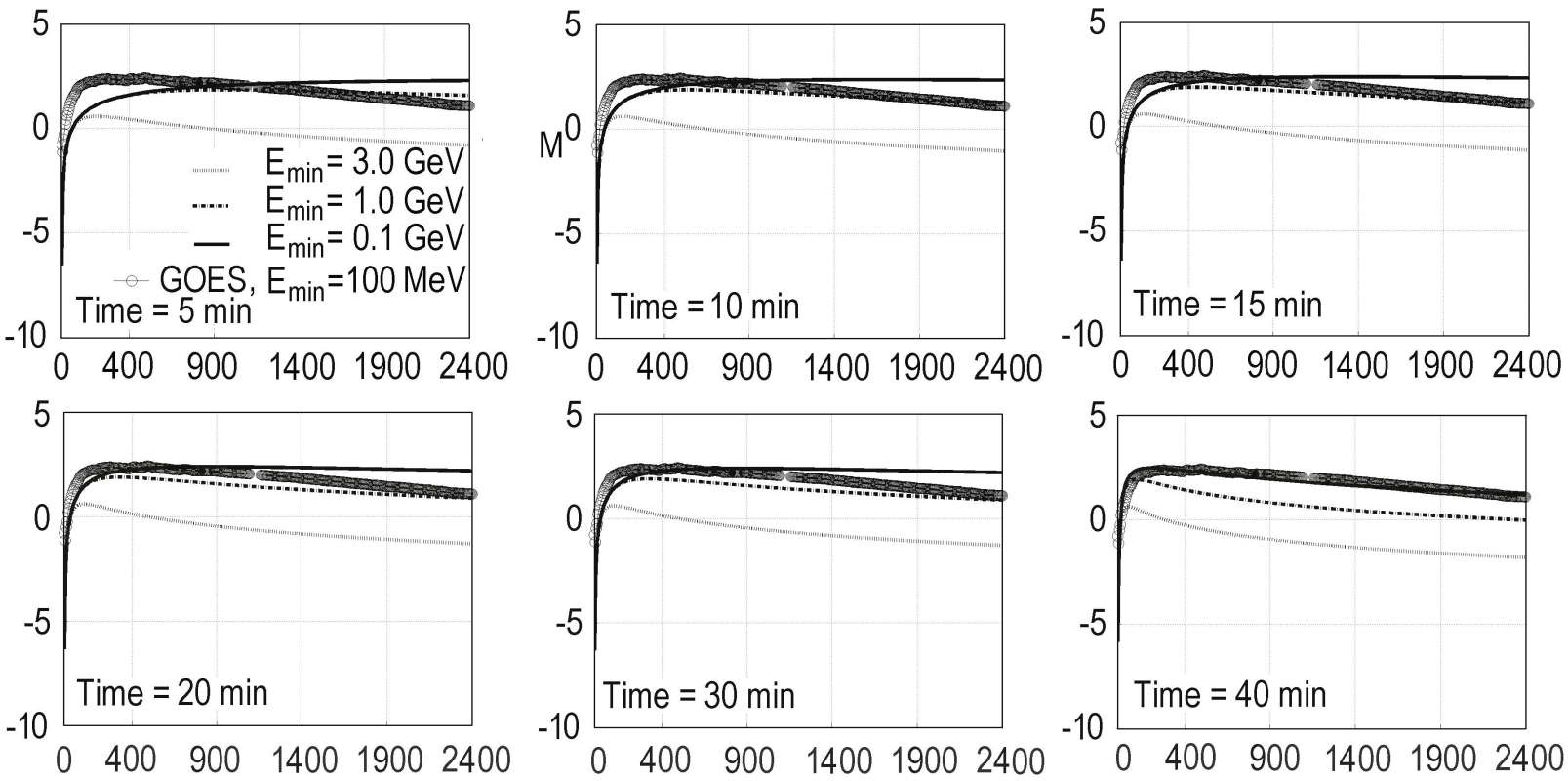

Fig. 31. Predicted SEP integral fluxes for $E_k \geq E_{min}$ = 0.1, 1.0, and 3.0 GeV. The forecasted integral flux for $E_k \geq E_{min}$ = 0.1 GeV is compared with the observed fluxes for $E_k \geq$ 100 MeV on GOES satellite. The ordinate is log10 of the SEP integral flux (in cm-2sec^{-1}sr^{-1}), and the abscissa is time in minutes from 11.40 UT of September 29, 1989. From *[Dorman et al. 2005 a,b]*.

Results of comparison presented in **Fig. 30** and **Fig. 31** show that by using on-line data from ground NM in the high energy range and from satellite in the low energy range during the first 30-40 minutes after the start of the SEP event, it is possible by using only CR data to solve the inverse problem by formulas in Sections 7.2 and 7.3: to determine the properties of SEP

source on the Sun (time of ejection into solar wind, source SEP energy spectrum, and total flux of accelerated particles) and parameters of SEP propagation in the interplanetary space (diffusion coefficient and its dependence from particle energy and from the distance from the Sun).

7.5. The inverse problems for great SEP events and space weather

Let us note that the solving of inverse problems for great SEP events has important practical sense: to predict the expected SEP differential energy spectrum on the Earth's orbit and integral fluxes for different threshold energies up to many hours (and even up to few days) ahead. The total (event-integrated) fluency of the SEP event, and the expected radiation hazards can also be estimated on the basis of the first 30—40 minutes after the start of the SEP event and corresponding Alerts to experts operating different objects in space, in magnetosphere, and in atmosphere at different altitudes and at different cut-off rigidities can be sent automatically. These experts should decide what to do operationally (for example, for space-probes in space and satellites in the magnetosphere to switch-off the electric power for few hours to save the memory of computers and high level electronics; for jets to decrease their altitudes from 10 km to 4—5 km to protect crew and passengers from great radiation hazard, and so on). From this point of view especially important is the solving of inverse problems for great SEP by using on-line data of many NM and several satellites in the frame of models in which CR propagation described by the theory of anisotropic diffusion or by kinetic theory. The solving of these inverse problems will made possible on the basis of world-wide CR Observatories and satellite data (in real scale time, applicable from Internet) to made forecasting on radiation hazard for much shorter time after SEP event beginning.

8. Forecasting of radiation hazard and the inverse problem for SEP propagation and generation in the frame of anisotropic diffusion and in kinetic approach

8.1. Kinetic and anisotropic diffusion cases

In this approach we will be based mainly on theoretical works *[Fedorov et al. 2002; Dorman et al. 2003; Dorman 2008 a]* according to which the evolution of the particle distribution function $f(y,\tau,\mu)$ follows from the kinetic equation written in the drift approximation:

$$\frac{\partial f}{\partial \tau}+\frac{\mu\partial f}{\partial y}+f-\frac{1}{2}\int_{-1}^{1} f d\mu=\frac{\nu_s}{\nu}\delta(y)\delta(\tau)\varphi(\mu), \qquad (122)$$

where y is coordinate along regular IMF and τ is time in dimensionless units $y = z\nu_s/v, \tau = \nu_s t$; $\nu_s = v/\Lambda$; is the collision frequency of SEP with magnetic inhomogeneities; $\mu = \cos\theta$, and θ is the particle pitch-angle. The right-hand side of **Eq. 122** describes an instantaneous injection of SEP with an initial angular distribution

$$\varphi(\mu)=\frac{a_\mu\Delta_\mu}{2\left(\Delta_\mu^2+(\mu-\mu_o)^2\right)}. \qquad (123)$$

For the finite time injection in the right-hand side of **Eq. 122** instead of $\delta(\tau)$ will be

$$\chi(\tau)=\nu_o^2\tau\exp(-\nu_o\tau), \qquad (124)$$

where ν_o^{-1} characterizes the mean duration of the injection. In this case the solution of **Eq. 122**, obtained by the method of direct and inverse Fourier — Laplace transform, will be

$$G(y,\tau)=\int_0^\tau d\xi\int_{-1}^{1} d\mu\chi(\tau-\xi)f(y,\xi,\mu)\psi(\mu). \qquad (125)$$

This solution consists from three terms

$$G(y,\tau)=G_{us}(y,\tau)+G_s^o(y,\tau)+G_s^d(y,\tau). \qquad (126)$$

The first component describes a contribution of the un-scattered particles which exponentially decreases with time τ:

$$G_{us}(y,\tau)=\frac{\nu_s\nu_o^2\exp(-\nu_o\tau)}{v}\times\int_0^\tau\frac{d\xi}{\xi}(\tau-\xi)\varphi\left(\frac{y}{\xi}\right)\psi\left(\frac{y}{\xi}\right)\exp(\xi(\nu_o-1)). \qquad (127)$$

A contribution of the scattered particles can be divided into two parts. One, the non-diffusive term $G_s^o(y,\tau)$, also exponentially decreases with time, and another term, $G_s^d(y,\tau)$, has a leading meaning in the diffusive limit of $\tau \gg 1$. Namely, the non-diffusive term reads

$$G_s^o(y,\tau)=\frac{\nu_s\nu_o^2\exp(-\nu_o\tau)}{8\pi v}\left\{\int_0^{y/\tau}d\eta\Psi(y,\tau,\eta)[S(\tau)-S(y)]+\int_{y/\tau}^{1}d\eta\Psi(y,\tau,\eta)[S(y/\eta)-S(y)]\right\}, \qquad (128)$$

where

$$\Psi(y,\tau,\eta)=\frac{\exp\left(y\Lambda(\eta)/2\right)}{\left((\mu_o-\eta)^2+\Delta_\mu^2\right)\left((\lambda_o-\eta)^2+\Delta_\lambda^2\right)}. \qquad (129)$$

The last (diffusive non-vanishing) term in **Eq. 126** has a sense only for $|y| < \tau$ and reads as

$$G_s^d(y,\tau)=\frac{\nu_s\nu_o^2}{4\pi v}\int_{-\pi/2}^{\pi/2}\frac{dk}{k^2}\Phi(y,k)\times\left\{e^{\tau\kappa}-e^{(y-\tau)\nu_o+y\kappa}\left[1+(\tau-y)(\nu_o+\kappa)\right]\right\}. \qquad (130)$$

where $\kappa \equiv k\cot k - 1$, and

$$\Phi(y,k)=\frac{\left(B_\mu B_\lambda-\Gamma_\mu\Gamma_\lambda\right)\cos(ky)+\left(B_\mu\Gamma_\lambda+\Gamma_\mu B_\lambda\right)\sin(ky)}{D_\mu D_\lambda\cos^2 k}. \qquad (131)$$

8.2. Expected temporal profiles for NM and comparison with observations

For example, some selected NM data for the 24 May 1990 are demonstrated in **Fig. 32**.

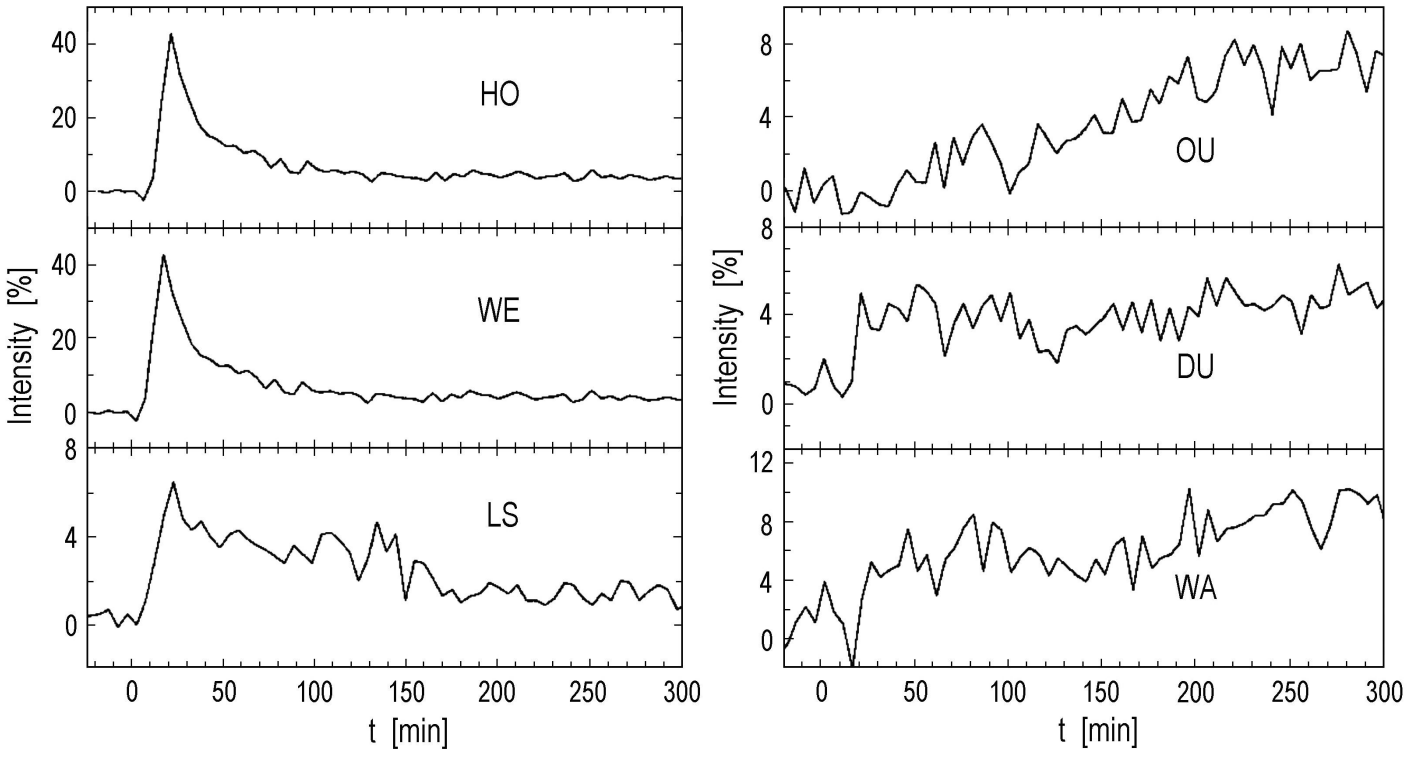

Fig 32. Two groups of NM records of the event on 24 May 1990. Left — have the narrow peak of the anisotropic stream of the first fast particles (HO — Ho-bart, WE— Mt. Wel-lington, LS — Lom-nický Štít); right — show a diffusive tail with a wide maximum at a later time (OU – Ou-lu, DU — Durham, WA— Mt.Washington). From *[Fedorov et al. 2002].*

In **Fig. 32** the time (in min) is measured from the onset of particle injection taken as 20.50 UT of May 24, 1990. The theo-retically predicted temporal profiles for the selected NM in the model described above are demonstrated in **Fig. 33**, left and right panels, respectively, using the calculated asymptotic direction for each NM station.

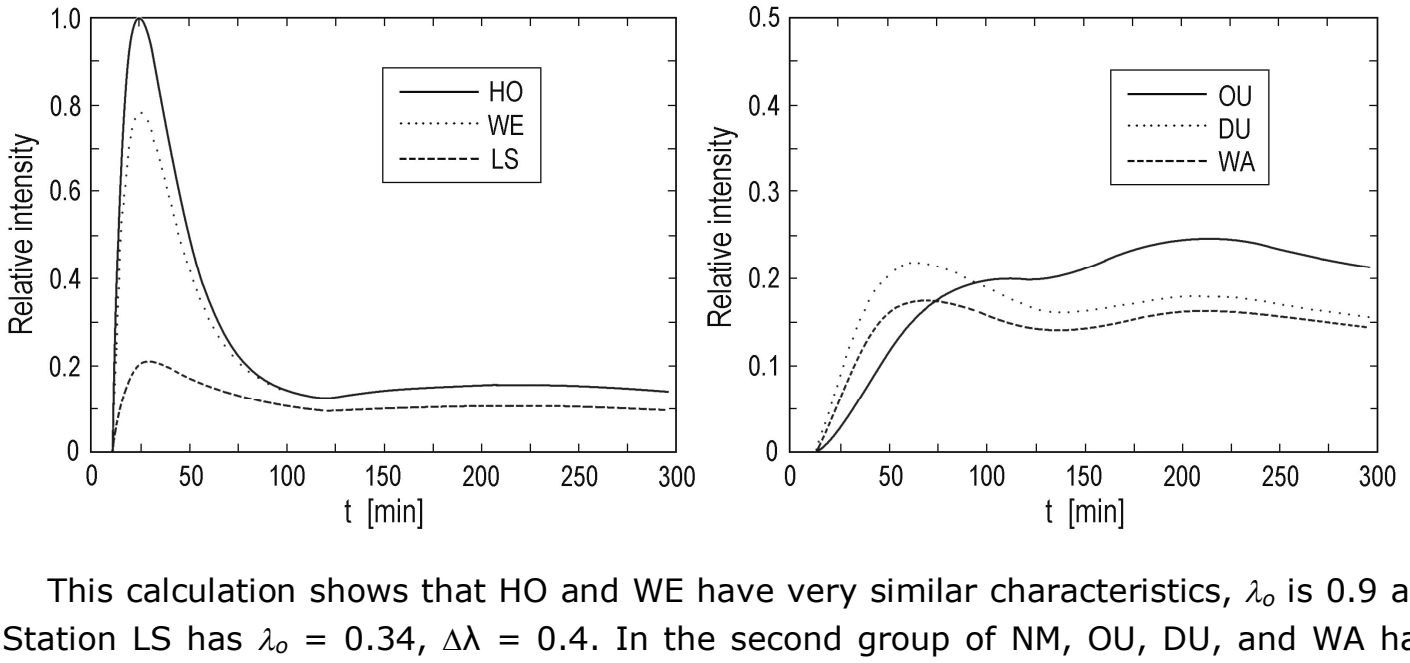

Fig. 33. Theoretical prediction of tem-poral profiles for the selected NM using cal-culated parameters λ_o, $\Delta\lambda$ and mean $\overline{R}$ for each NM. On the ordinate axis are shown expected intensity relative to HO in maxi-mum. According to *[Fedorov et al. 2002)]*

This calculation shows that HO and WE have very similar characteristics, λ_o is 0.9 and 0.86, respectively, with $\Delta\lambda = -0.26$. Station LS has $\lambda_o = 0.34$, $\Delta\lambda = 0.4$. In the second group of NM, OU, DU, and WA have $\lambda_o = -0.94, -0.9, -0.85$ and $\Delta\lambda = 0.06, 0.1, 0.3$, respectively. Oulu and Apatity give absolutely the same theoretical curves resulting from their similar charac-teristics and very similar temporal profiles of the event. The last two NMs (DU and WA) experienced small increases at 1—2 hours after onset, as the theory predicts, see **Fig. 32** (right panel), owing to smaller λ_o and larger $\Delta\lambda$ and larger mean $\overline{R}$.

8.3. Seven steps for forecasting of radiation hazard during SEP events

For realization of the **first step** of forecasting we need one minute real-time data from about all NM of the world network. On the each NM must work automatically the program for the search of the start SEP events as it was described in Sections

1—3. This search will help to determine which NM from about 50 of total number operated in the world network show the narrow peak of the anisotropic stream of the first arrived solar CR (NM of the 1-st type) and which show a diffusive tail with a wide maximum at a later time (NM of the 2-nd type). In the **second step** we determine rigidity spectrum of arrived SEP $I_s(R)$ above each NM outside of the atmosphere, and then separately for NM of the 1-st type and 2-nd type by using method of coupling functions as it was described above in Section 5 (in more detail see Chapter 3 in *[Dorman M2004]*. In the **third step** we should try to use the model of isotropic diffusion for a rough estimation of expected radiation hazard (see Sections 6 and 7). In the **fourth step** we should determine for different NM the mean $\overline{R}$, λ_o and $\Delta\lambda$ characterizing for this event. By using these parameters and experimental data on NM time profiles in the beginning time we cane determine parameters of SEP non-scattering and diffusive propagation, described in Sections 8.1 and 8.2 (the **fifth step**). On the basis of determined parameters of SEP non-scattering and diffusive propagation we then determine expected SEP fluxes and pitch-angle distribution during total event in interplanetary space in dependence of time after ejection (the **sixth step**).

In the **seventh step** by using again method of coupling functions we should determine expected radiation doze which will be obtain during this event inside space probes in interplanetary space, satellites in the magnetosphere, aircrafts at different altitudes and cutoff rigidities, for people and technologies on the ground.

9. Effects of great magnetic storms (caused big CR Forbush effects) on the frequency of infarct myocardial, brain strokes, care accidents, and technology; extended NOAA classification

There are numerous indications that natural, solar variability-driven time variations of the Earth's magnetic field can be hazardous in relation to health and safety. There are two lines of their possible influence: effects on physical systems and on human beings as biological systems. High frequency radio communications are disrupted, electric power distribution grids are blacked out when geomagnetically induced currents cause safety devices to trip, and atmospheric warming causes increased drag on satellites. An example of a major disruption on high technology operations by magnetic variations of large extent occurred in March 1989, when an intense geomagnetic storm upset communication systems, orbiting satellites, and electric power systems around the world. Several large power transformers also failed in Canada and United States, and there were hundreds of misoperations of relays and protective systems *[Kappenman and Albertson 1990; Hruska and Shea 1993]*. Some evidence has been also reported on the association between geomagnetic disturbances and increases in work and traffic accidents *[Ptitsyna et al. 1998 and refs. therein]*. These studies were based on the hypothesis that a significant part of traffic accidents could be caused by the incorrect or retarded reaction of drivers to the traffic circumstances, the capability to react correctly being influenced by the environmental magnetic and electric fields. The analysis of accidents caused by human factors in the biggest atomic station of former USSR, "Kurskaya", during 1985—1989, showed that ~70% of these accidents happened in the days of geomagnetic storms. In *[Reiter 1954, 1955]* it was found that work and traffic accidents in Germany were associated with disturbances in atmospheric electricity and in geomagnetic field (defined by sudden perturbations in radio wave propagation). On the basis of 25 reaction tests, it was found also that the human reaction time, during these disturbed periods, was considerably retarded. Retarded reaction in connection with naturally occurred magnetic field disturbances was observed also by *[Koenig and Ankermueller 1982]*. Moreover, a number of investigations showed significant correlation between the incidence of clinically important pathologies and strong geomagnetic field variations. The most significant results have been those on cardiovascular and nervous system diseases, showing some association with geomagnetic activity; a number of laboratory results on correlation between human blood system and solar and geomagnetic activity supported these findings *[Ptitsyna et al. 1998 and refs. therein]*. Recently, the monitoring of cardiovascular function among cosmonauts of "MIR" space station revealed a reduction of heart rate variability during geomagnetic storms *[Baevsky et al. 1996]*; the reduction in heart rate variability has been associated with 550% increase in the risk of coronary artery diseases *[Baevsky et al. 1997 and refs. therein]*. On the basis of great statistical data on several millions medical events in Moscow and in St. Petersburg were found an sufficient influence of geomagnetic storms accompanied with CR Forbush-decreases on the frequency of myocardial infarcts, brain strokes and car accident road traumas *[Villoresi et al. 1994, 1995]*. Earlier we found that among all characteristics of geomagnetic activity, Forbush decreases are better related to hazardous effects of solar variability-driven disturbances of the geomagnetic field *[Ptitsyna et al. 1998]*. **Fig. 34** shows the correlation between cardiovascular diseases, car accidents and different characteristics of geomagnetic activity (planetary index AA, major geomagnetic storms MGS, sudden commencement of geomagnetic storm SSC, occurrence of downward vertical component of the interplanetary magnetic field Bz and also decreasing phase of Forbush decreases (FD)). The most remarkable and statistically significant effects have been observed during days of geomagnetic perturbations defined by the days of the declining phase of Forbush decreases in CR intensity. During these days the average numbers of traffic accidents, infarctions, and brain strokes increase by (17.4±3.1)%, (10.5±1.2)% and (7.0±1.7)% respectively.

In **Fig. 35** we show the effect on pathology rates during the time development of FD. All FD have been divided into two groups, according to the time duration T of the FD decreasing phase. Then, the average incidence of infarctions and traffic accidents was computed beginning from one day before the FD-onset till 5 days after. For the first group (T<1 day) the average

daily incidence of infarctions and traffic incidence increases only in the first day of FD; no effect is observed during the recovery phase (that usually lasts for several days). Also for the second group (1 day<T<2 days) the increase in incidence rates is observed only during the 2-days period of the decreasing phase of FD.

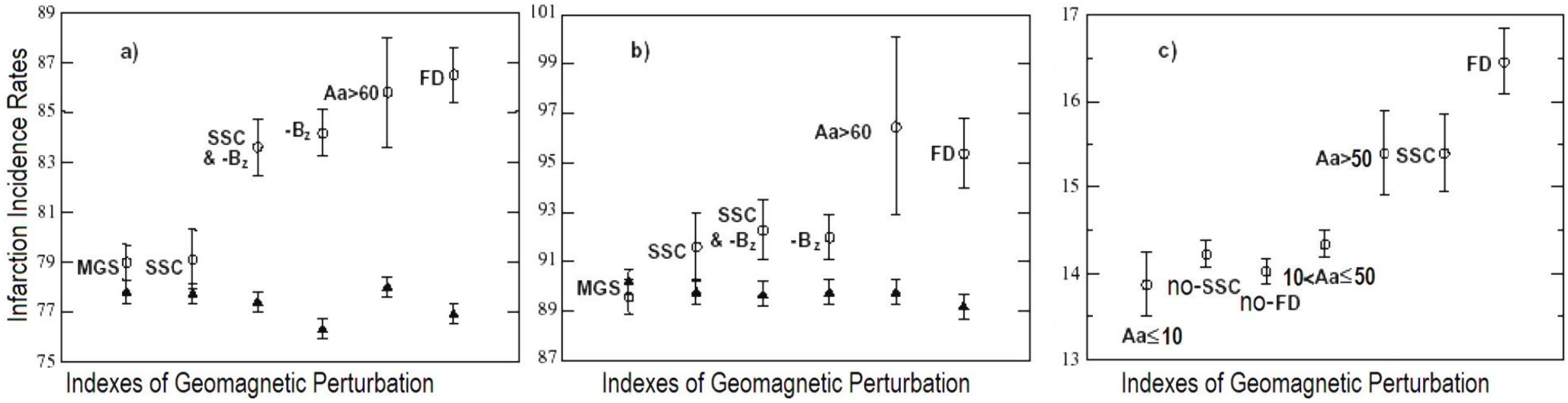

Fig. 34: Myocardial infarction (**a**), brain stroke (**b**) and road accident (**c**) incidence rates per day during geomagnetic quiet and perturbed days according to different indexes of activity.

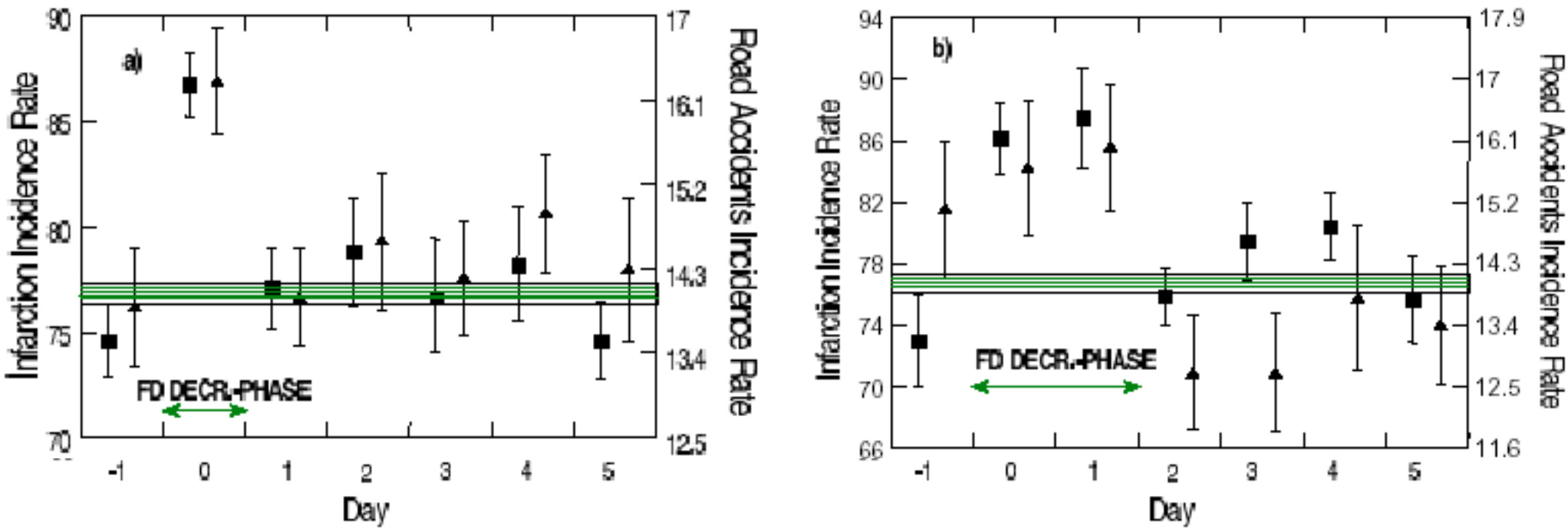

Fig 35: Infarction (full squares) and road accidents (full triangles) incidence during the time development of FD. (**a**): CR decrease phase T<1 day; (**b**): CR decrease phase 1 day<T<2 days.

In **Table 3** are shown NOAA scale of geomagnetic storms influence on power systems, on spacecraft operations, and on other systems (greatest three types, mostly accompanied with Forbush-decreases). We expect that for these three types of geomagnetic storms can be useful on-line one-hour CR data of neutron monitors and muon telescopes for automatically on-line forecasting (at least before 15-20 hours of SSC). In **Table 3** we added some preliminary information on possible biological effects according to our results discussed above (see **Fig. 34** and **Fig. 35**).

Table 3

The extended NOAA scale of geomagnetic storms influence on people health, power systems, on spacecraft operations, and on other systems (greatest three types, mostly accompanied with Forbush-decreases). In the original NOAA scale are included biological effects according to results discussed above

Geomagnetic Storms			Kp values	Number per solar cycle
G5	**Extreme**	**Biological effects:** increasing on more than 10-15% of the daily rate of infarct myocardial, brain strokes and car road accidents traumas for people population on the ground. **Power systems:** widespread voltage control problems and protective system problems can occur, some grid systems may experience complete collapse or blackouts. Transformers may experience damage. **Spacecraft operations:** may experience extensive surface charging, problems with orientation, uplink/downlink and tracking satellites. **Other systems:** pipeline currents can reach hundreds of amps, HF (high frequency) radio propagation may be impossible in many areas for one to two days, satellite navigation may be degraded for days, low-frequency radio navigation can be out for hours.	**Kp = 9**	**4 per cycle (4-8 days per cycle)**

Table 3 (continuation)

The extended NOAA scale of geomagnetic storms influence on people health, power systems, on spacecraft operations, and on other systems (greatest three types, mostly accompanied with Forbush-decreases). In the original NOAA scale are included biological effects according to results discussed above

Geomagnetic Storms			Kp values	Number per solar cycle
G4	**Severe**	**Biological effects:** increasing on several percents (up to 10-15%) of the daily rate of infarct myocardial, brain strokes and car road accidents traumas for people population on the ground **Power systems:** possible widespread voltage control problems and some protective systems will mistakenly trip out key assets from the grid. **Spacecraft operations:** may experience surface charging and tracking problems, corrections may be needed for orientation problems. **Other systems:** induced pipeline currents affect preventive measures, HF radio propagation sporadic, satellite navigation degraded for hours, low-frequency radio navigation disrupted.	**Kp = 8, including a 9-**	**100 per cycle (100-200 days per cycle)**
G3	**Strong**	**Biological effects:** increasing on few percents of the daily rate of infarct myocardial, brain strokes and car road accidents traumas for people population on the ground **Power systems:** voltage corrections may be required, false alarms triggered on some protection devices. **Spacecraft operations:** surface charging may occur on satellite components, drag may increase on low-Earth-orbit satellites, and corrections may be needed for orientation problems. **Other systems:** intermittent satellite navigation and low-frequency radio navigation problems may occur, HF radio may be intermittent.	**Kp = 7**	**200 per cycle (200-400 days per cycle)**

10. Cosmic ray on-line one-hour data using for forecasting of dangerous geomagnetic storms accompanied with Forbush-decreases; formation of International Cosmic Ray Service (ICRS)

Thus, FD events can be used as reliable indicators of health- and safety-related harmful geomagnetic storms. For a practical realization of forecasting hazardous geomagnetic storms by means of FD indicators, it will be necessary to get data from most CR stations in real-time (now main part of data are available only after about one month). Therefore, it is necessary to found a special Real-Time Cosmic Ray World Data Center to transform the cosmic ray station network in a real-time International Cosmic Ray Service (ICRS) *[Dorman et al. 1993]* We present here basic ideas of the organization of such real-time data collection and processing, for providing a reliable forecast-service of FD and related dangerous disturbances of geomagnetic field. The main features observed in CR intensity before the beginning of FD that can be used for FD forecasting are the following (see **Fig. 36**):

1. CR pre-increase *[Blokh et al. 1959; Dorman 1959; see review in Dorman 1963a,b]*. The discovery of this effect in 1959 *[Blokh et al. 1959]* stimulated to develop the mechanism of galactic CR interactions with interplanetary shock waves *[Dorman 1959; Dorman and Freidman 1959]* and further analyses *[Dorman 1995, Belov et al. 1995]* showing that this effect is related to particle interaction and acceleration by interplanetary shock waves;

2. CR pre-decrease *[McCracken and Parsons 1958; Fenton et al 1959; see review in Dorman 1963a,b]*. This effect was analyzed recently both theoretically [Dorman et al. 1995] and experimentally on the basis of the network of CR stations *[Belov et al. 1995]*. The pre-decrease effect can be due to a magnetic connection of the Earth with regions (moving from the Sun) with reduced CR density; this lower density can be observed at the Earth along the actual direction of IMF lines *[Nagashima et al. 1990, Bavassano et al. 1994]*;

3. CR fluctuations. Many authors found some peculiarities in behavior of CR fluctuations before FD: changes in frequency spectrum; appearance of peaks in spectrum at some frequencies; variations in some special parameter introduced for characterizing the variability of fluctuations. Though the obtained results are often contradictory *[Dorman et al. 1995]*, sometimes CR fluctuations appear as reliable phenomena for FD prediction, as expected from additional Alfven turbulence produced by kinetic stream instability of low-energy particles accelerated by shock waves *[Berezhko et al. 1997]*;

4. Change in 3-D anisotropy. The CR longitudinal dependence changes abruptly in directions close to usual directions of interplanetary magnetic field and depends on the character and source of the disturbance. These effects, appearing much before Forbush decreases (up to 1 day) may be considered as predictors of FD. Estimation of CR anisotropy vector may be done by the global survey method described in *[Belov et al. 1997]*.

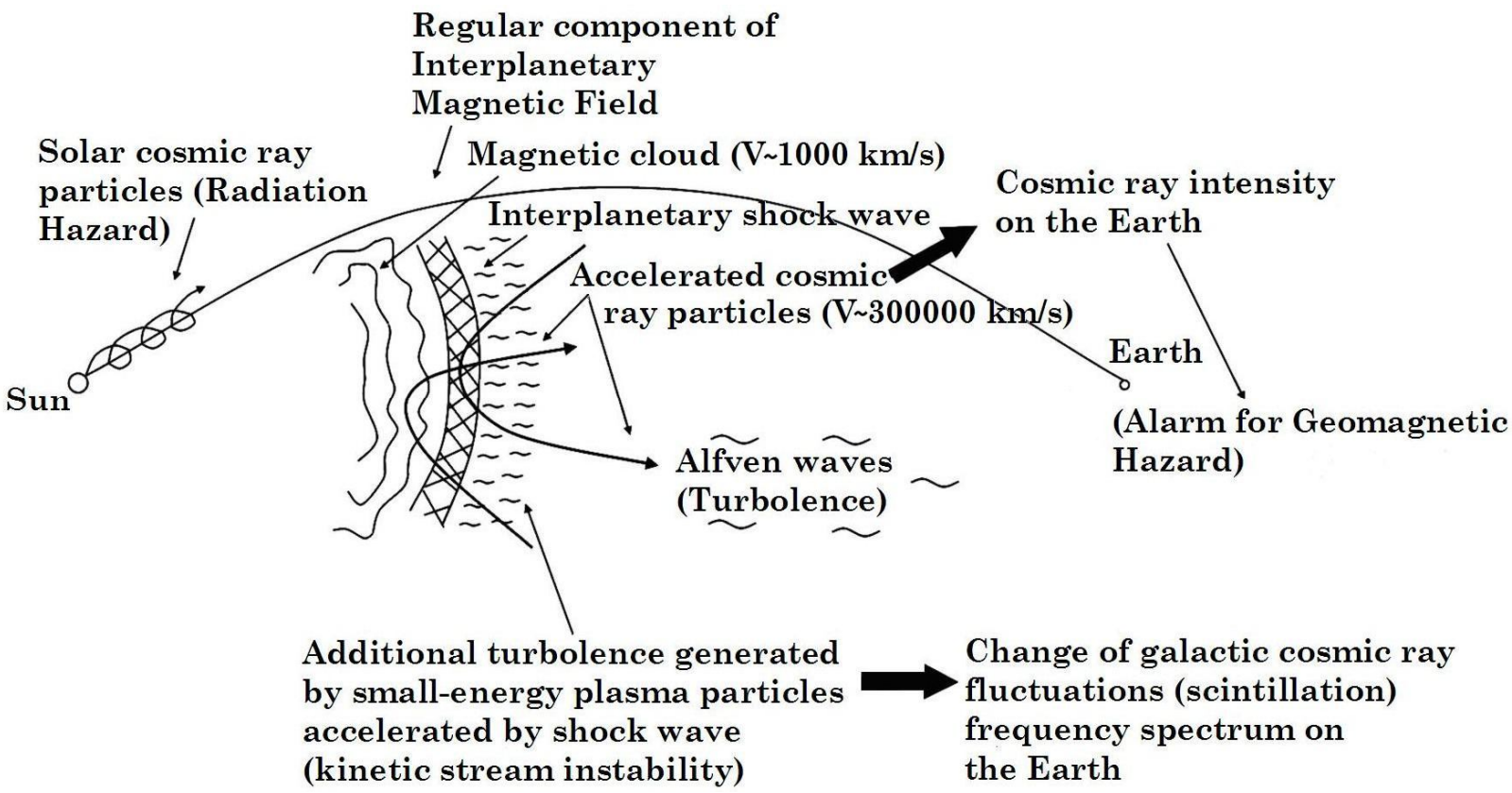

Fig. 36. Scheme of mechanisms of possible precursory effects in CR

In **Fig. 37** we show an example of such estimation done for the 9.09.1992 event represented the longitude-time CR intensity distribution. The grey circles mark the CR intensity decrease and white circles mark the CR intensity increase (in both cases bigger diameter of circle means bigger amplitude of intensity variation). The vertical line marks the time of Sudden Storm Commencement (SSC).

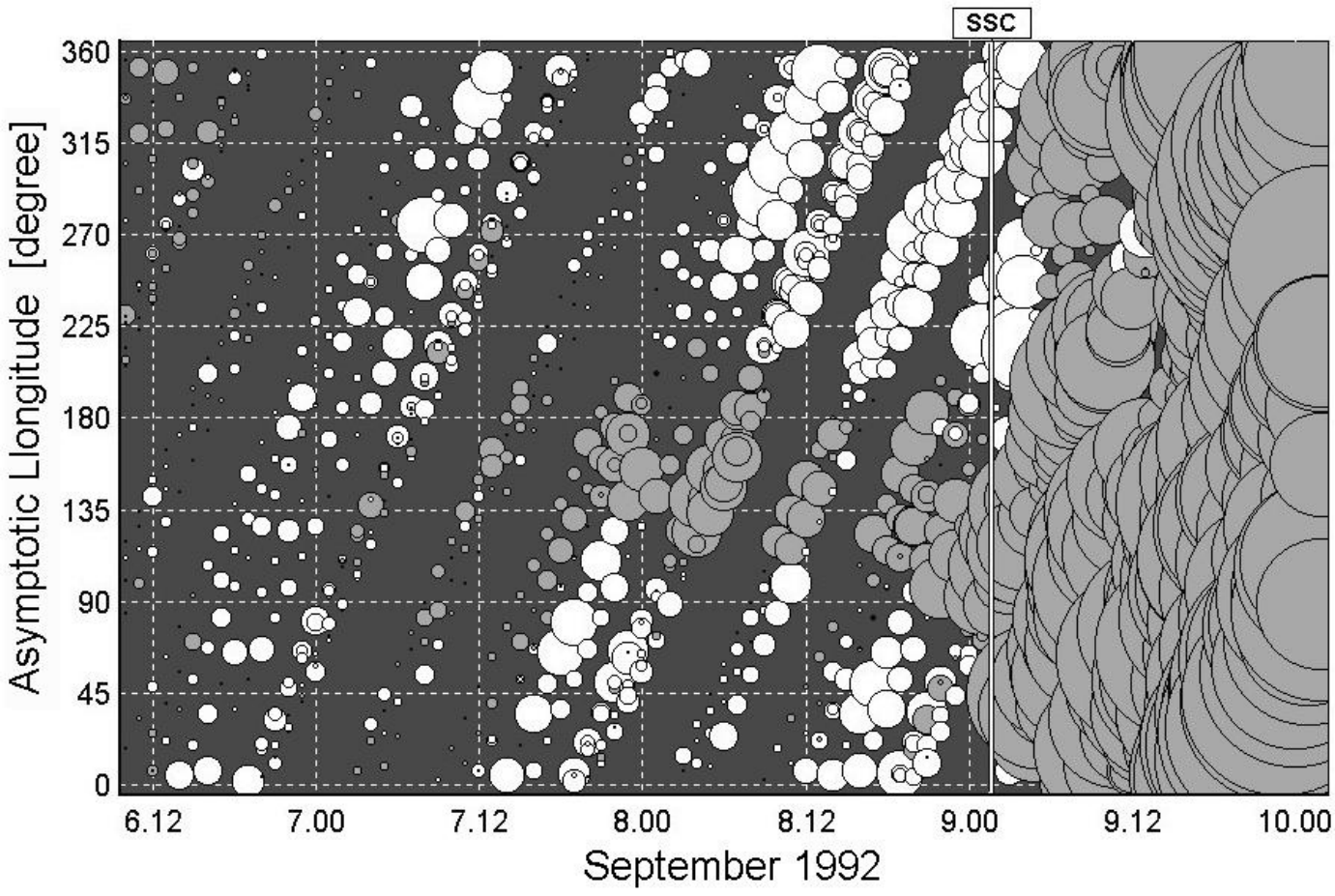

Fig. 37. Galactic cosmic ray pre-increase (white circles) and pre-decrease (grey circles) effects before the Sudden Storm Commencement (SSC) of great magnetic storm in September 1992, accompanied with Forbush-decrease.

From **Fig. 37** one can see that the pre-increase, as well as the pre-decrease, occurs some hours (at least, 15—20 hours) before the SSC. As it was shown recently by *[Munakata et al. 2000]*, the CR pre-increase and pre-decrease effects can be observed very clear also by multidirectional muon telescope world network. They investigated 14 "major" geomagnetic storms characterized by $K_p \geq 8$– and 25 large storms characterized by $Kp \geq 7$– observed in 1992—1998. It was shown that 89% of "major" geomagnetic storms have clear precursor effects what can be used for forecasting (the probability of exact forecasting increased with increasing of the value of storm).

We suppose that this type of analysis on the basis of on-line one-hour neutron monitor and muon telescope data from the world network CR Observatories can be made in near future automatically with forecasting of great geomagnetic storms. This important problem can be solved, for example by formation of the International Cosmic Ray Service (ICRS), what will be based on real-time collection and exchange through Internet of the data from about all cosmic-ray stations of the network (the possible scheme of ICRS working is shown in **Fig. 38** and **Fig. 39**).

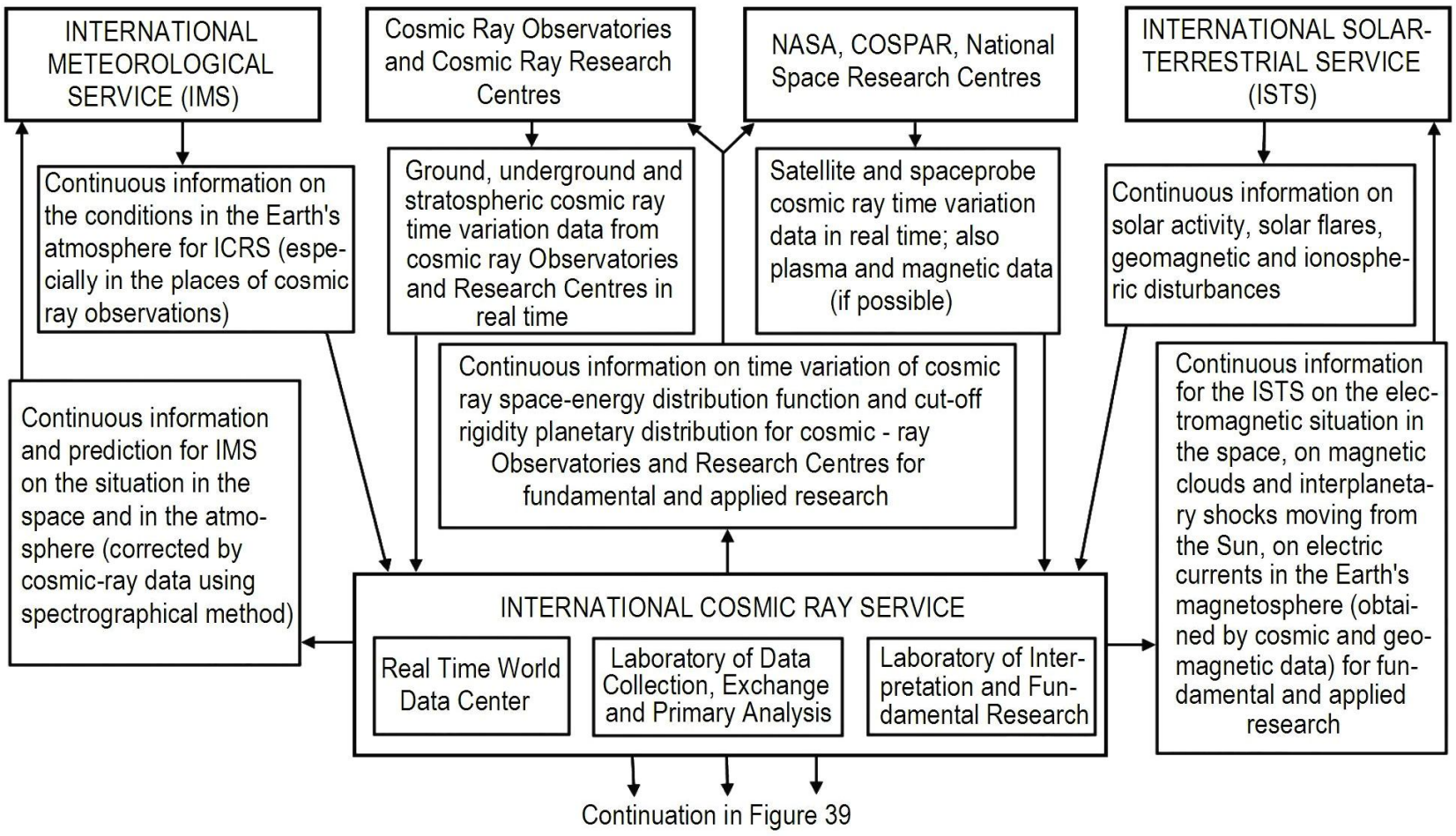

Fig. 38. Supposed scheme of exchange data between collaborated CR Observatories in the frame of ICRS.

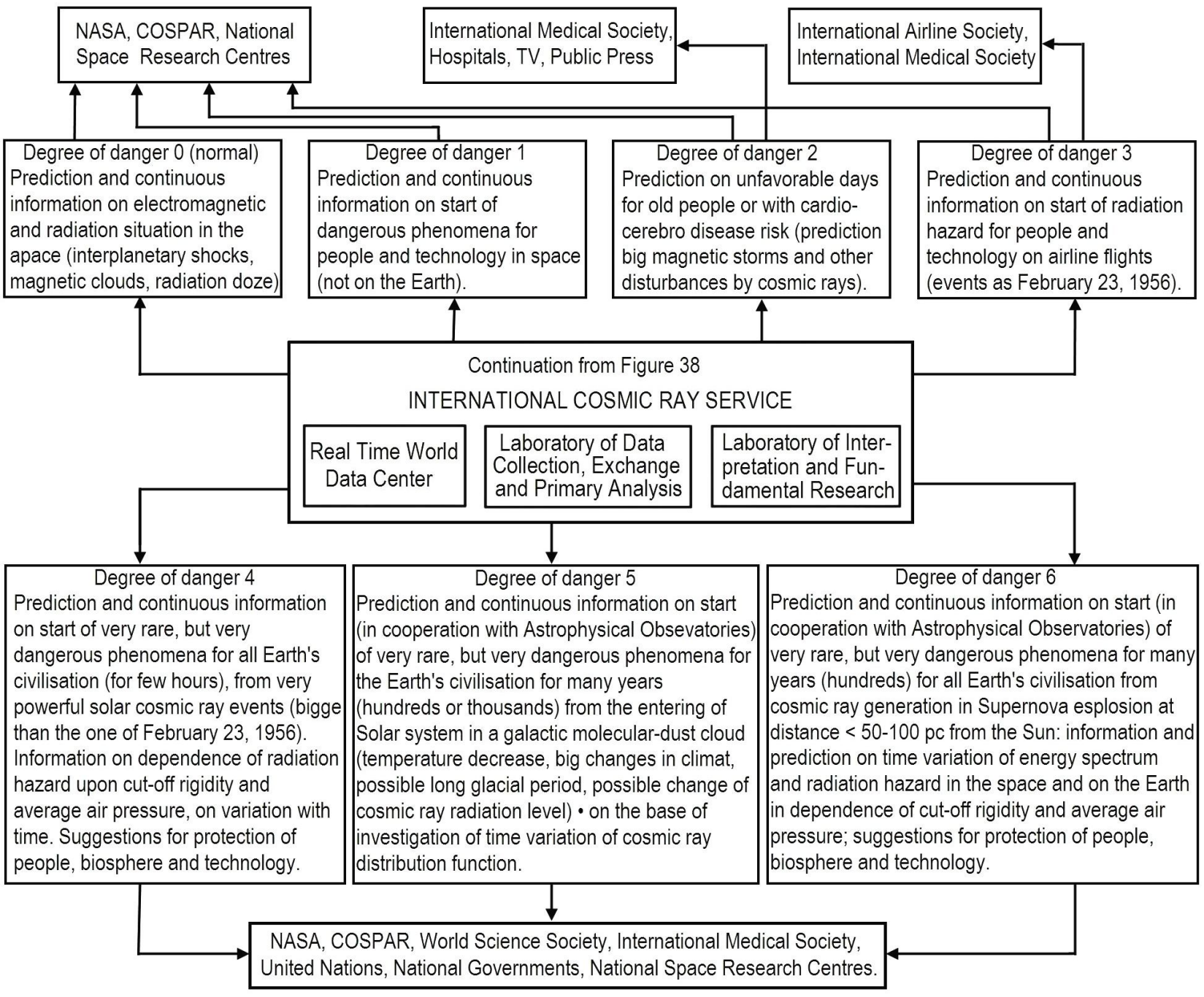

Fig. 39. Output information on space weather and dangerous situations of different levels from ICRS to collaborated organizations.

Then, computerized data analysis and interpretation will be done on the basis of modern theories listed above and, as we hope, will be developed father in near future. It will be necessary to use also related spacecraft data in real time: cosmic ray variations in small and very small energy regions, interplanetary magnetic field and solar wind data. For this purpose neutron

monitor stations of the network should have a data collection time of 1 minute and 1 hour. The organization of ICRS and continue automatically forecast will provide necessary information to space agencies, health authorities, road police and other organizations to apply the appropriate preventive procedures for saving people and technologies from negative CR and other Space Weather factors negative effects.

11. CR and other space weather factors influenced on the Earth's climate

11.1. Periodicities and long-term variations in climate change

About two hundred years ago, the famous astronomer William Herschel (1801) suggested that the price of wheat in England was directly related to the number of sunspots. He noticed that less rain fell when the number of sunspots was high (Joseph in the Bible, recognized a similar periodicity in food production in Egypt, about four thousand years ago). The solar activity level is known from direct observations over the past 450 years and from data of cosmogenic nuclides (through CR intensity variations) for more than 10 thousand years *[Eddy 1976; see review in Dorman M2004]*. Over this period there is a striking qualitative correlation between cold and warm climate periods and high and low levels of galactic CR intensity (low and high solar activity). As an example, **Fig. 40** shows the change in the concentration of radiocarbon during the last millennium (a higher concentration of ^{14}C corresponds to a higher intensity of galactic CR and to lower solar activity).

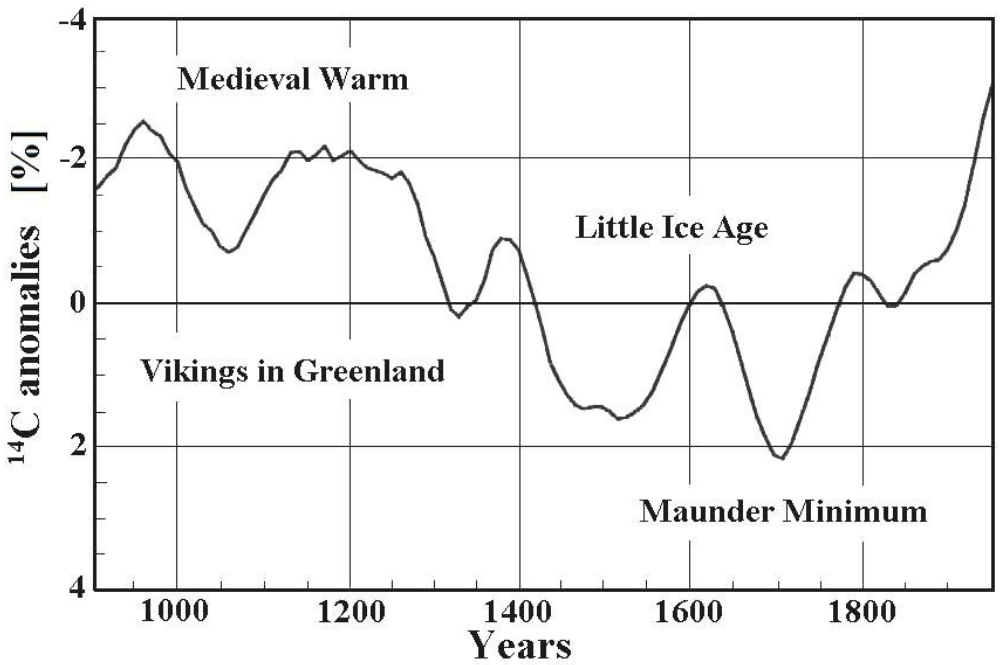

Fig. 40. The change of CR intensity reflected in radiocarbon concentration during the last millennium. The Maunder minimum refers to the period 1645—1715, when sunspots were rare. From *[Swensmark 2000]*.

It can be seen from **Fig. 40** that during 1000—1300 AD the CR intensity was low and solar activity high, which coincided with the warm medieval period (during this period Vikings settled in Greenland). After 1300 AD solar activity decreased and CR intensity increased, and a long cold period followed (the so called Little Ice Age, which included the Maunder minimum 1645—1715 AD and lasted until the middle of 19th century).

11.2. The possible role of solar activity and solar irradiance in climate change

Friis-Christiansen and Lassen found *[Friis-Christiansen & Lassen 1991; Lassen & Friis-Christiansen 1995]*, from four hundred years of data, that the filtered solar activity cycle length is closely connected to variations of the average surface temperature in the northern hemisphere. *[Labitzke and Van Loon 1993]* showed, from solar cycle data, that the air temperature increases with increasing levels of solar activity. *[Swensmark 2000]* also discussed the problem of the possible influence of solar activity on the Earth's climate through changes in solar irradiance. But the direct satellite measurements of the solar irradiance during the last two solar cycles showed that the variations during a solar cycle was only about 0.1%, corresponding to about 0.3 $W \cdot m^{-2}$. This value is too small to explain the present observed climate changes *[Lean et al. 1995]*. Much bigger changes during solar cycle occur in UV radiation (about 10%, which is important in the formation of the ozone layer). *[High 1996; Shindell et al. 1999]* suggested that the heating of the stratosphere by UV radiation can be dynamically transported into the troposphere. This effect might be responsible for small contributions towards 11 and 22 years cycle modulation of climate but not to the 100 years of climate change that we are presently experiencing.

11.3. Cosmic rays as an important link between solar activity and climate change

Many authors have considered the influence of galactic and solar CR on the Earth's climate. Cosmic radiation is the main source of air ionization below 40—35 km; only near the ground level, lower than 1 km, are radioactive gases from the soil also important in air ionization *[see review in Dorman M2004]*. The first to suggest a possible influence of air ionization by CR on the climate was Ney (1959). *[Swensmark 2000]* noted that the variation in air ionization caused by CR could potentially influence the optical transparency of the atmosphere, by either a change in aerosol formation or influence the transition between the different phases of water. Many other authors considered these possibilities *[Ney 1959; Dickinson 1975; Pudovkin and Raspopov*

1992; Pudovkin and Veretenenko 1995, 1996; Tinsley 1996; Swensmark and Friis-Christiansen 1997; Swensmark 1998; Marsh and Swensmark 2000a,b; Dorman 2009, 2012]. The possible statistical connections between the solar activity cycle and the corresponding long term CR intensity variations with characteristics of climate change were considered in *[Dorman et al. 1987, 1988a,b]*. *[Dorman et al. 1997]* reconstructed CR intensity variations over the last four hundred years on the basis of solar activity data and compared the results with radiocarbon and climate change data.

Cosmic radiation plays a key role in the formation of thunderstorms and lightnings (see extended review in Chapter 11 in *[Dorman M2004]*. Many authors *[Markson 1978; Price 2000; Tinsley 2000; Schlegel et al. 2001; Dorman et al. 2003; Dorman and Dorman 2005]* have considered atmospheric electric field phenomena as a possible link between solar activity and the Earth's climate. Also important in the relationship between CR and climate, is the influence of long term changes in the geomagnetic field on CR intensity through the changes of cutoff rigidity (see extended review in Chapter 7 in *[Dorman M2009]*). One can consider the general hierarchical relationship to be: **(solar activity cycles + long-term changes in the geomagnetic field) → (CR long term modulation in the Heliosphere + long term variation of cutoff rigidity) → (long term variation of clouds covering + atmospheric electric field effects) → climate change**.

11.4. The Connection between galactic CR solar cycles and the Earth's cloud coverage

Recent research has shown that the Earth's cloud coverage (observed by satellites) is strongly influenced by CR intensity *[Swensmark 2000; Tinsley 1996; Swensmark 1998; Marsh and Swensmark 2000a,b]*. Clouds influence the irradiative properties of the atmosphere by both cooling through reflection of incoming short wave solar radiation, and heating through trapping of outgoing long wave radiation (the greenhouse effect). The overall result depends largely on the height of the clouds. According to *[Hartmann 1993]*, high optically thin clouds tend to heat while low optically thick clouds tend to cool (see **Table 4**).

Table 4

**Global annual mean forcing due to various types of clouds,
from the Earth Radiation Budget Experiment (ERBE), according to** *[Hartmann 1993]*
The positive forcing increases the net radiation budget of the Earth and leads to a warming;
negative forcing decreases the net radiation and causes a cooling
(Note that the global fraction implies that 36.7% of the Earth is cloud free)

Parameter	High clouds		Middle clouds		Low clouds	Total
	Thin	Thick	Thin	Thick	All	
Global fraction /(%)	10.1	8.6	10.7	7.3	26.6	63.3
Forcing (relative to clear sky):						
Albedo (SW radiation)/($W{\cdot}m^{-2}$)	-4.1	-15.6	-3.7	-9.9	-20.2	-53.5
Outgoing LW radiation /($W{\cdot}m^{-2}$)	6.5	8.6	4.8	2.4	3.5	25.8
Net forcing /($W{\cdot}m^{-2}$)	2.4	-7.0	1.1	-7.5	-16.7	-27.7

From **Table 4** it can be seen that low clouds result in a cooling effect of about 17 $W{\cdot}m^{-2}$, which means that they play an important role in the Earth's radiation budget *[Ohring and Clapp 1980; Ramanathan et al. 1989; Ardanuy 1991]*. The important issue is that even small changes in the lower cloud coverage can result in important changes in the radiation budget and hence has a considerably influence on the Earth's climate (let us remember that the solar irradiance changes during solar cycles is only about 0.3 $W{\cdot}m^{-2}$). **Fig. 41** shows a comparison of the Earth's total cloud coverage (from satellite observations) with CR intensities (from the Climax neutron monitor) and solar activity data over 20 years.

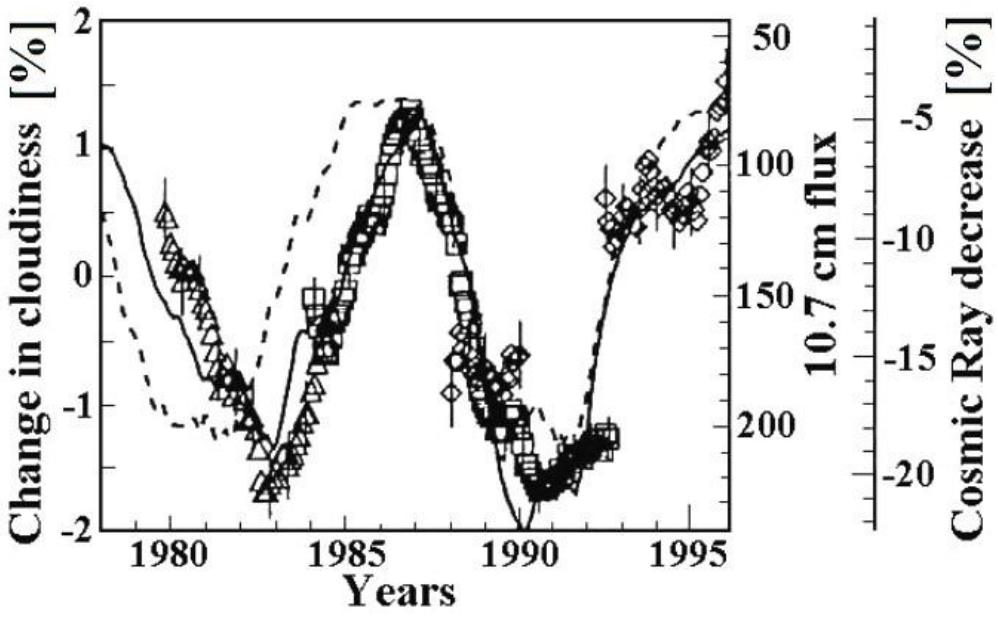

Fig. 41. Changes in the Earth's cloud coverage: triangles — from satellite Nimbus 7, CMATRIX project *[Stowe et al. 1988]*; squares — from the International Satellite Cloud Climatology Project, ISCCP *[Rossow and Shiffer 199]*; diamonds — from the Defense Meteorological Satellite Program, DMSP *[Weng and Grody 1994; Ferraro et al. 1996)]* Solid curve — CR intensity variation according to Climax NM, normalized to May 1965. Broken curve — solar radio flux at 10.7 cm. All data are smoothed using twelve months running mean. From *[Swensmark 2000]*.

From **Fig. 41** it can be seen that the correlation of global cloud coverage with CR intensity is much better than with solar activity. Marsh and Swensmark *[Marsh and Swensmark 2000a]* came to conclusion that CR intensity relates well with low global cloud coverage, but not with high and middle clouds (see **Fig. 42**).

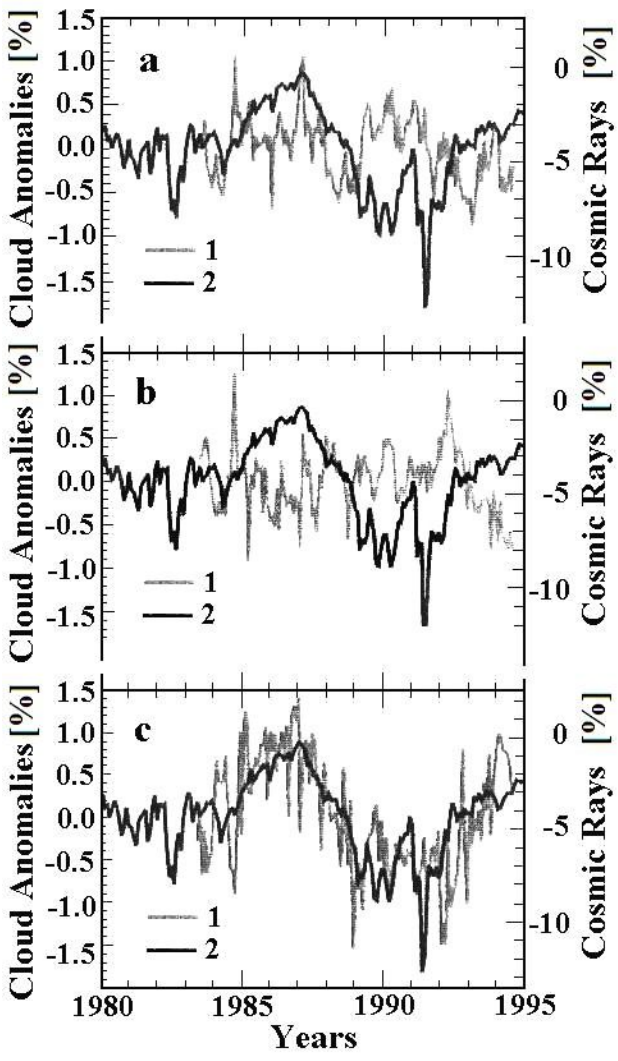

Fig. 42. CR intensity obtained at the Huancayo/Haleakala Neutron Monitor (normalized to October 1965, curve 2) in comparison with global average monthly cloud coverage anomalies (curves 1) at heights, H, for: **a** — high clouds, H > 6.5 km, **b** — middle clouds, 6.5 km >H > 3.2 km, and **c** — low clouds, H < 3.2 km. From *[Marsh and Swensmark 2000a]*.

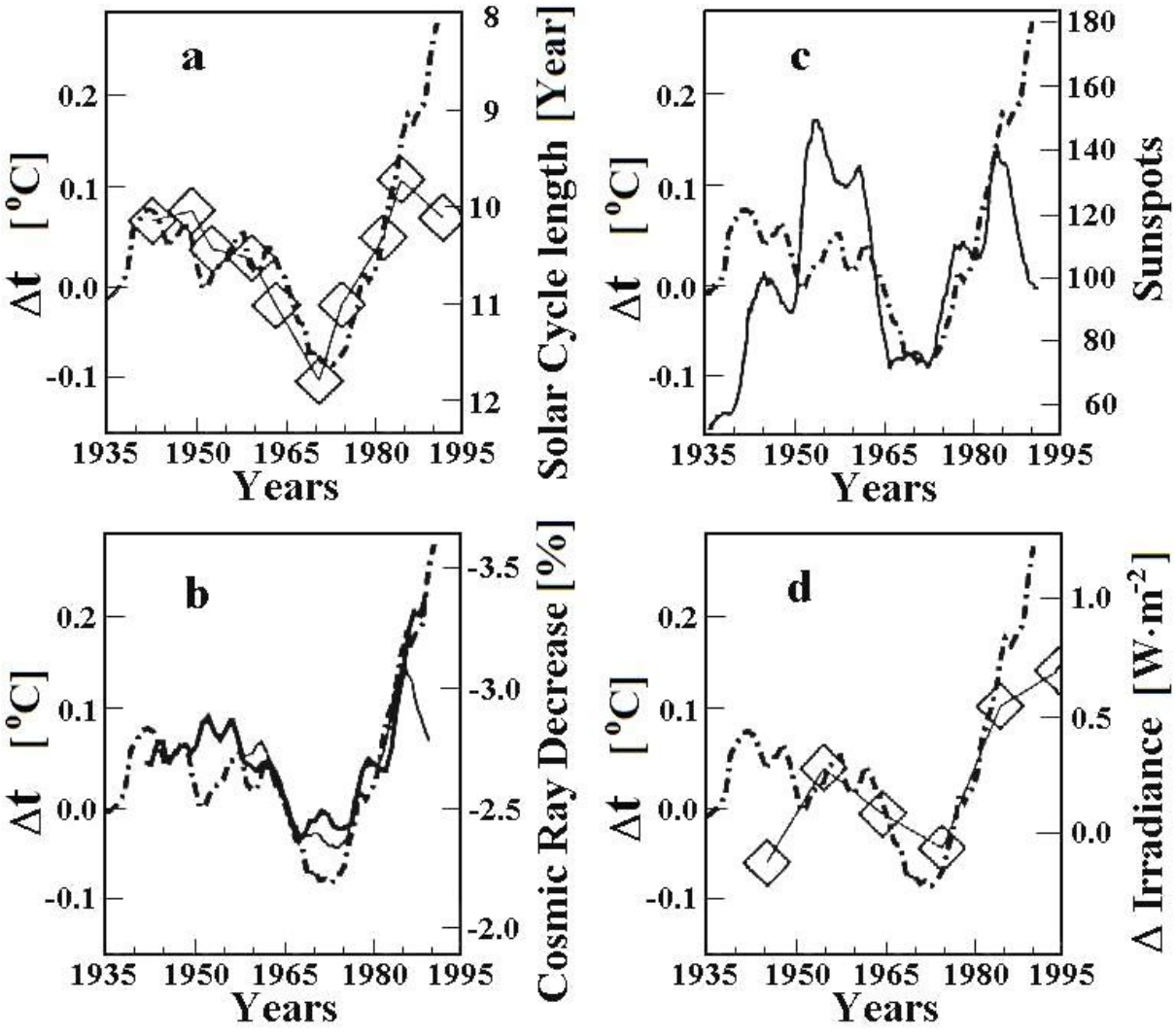

Fig. 43. Eleven year average Northern hemisphere marine and land air temperature anomalies, Δt, (broken curve) compared with: (**a**) unfiltered solar cycle length; (**b**) Eleven year average CR intensity (thick solid curve — from ion chambers 1937—1994, normalized to 1965, and thin solid curve — from Climax NM, normalized to ion chambers); (**c**) Eleven year average of sunspot numbers; and (**d**) decade variation in reconstructed solar irradiance from *[Lean et al. 1995]* (zero level corresponds to 1367 $W \cdot m^{-2}$). From *[Swensmark 2000]*.

It is important to note that low clouds lead, as rule, to the cooling of the atmosphere. It means that with increasing CR intensity and cloud coverage (see **Fig. 41**), we can expect the surface temperature to decrease. It is in good agreement with the situation shown in **Fig. 40** for the last thousand years, and with direct measurements of the surface temperature over the last four solar cycles (see section 2.5, below).

11.5. The influence of CR on the Earth's temperature

Fig. 43 shows a comparison of eleven year moving average Northern Hemisphere marine and land air temperature anomalies for 1935—1995 with CR intensity (constructed for Cheltenham/Fredericksburg for 1937—1975 and Yakutsk for 1953—1994, according to *[Ahluwalia 1997]* and Climax NM data, as well as with other parameters (unfiltered solar cycle length, sunspot numbers, and reconstructed solar irradiance). From **Fig. 43** one can see that the best correlation of global air temperature is with CR intensity, in accordance with the results described in sections 2.1—2.4 above. According to *[Swensmark 2000]*, the comparison of **Fig. 43** with **Fig. 41** shows that the increase of air temperature by 0.3°C corresponds to a decrease of CR intensity of 3.5% and a decrease of global cloudiness of 3%; this is equivalent to an increase of solar irradiance on the Earth's surface of about 1.5 $W.m^{-2}$ *[Rossow and Cairns 1995]* and is about 5 times bigger than the solar cycle change of solar irradiance, which as we have seen, s only 0.3 $W \cdot m^{-2}$.

11.6. CR influence on climate during Maunder minimum

Fig. 44 shows the situation in the Maunder minimum (a time when sunspots were very rare) for: solar irradiance *[Lean et al. 1992, 1995]*; concentration of the cosmogenic isotope ^{10}Be according to *[Beer et al. 1991]* (as a measure of CR intensity, see extended review in Chapter 10 in *[Dorman M2004]*); and reconstructed air surface temperature for the northern hemisphere *[Jones et al. 1998]*.

The solar irradiance is almost constant during the Maunder minimum and about 0.24% (or about 0.82 $W \cdot m^{-2}$) lower than the present value (see Panel **a** in **Fig. 44**), but CR intensity and air surface temperature vary in a similar manner — see above

sections; with increasing CR intensity there is a decrease in air surface temperature (see Panels **b** and **c** in **Fig. 44**). The highest level of CR intensity was between 1690—1700, which corresponds to the minimum of air surface temperature *[Mann et al. 1998]* and also to the coldest decade (1690—1700).

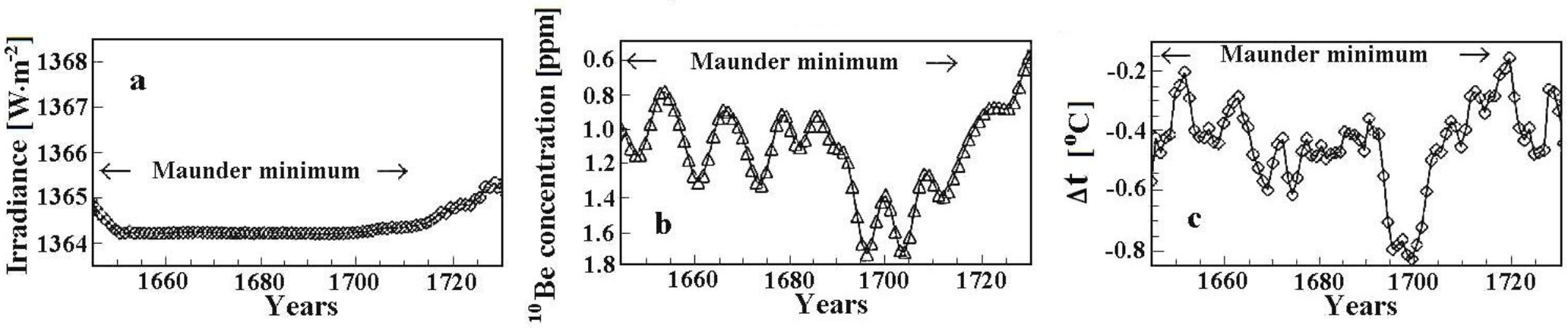

Fig. 44. Situation in the Maunder minimum: **a** — reconstructed solar irradiance *[Labitzke and Loon 1993]*; **b** — cosmogenic ^{10}Be concentration *[Beer et al. 1991]*; **c** - reconstructed relative change of air surface temperature, Δt, for the northern hemisphere *[Jones et al. 1998]*. From *[Swensmark 2000]*.

11.7. The connection between ion generation in the atmosphere by CR and total surface of clouds

The time variation of the integral rate of ion generation, q, (approximately proportional to CR intensity) in the middle latitude atmosphere at an altitude between 2–5 km was found by *[Stozhkov et al. 2001]* for the period January 1984–August 1990 using regular CR balloon measurements. The relative change in *q*, $\Delta q/q$, have been compared with the relative changes of the total surface of clouds over the Atlantic Ocean, $^{\Delta S/S}$, and are shown in **Fig. 45**: the correlation coefficient is 0.91 ± 0.04. This result is in good agreement with results described above (see panel **b** in **Fig. 43** and panel **c** in **Fig. 44**) and shows that there is a direct correlation between cloud cover and CR generated ions.

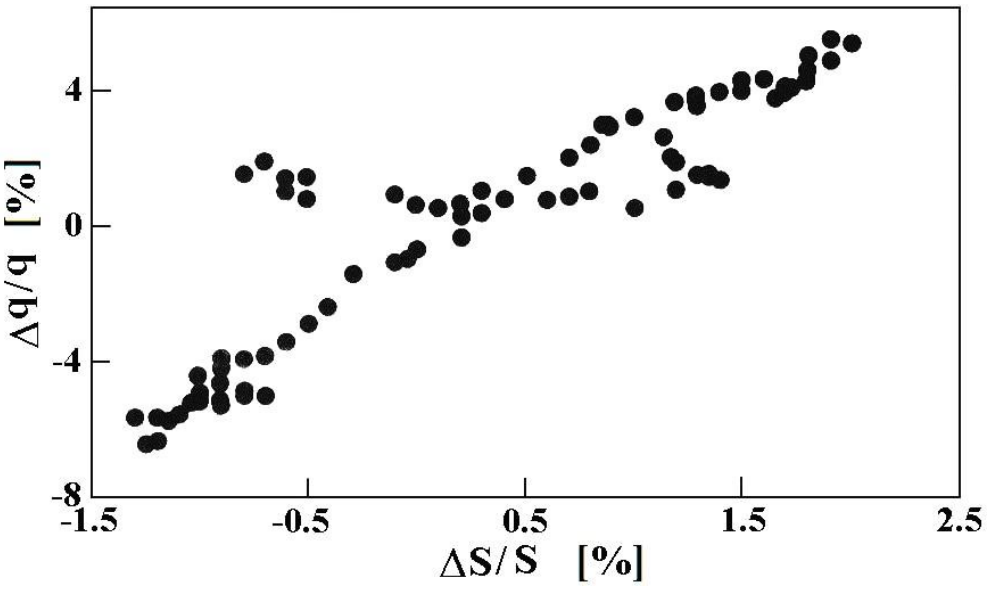

Fig. 45. The positive relationship between the relative changes of total clouds covering surface over Atlantic Ocean, $\Delta S/S$, in the period January 1984—August 1990 *[Swensmark and Friis-Christiansen 1997]* and the relative changes of integral rate of ion generation $\Delta q/q$ in the middle latitude atmosphere in the altitude interval 2–5 km. From *[Stozhkov et al. 2001]*.

11.8. The influence of big CR Forbush decreases and solar CR events on rainfall

A decrease of atmospheric ionization leads to a decrease in the concentration of charge condensation centers. In these periods, a decrease of total cloudiness and atmosphere turbulence together with an increase in isobaric levels is observed *[Veretenenko and Pudovkin 1994]*. As a result, a decrease of rainfall is also expected. Stozhkov *[Stozhkov et al. 1995a,b, 1996; Stozhkov 2002]* analyzed 70 events of CR Forbush decreases (defined as a rapid decrease in observed galactic CR intensity, and caused by big geomagnetic storms) observed in 1956—1993and compared these events with rainfall data over the former USSR. It was found that during the main phase of the Forbush decrease, the daily rainfall levels decreases by about 17%. Similarly, Todd and Kniveton *[Todd and Kniveton 2001, 2004]* investigating 32 Forbush decreases events over the period 1983—2000found reduced cloud cover of 12—18%.

During big solar CR events, when CR intensity and ionization in the atmosphere significantly increases, an inverse situation is expected and the increase in cloudiness leads to an increase in rainfall. A studies *[Stozhkov et al. 1995a,b, 1996; Stozhkov 2002]*, involving 53 events of solar CR enhancements, between 1942—1993 showed a positive increase of about 13% in the total rainfall over the former USSR.

11.9. The influence of geomagnetic disturbances and solar activity on the climate through energetic particle precipitation from inner radiation belt

The relationship between solar and geomagnetic activity and climate parameters (cloudiness, temperature, rainfall, etc) was considered above and is the subject of much ongoing research. The clearly pronounced relationship observed at high and middle

latitudes, is explained by the decrease of galactic CR intensity (energies in the range of MeV and GeV) with increasing solar and geomagnetic activity, and by the appearance of solar CR fluxes ionizing the atmosphere *[Tinsley and Deen 1991]*. This mechanism works efficiently at high latitudes, because CR particles with energy up to 1 GeV penetrate this region more easily to due to its very low cutoff rigidity. Near the equator, in the Brazilian Magnetic Anomaly (BMA) region, the main part of galactic and solar CR is shielded by a geomagnetic field. This field is at an altitude of 200—300 km and contains large fluxes of energetic protons and electrons trapped in the inner radiation belt. Significant magnetic disturbances can produce precipitation of these particles and subsequent ionization of the atmosphere. The influence of solar-terrestrial connections on climate in the BMA region was studied by *[Pugacheva et al. 1995]*. Two types of correlations were observed: 1) a significant short and long time scale correlation between the index of geomagnetic activity Kp and rainfall in Sao Paulo State; 2) the correlation-anti-correlation of rainfalls with the 11 and 22 year cycles of solar activity for 1860—1990 in Fortaleza. **Fig. 46** shows the time relationship between Kp-index and rain in Campinas (23° S, 47° W) and in Ubajara (3° S, 41° W), during 1986. From **Fig. 46**, it can be seen that, with a delay of 5—11 days, almost every significant (> 3.0) increase of the Kp-index is accompanied by an increase in rainfall. The effect is most noticeable at the time of the great geomagnetic storm of February 8 1986, when the electron fluxes of inner radiation belt reached the atmosphere between 18—21 February *[Martin et al. 1995]* and the greatest rainfall of the 1986 was recorded on 19 February. Again, after a series of solar flares, great magnetic disturbances were registered between 19—22 March, 1991. On the 22 March the Sao Paolo meteorological station showed the greatest rainfall of the year.

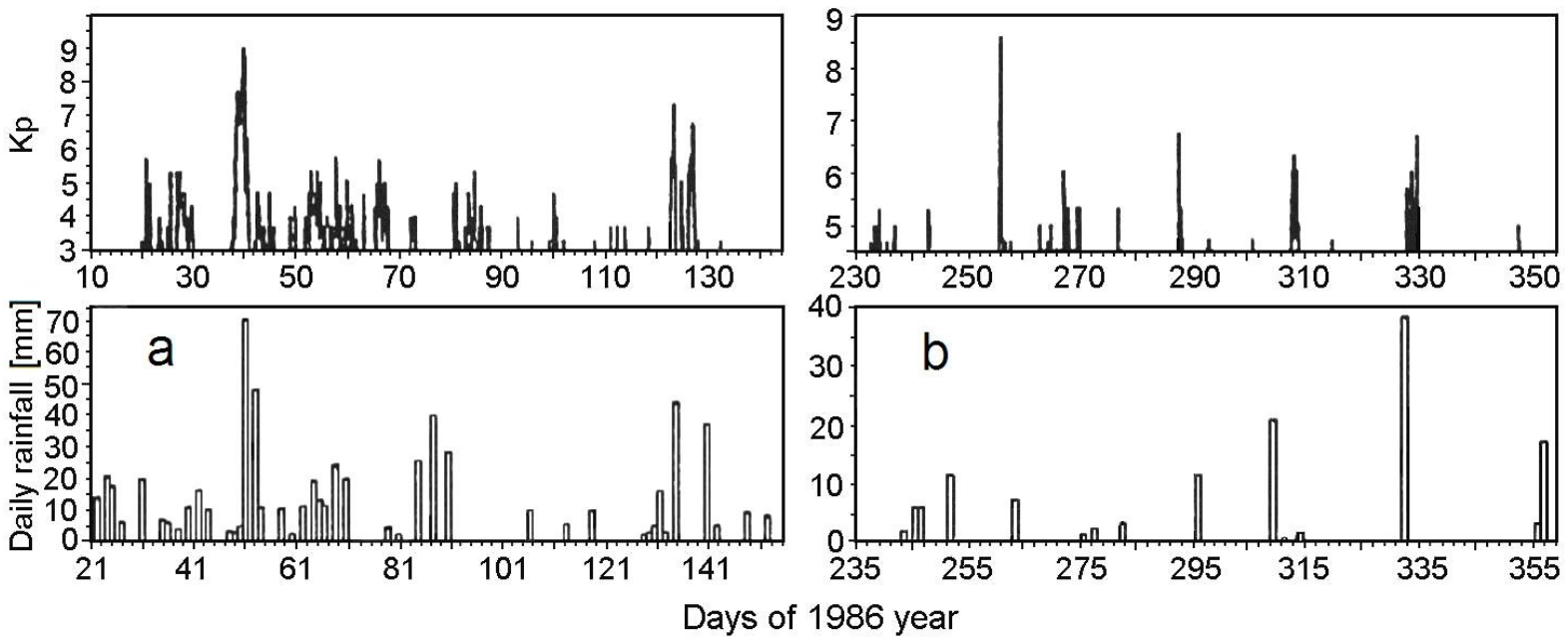

Fig. 46. The Kp-index of geomagnetic activity (top panels) and rainfall level (bottom panels) in Campinas (left panels **a**) and in Ubajara (right panels **b**) in 1986. According to *[Pugacheva et al. 1995]*.

The relationship between long term variations of annual rainfall at Campinas, the Kp-index and sunspot numbers are shown in **Figs. 47** and **48**.

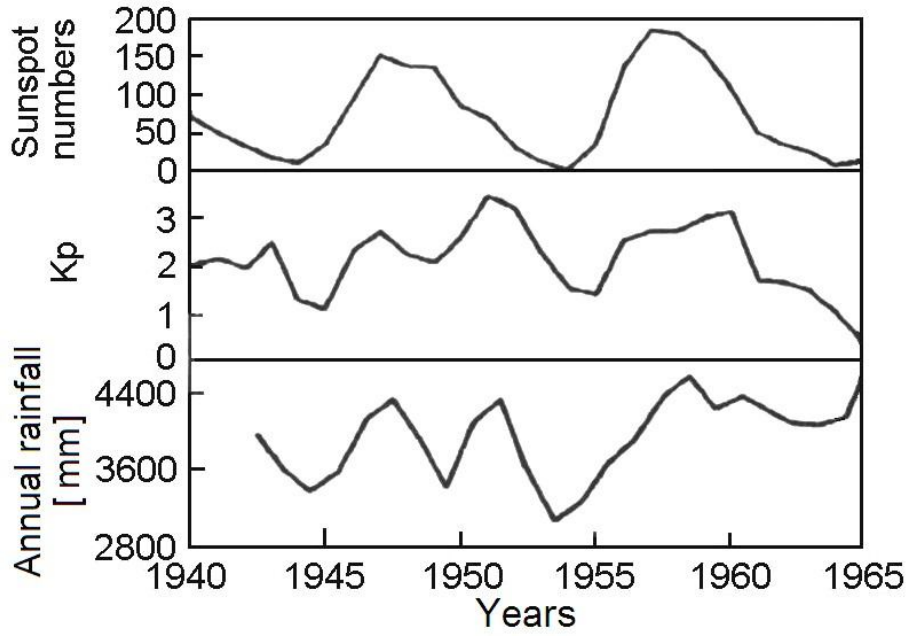

Fig. 47. Long-term variations of rainfalls (Campinas, the bottom panel) in comparison with variations of solar and geomagnetic activity (the top and middle panels, respectively) for 1940—1965. From *[Pugacheva et al. 1995]*.

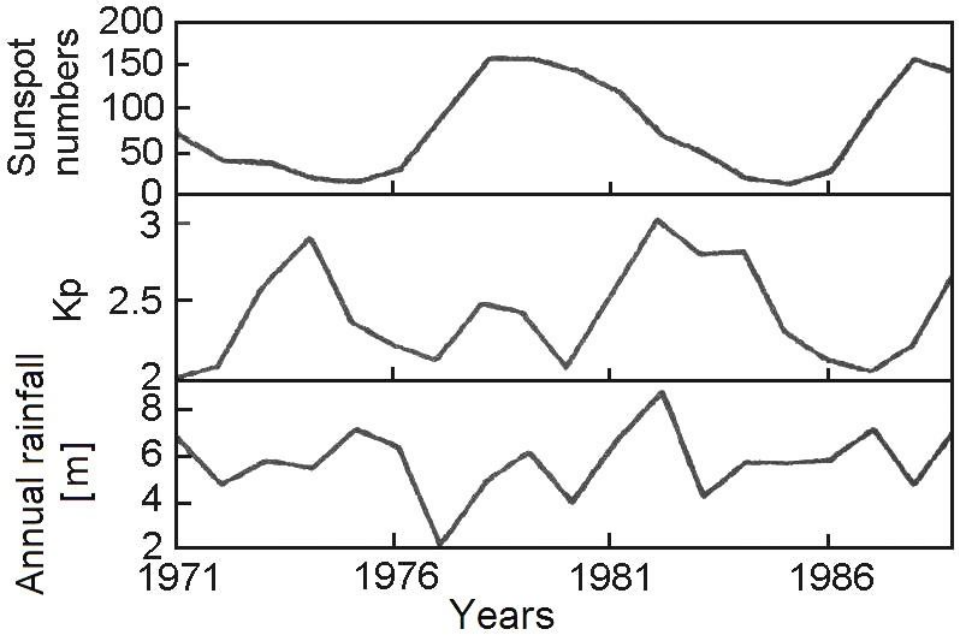

Fig. 48. The same as in **Fig. 47**, but for 1971—1990. From Pugacheva et al. (1995).

Figs. 47 and **48** show the double peak structure of rainfall variation compared to the Kp-index. Only during the 20th solar cycle (1964—1975), weakest of the shown 6 cycles, an anti-correlation between rainfalls and sunspot numbers is observed in most of Brazil. The Kp — rainfall correlation is more pronounced in the regions connected with magnetic lines occupied by trapped particles.

In Fortaleza (4° S, 39° W), located in an empty magnetic tube (L = 1.054), it is the other kind of correlation (see **Fig. 49**).

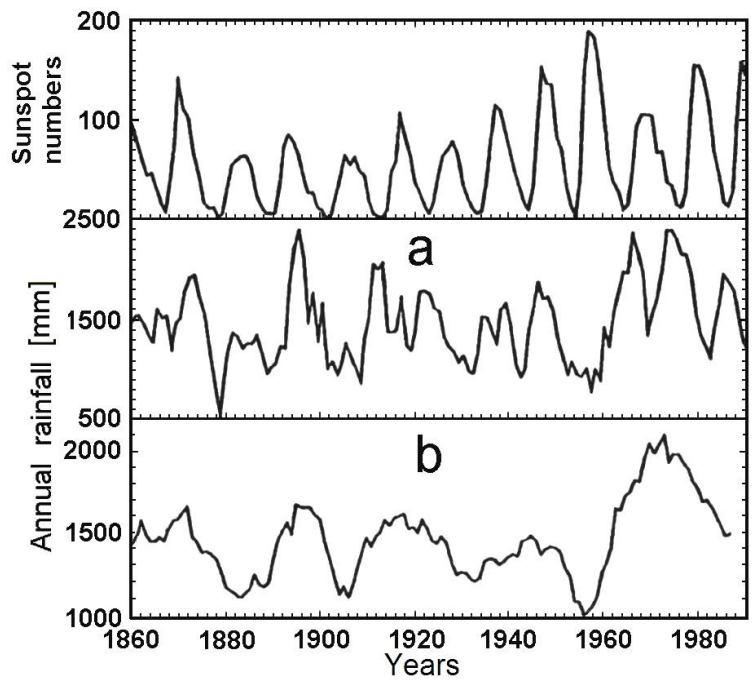

Fig. 49. The comparison of yearly sunspot numbers long-term variation (the top panel) with 3 years and 11 years running averaged rainfalls (panels **a** and **b**, respectively) in Fortaleza (4°S, 39°W) during 1860—1990. From *[Pugacheva et al. 1995]*.

From **Fig. 49** can be seen that a correlation exists between sunspot numbers and rainfall between 1860—1900 (11^{th}—13^{th} solar cycles) and 1933—1954 (17^{th} and 18^{th} cycles). The anti-correlation was observed during 1900—1933 (cycles 14^{th}—16^{th}) and during 1954—1990 (cycles 19^{th}—21^{th}). As far as sunspot numbers mainly anti-correlate with the galactic CR flux, an anti-correlation of sunspot numbers with rainfalls could be interpreted as a correlation of rainfalls with the CR. The positive and negative phases of the correlation interchange several times during the long time interval 1860—1990, that was observed earlier in North America *[King 1975]*. Some climate events have a 22 years periodicity similar to the 22 years solar magnetic cycle. The panel b in **Fig. 49** demonstrate 22 years periodicity of 11 years running averaged rainfalls in Fortaleza. The phenomenon is observed during 5 periods from 1860 to 1990. During the 11^{th}—16^{th} solar cycles (from 1860 until 1930), the maxima of rainfalls correspond to the maxima of sunspot numbers of odd solar cycles 11^{th}, 13^{th}, 15^{th} and minima of rainfalls correspond to maxima of even solar cycles 12^{th}, 14^{th}, 16^{th}. During the 17^{th} solar cycle the phase of the 22 years periodicity is changed to the opposite and the sunspot number maxima of odd cycles 19^{th} and 21^{th} correspond to the minima of rainfall. The effect is not pronounced (excluding years 1957—1997) in Sao Paolo.

The difference in results obtained in *[Stozhkov 2002; Todd and Kniveton 2001, 2004; Pugacheva et al. 1995]* can be easy understand if we take into account the large value of the cutoff rigidity in the BMA region. This is the reason why the variations in galactic and solar CR intensity in the BMA region, are not reflected in the ionization of the air and hence do not influenced the climate. However in the BMA region other mechanism of solar and magnetic activity can influence climatic parameters such as energetic particle precipitation coming from the inner radiation belt.

11.10. On the possible influence of galactic CR on formation of cirrus hole and global warming

According to *[Ely and Huang 1987; Ely et al. 1995]*, there are expected variations of upper tropospheric ionization caused by long-term variations of galactic CR intensity. These variations have resulted in the formation of the cirrus hole (a strong latitude dependent modulation of cirrus clouds). The upper tropospheric ionization is caused, largely, by particles with energy smaller than 1 GeV but bigger than about 500 MeV. In **Fig. 50** is shown the long term modulation of the difference between NM at Mt. Washington and Durham for protons with kinetic energy 650—850 MeV.

Fig. 50 clearly shows the 22 years modulation of galactic CR intensity in the range 650—850 MeV with an amplitude of more than 3%. Variations of upper tropospheric ionization do have some influence on the cirrus covering and the "cirrus hole" is expected to correspond to a decrease in CR intensity.

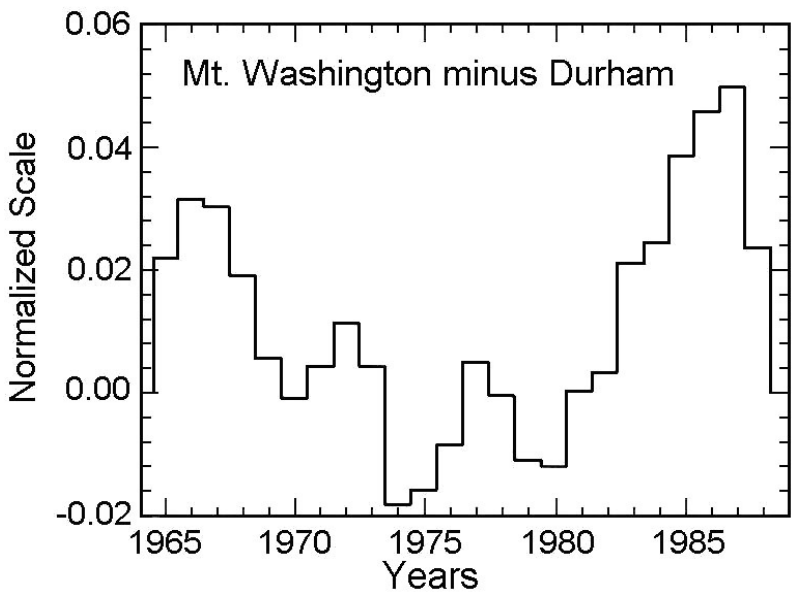

Fig. 50. The observed 22 years modulation of galactic CR between 1.24—1.41 GV rigidity (i.e., protons with kinetic energy between 650—850 MeV, ionizing heavily in the layer 200—300g/cm^2). From *[Ely et al. 1995]*.

According to *[Ely et al. 1995]*, the "cirrus hole" was observed in different latitude zones over the whole world between 1962 and 1971, centered at 1966 (see **Fig. 51**).

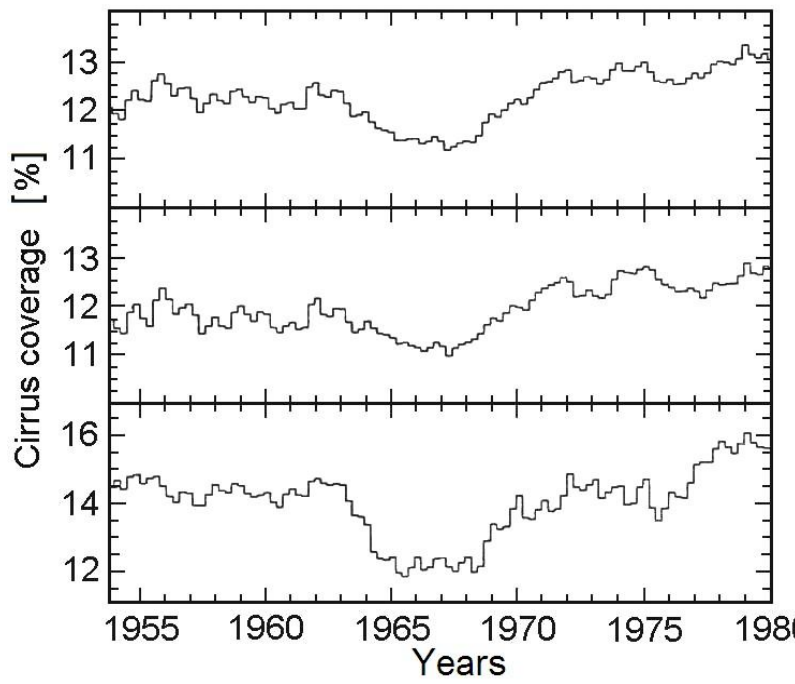

Fig. 51. The 'cirrus hole' of the 1960's for: the whole world (the top panel); the equatorial zone (30°S—30°N; middle panel); the northern zone (bottom panel). From *[Ely et al. 1995]*.

Fig. 51 gives the cirrus cloud cover data over a 25 a period, for the whole world, the equatorial zone (30°S—30°N) and the northern zone (30°N—90°N), showing fractional decreases in cirrus coverage of 7%, 4%, and 17%, respectively. The decrease of cirrus covering leads to an increase in heat loss to outer space (note, that only a 4% change in total cloud cover is equivalent to twice the present greenhouse effect due to anthropogenic carbon dioxide). The influence of cirrus hole in the northern latitude zone (30°N—90°N), where the cirrus covering was reduced by 17%, is expected to be great (this effect of the cirrus hole is reduced in summer by the increase of lower clouds resulting in enhanced insulation) The low temperatures produced from mid to high latitude significantly increase the pressure of the polar air mass and cause frequent 'polar break troughs' at various longitudes in which, for example, cold air from Canada may go all the way to Florida and freeze the grapefruit *[Ely et al. 1995]*. However, when the cirrus hole is not present, the heat loss from mid to high latitudes is much less, and the switching of the circulation patterns (Rossby waves) is much less frequent.

11.11. Description of long-term galactic CR variation by both convection-diffusion and drift mechanisms with possibility of forecasting of some part of climate change in near future caused by CR

It was shown in previous sections that CR might be considered as sufficient links determined some part of space weather influence on the climate change. From this point of view, it is important to understand mechanisms of galactic CR long-term variations and on this basis to forecast expected CR intensity in near future. In *[Dorman 2005a,b, 2006]* it was made on basis of monthly sunspot numbers with taking into account time-lag between processes on the Sun and situation in the interplanetary space as well as the sign of general magnetic field (see **Fig. 52**); in *[Belov et al. 2005]* – mainly on basis of monthly data of solar general magnetic field (see **Fig. 53**).

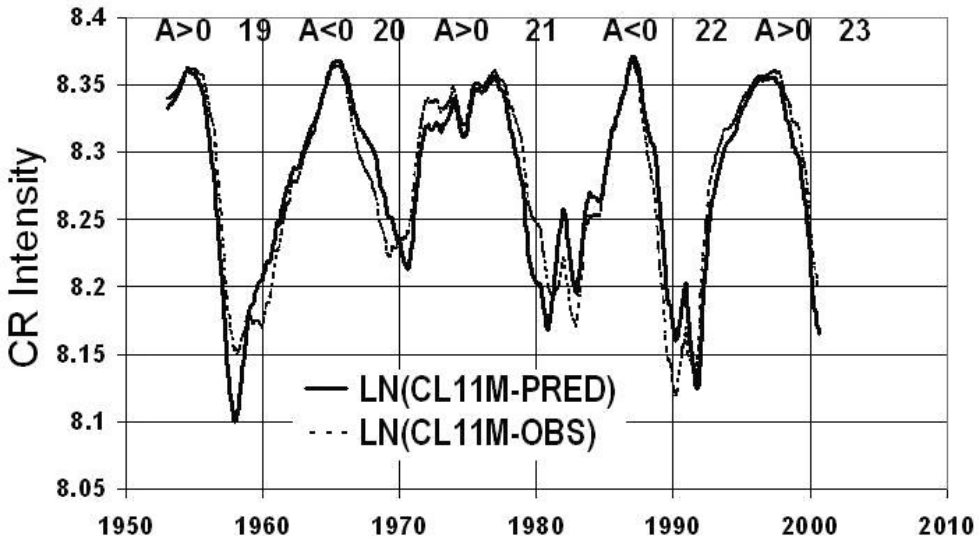

Fig. 52. Comparison of observed by Climax neutron monitor CR intensity averaging with moving period eleven month LN(CL11M-OBS) with predicted on the basis of monthly sunspot numbers from model of convection-diffusion modulation, corrected on drift effects LN(CL11M-PRED). Correlation coefficient between both curves 0.97. From *[Dorman 2006]*.

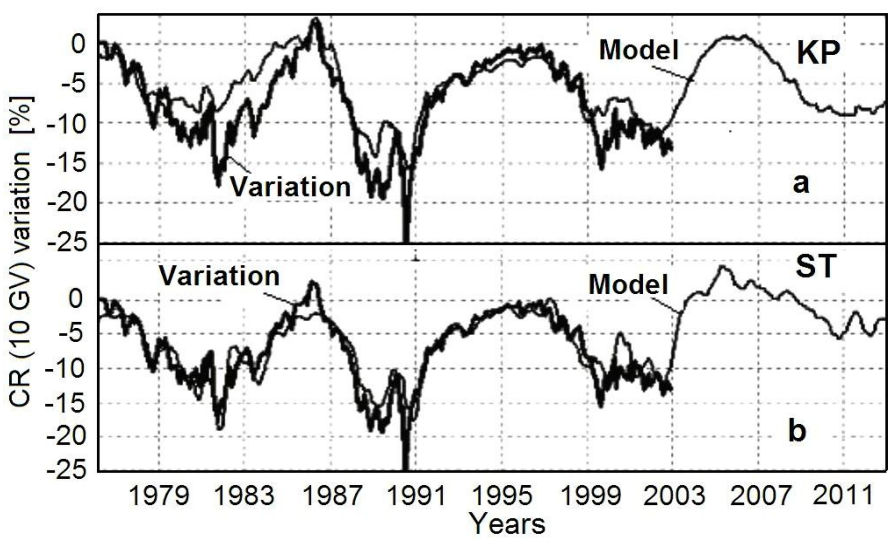

Fig. 53. The forecast of galactic CR behavior based on the predicted values of the global characteristics of the solar magnetic field, thick line — data of CR intensity observations (Moscow NM), thin line — the predicted CR variation up to 2013 based on data of Kitt Peak Observatory (upper panel) and based on data of Stanford Observatory (bottom panel). From *[Belov et al. 2005]*.

From **Fig. 52** follows that in the frame of used in *[Dorman 2005a,b, 2006]* convection-diffusion and drift models can be determined with very good accuracy expected galactic CR intensity in the past (when monthly sunspot numbers are known) as

well as behavior of CR intensity in future if monthly sunspot numbers can be well forecasted. According to *[Belov et al. 2005]*, the same can be made with good accuracy on the basis of monthly data on the solar general magnetic field (see **Fig. 53**). Let us note that described above results obtained in *[Dorman 2005a,b, 2006]*; and *[Belov et al. 2005]* give possibility to forecast some part of climate change connected with CR.

11.12. Influence of long-term variation of main geomagnetic field on global climate change through CR cutoff rigidity variation

The sufficient change of main geomagnetic field leads to change of planetary distribution of cutoff rigidities R_c and to corresponding change of the i-th component of CR intensity $N_i(R_c,h_o)$ at some level h_o in the Earth's atmosphere $\Delta N_i(R_c,h_o)/N_{io} = -\Delta R_c W_i(R_c,h_o)$ where $W_i(R_c,h_o)$ is the coupling function (see details in Chapter 3 in *[Dorman M2004]*). Variations of CR intensity caused by change of R_c are described in detail in Chapter 7 in *[Dorman M2009]*, and here we will demonstrate results of *[Shea and Smart 2003]* on R_c changing for the last 300 and 400 years (see **Fig. 54** and **Table 5**, correspondingly).

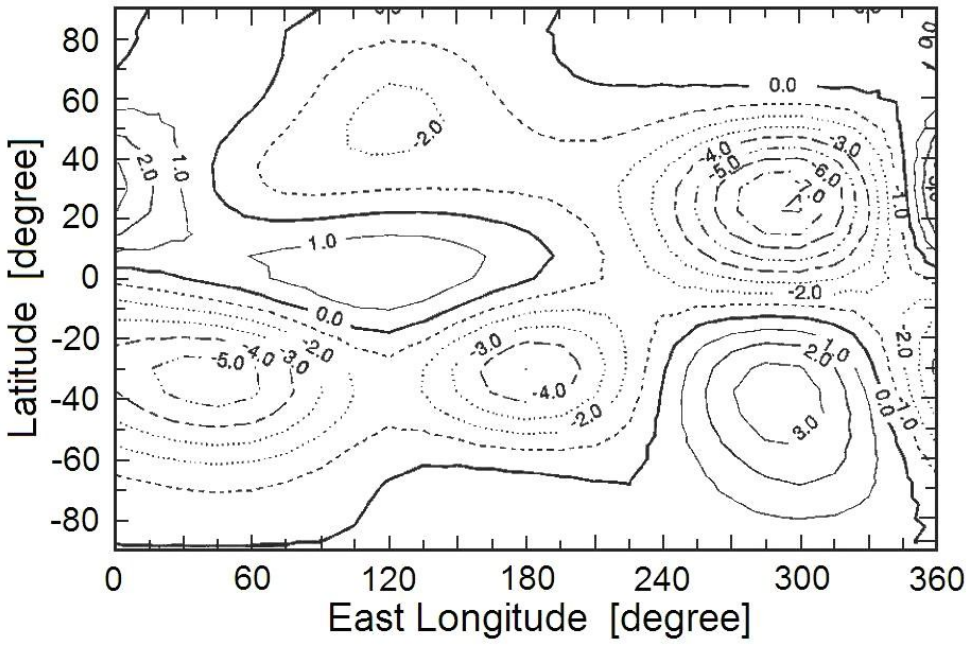

Fig. 54. Contours of the change in vertical cutoff rigidity values (in GV) between 1600 and 1900. Full lines reflect positive trend (increasing of cutoff rigidity from 1600 to 1900); dotted lines reflect negative trend. According to *[Shea and Smart 2003]*.

Table 5

Vertical cutoff rigidities (in GV) for various epochs 1600, 1700, 1800, 1900, and 2000, as well as change from 1900 to 2000 owed to changes of geomagnetic field

According to *[Shea and Smart 2003]*

Lat.	Long. (E)	Epoch 2000	Epoch 1900	Epoch 1800	Epoch 1700	Epoch 1600	Change 1900−2000	Region
55	30	2.30	2.84	2.31	1.49	1.31	−0.54	Europe
50	0	3.36	2.94	2.01	1.33	1.81	+0.42	Europe
50	15	3.52	3.83	2.85	1.69	1.76	−0.31	Europe
40	15	7.22	7.62	5.86	3.98	3.97	−0.40	Europe
45	285	1.45	1.20	1.52	2.36	4.1	+0.25	N. Amer.
40	255	2.55	3.18	4.08	4.88	5.89	−0.63	N. Amer.
20	255	8.67	12.02	14.11	15.05	16.85	−3.35	N. Amer.
20	300	10.01	7.36	9.24	12.31	15.41	+2.65	N. Amer.
50	105	4.25	4.65	5.08	5.79	8.60	−0.40	Asia
40	120	9.25	9.48	10.24	11.28	13.88	−0.23	Asia
35	135	11.79	11.68	12.40	13.13	14.39	+0.11	Japan
−25	150	8.56	9.75	10.41	11.54	11.35	−1.19	Australia
−35	15	4.40	5.93	8.41	11.29	12.19	−1.53	S. Africa
−35	300	8.94	12.07	13.09	10.84	8.10	−3.13	S. Amer.

Table 5 shows that the change of geomagnetic cutoffs, in the period 1600 to 1900, is not homogeneous: of the 14 selected regions, 5 showed increasing cutoffs with decreasing CR intensity, and 9 regions showed decreasing cutoffs with increasing CR intensity. From **Table 5** can be seen also that at present time (from 1900 to 2000) there are sufficient change in cutoff rigidities: decreasing (with corresponding increasing of CR intensity) in 10 regions, and increasing (with corresponding decreasing of CR intensity) in 3 regions. These changes give trend in CR intensity change what we need to take into account together with CR 11 and 22 years modulation by solar activity, considered in section 11.11.

11.13. Atmospheric ionization by CR: the altitude dependence and planetary distribution

The main process in the link between CR and cloudiness is the air ionization which triggers chemical processes in the atmosphere. **Fig. 55** illustrates the total ionization of atmosphere by galactic CR (primary and secondary) as a function of altitude.

The planetary distribution of ionization at the altitude of 3 km according to *[Usoskin et al. 2004]*, is shown in *Fig. 56* for the year 2000.

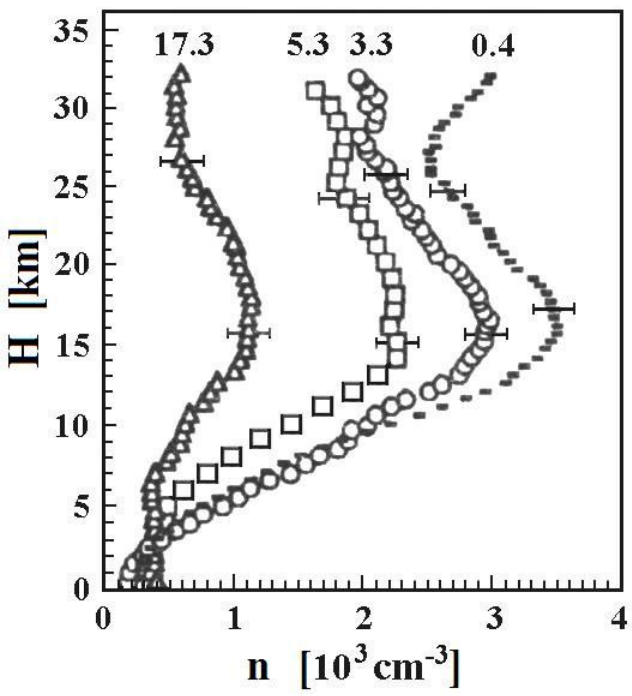

Fig. 55. The ion concentration, n, profiles as a function of altitude, H, for different geomagnetic cutoff rigidities (numbers at the top are in units of GV). The horizontal bars indicate the standard deviations. From *[Ermakov et al. 1997]*.

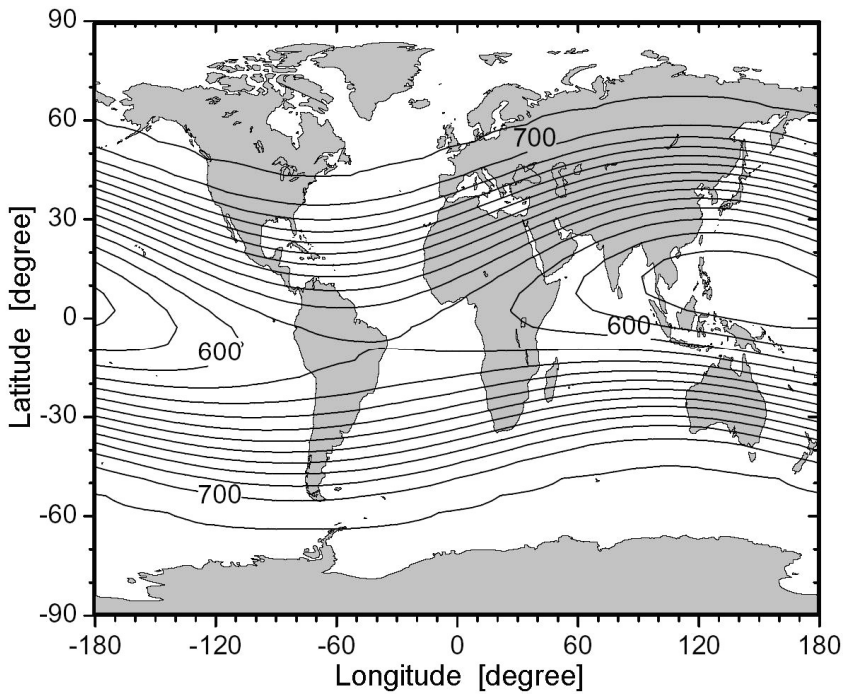

Fig. 56. Planetary distribution of calculated equilibrium galactic CR induced ionization at the altitude of 3 km (h = 725 g/cm^2) for the year 2000. Contour lines are given the number of ion pairs per cm^3 in steps of 10 cm^{-3}. From *[Usoskin et al. 2004]*.

11.14. Project 'Cloud' as an important step in understanding the link between CR and cloud formation

The many unanswered questions in understanding the relationship between CR and cloud formation is being investigated by a special collaboration, within the framework of European Organization for Nuclear Research, involving 17 Institutes and Universities *[Fastrup et al. 2000]*. The experiment, which is named 'CLOUD', is based on a cloud chamber (which is designed to duplicate the conditions prevailing in the atmosphere) and 'cosmic rays' from CERN Proton Synchrotron. The Project will consider possible links between CR, variable Sun intensities and the Earth's climate change (see **Fig. 57**).

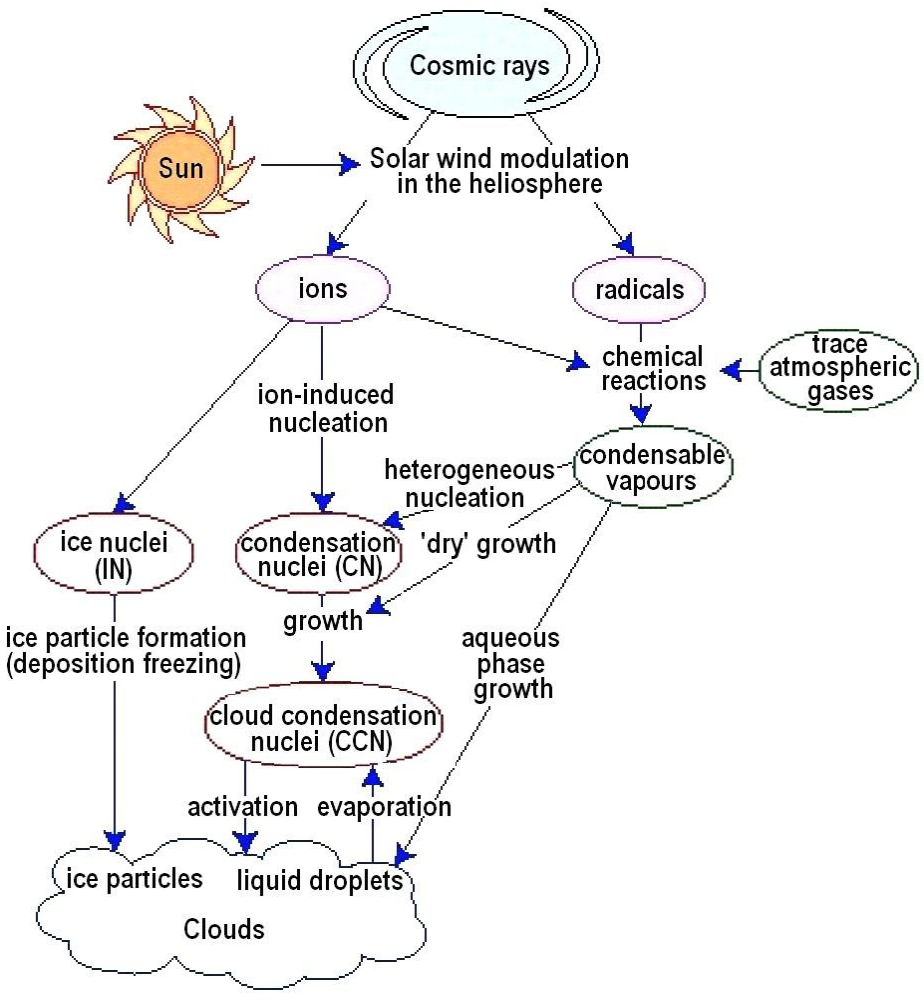

Fig. 57. Possible paths of solar modulated CR influence on different processes in the atmosphere leading to the formation of clouds and their influence on climate. From *[Fastrup et al. 2000]*.

11.15. The influence on the Earth's climate of the solar system moving around the galactic centre and crossing Galaxy arms

The influence of space dust on the Earth's climate has been reviewed in *[Veizer et al. 2000]*. **Fig. 58** shows the changes of planetary surface temperature for the last 520 Ma according to *[Veizer et al. 2000]*. These data were obtained from the paleoenvironmental records. During this period the solar system crossed Galaxy arms four times. In doing so, there were four alternating warming and cooling periods with planetary temperature changes of more than 5°C.

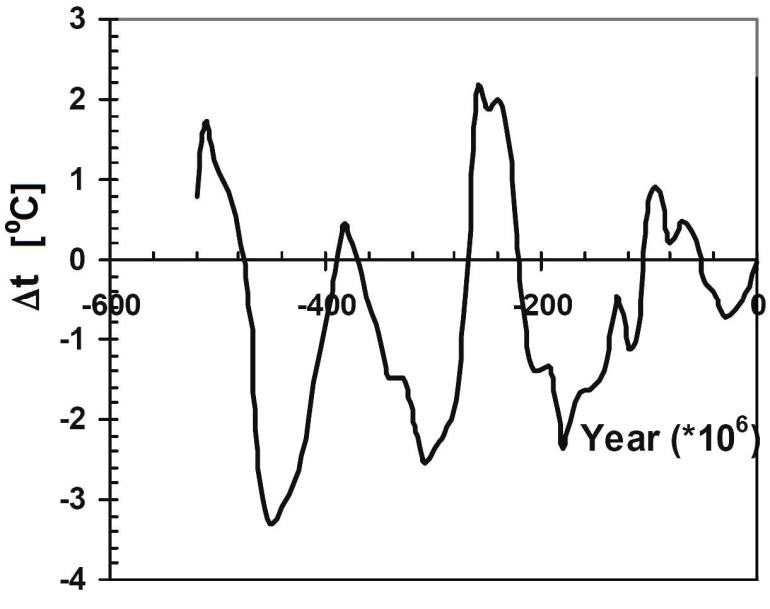

Fig. 58. Changes of air temperature, Δt, near the Earth's surface for the last 520 million years according to the pale-environmental records *[Veizer et al. 2000]*. From *[Ermakov et al. 2006]*.

The amount of matter inside the galactic arms is more than on the outside. The gravitation influence of this matter attracts the inflow of comets from Oort's cloud to solar system *[Fuhrer et al. 1999; Maseeva 2004]*. It results in an increase in concentration of interplanetary dust in zodiac cloud and a cooling of the Earth's climate *[Hansen et al. 1999]*.

11.16. The influence of molecular-dust galactic clouds on the Earth's climate

The solar system moves relative to interstellar matter with a velocity about 30 km/s and sometimes passes through molecular-dust clouds. During these periods, we can expect a decrease in sea level air temperature. According to *[Dorman 2008b]*, the prediction of the interaction of a dust-molecular cloud with the solar system can be performed by measurements of changes in the galactic CR distribution function. From the past, we know that the dust between the Sun and the Earth has led to decreases of solar irradiation flux resulting in reduced global planetary temperatures (by 5—7°C). The plasma in a moving molecular dust cloud contains a frozen-in magnetic field; this moving field will modify the stationary galactic CR distribution outside the Heliosphere. The change in the distribution function can be significant, and it should be possible to identify these changes when the distance between the cloud and the Sun becomes comparable with the dimension of the cloud. The continuous observation of the time variation of CR distribution function for many years should make it possible to determining the direction, geometry and the speed of the dust-molecular cloud relative to the Sun. Therefore, it should, in future, be possible to forecast climatic changes caused by this molecular-dust cloud.

Fig. 59 shows the temperature changes at the Antarctic station Vostok (bottom curve), which took place over the last 420,000 years according to *[Petit et al. 1999]*. These data were obtained from isotopic analysis of O and H extracted from the ice cores at a depth 3,300 m. It is seen from **Fig. 59** that during this time the warming and cooling periods changed many times and that the temperature changes amounted up to 9 °C. Data obtained from isotope analysis of ice cores in Greenland, which cover the last 100,000 years *[Fuhrer et al. 1999]*, confirm the existence of large changes in climate.

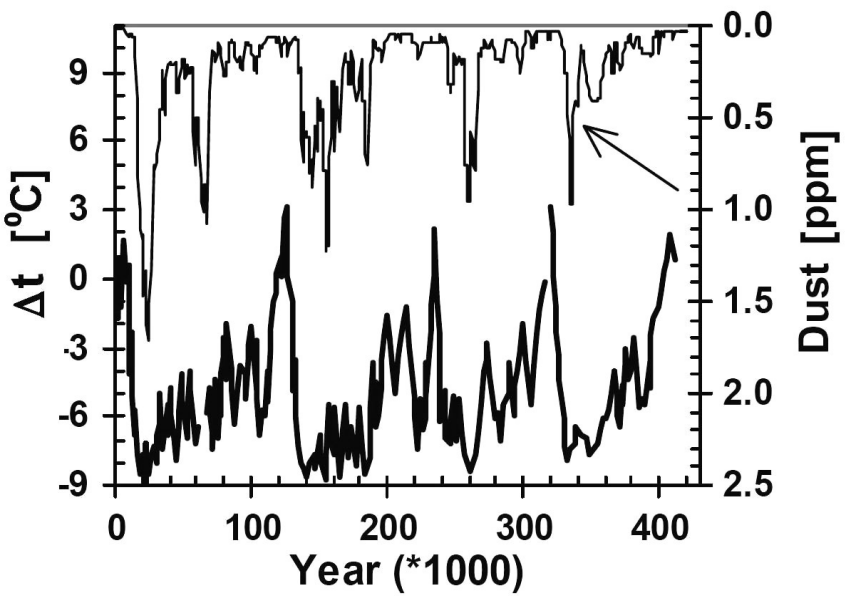

Fig. 59. Changes of temperature, Δt, relative to modern epoch (bottom thick curve) and dust concentration (upper thin curve) over the last 420 000 years *[Petit et al. 1999]*. From *[Ermakov et al. 2006]*.

11.17. The influence of interplanetary dust sources on the Earth's climate and forecasting for the next half-century

According to *[Ermakov et al. 2006a,b]*, the dust of zodiac cloud is a major contributory factor to climate changes in the past and at the present time. The proposed mechanism of cosmic dust influence is as follows: dust from interplanetary space enters the Earth's atmosphere during the yearly rotation of the Earth around the Sun. The space dust participates in the processes of cloud formation. The clouds reflect some part of solar irradiance back to space. In this way, the dust influences climate. The main sources of interplanetary dust are comets, asteroids, and meteor fluxes. The rate of dust production is continually changing. The effect of volcanic dust on the Earth's air temperature is illustrated in **Fig. 60** *[Hansen et al. 1999]*.

According to *[Ermakov et al. 2006a]*, the spectral analysis of global surface temperature during 1880—2005 shows the presence of several spectral lines that can be identified with the periods of meteor fluxes, comets, and asteroids. The results of analysis have been used in *[Ermakov et al. 2006a,b]* to predict changes in climate over the next half-century: the interplanetary dust factor of cooling in the next few decades will be more important than the warming from greenhouse effect (see **Fig. 61**).

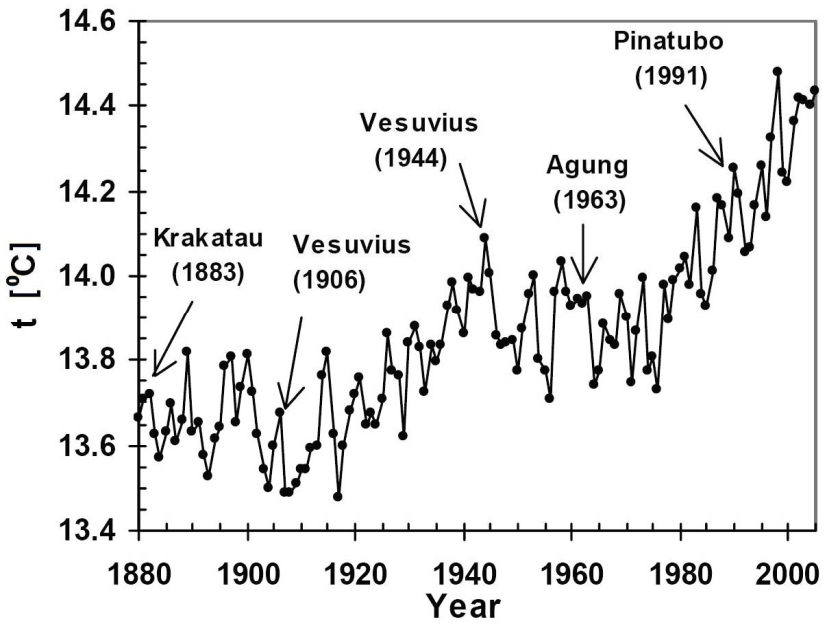

Fig. 60. Yearly average values of the global air temperature, *t*, near the Earth's surface for the period from 1880 to 2005 according to *[Hansen et al. 1999]*. Arrows show the dates of the volcano eruptions with the dust emission to the stratosphere and short times cooling after eruptions. From *[Ermakov et al. 2006a]*.

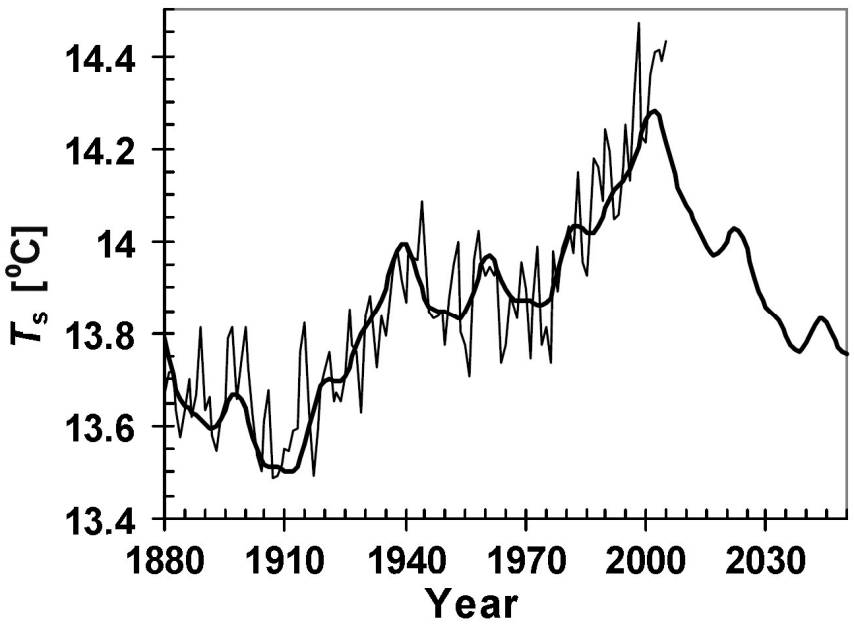

Fig. 61. Forecasting of the planetary air-surface temperature for the next half-century. Thin line — measurements, thick line — calculated based on main harmonics. According to *[Ermakov et al. 2006a,b]*.

11.18. Space factors and global warming

It is now commonly thought of that the current trend of the global warming is causally related to the accelerating consumption of fossil fuels by the industrial nations. However, it has been suggested that this warming is a result of a gradual increase of solar and magnetic activity over the last 100 years. According to *[Pulkkinen et al. 2001]*, as shown in **Fig. 62**, the solar and magnetic activity has been increasing since the year 1900 with decreases in 1970 and post 1980. This figure shows that the aa index of geomagnetic activity (a measure of the variability of the interplanetary magnetic field, IMF), varies, almost in parallel, with the global temperature anomaly.

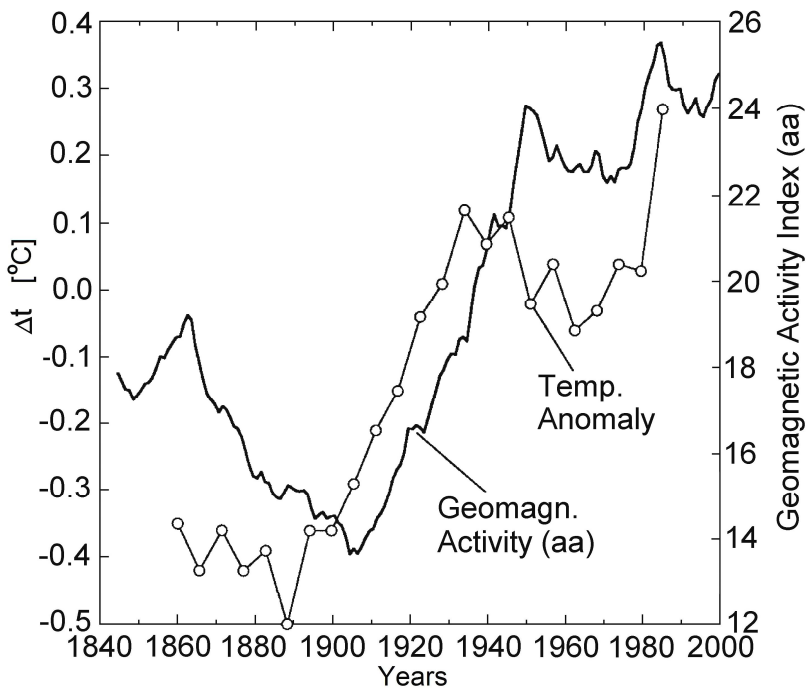

Fig. 62. The geomagnetic activity (index aa) at the minimum of solar activity variation of the global temperature anomaly, Δt, from 1840 to 2000. From *[Pulkkinen et al. 2001]*.

It has been well established that the brightness of the Sun varies in proportion to solar activity. The brightness changes are very small and cannot explain all of the present global warming. However, the gradual increase of solar activity over the last hundred years has been accompanied by a gradual decrease of CR intensity in interplanetary space *[Lockwood et al. 1999]*. The direct measurements of CR intensity on the ground by the global network of neutron monitors (NM) as well as regular CR intensity measurements from balloons in the troposphere and stratosphere over a period of more than 40 a, show that there is a small negative trend of galactic CR intensity *[Stozhkovet al. 2000]* of about 0.08% per year. Extrapolating this trend to a hundred years, it gives a CR intensity decrease on 8%. From **Fig. 41** it can be seen that the decreasing of CR intensity by 8% will lead to a decrease of cloud coverage of about 2%. According to *[Dickinson 1975]*, decreasing cloud coverage by 2% corresponds to increasing the solar radiation falling on the Earth by about 0.5%. Using this information, *[Stozhkov et al. 2001]* concluded that the observed increase of average planetary ground temperature of 0.4—0.8°C over the last 100 years, may be a result of this negative trend of CR intensity. Sakurai *[Sakurai 2003]* came to the same conclusion on the basis of analyzing data of solar activity and CR intensity.

11.19. Discussion on CR and other space factors effect the earth's Climate

Many factors from space and from anthropogenic activities influenced the Earth's climate. The initial response is that space factors are unlikely to be responsible for most of our present climate change. However, it is important that all possible space factors be considered, and from an analysis of past climate changes, we can identify our present phase and can predict future climate change. During the last several hundred million years, the Sun has rotated around the galactic centre several times with resultant climate changes. For example, considering the effects due to galactic molecular-dust concentrated in the galactic arms, as given in **Fig. 58**, we can see that during the past 520 million years, there were four periods with surface temperatures lower than what we are presently experiencing and four periods with higher temperatures. On the other hand, during the past 420 thousand years (**Fig. 59**) there were four decreases of temperature (the last one was about 20—40 thousand years ago: the so called big ice period), and five increases of temperature, the last of which happened few thousand years ago. At present, the Earth is in a slight cooling phase (of the order of one degree centigrade over several thousand years).

When considering CR variations as one of the possible causes of long-term climate change we need to take into account not only CR modulation by solar activity but also the change of geomagnetic cutoff rigidities (see **Table 5**). It is especially important when we consider climate change on a scale of between thousand and million years: pale-magnetic investigations show that during the last 3.6 million years the magnetic field of the Earth changed sign nine times, and the Earth's magnetic moment changed — sometimes having a value of only one-fifth of its present value *[Cox et al. 1967]* — corresponding to increases of CR intensity and decreases of the surface temperature. The effects of space factors on our climate can be divided into two types:

- the 'gradual' type, related to changes on time scales ranging from 10^8 years to 11—22 years, producing effects which could be greater than that produced from anthropogenic factors, and
- the 'sudden' type, coming from Supernova explosions and asteroid impacts, for example, and which may indeed be catastrophic to our civilization. Volcanic and anthropogenic factors are also in a sense, 'sudden' factors in their effect on climate change.

It is necessary to investigate all of the possible 'sudden' factors and to develop methods of forecasting and also for protecting the biosphere and the Earth's civilization from big changes in climate and environment. We cannot completely exclude the possibility that a Supernova explosion, for example, took place twenty years ago at a distance of say thirty light years away. In this case its influence on our climate and environment will be felt in ten years time. According to *[Ellis and Schramm 1995]*, in this case, UV radiation would destroy the Earth's ozone layer over a period of about 300 years. The recent observations of Geminga, PSR J0437-4715, and SN 1987A strengthen the case for one or more supernova extinctions having taken place during the Phanerozoic era. In this case, a nearby supernova explosion would have depleted the ozone layer, exposing both marine and terrestrial organisms to potentially lethal solar ultraviolet radiation. In particular, photosynthesizing organisms including phytoplankton and reef communities would most likely have been badly affected.

As *[Quante 2004]* noted, clouds play a key role in our climate system. They strongly modulate the energy budget of the Earth and are a vital factor in the global water cycle. Furthermore, clouds significantly affect the vertical transport in the atmosphere and determine, in a major way, the redistribution of trace gases and aerosols through precipitation. In our present-day climate, on average, clouds cool our planet; the net cloud radiative forcing at the top of the atmosphere is about — 20 $W \cdot m^{-2}$. Any change in the amount of cloud or a shift in the vertical distribution of clouds, can lead to considerable changes in the global energy budget and thus affect climate.

Many of the 'gradual' types of space factors are linked to cloud formation. *[Quante 2004]* noted that galactic CR *[Swensmark and Friis-Christiansen 1997; Swensmark 1998; Marsh and Swensmark 2000a,b]* was an important link between solar activity and low cloud cover. However, new data after 1995 shows that the problem is more complicated and the correlation no longer holds *[Kristjánsson et al. 2002]*. *[Kristjánsson et al. 2004]* point out that still many details are missing for a complete analysis, but a cosmic ray modulation of the low cloud cover seems less likely to be the major factor in our present climate change, but its role in future climate changes must not be ruled out.

In this Section much emphasis has been given to the formation of clouds and the influence CR plays (through ionization and influence on chemical processes in atmosphere) in their formation. This does not imply that CR is the only factor in their formation; dust, aerosols, precipitation of energetic particles from radiation belts and greenhouse gases, all play their part. However, the influence of CR is important and has been demonstrated here through:

- a direct correlation during one solar cycle and also for much longer periods,
- the correlation of CR intensity with the planetary surface temperature,
- by the direct relationship between cloud formation and CR air ionization,
- by the relationship between geomagnetic activity and rainfall through precipitation of energetic particles from radiation belts and
- by linking CR intensities with the cirrus holes.

The importance of CR cannot be stressed highly enough and it is important to develop methods for determining, with high accuracy, galactic CR intensity variations for the past, the present and for the near future.

In this Section several attempts have been made to explain the present climate change (the relatively rapid warming of the

Earth discussed in Section 6 for 1937—1994), using space factors:

- through eleven year average CR intensities,
- by the increasing geomagnetic activity,
- by the decreasing CR intensity (of 8% over the past one hundred years) and
- by relating the spectral analysis of *[Ermakov et al. 2006a]* to global temperature during 1880—2005.

Their results show the presence of several spectral lines that can be identified with the periods of meteor fluxes, comets, and asteroids. On the basis of this work *[Ermakov et al. 2006a,b]* has predicted a cooling of the Earth's climate over the next half-century which they believe will be more important than warming from greenhouse effect.

Finally, it appears that our present climate change (including a rapid warming of about 0.8°C over the past hundred years) is caused by a collective action of several space factors, volcano activities (with the dust emission rising to the stratosphere, resulting in short term cooling after eruptions), as well as by anthropogenic factors with their own cooling and warming contributions. The relation between these contributions will determine the final outcome. At present the warming effect is stronger than the cooling effect. It is also very possible that the present dominant influence is anthropogenic in origin.

From **Fig. 59** can be seen that now we are near the maximum global temperature reached over the last 400 thousand years, so an additional rapid increase of even a few °C could lead to an unprecedented and catastrophic situation. It is necessary that urgent and collective action be taken now by the main industrial countries and by the UN, to minimize the anthropogenic influence on our climate before it became too late. On the other hand, in future, if the natural change of climate results in a cooling of the planet (see **Figs. 58** and **59**), then special man-made factors, resulting in warming, may have to be used to compensate.

We considered above the change of planetary climate as caused mostly by two space factors: cosmic rays and space dust. This we advocate with the use of results obtained over long time periods, from about ten thousand years to many millions of years. We also considered very short events of only one or a few days, such as Forbush effects and Ground Level Enhancements (GLE). In these cases, it is necessary to use a superposed method, summing over many events to sufficiently reduce the relative role of meteorological factors, active incident to the aforementioned short events (see Section 9).

Analysis of *[Kristjánsson and Kristiansen 2000]* contradicts the simple relationship between cloud cover and radiation assumed in the CR-cloud-climate hypothesis, because this relationship really is much more complicated and is not the main climate-causal relationship. We agree with this result and with result of *[Erlykin et al. 2009a,b]* and *[Erlykin and Wolfendale 2011]* that there is no simple causal connection between CR and low cloud coverage (LCC), that there is no correlation between CR and LCC for short-term variations, and that while there is correlation between CR and LCC for long-term variations, that this connection can explain not more than about 20% of observed climate change. But the supposition of *[Erlykin et al. 2009a,b]* that the observed long-term correlation between cosmic ray intensity and cloudiness may be caused by parallel separate correlations between CR, cloudiness and solar activity contradicts the existence of the hysteresis effect in CR caused by the big dimensions of the Heliosphere *[Dorman and Dorman 1967a,b; Dorman et al. 1997; Dorman 2005a,b, 2006]*. This effect, which formed a time-lag of CR relative to solar activity of more than one year (different in consequent solar cycles and increasing inverse to particle energy), gives the possibility of distinguishing phenomena caused by CR from phenomena caused directly by solar activity (i.e. activity without time lag). The importance of cosmic ray influence on climate compared with the influence of solar irradiation can be seen clearly during the Maunder minimum (see **Fig. 44**). Cosmic ray influence on climate over a very long timescale of many hundreds of years can be seen from **Fig 40** (through variation of ^{14}C).

It is necessary to take into account that the main factors influencing climate are meteorological processes: cyclones and anticyclones; air mass moving in vertical and horizontal directions; precipitation of ice and snow (which changes the planetary radiation balance, see *[Waliser et al. 2011]*); and so on. Only after averaging for long periods (from one-ten years up to 100—1000 years and even million of years) did it become possible to determine much smaller factors that influence the climate, such as CR, dust, solar irradiation, and so on. For example, *[Zecca and Chiari 2009]* show that the dust from comet 1P/Halley, according to data of about the last 2000 years, produces periodic variations in planetary surface temperature (an average cooling of about 0.08°C) with a period 72 ± 5 years. Cosmic dust of interplanetary and interstellar origin, as well as galactic CR entering the Earth's atmosphere, have an impact on the Earth's climate *[Ermakov et al. 2006, 2007, 2009; Kasatkina et al. 2007a,b; Dorman 2009, 2012]*. *[Ermakov et al. 2006, 2009]* hypothesized that the particles of extraterrestrial origin residing in the atmosphere may serve as condensation nuclei and, thereby, may affect the cloud cover. *[Kasatkina et al. 2007a,b]* conjectured that interstellar dust particles may serve as atmospheric condensation nuclei, change atmospheric transparency and, as a consequence, affect the radiation balance. *[Ogurtsov and Raspopov 2011]* show that the meteoric dust in the Earth's atmosphere is potentially one of the important climate forming agents in two ways: (i) particles of meteoric haze may serve as condensation nuclei in the troposphere and stratosphere; (ii) charged meteor particles residing in the mesosphere may markedly change (by a few percent) the total atmospheric resistance and thereby, affect the global current circuit. Changes in the global electric circuit, in turn, may influence cloud formation processes.

Let us underline that there is also one additional mechanism by which CR influence lower cloud formation, precipitation, and climate change: the nucleation by cosmic energetic particles of aerosol and dust, and through aerosol and dust — increasing of cloudiness. It was shown by *[Enghoff et al. 2011]* in the frame of the CLOUD experiment at CERN that the irradiation by energetic particles (about 580 MeV) of the air at normal conditions in the closed chamber led to aerosol nucleation (induced by high energy particles), and simultaneously to an increase in ionization (see also *[Kirkby et al. 2011]*).

Let us note that in this Section, we considered CR and dust aerosols separately, but acting in the same direction. Increasing CR intensity and increasing of aerosols and dust leads to increasing of cloudiness and a corresponding decrease of planetary surface temperature. Now, consistent with the experimental results of *[Enghoff et al. 2011]* on aerosol nucleation in the frame of the CLOUD Project on the accelerator at CERN (see short description of this Project in *[Dorman M2004]*), it was found that with increasing intensity of energetic particles, the rate of formation of aerosol nucleation in the air at normal conditions increased sufficiently. This result can be considered as some additional physical evidence of the CR — cloud connection hypothesis.

12. Does CR and other space weather factors influence on agricultural markets? Necessary conditions, possible scenarios, and case studies

12.1. The matter of the problem

The problem of the possible influence of solar activity on the Earth agriculture has a history of almost three centuries. One of the first records of this influence appears in the description of the Royal Society of Britain made by Jonathan Swift, a famous professor of theology and the father of the European satire, in his book devoted to the third travel of Gulliver to the island of Laputa *[Swift 1726]*. In this biting satire, Swift mentions the main fears of Laputians as follows:

a) The Earth can find itself in the burning hot comet tail and enter into the period of global warming threatening loss of all life.
b) The Sun daily spending its rays without any nutriment to supply them, will at last be wholly consumed and annihilated which must be attended with the Destruction of this Earth.

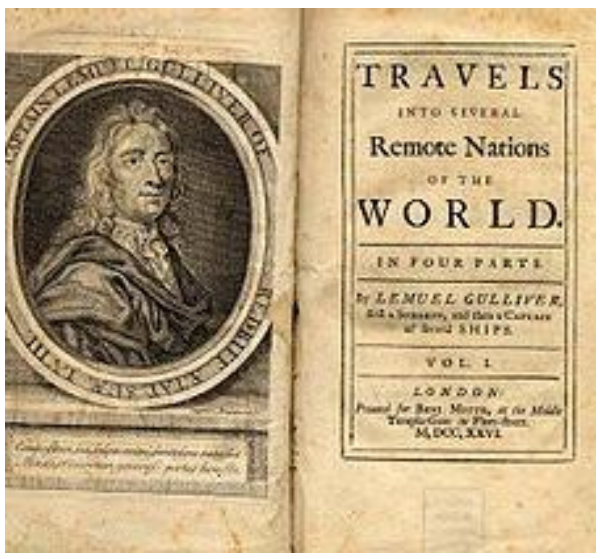

First edition of Gulliver's Travels

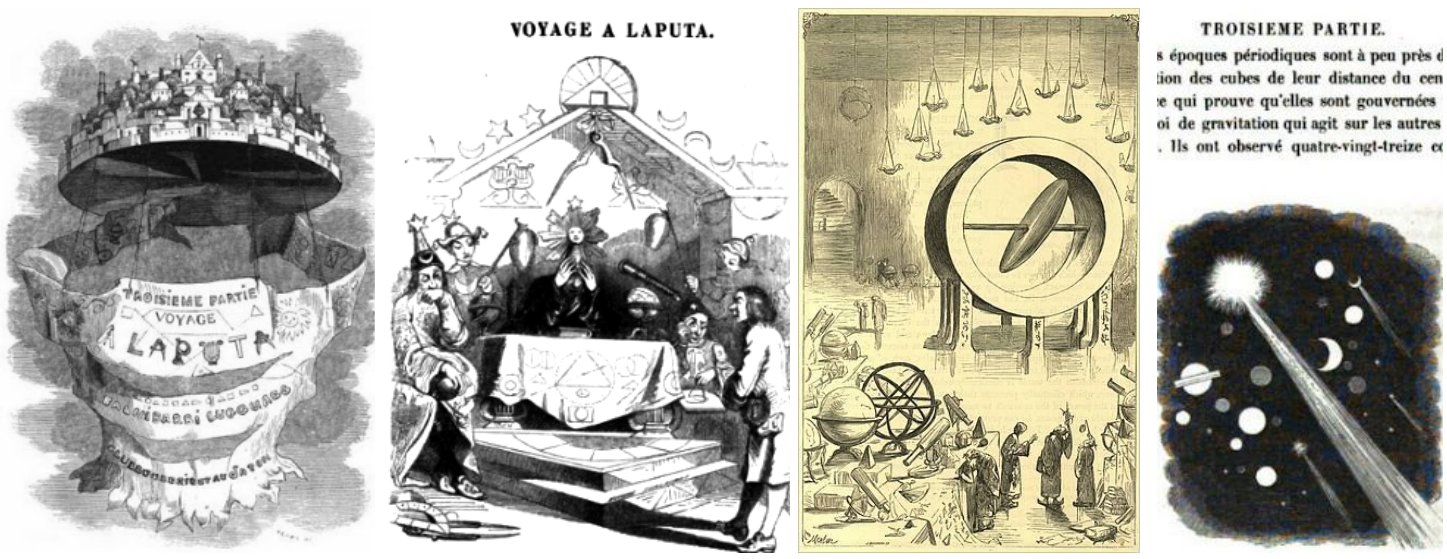

Part III: A Voyage to Laputa (illustration by J.J. Grandville, 1838)

These fears reflected theories prevailing in Swift's contemporary scientific society, particularly to the Derham's theory that sunspots arise from solar volcanoes *[Renaker 1979]*. Interesting how enduring these fears are that can be met nowadays in science fiction novels and disaster films.

The next statement of the possible influence of the space weather on the agriculture was made by the father of the observational astronomy William Herschel, famous for the discovery of Uranius. He compared the grain prices from the fundamental study of Adam Smith (1776) with the data on the sunspots number, and made a far-reaching conclusion about the coincidence of the five long periods of few sunspots with the periods of rise in wheat prices *[Herschel 1801]*. This work was presented to the Royal Society, and it was met extremely negatively by other members of the Society. According to a very sharp opinion of one of the Society's leaders (Lord Brougham), "since the publication of Gulliver's voyage to Laputa, nothing so ridiculous has ever been offered to the world" *[Soon and Yaskell, 2003]*.

Sir Frederick William Herschel (1738 —1822)

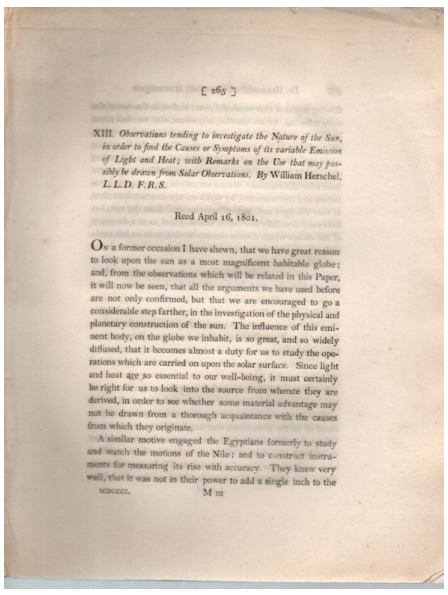

XIII. *Observations tending to investigate the Nature of the Sun, in order to find the Causes or Symptoms of its variable Emission of Light and Heat; with Remarks on the Use that may possibly be drawn from Solar Observations.* By William Herschel, *L. L. D. F. R. S.*

Read April 16, 1801.

First page of W. Herschel's "Observations tending to investigate the Nature of the Sun in order to find the Cause of Symptoms of its Variable Emission of Light and Heat". (Philosophical Transactions, 1801).

William Jevons, one of the founders of the mathematical school in economics, was the next victim of the interest to this problem. He was one of the first economists that paid attention on cyclicity in economic processes, and particularly, on cyclic recurrence of economic crises which average length he estimated as 10.2 years *[Jevons 1875, 1878, 1879]*.

William Stanley Jevons (1835—1882), a British economist and logician. Professor of Political Economy at University College, London

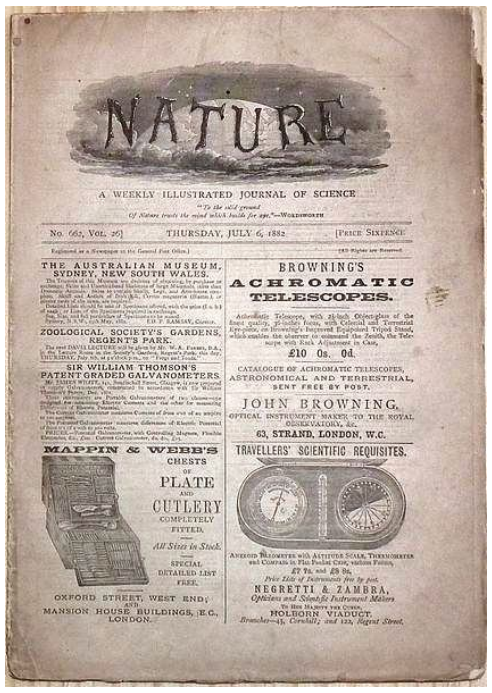

Jevons, William Stanley. The Solar-Commercial Cycle. 'Nature'. A Weekly Illustrated Journal of Science. Vol.26, no.662, July 6th. 1882. pp. 226—228.

Because of the striking closeness of the crises cycle length to the 11-year length of the sunspots cycle, discovered shortly before the works of Jevons, he assumed that the solar activity modulates economic processes in some way. As a possible causal-effect relationship that could explain the coincidence of the both cycle's length, Jevons assumed that in years of "unfavorable" solar activity weather anomalies happen. They cause to bad harvests, and consequently — to the rise in food price that generates stock exchange crisis. Moreover, Jevons extrapolated the series of coincidences between the times of the previous five stock exchange crises and the periods of the minimal solar activity, and also put attention on the rises in stock exchange activity immediately after those minimums. He dared to forecast the next economic crisis in the period of the next minimum of solar activity expected in 1879, and this caused the natural reaction in the stock exchange and in the media. Because neither in 1879 nor in later years the promised crisis did not happen[1], the Jevons theory was completely discredited, and the new term "sun-spot equilibria" appeared in economic science.

[1] In fact, the forecast of Jevons came true, in part. In the period of the minimal solar activity of 1876—1878 he mentioned, the monsoon transfer of the moist ocean air to the Southern India (the major part of the British Empire of that time) disappeared for three years. This caused a severe draught that brought to the humanitarian catastrophe known as Great Famine in India. As much as 6—10 million people died of starvation and another 60 million people turned into refugees.

[2] This term reflects high stock exchange sensitivity to any "significant" scientific, economic, or political information about threats to its stability. Such information forms pessimistic expectations of many participants of the stock exchange trade and can invite real panic in spite of unreliability of the initial forecast. The example of Jevons's forecast lays in the basis of the term "sunspot equilibria" in the modern economics. This is the state where speculators' expectations formed by a priori information, are taken into account. This information even being essentially irrelevant, can determine the speculators' behavior and influence the forecasted reality (Azariadis, 1981).

Further discovery of the exceptional constancy, within the range of 0.1%, of the level of solar radiation that reaches the Earth (received the name of the solar constant) deprived supporters of the solar activity influence on the Earth processes of their physical arguments for a long time. This "pessimistic" period continued till discovery of new channels of the solar activity influence on the Earth, united now by the term "space weather".

12.2. The Earth weather influence on harvest

The fact of the harvest dependence on weather conditions is trivial and well-known. However, the threshold character of this dependence often is overlooked. For example, occasional light frosts in the period of blossoming or pouring rains at harvest can during a few days reduce productivity almost to zero. At the same time, average annual or monthly weather indices (of temperature, humidity, precipitation) for this region can remain almost the same. For various crops, the critical agrotechnical and weather conditions can be different. Thus, for the perennial crop like grapes high enough temperatures in the period of ripening is very important, and for annual grain crops the air humidity can be critical.

To minimize losses of harvest because of weather anomalies, the practice of long-term selection and zoning of the most suitable crops is used, as well as agrotechnologies optimal for type of weather prevailing in the region. However, it is this long-term crops zoning for standard weather that under conditions of fast climate change can cause a shift of dominating crops to the state of risky

agriculture very sensitive to small local weather anomalies[3]. The importance of localized efforts to increase local adaptive capacity,

[3] Shifts in the opposite direction are possible when climate changes lead to an increase in productivity and a decrease in its variability for crops traditional in the region. This is the conclusion of the study of Richter and Semenov (2005) where the influence of possible climate changes on winter wheat yield in England and Wales is modeled.

take advantage of climate changes that may lead to increased agriculture productivity where this is possible, and to buffer the situations where increased stresses are likely, is underlined in the study of Thornton et al. (2009) who simulated cropping for Eastern Africa. A similar conclusion that climate change takes expression in local processes such as increased climatic variability, is made in *[Head et al. 2011]* using data of Australian wheat farming households.

12.3. Yield deficit and grain market

In free market, the deficit of first-necessity goods (agricultural goods belong to this category, of course) causes price spikes that reduces the demand and brings the market to the state determined by the equilibrium between supply and demand. Shortages (or surpluses) can cause the market reaction in a form of panic when prices spikes (or slumps) make them much higher (or lower) than the equilibrium level[4]. Such market panic reaction can be revealed in the case of food deficit caused by bad yield

[4] Shiller (1990) studied stock market crashes and "hot" real estate markets in USA and Japan. Most of the respondents in this study picked up the answer "There is panic buying, and price becomes irrelevant" explaining the burst in housing prices.

because of local weather anomalies. The food prices bursts stimulate import from regions not stricken with the bad weather what serves to dampen prices and to restore the market equilibrium. This mechanism, however, not always works effectively. First, transport costs are included into the final price of agricultural products. Second, transfer of agricultural goods is restricted often by geographic, economic, and political barriers — relative market isolation, high customs, and low quotes protecting local producers[5].

[5] Other possible solution of the supply deficit and panic increase in vital goods prices (food, fuel) is imposition of a rationing system. In this system ration, cards distributed by the authorities are used to balance between supply and demand, and not prices (widely used in USSR and many European countries during and after the World War II).

Thus, in the markets isolated from the external supply and/or needed to pay expensive transport costs[6], there can be a panic

[6] Here is an example of influence of transport costs on the grain market: the difference between prices in Britain (importer) and in the USA (exporter) was reduced significantly in the end of the 19 century after beginning of wide use of inexpensive steamships for freight transport *[Ejrnæs et al. 2008]*.

reaction to the deficit of agricultural products, particularly, of grain, with burst price spikes.

12.4. Three necessary conditions for implementation of the relationship between space weather and the Earth prices

Summarizing the above analysis, we formulate the following three necessary conditions for a possible implementation of the causal relationship between anomalies of the space weather and grain prices bursts caused by them:

1. High sensitivity of weather (local — in space and time) to the space weather factors, for example — to cosmic rays, sun ultraviolet radiation, and magnetosphere activity).
2. High sensitivity of the major grain crops yield in the region to weather anomalies (belonging to a risky agricultural region) in the studied period.
3. High sensitivity of the grain market to the supply deficit due to limited import capacity that can cause burst (panic) price leaps.

12.5. Causal relationships between space weather and grain markets

The scheme in Fig. 63 illustrates a possible chain of relationships that lead to the prices reaction to the unfavorable states of space weather in the regions where the above necessary conditions are fulfilled.

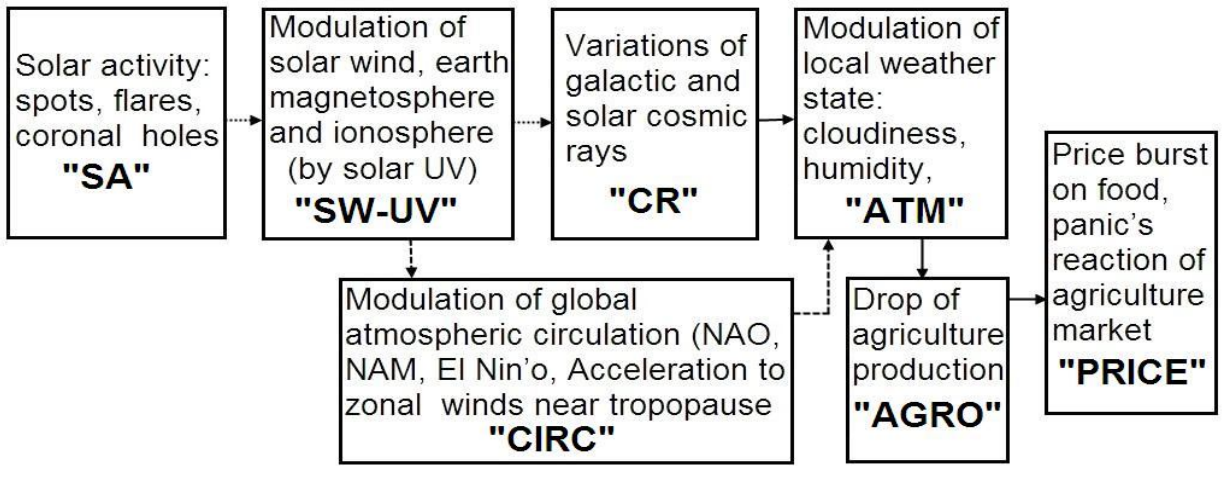

Fig. 62. A possible causal chains between space weather and earth agriculture markets. Thin arrows — direct relations without threshold effects, bold arrows — non-linear relations and existence of threshold states.

Main specific of this scheme is existence of nonlinear sensitivity between selected elements of the scheme (imaged by bold arrows). In result, final connection "solar activity — price level" in terms of theory of catastrophes *[Arnold, M1992]* must be presented not as "hard dependence" like to $Y = \sum k_i X_i + Noise$, but as "soft type dependence" $Y = \sum k_i(X_i, Y) * X_i(t - \tau) + Noise$ taking in account both feedback, possible phase delay and existence of external factors of influence caused by sources of another nature. Here *X* is vector of inputted variables (solar activity space weather state, conditions in the Earth atmosphere, market state), *Y* — output response (prices, social reaction), k_i — coefficients (functions) of connection, *r* — phase delay.

12.6. Four possible scenarios of price reaction on space weather

In the frame of the proposed causal scheme, four variants of the agriculture reaction on space weather/local weather are possible for different climatic zones and for different crops. The proposed set of scenarios is based on cosmic rays as a modulation factor that initiates cloudiness, deficit of radiation, lower temperature and excess of participation. We would like to note here that a possible space weather — earth weather relationship through the causal chain "cosmic ray" — "cloudiness" is not a unique channel of space weather influence. A full list of possible influence mechanisms is wider. In this paragraph, we limit our analysis by this only chain to illustrate possible scenarios of response that depend on local climate state and agriculture conditions. All these scenarios are presented in **Fig. 63** and include:

A. Zone I of risky agriculture is sensitive to deficit of solar irradiance, cold weather and redundant rains. The most probable candidates are northern Europe, particularly England. The most unfavorable state of space weather/solar activity is a minimum of sunspots with minimal solar wind and maximal cosmic ray flux that penetrate into the Earth's atmosphere and stimulate cloudiness formation in regions sensitive to this link (e.g., Northern Atlantic).
B. Zone II of risky agriculture is sensitive to dry and hot weather with droughts. The most probable candidates are southern Europe and the Mediterranean (Italy, Spain, North Africa). The most unfavorable state of space weather/solar activity is a maximum of sunspots with maximal solar wind and minimal cosmic ray flux that diminishes cloudiness formation above Atlantics.
C. Zone III includes specific cases of risky agriculture which is sensitive either to a deficit of precipitation (droughts) or to excess rains/cloudiness. This situation may take place in zones with the climate unfavorable for agriculture where it can succeed only in a very narrow range of weather condition (rains, temperature, humidity, solar irradiation). In this specific situation we can expect unfavorable conditions for agriculture production both in maximum and minimum states of solar activity. A possible candidate is Iceland in the18-th and 19-th centuries.
D. Zone IV where agriculture is not risky and its sensitivity to local weather fluctuations is relatively low. This situation leads to a neutral reaction of the agriculture market on the space weather and the phase of solar activity. The most probable candidate is Central Europe.

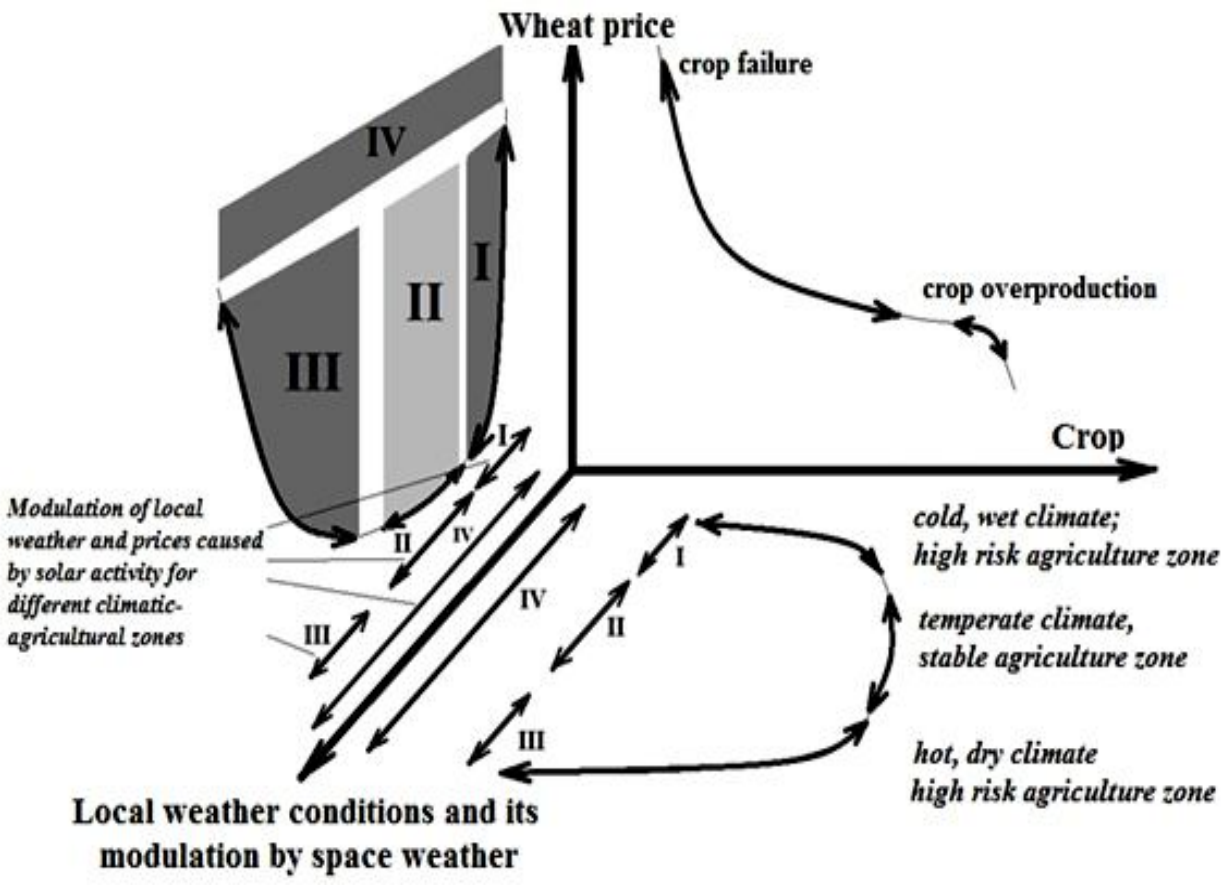

Fig. 63. Four possible scenarios of responses of agricultural production and markets on possible modulation of local weather by solar activity/space weather.

These four types of reactions describe possible scenarios of causal chains between the space weather and the Earth agriculture production for the suggested relationship "cosmic ray" — "cloudiness". Our analysis aims to reveal examples of the above scenarios in specific regions and historical periods in Europe and North America.

According to the above description, we may expect systematical price bursts in solar minimum states for cold and wet regions (zone I in **Fig. 63**). Similar price bursts are expected in hot and dry regions in states of solar maximum (zone III on **Fig. 63**). For

these two cases a typical time interval between price bursts is caused by a period of solar activity — 9—13 years. For specific regions, crops sensitive both to excess of participation and to its deficit (zone IV) can fail, and thus price bursts are possible both in minimal and maximal states of solar activity with typical time intervals between price bursts close to half of a solar cycle period — 4—6 years. The same typical time of price bursts can be caused by a formal mixing of data from different zones with opposite type of price reaction into one joined series. The example can be found in the work of Beveridge (1921) where the "Beveridge index of price" was calculated by averaging price indexes for approximately 50 markets from Western and Central Europe. In this work, Fourier response was revealed on periods 4—5 years.

12.7. Using data

The main source of data on solar activity that is the driver of space weather is "sunspot number". In spite of starting observations in 1611 after Galileo discovered these numbers, the further minimum of Maunder interrupted regular sunspot observations. Regular and daily sunspot observations were renewed by several scientists only in the 18-th century after solar activity returned. It allowed constructing a catalog of solar activity (sunspots numbers) from 1700 up to present time (http://sidc.oma.be/DATA/yearssn.dat). Later, sunspot data were restored for the previous period (the 17-th century) using days when any manifestations of sunspots were observed on the Sun episodically[7].

[7] Results of restoration are discussed in *[Ogurtsov et al. 2003; Nagovitsyn 2007]* and presented in free FTP site of NOAA/NGDC: ftp://ftp.ngdc.noaa.gov/STP/SOLAR_DATA/SUNSPOT_NUMBERS/ANCIENT_DATA/earlyssn.dat

Another approach used for estimation of solar activity in the period of Maunder Minimum and the previous period is an indirect method of restoration of the solar activity level based on the measurement of isotope Be^{10} in the Greenland ice *[Beer et al, 1998]*. Although this method cannot give reliable quantitative estimation of sunspot numbers themselves, it enables identifying moments of maximal and minimal states of solar activity. We would like to note here that the data based on Be^{10} measurement are sensitive directly to cosmic ray flux penetrated into atmosphere that is much more important than sunspot numbers. Cosmic rays are an agent of direct influence of space weather on atmospheric processes, controlled ionization and vapor condensation. On the opposite, the causal chain from sunspots to atmospheric process includes a lot of intermediate elements (solar wind, state of Earth magnetosphere and global atmospheric circulation). These intermediate elements in the causal chain are able to mask a possible link between sunspots and local atmosphere states.

The first data on wheat price used by William Hershel for his analysis was published in the famous work of Adam Smith (1776). The most full and reliable database on wheat prices in the Middle Age England was created one hundred years later as a result of selfless work of a great economist and statistician Prof. Rodgers (1887).

His database:

1. Cover the period from 1259 to the middle of the 18-th century.
2. Uses only price data for wheat purchased by monasteries and colleges that enjoyed from tax exemption in this period. This circumstance made unnecessary "tax optimization" considerations during registration of the transactions that increased reliability of this data source.

In addition to data on wheat prices, in our analysis we use the 700 years database (1264—1954) on consumable basket prices *[Brown and Hopkins 1956]*. An additional database that we used was an archive of wheat prices for 90 wheat markets of Middle Age Europe. We used the fullest part of the database from the period of 1590—1702 that covered the period of Maunder Minimum and the small Ice Age in Europe. The source of this database is the International Institute of Social History (2005).

To search for possible manifestations of space weather influence on agriculture markets in the New Time we used data of Agriculture Department of USA for the period of 1866—2002 of "durum" wheat prices (durum wheat is used for bread and bakery). We used also the comparative analyses of wheat production and wheat prices in Middle Age England and France *[Appleby 1979]*; the wheat prices analysis for Middle Age England from *[Beveridge 1921]*; the analysis of the correlation between local weather and crops in the end of 19-th century — first decades of 20-th century from the work *[Hooker 1907]*; analysis of wheat production in USA during first decades of 20-th century from the article *[Acrtowski 1910]*. To analyze a possible influence of forage crop failure on drop of livestock in Iceland 18-19-th centuries that in turn caused famine and increased mortality toll we used the work *[Vasey 2001]*.

12.8. Using methods of analysis

The main difficulties in search for response of agriculture indices used as indicators of possible relationships, on abnormal states of space weather/solar activity are caused by the following two factors:

1. Solar cycles of activity as a generator of variations in space weather is not stable both in frequencies of variations and in amplitudes of cycles. Time intervals between minimums of solar activity (a cycle period) change in a wide interval from 8 to 15 years. The amplitude of cycles described as Wolf numbers changes from tens to hundreds and often decreases to zero on periods of a few tens of years.

2. Solar activity includes different components (sunspots, flares, coronal holes) formed by different elements of dynamo process or by their combinations (poloidal and azimuthal magnetic fields under photosphere, convection, differen-

tial rotation and meridional circulation). As a result, different components of solar activity have different phase patterns (change with phase during cycle) and their behavior during a cycle of activity changes. For example, input of coronal holes (and recurrent fluxes in solar wind accelerated from coronal holes) to space weather is maximal in minimum state of solar activity and is absent in maximal state. Solar flares of small amplitude have a very good correlation with sunspot numbers but for big solar flares with coronal mass ejections and acceleration of strong proton fluxes the situation is much more complicated and dynamic. The distribution of proton flares changes from cycle to cycle radically, and for some cycles their frequency is maximal not in the maximum of sunspot number but predominantly in the phase of rise or decay of sunspot activity *[Shea and Smart 1992]*. Additional difficulties are caused by instability of a relative input of different components of solar activity into space weather formation. It explains, for example, the observed drastic change during the last 100 years in the phase pattern of geomagnetic activity as a result of the change of relative input of coronal holes and sunspot during dynamo process in the Sun *[Georgieva and Kirov 2011; Kishcha, Dmitrieva and Obridko 1999]*.

The impact of space weather factors on the Earth atmosphere has a place on the background of complex and yet not explained global atmospheric circulation with effects of long-range action[8], phase instability and possible transitions like a strange attractor *[Ruzmaikin 2007]*.

[8] This effect may be illustrated by a situation when a local weather cataclysm like El-Nino near the west coast of South and Central America leads to a drastic weather response in the opposite side of the Earth in North Atlantics as a result of the atmospheric and oceanic mass and heat transfers. There are researchers that claim a relationship between solar activity and El Nino is possible *[Ruzmaikin 1999]*.

Influence of the space weather on the local weather and on agriculture markets, if it has place, must happen on the background of another factors of influences that act simultaneously with space weather factors. These influences may have a comparable amplitude and may have both random and regular nature with periodical components on the same times as space weather (10—20 years). As examples, we may refer on climate variations, political or military events that lead to economic shocks, scientific and technological revolutions.

This situation makes use of classical statistical methods non-effective. As an example, we can mention methods aimed at selection of a harmonic signal (Fourier analysis, periodogram analysis) with a selected period (for example, 11-year period), or at search for a direct linear relationship (regression or correlation analysis). It means that to search for a space weather influence we have to use another methods and statistics, much more robust to variability of period of solar cycle and amplitude of solar activity, to non-stability of atmospheric circulation and other external factors.

In the frame of our approach we may use the next robust statistics:

a. Comparison of interval statistics both between price bursts and between extreme states of solar activity (minimums, for example).
b. Search of a systematical phase asymmetry of wheat prices in "favorable" and "unfavorable" states of space weather/solar activity.
c. Regression analysis that uses dichotomous "dummy" variables "yes"/"no" related to the solar activity state (for example, "yes" or "no" for the minimum of solar activity).

In some regions, we must take into account a possibility of "long-range action" when regions located far from a region of space weather influence on the earth weather may be nevertheless sensitive to space weather action as a result of global circulation and cyclonic transfer of formed clouds over thousands kilometers (for example, from North Atlantics to East Siberia).

Another effect that we have to take into account is a possible phase delay in price reaction on "unfavorable" sates of space weather. These delays may be caused by reserves of the crop from the previous yield and by a natural inertia of agricultural markets. Sensitivity of agriculture production to local weather conditions may be much higher in a case when a crop is concentrated in a compacted region with a certain type of weather conditions than in a case of a crop dispersed through thousands of kilometres with different climate conditions in different regions and, accordingly, with different (or even opposite) type of sensitivity to external factors.These are factors and parameters we take into account in the analysis of data for different regions in different historical periods that meet the above defined criteria

12.9. Wheat markets sensitivity to the space weather in Medieval England

Medieval England is an ideal testing region for searching for manifestations of space weather influence on agricultural prices. In this period, this region met all three the above mentioned conditions necessary for this relationship to be realized:

1. The weather in the region depends on the space weather factors in the zone of cloudiness formation in the North Atlantics that is sensitive to the cosmic rays variations during changes of solar activity.
2. The region belonged to the zone of risky agriculture, particularly, for wheat that is highly sensitive to weather anomalies in the vegetation period.
3. Relative isolation from European markets amplified price reaction to shortage in grain.

Another advantage of using this region in the research is availability of the reliable data collection of grain prices from 1259 to the 18th century due to the distinguished effort of Prof. Rogers (1887). The initial curve of the changes of yearly wheat pric-

es is presented in **Fig. 64a**. To search for space weather influences we used the above described methods of comparison between statistics of intervals and of search for price asymmetry.

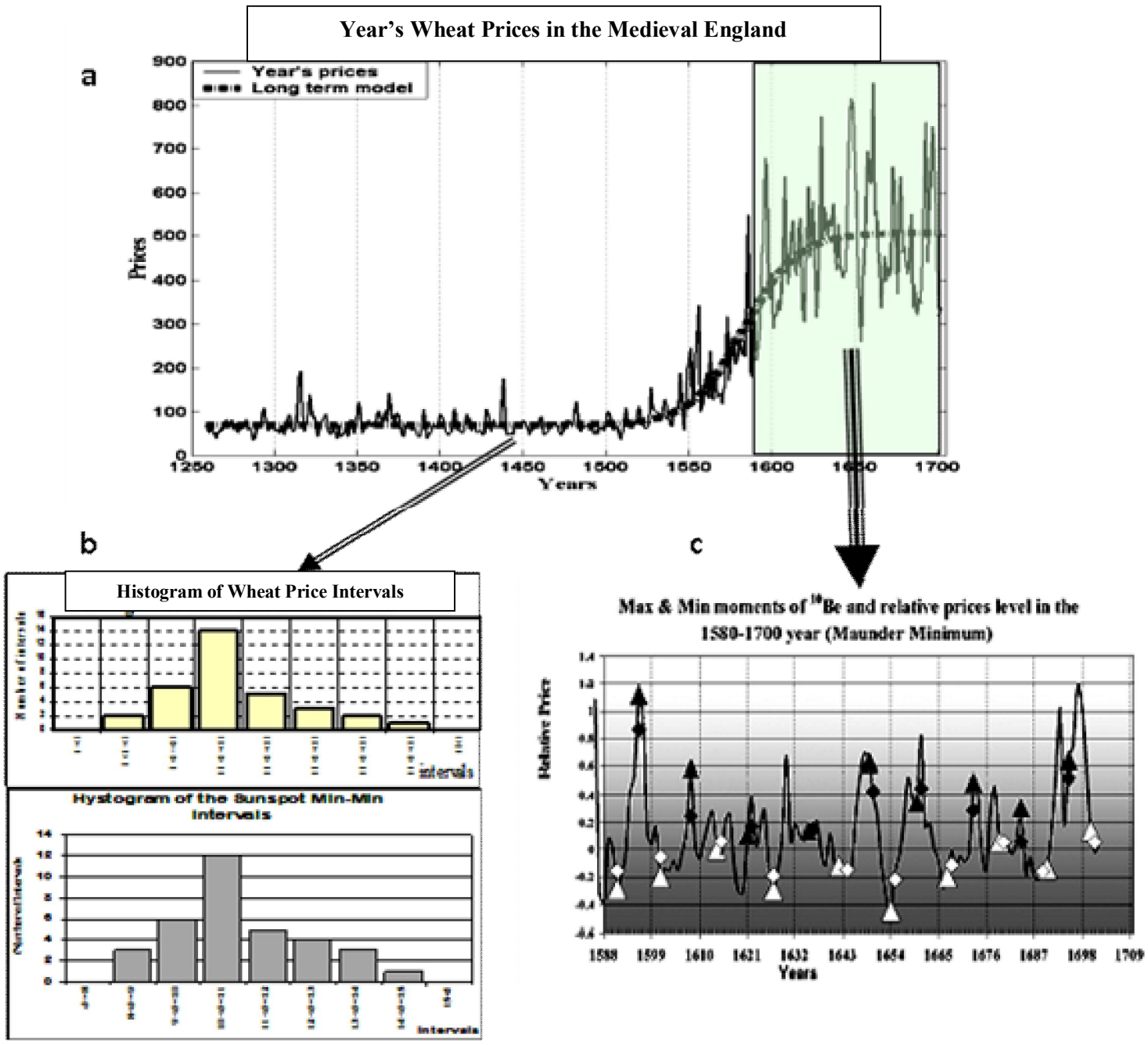

Fig. 64. Panel **a** — wheat prices in Medieval England smoothed by a logistic function; **b** — comparison of histograms of intervals between minimal states of solar activity and of intervals between wheat price bursts. The range of intervals is 8—16 years. For both histograms the maximum is achieved in the point of 11 years; **c** — price asymmetry in states of minimum/maximum of solar activity identified by the method of Be^{10} in Maunder Minimum: white triangular are prices in states of maximum, white diamonds are prices average for three years that include the state of maximum, black triangular and diamonds are prices defined similarly for states of minimum of solar activity.

First, we compared statistics of intervals between wheat price bursts and of intervals between states of solar activity minimum *[Pustil'nik et al. 2003; Pustil'nik and Yom Din 2004a,b]*. The statistics were compared both for the distributions of the intervals by length (**Fig. 64b,c**) and for statistical characteristics of these distributions (average length of the intervals, medians, standard deviations — **Table 6**).

Table 6

Statistical characteristics (average, median, standard deviation) for two samples of intervals between price bursts (wheat price and consumer basket price) and for the sample of intervals between minimal states of solar activity

Samples	Median	Average	Standard deviation
Min-Min intervals for sunspots	10.7	11.02	1.53
Intervals between wheat price bursts	11.00	11.14	1.44
Intervals between consumer basket price bursts	11.00	10.5	1.28

It follows both from the results in **Table 6** for statistical characteristics and from the histograms of these characteristics (**Fig. 64b**) that the hypothesis that the distributions of intervals for wheat price and consumer basket price bursts and the distribution of solar activity minimums are not different one from another is significant (99%). Highly significant price asymmetry for minimum and maximum states of solar activity in the period of Maunder Minimum is another evidence of the space weather influence on wheat prices in Medieval England (**Fig. 64c**). As it is seen in this figure, wheat prices in years of solar activity minimum are higher (on the average, twice as many) than prices in years of the nearest solar activity maximum for all nine cycles of solar activity. In this examination, the significance level is 99%, too.

These results show that realization of the above described causal chain between the space weather and grain markets is possible for the case study of Medieval England. The observed market reaction corresponds to case I (zone of risky agriculture sensitive to deficit of solar irradiance, cold weather and redundant rains) described in Section 12.8. The results are in good agreement with those expected for this climatic zone.

12.10. Wheat markets sensitivity to space weather in Medieval Europe

In the next stage of the analysis we tried to answer the following question. Is the discovered sensitivity of the grain markets in Medieval England a universal feature for all markets in the earth (like dependence of the same prices on the seasonal "winter — summer" changes) or this feature realizes only in isolated zones and in certain historic periods when the three necessary conditions for the causal chain "space weather" — "earth prices" are satisfied? To answer the question we fulfilled regression analysis of data from 22 European grain markets that were presented by relatively full data from all markets in the database of the International Institute of Social History (2005).

We used the well-known method of regression analysis with dummy variables (first introduced by *[Suits 1957]*)[9]. In our study,

[9] These variables describe qualitative data, for example, of the kind "yes" — "no".

we used this method for establishing relationships between states of grain markets with states of minimum or maximum of solar activity. We tested the hypothesis of existence of such relationship between solar activity and prices, and estimated its significance for samples for markets from different European zones. For this purpose, we introduced a dummy variable d_{min} that takes a value 1 in the years of solar activity minimum, and a value 0 otherwise. In a similar way, we introduced a dummy variable d_{max} for years of solar activity maximum. In a certain way, this method develops the method of the direct search for the price asymmetry of minimal and maximal phases of solar activity used above for the wheat market in Medieval England (**Fig. 64c**). However, the method of dummy variables is more accurate and enables clear estimating of the significance level of the hypothesis about existence of such phase asymmetry.

For our analysis we used the period of 1590—1702 that includes the Maunder Minimum when the solar activity fell sharply. The following two reasons led to choose this period:

1. Europe went through a little ice age in this period. A considerable part of areas moved to risky agriculture zones with an increased influence of weather anomalies on grain production.
2. Only for this period special measurements of the isotope Be^{10} were carried out to reflect directly contribution of cosmic rays that are a probable factor of influence on weather *[Beer 1998]*[10].

[10] Additional analysis for other periods using regression with dummy variables showed a significant relationship between solar activity extrema and wheat prices in England up to 1840's (the results can be sent by the authors by request). Weak market sensitivity to the space weather after this period we explain by a sharp increase of the grain import — from 5%-8% during 1801—1840 up to 17%—18% beginning from 1841 *[Ejrnaes et al. 2008]*. This growth of import broke the causal chain in the part "sensitivity of the isolated market to supply shortage"

We present significance level of the influence of minimal and maximal states of solar activity on wheat prices for a number of markets in **Fig. 65** where the Europe map of precipitation is shown.

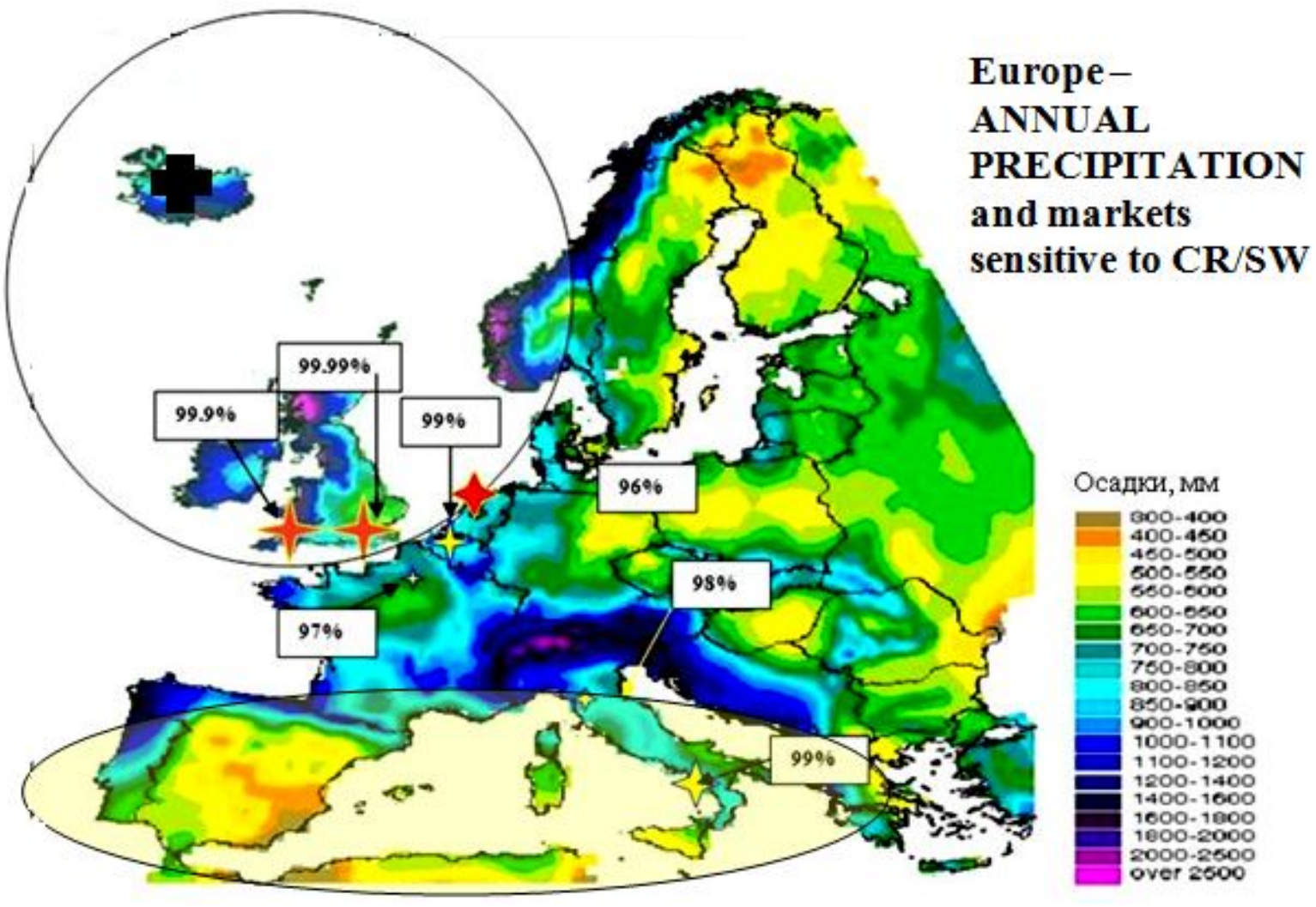

Fig. 65. The Europe map of precipitation. Localization of wheat markets that show high sensitivity to the space weather and its significance level, are shown. Red stars show markets sensitive to states of minimal solar activity (London, Exeter — England; Leiden — the Netherlands), yellow stars show markets sensitive to states of maximal solar activity (Napoli, Bassano — Italy). The stars size corresponds to the significance level.

As it is shown in this figure, in the researched period all grain markets in England were highly sensitive (larger than 99%) to space weather states of both minimal (d_{min}) and maximal (d_{max}) solar activity. The wheat market in Leiden, the Nether-

lands, where climate is similar to England, was sensitive (95%) to solar activity minimums, too. At the same time, some of the markets in Belgium, France and especially in Italy (Napoli, Bassano) demonstrated high sensitivity to solar activity maximums.

Because modulation of cloudiness in the North Atlantics by a cosmic rays flux is one of the channels of the possible influence of the space weather on the Earth weather, one can expect excess precipitation and deficit of solar radiation (unfavorable for agriculture in cold and damp climate) in states of minimal solar activity. At the same time, the cosmic rays flux and the related cloudiness drop in states of maximal solar activity, and draughts are possible. The latter are unfavorable for agriculture in the South Europe influenced by hot and dry North Africa climate, especially in Italy and Spain.

These results show that the observed sensitivity of wheat markets to the space weather is not a universal property invariable for all regions and periods. On the contrary, depending on satisfaction (full or partial) of the above formulated conditions a few cases are possible:

1. Any influence of the space weather/solar activity cannot be observed (for most markets of Central Europe).
2. Highly significant sensitivity to states of minimal solar activity is observed (England and neighboring markets of the continental Europe).
3. Significant influence of states of maximal solar activity in zones sensitive to draughts is observed (particularly, in Italy influenced by North Africa climate).

Thus either the observed distribution of zones sensitive to the space weather or the sign of this sensitivity are in good agreement with the above described scheme of the causal relationships between the space weather and grain markets.

12.11. The US wheat market sensitivity to the space weather in 20th century

The previous analysis regarded grain markets in the Middle Ages or in the very beginning of the New Time. Our next question is whether the above described scenarios of the space weather influence on Earth markets can be observed in the New Time? From the first glance, the all over the world implementation of modern agro techniques methods that increase the plant resistance to unfavorable weather, should cause breaking the second condition — belonging to risky agriculture — necessary for the above influence. Another factor of suppressing a possible sensitivity of grain markets to external anomalies is globalization of the world economics in the 20th century. This process made it easier in a drastic way to access external supply for markets with supply deficit. Nevertheless, we decided to analyze the US grain market in the New Time searching for possible manifestation of the space weather influence on prices. For this purpose, we used wheat prices from the period 1908-1993 based on data of USDA (2004). Wheat price variability for the researched period is shown in **Fig. 66**.

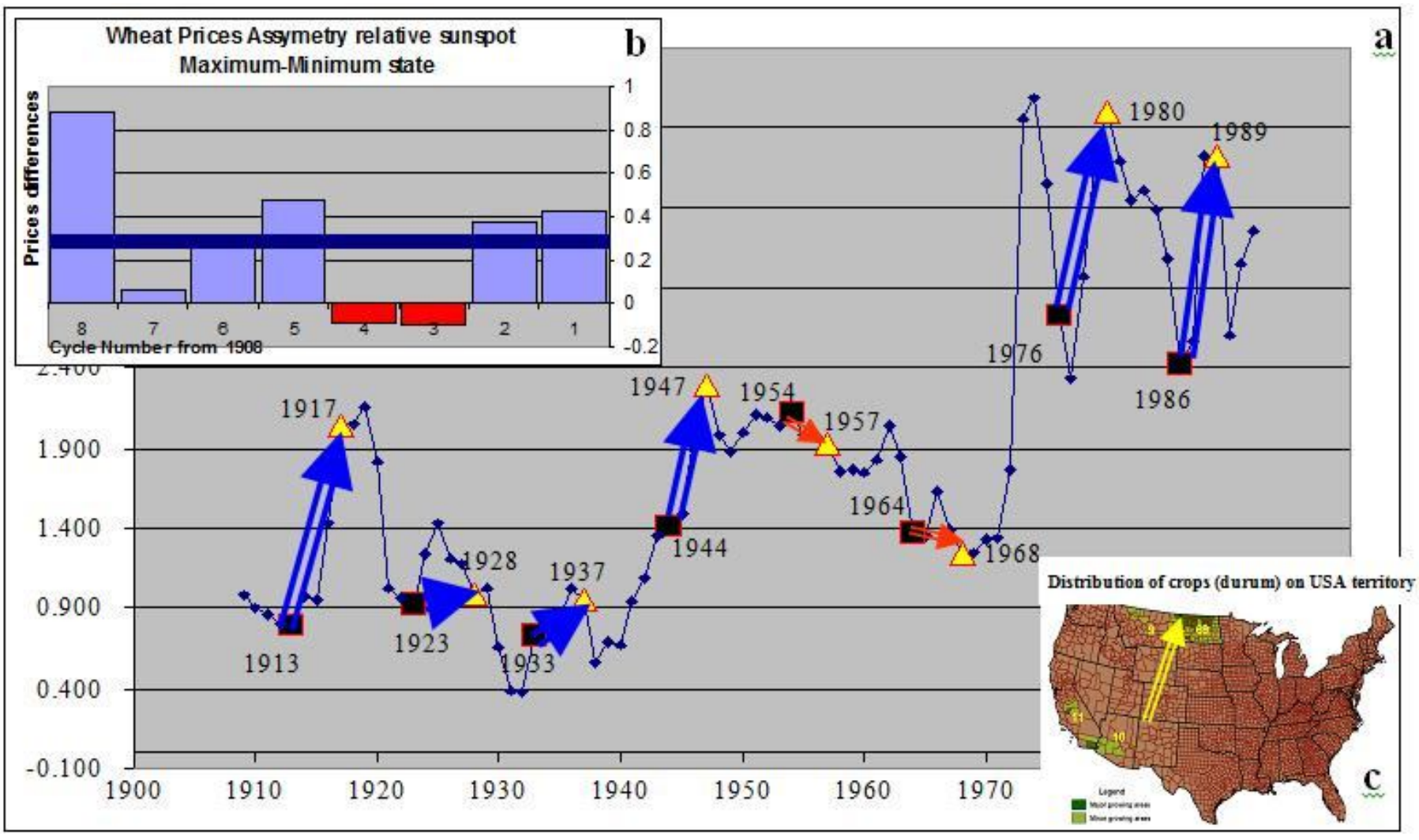

Fig. 66. Panel **a** — changes in durum wheat prices in USA in the period 1908-1993. Blue points and lines show price dynamics, yellow triangular — years of solar activity maximums, black squares — years of solar activity minimums, blue double arrows — price changes from solar activity minimum to the next maximum. **b** — a histogram of price asymmetry — a price difference between the maximum and the predecessor minimum of solar activity — depending on the solar activity cycle. **c** — high concentration of the durum wheat crop: more than 2/3 of the harvest area is concentrated in 3% of the USA area, in the state of North Dakota.

The small sample that includes only 8 solar activity cycles does not enable researching statistical properties of the intervals between price bursts as this was made for Medieval England where the 500 years statistics is available. In this situation we can hope only that the phase asymmetry of prices can be revealed with significant differences between prices in states of maximal and minimal solar activity. As it is shown in **Fig. 66**, for the researched sample, indeed, a significant price asymmetry for maximums and minimums of solar activity is observed: prices in states of maximal solar activity are systematically higher than prices in states of minimal solar activity. To estimate significance level of this asymmetry we used the Student criterion. For the average price asymmetry $\overline{\Delta\text{Price}} = 0.29$ (as it is defined in the legend of **Fig. 66b**) and standard deviation $s(\overline{\Delta\text{Price}}) = 0.12$ the significance level for rejecting the zero hypothesis of asymmetry is 97%.

Therefore, for the researched sample of wheat prices in USA one can infer that even in the New Times a significant influence of the space weather on agricultural markets is observed though the significance is a bit lower that that for observations during the Maunder Minimum (**Fig. 64c**). This unexpected, to some extent, result can be explained, maybe, by a very high concentration of the durum crop in a small area in North Dakota on the border with Canada (**Fig. 66c**). This zone is influenced by the North Atlantic Oscillation (NAO) that, in turn, is sensitive to the space weather. Using the method of regression with dummy variables gave a similar significance level of 96% for the relationship "solar activity — prices".

12.12. Manifestation of space weather influence on famines and death toll: a case study of Iceland of 18—19 centuries

One of the most tragic manifestations of sharp rises of grain prices caused by poor harvest under adverse weather conditions is famine and mortality from it. The above described effect of the space weather influence on the Earth weather that becomes apparent in a form of bad harvest and grain price rises, generally speaking should remain a trace in this sad statistics too. Obviously, such manifestation of the space weather can take place only in that regions and periods for which all three necessary conditions of the relationship "space weather" — "agricultural prices" take place. We chose Iceland of 18—19 centuries as a possible region for searching for such manifestations[11]. The key source of data about bad feed harvest and the caused cases of decrease in population

[11] The reasons for choosing just this region and period are as follows:

is the work of the US researcher Vasey (2001). As this is shown in this work, all periods of decrease in population of Iceland coincide with falls in livestock caused by bad feed harvest. The appropriate famine periods are marked by yellow triangular in **Fig. 67a**. It is striking that the periods of famine years always coincide or close to extremes of solar activity (minima or maxima). To examine this hypothesis we marked out the periods of cycles around famine years. These periods were marked out from minimum to minimum for events that happened during the period of the cycle maximum, and on the opposite, from maximum to maximum for events that happened during the period of the cycle minimum. To combine data from various cycles that differ one from another in duration and amplitude, in one homogeneous sample, sunspots numbers were normalized in relative amplitudes and times were normalized in relative phases of the cycle. For this purpose, for events close to the cycle maximum the normalized amplitude y_{norm} was defined as deviation from the minimal value normalized by the range of changes during the cycle:

$$y_{norm} = \left(ssn_i - ssn_{\min}\right)/\left(ssn_{\max} - ssn_{\min}\right), \quad \textbf{(132)}$$

where ssn_i is a sun spots number in year i, $ssn_{min}$is a number of sun spots in year of minimum, ssn_{max} is a number of sun spots in year of maximum, and for events in the neighborhood of the cycle minimum the absolute value of deviation from the maximal value was used, also normalized by the range of changes:

$$y_{norm} = \left(ssn_{\max} - ssn_i\right)/\left(ssn_{\max} - ssn_{\min}\right). \quad \textbf{(133)}$$

The times t_i were recalculated as cycle phases Φ_i according to the following formula:

$$\Phi_i = \left|t_i - t_{ext}\right| / T_{cycle}, \quad \textbf{(134)}$$

where t_{ext} are times of minimum or maximum of the cycle where famine has had happened, T_{cycle} is duration of the cycle. Normalized phase data for 6 cycles during which mass population decrease happened because of bad harvest and famine, are united in a sample presented in **Fig. 67b**. As it is seen in this figure, all 6 events of population decrease because of famine in Iceland in the period 1784-1900 are concentrated in a small part (20%) of the phase space of sun cycle around the cycle extremes (maximum or minimum). Probability of the random realization of such accurate phasing of two independent processes is estimated as $\mathbf{P = (1/5)^6 < 10^{-4}}$. The revealed phase linkage of the periods of famine because of weather anomalies in Iceland, to the solar activity extremes enables to claim about the highly significant manifestation of the negative influence of the space weather/solar activity on the state of the agricultural market in the region at the researched period.

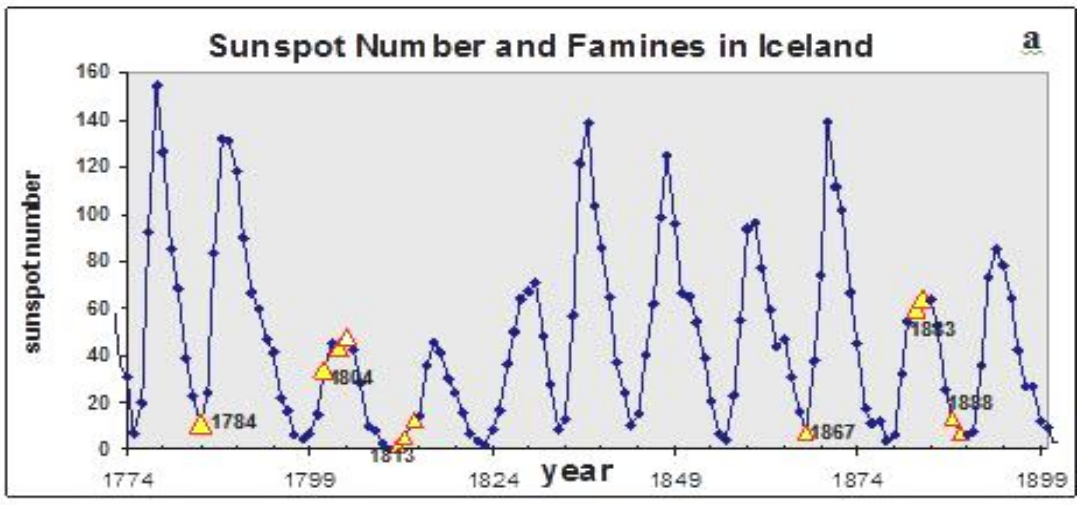

Fig. 67. Panel **a** —relationship between solar activity and periods of famine/decrease in population in Iceland of 18—19 centuries, in the phase curve of changes in number of sun spots; **b** — a phase diagram of the result of superposition of 6 solar activity periods during which fall in population happened because of the famine caused by decrease in livestock. In the horizontal axes phases of the cycle related to the cycle extremes (maximum or minimum) are marked when blue diamonds are sun spots numbers and red triangular are years of famine beginning. The rectangle in the center of the figure bounds the part of the phase space of cycles during which famines happened and population decreased.

12.13. Summary on research of space weather influence on agricultural markets

In this study the model of a possible influence of the space weather on the agricultural markets is presented based on the causal chain "space weather" — "earth weather" — "agricultural production' — "market prices". Main results are following:

1. It is marked that realization of this causal chain demands simultaneous satisfaction of several necessary conditions for specific zone and period. The influence of the space weather on agricultural markets is not a universal phenomenon, but reveals only in that zones and periods when and where all necessary conditions are satisfied (atmospheric, agro climatic, market).
2. A significant manifestation of this influence for the case of Medieval England is shown, particularly, for the period of the Maunder Minimum.
3. The dependence of the European markets sensitivity to the space weather (including the direction of this sensitivity) on localization in the corresponding climatic zone is shown.
4. It is shown that even in the New Time the dependence on the space weather/solar activity is observed in the USA. This dependence is revealed for durum wheat produced in a small zone sensitive to the influence of the North Atlantic Oscillation.
5. The coincidence of the periods of decrease in population in Iceland of the 18—19 centuries (caused by bad feed harvest and the following drop of livestock), from the one hand, and phases of solar activity extreme, from the other hand, is shown. We explain this coincidence as a manifestation of the earth markets dependence on the space weather we research in this study.
6. The presented results clearly indicate on significant space weather influence on the Earth agricultural markets, and first of all, on grain markets. This is true for the zones where the presented necessary conditions for the causal chains (**Fig. 63**) are satisfied in the researched period.

Let us note that continuous progress in the development of agro technology using achievements in gene engineering, biotechnology, irrigation, agro chemistry and plant protection should result in augmentation of steadiness of crops toward external factors like weather anomalies. This process should disturb the causal chain "space weather" — "agricultural prices" breaking the key link "weather — yield". Accordingly, in the nearest future one could assume gradual weakening of grain and other crops prices sensitivity to the space weather. Unfortunately, the global and sharp climate change observed in the last years can bring to the opposite results. The main feature of this change is the sharp growth of the amount and amplitude of weather anomalies especially shifts of the usual time bounds of seasonal weather states. Under these conditions, in many regions the long-term selection of crops most suitable for the zone can turn out to be not optimal. Sharp deviations of the local weather from the "standard" can move zones to the category of risky agriculture zones highly sensitive to weather anomalies. If such movement happens in the zone where the weather, in turn, is sensitive to the solar activity state and the external supply of agricultural production is limited for some reasons, the causal chain "space weather" — "agricultural prices" can become work-

ing even under the modern conditions of the technological progress and globalization. For a more specific identification of the regions where this negative phenomenon can take place in the nearest future, a progress in understanding various physical and technological processes is needed — global climate change and its consequences for local weather in various regions, zoned crops steadiness and mechanisms of solar-earth relationships regarding their influence on weather in the researched regions. To cope with this problem joined efforts of specialists from various fields are needed — agrarian researchers and meteorologists, astrophysics, and specialists in the space weather.

Acknowledgements. We would like cordially to thank H.S. Ahluwalia, J. Allen, A.V. Belov, E.B. Berezhko, J.W. Bieber, A. Chilingaryan, M. Duldig, E.A. Eroshenko, N. Iucci, K. Kudela, V. Kuznetsov, K. Munakata, Y. Muraki, M. Murat, M. Panasyuk, M. Parisi, N.G. Ptitsyna, M.A. Shea, D.F. Smart, A. Sternlieb, M. Storini, J.F. Valdes-Galicia, P. Velinov, G. Villoresi, A. Wolfendale, V.G. Yanke, I.G. Zukerman for interesting discussions, Itzik ben Israel and Uri Dai for constant interest and support of Israel Cosmic Ray & Space Weather Center and Israel-Italian Emilio Sergé Observatory.

REFERENCES

1. Ahluwalia H.S., 1997. "Three activity cycle periodicity in galactic cosmic rays", *Proc. 25th Intern.* Cosmic *Ray Conf.*, Durban, **2**, 109—112.
2. Allen J.H. and D.C. Wilkinson, 1993. "Solar-terrestrial activity affecting systems in space and on Earth", in *Proc. Workshop "Solar-Terrestrial Predictions-IV"*, Ottawa, Canada, 1992, edited by Hruska, J., M.A. Shea, D.F., Smart, and G. Heckman, NOAA Environ. Res. Lab., Boulder, CO, **1**, 75—107.
3. Appleby A.B. 1979, "Grain Prices and Subsistence Crises in England and France, 1590-1740". *The Journal of Economic History*, **39**(4): 865—887.
4. Arctowski H., 1910. "Studies on climate and crops". *Bulletin of the American Geographical Society*, XLII(4): 270-282, XLII(7): 481—495.
5. Ardanuy P.E., L.L. Stowe, A. Gruber, and M. Weiss, 1989. "Shortwave, longwave and net cloud-radiative forcing as determined from NIMBUS-7 observations", *J. Geophys. Res.*, **96**, 18537—18549.
6. Arnold, V. I., M1992. *Catastrophe Theory*. 3rd ed. Berlin: Springer-Verlag.
7. Artamonova I. and S. Veretenenko "Galactic cosmic ray variation influence on baric system dynamics at middle latitudes", *J. Atmosph. and Solar-Terrestrial Physics*, **73**, 366—370, 2011.
8. Azariadis C., 1981. "Self-Fulfilling Prophecies", *Journal of Economic Theory*, **25**, 380—396.
9. Baevsky, R.M. et al. 1996, *Proc. MEFA Int. Fair of Medical Technology & Pharmacy* (Brno, Chec Republic).
10. Baevsky R.M., V.M. Petrov, G. Cornelissen, F. Halberg, K. Orth-Gomur, T. Ekerstedt, K. Otsuka, T. Breus, J. Siegelova, J. Dusek, and B. Fiser, 1997. "Meta-analyzed heart rate variability, exposure to geomagnetic storms, and the risk of ischemic heart disease", *Scripta medica,* **70**, No. 4—5, 201—206.
11. Barnard L., M. Lockwood, M.A. Hapgood, M.J. Owens, C.J. Davis, and F. Steinhilber, 2011. "Predicting space climate change", Geophys. Res. Lett., 38, L16103, doi:10.1029/2011GL048489.
12. Bavassano B., N. Iucci, R.P Lepping, C. Signorini, E.J. Smith, and G.Villoresi, 1994. "Galactic cosmic ray modulation and interplanetary medium perturbations due to a long-living active region during October 1989", *J. Geophys. Res.*, **99**, No. A3, 4227—4234.
13. Beer J., G.M. Raisbeck, and F. Yiou, 1991. "Time variations of ^{10}Be and solar activity", in C.P. Sonett, M.S. Giampapa, and M.S. Matthews (eds.) *The Sun in time*, University of Arizona Press, 343—359.
14. Beer J., S. Tobias, and N. Weiss, 1998. "An active Sun throughout the Maunder minimum", *Solar Phys.*, **181**, 237—249.
15. Belov A.V., Dorman L.I., Eroshenko E.A., Iucci N., Villoresi G. and Yanke V.G., 1995a. "Search for predictors of Forbush-decreases". *Proc. 24-th Intern. Cosmic Ray Conf.,* Rome, **4**, 888—891.
16. Belov A.V., Dorman L.I., Eroshenko E.A., Iucci N., Villoresi G. and Yanke V.G., 1995b. "Anisotropy of cosmic rays and Forbush-decreases in 1991". *Proc. 24-th Intern. Cosmic Ray Conf.*, Rome, **4**, 912—915.
17. Belov A.V., E.A. Eroshenko, and V.G. Yanke, 1997. "Modulation Effects in 1991-1992 Years", *Proc. 25th Intern. Cosmic Ray Conf.*, 1997, Durban, South Africa, **1**, 437—440.
18. Belov A., L. Dorman I., E. Eroshenko, L. Gromova, N. Iucci, D. Ivanus, O. Kryakunova, A. Levitin, M. Parisi, N. Ptitsyna, M. Tyasto, E. Vernova, G. Villoresi, and V. Yanke, 2003. "The relation between malfunctions of satellites at different orbits and cosmic ray variations", *Proc. 28th Intern. Cosmic Ray Conf.*, 2003, Tsukuba, Japan, **7**, 4213—4216.
19. Belov A.V., L.I. Dorman, R.T. Gushchina, V.N. Obridko, B.D. Shelting and V.G. Yanke, 2005. "Prediction of expected global climate change by forecasting of galactic cosmic ray intensity time variation in near future based on solar magnetic field data", *Adv. Space Res.*, **35**, No. 3 , 491—495.
20. Berezhko E.G., V.I. Kozlov, A.I. Kuzmin, and N.N. Tugolukov, 1987. "Cosmic ray intensity micropulsations associated with disturbances of electromagnetic conditions in the heliosphere", *Proc. 20th Intern. Cosmic Ray Conf.*, 1987, Moscow, USSR, **4**, 99—102.
21. Beveridge W.H.B., M1939. *Prices and Wages in England from the Twelfth to the Nineteenth Century*. Longmans, Green: London, New York.
22. Beveridge William H., 1921. "Weather and Harvest Cycles," *Economic Journal*, XXXI, 429—453.
23. Bhattacharyya A. and B. Mitra, 1997. "Changes in cosmic ray cut-off rigidities due to secular variations of the geomagnetic field", *Ann. Geophys.*, **15**, No. 6, 734—739.
24. Blokh Ya.L., Glokova E.S., Dorman L.I. and Inozemtseva O.I., 1959. "Electromagnetic conditions in interplanetary space in the period from August 29 to September 10, 1957 determined by cosmic ray variation data". *Proc. 6-th Intern. Cosmic Ray Conf.*, Moscow, **4**, 172—177.
25. Boberg F., Lundstedt H., 2002. "Solar Wind Variations Related to Fluctuations of the North Atlantic Oscillation", *Geophysical Research Letters*, **29**(15): 13—19.
26. Brázdil R, Dobrovolný P, Luterbacher J, Moberg A, Pfister C, Wheeler D, Zorita E., 2010. "European climate of the past 500 years: new challenges for historical climatology". *Climatic Change*, **101**, 7—40.
27. Breus, T., Siegelova, J., Dusek, J., and Fiser, B. 1997, *Scripta Medica* **70**, 199
28. Brown E. H. P. and Hopkins S. V., 1956. "Seven centuries of the prices of consumables, compared with builders' wage-rates". *Economica*, XXIII (89-92): 296—314.
29. Cox A., G.B. Dalrymple, and R.R. Doedl, 1967. "Reversals of the Earth's magnetic field", *Sci. American*, **216**, No. 2, 44—54.

30. Dickinson R.E., 1975. "Solar variability and the lower atmosphere", *Bull. Am. Met. Soc*., **56**, 1240—1248.
31. Dobrica V., C. Demetrescu, C. Boroneant, G. Maris, 2009. "Solar and geomagnetic activity effects on climate at regional and global scales: Case study-Romania", *J. Atmospheric and Solar-Terrestrial Physics*, **71**, 1727— 1735.
32. Dorman L.I., 1959. "On the energetic spectrum and lengthy of cosmic ray intensity increase on the Earth caused by shock wave and albedo from magnetized front of corpuscular stream.. *Proc. 6-th Intern. Cosmic Ray Conf.*, Moscow, **4**, 132—139.
33. Dorman L.I., 1960. "On the energetic spectrum and prolongation of the cosmic ray intensity increase on the Earth caused by shock wave of corpuscular stream". *Proc.of Yakutsk Filial of Academy of Sciences*, Ser. Phys., Academy of Sciences of USSR Press, Moscow, No. 3, 145—147.
34. Dorman L.I., M1963a. *Cosmic Ray Variations and Space Explorations.* NAUKA, Moscow, pp 1023.
35. Dorman L.I., M1963b. G*eophysical and Astrophysical Aspects of Cosmic Rays.* North-Holland Publ. Co., Amsterdam (In series "Progress in Physics of Cosmic Ray and Elementary Particles",ed. by J.G.Wilson and S.A.Wouthuysen, Vol. 7), pp 320.
36. Dorman L.I., M1972. *Acceleration Processes in Space*. VINITI, Moscow (in series "Summary of Science", Astronomy, Vol. 7).
37. Dorman L.I., M1974. *Cosmic Rays: Variations and Space Exploration.* North-Holland Publ. Co., Amsterdam. pp 675.
38. Dorman L.I., M1978. *Cosmic Rays of Solar Origin.* VINITI, Moscow (in series "Summary of Science", Space Investigations, Vol.12).
39. Dorman L.I., 2002. "Solar Energetic Particle Events and Geomagnetic Storms Influence on People's Health and Technology; Principles of Monitoring and Forecasting of Space Dangerous Phenomena by Using On-Line Cosmic Ray Data", in *Proc. 22nd ISTC Japan Workshop on Space Weather Forecast in Russia/CIS*, Nagoya, Japan, June 2002, edited by Muraki Y., Nagoya University, **2**, 133—151.
40. Dorman L.I., M2004. *Cosmic Rays in the Earth's Atmosphere and Underground*, Kluwer Academic Publishers, Dordrecht/Boston/London.
41. Dorman L.I., 2005a. "Prediction of galactic cosmic ray intensity variation for a few (up to 10—12) years ahead on the *basis* of convection-diffusion and drift model", *Annales Geophysicae*, **23**, No. 9, 3003—3007.
42. Dorman L.I., 2005b. "*Estimation* of long-term cosmic ray intensity variation in near future and prediction of their contribution in expected global climate change", *Adv. Space Res*., **35**, 496—503.
43. Dorman L.I., 2006. "Long-term cosmic ray intensity variation and part of global climate change, controlled by solar activity through cosmic rays", Adv. Space Res., 37, 1621—1628.
44. Dorman L.I., M2006. *Cosmic Ray Interactions, Propagation, and Acceleration in Space,* Springer, Netherlands.
45. L.I. Dorman, 2008a. "Forecasting of radiation hazard and the inverse problem for SEP propagation and generation in the frame of anisotropic diffusion and in kinetic approach", *Proc. 30-th Intern. Cosmic Ray Conf*., Merida, Mexico, **1**, 175—178.
46. Dorman L.I., 2008b. "Natural hazards for the Earth's civilization from space, 1. Cosmic ray influence on atmospheric processes", *Adv. Geosci*., **14**, 281-286.
47. Dorman L.I., 2009. "Chapter 3. The Role of Space Weather and Cosmic Ray Effects in Climate Change", in book *Climate Change: Observed Impacts on Planet Earth*, Edited by Trevor M. Letcher, Elsevier.
48. Dorman L.I., M2009. *Cosmic Rays in Magnetospheres of the Earth and other Planets*, Springer, Netherlands.
49. Dorman L.I., M2010. *Solar Neutrons and Related Phenomena*, Springer, Netherlands.
50. Dorman L.I., 2012. "Cosmic rays and space weather: effects on global climate change", *Ann. Geophys*., **30**, No. 1, 9—19.
51. Dorman I.V. and L.I. Dorman, 1967a. "Solar wind properties obtained from the study of the 11-year cosmic ray cycle. 1", *J. Geophys. Res*., **72**, No. 5, 1513—l520.
52. Dorman I.V. and L.I. Dorman, 1967b. "Propagation of energetic particles through interplanetary space according to the data of 11-year cosmic ray variations", *J. Atmosph. and Terr. Phys*., **29**, No. 4, 429—449.
53. Dorman L.I. and I.V. Dorman, 2005. "Possible influence of cosmic rays on climate through thunderstorm clouds", *Adv. Space Res*., **35**, 476—483.
54. Dorman L.I. and Freidman G.I., 1959. "On the possibility of charged particle acceleration by shock waves in the magnetized plasma". *Proc. on All-Union Conf. on Magnetohydrodinamics and Plasma Physics*, Latvia SSR Academy of Sciences Press, Riga, pp. 77—81.
55. Dorman L.I. and Miroshnichenko L.I., M1968. *Solar Cosmic Rays*. FIZMATGIZ, Moscow, pp 508. English translation published for the National Aeronautics and Space Administration and National Science Foundation in 1976 (TT 70-57262/ NASA TT F-624), Washington, D.C.
56. Dorman L.I. and L.A. Pustil'nik, 1999. "Statistical characteristics of SEP events and their connection with acceleration, escaping and propagation mechanisms", *Proc. 26-th Intern. Cosmic Ray Conference*, Salt Lake City, **6**, 407—410.
57. Dorman L.I., I.Ya. Libin, M.M. Mikalayunas, and K.F. Yudakhin, 1987. "On the connection between cosmophysical and geophysical parameters in 19-20 cycles of solar activity", *Geomagnetism and Aeronomy*, **27**, No. 2, 303—305.
58. Dorman L.I., I.Ya. Libin, and M.M. Mikalajunas, 1988a. "About the possibility of the influence of cosmic factors on weather, spectral analysis: cosmic factors and intensity of storms", *The Regional Hidrometeorology (Vilnius)*, **12**, 119—134.
59. Dorman L.I., I.Ya. Libin, and M.M. Mikalajunas, 1988b. "About the possible influence of the cosmic factors on the weather. Solar activity and sea storms: instantaneous power spectra", *The Regional Hidrometeorology (Vilnius)*, **12**, 135—143.
60. Dorman L.I, Iucci N., Villoresi G., 1993a. "The use of cosmic rays for continuos monitoring and prediction of some dangerous phenomena for the Earth's civilization". *Astrophysics and Space Science*, **208**, 55—68.
61. Dorman L.I., Iucci N. and Villoresi G., 1993b. "Possible monitoring of space processes by cosmic rays". *Proc. 23-th Intern. Cosmic Ray Conf*., Calgary, **4**, 695—698.
62. Dorman L.I., Iucci N. and Villoresi G., 1993c. "Space dangerous phenomena and their possible prediction by cosmic rays". *Proc. 23-th Intern. Cosmic Ray Conf*., Calgary, **4**, 699—702.
63. Dorman L.I., Iucci N., Villoresi G., 1995a. "The nature of cosmic ray Forbush-decrease and precursory effects". *Proc. 24-th Intern. Cosmic Ray Conf*., Rome, **4**, 892—895.
64. Dorman L.I., Villoresi G., Belov A.V., Eroshenko E.A., Iucci N., Yanke V.G., Yudakhin K.F., Bavassano B., Ptitsyna N.G., Tyasto M.I., 1995b. "Cosmic-ray forecasting features for big Forbush-decreases". *Nuclear Physics B*,. **49A**, 136—144.
65. Dorman L.I., Iucci N. and Villoresi G., 1997a. "Auto-model solution for nonstationary problem described the cosmic ray preincrease effect and Forbush-decrease". *Proc. of 25- th Intern. Cosmic Ray Conference,* Durban (South Africa), **1**, 413—416.
66. Dorman L.I., G. Villoresi, I.V. Dorman, N. Iucci, and M. Parisi, 1997b. "On the expected CR intensity global modulation in the Heliosphere in the last several hundred years". *Proc. 25-th Intern. Cosmic Ray Conference*, Durban (South Africa), **7**, 345—348.
67. Dorman L.I., N. Iucci, N.G. Ptitsyna, G. Villoresi, 1999. "Cosmic ray Forbush-decrease as indicators of space dangerous phenomenon and possible use of cosmic ray data for their prediction", *Proc. 26-th Intern. Cosmic Ray Conference*, Salt Lake City, **6**, 476—479.
68. Dorman L.I., B. A. Shakhov, and M. Stehlik, 2003a. "The second order pitch-angle approximation for the cosmic ray Fokker-Planck kinetic equations", *Proc. 28th Intern. Cosmic Ray Conf*., Tsukuba (Japan), **6**, 3535—3538.

69. Dorman L.I., I.V. Dorman, N. Iucci, M. Parisi, Y. Ne'eman, L.A. Pustil'nik, F. Signoretti, A. Sternlieb, G. Villoresi, and I.G. Zukerman, 2003b. "Thunderstorms Atmospheric Electric Field Effect in the Intensity of Cosmic Ray Muons and in Neutron Monitor Data", *J. Geophys. Res*., **108**, No. A5, 1181, SSH 2_1—8.
70. Eddy J.A., 1976. "The Maunder Minimum", *Science*, **192**, 1189—1202.
71. Ejrnæs M., Persson K.G., and Rich S., 2008. "Feeding the British: convergence and market efficiency in the nineteenth-century grain trade". *The Economic History Review*, **61**(s1): 140—171.
72. Ely J.T.A. and T.C. Huang, 1987. "Geomagnetic activity and local modulations of cosmic ray circa 1 GeV", Geophys*. Res. Lett*., **14**, No. 1, 72—75.
73. Ely J.T.A., J.J. Lord, and F.D. Lind, 1995. "GCR, the Cirrus hole, global warming and record floods", *Proc. 24th Intern. Cosmic Ray Conf*., Rome, **4**, 1137—1140.
74. Enghoff M.B., J.O.P. Pedersen, U.I. Uggerhøj, S.M. Paling, and H. Svensmark, 2011. "Aerosol nucleation induced by a high energy particle beam", *Geophys. Res. Lett*., **38**, L09805, doi:10.1029/2011GL047036.
75. Erlykin A.D. and A.W. Wolfendale, 2011. "Cosmic ray effects on cloud cover and the irrelevance to climate change", *J. Atm. and Solar-Terr. Physics*, **73**, 1681—1686.
76. Erlykin A.D., G. Gyalai, K. Kudela, T. Sloan and A.W. Wolfendale, 2009a. "Some aspects of ionization and the cloud cover, cosmic ray correlation problem", *J. Atmospheric and Solar-Terrestrial Physics*, **71**, 823—829.
77. Erlykin A.D., G. Gyalai, K. Kudela, T. Sloan, and A.W. Wolfendale, 2009b. "On the correlation between cosmic ray intensity and cloud cover", *J. Atm. and Solar-Terr. Physics*, **71**, 1794—1806.
78. Ermakov V.I., G.A. Bazilevskaya, P.E. Pokrevsky, and Yu. I. Stozhkov, 1997. "Cosmic rays and ion production in the atmosphere", *Proc. 25th Intern. Cosmic Ray Conf*., Durbin, **7**, 317—320.
79. Ermakov V, V. Okhlopkov, and Yu. Stozhkov, 2006a. "Influence of Zodiac Dust on the Earth's Climate", *Proc. European Cosmic Ray Symposium*, Lesboa, Paper 1—72.
80. Ermakov V.I., V.P. Okhlopkov, and Y.I. Stozhkov, 2006b. "Influence of cosmic dust on the Earth's climate," *Bulletin of Lebedev Physics Institute*, Russian Ac. of Sci., Moscow, No. 3, 41—51.
81. Ermakov V.I., V.P. Okhlopkov, and Yu.I. Stozhkov, 2006c. "Effect of cosmic dust on terrestrial climate", *Kratk. Soob'sh. Fiz. FIAN*, No. 3, 41—51. In Russian.
82. Ermakov V.I., V.P. Okhlopkov, and Yu.I. Stozhkov, 2007. "Effect of cosmic dust on cloudiness, albedo, and terrestrial climate", *Vestn. Mosk. Univ*., Ser. 3: Fiz. Astron., No. 5, 41—45. In Russian.
83. Ermakov V.I., V.P. Okhlopkov, and Yu.I. Stozhkov, 2009. "Cosmic rays and dust in the Earth's atmosphere", *Izv. Russ. Akad. Nauk*, Ser. Fiz., **73**, No. 3, 434—436. In Russian.
84. Fastrup B., E. Pedersen, E. Lillestol et al. (Collaboration CLOUD), 2000. "A study of the link between cosmic rays and clouds with a cloud chamber at the CERN PS", *Proposal CLOUD*, CERN/SPSC 2000-021.
85. Fedorov Yu., M. Stehlik, K. Kudela, and J. Kassovicova, 2002. "Non-diffusive particle pulse transport: Application to an anisotropic solar GLE", *Solar Physics*, **208**, No. 2, 325—334.
86. Fenton, A. G. et al. 1959, Can. J. Phys. 37, 970.
87. Ferraro R.R., F. Weng, N.C. Grody, and A. Basist, 1996. "An eight-year (1987-1994) time series of rainfall, clouds, water vapor, snow cover, and sea ice derived from SSM/I measurements", *Bull. Am. Met. Soc*., **77**, 891—905.
88. Friis-Christiansen E. and K. Lassen, 1991. "Length of the solar cycle: an indicator of solar activity closely associated with climate", *Science*, **254**, 698-700.
89. Fuhrer K., E.W. Wolff, S.J. Johnsen, 1999. "Timescales for dust variability in the Greenland Ice Core Project (GRIP) in the last 100,000 years," *J. Geophys. Res*., **104**, No. D24, 31043—31052.
90. Georgieva K. and Kirov B., 2011. "Solar dynamo and geomagnetic activity", *Journal of Atmospheric and Solar-Terrestrial Physics*, **73**, Issue 2—3, 207—222.
91. Haigh J.D., 1996. "The impact of solar variability on climate", *Science*, **272**, 981—984.
92. Haigh J.D., Winning A.R., Toumi R. and Harder J.W., 2010, "An influence of solar spectral variations on radiative forcing of climate", *Nature*, **467**, 7 Oct 2010, 696—699.
93. Hansen J., R. Ruedy, J. Glascoe, and M. Sato, 1999. "GISS analysis of surface temperature change", *J. Geophys. Res*., **104**, No. D24, 30997—31022.
94. Harrison G. and Stephenson D., 2006. "Empirical evidence for a non-linear effect of galactic cosmic rays on clouds", *Proceedings of the Royal Society A*, **A 462**, 2068, 1221—1233 doi: 10.1098/rspa.2005.1628.
95. Hartmann D.L., 1993. "Radiative effects of clouds on the Earth's climate in aerosol-cloud-climate interactions", in P.V. Hobbs (ed) *Aerosol-Cloud-Climate Interactions*, Academic Press, 151.
96. Head L., Atchison J., Gates A., Muir P., 2011. "A Fine-Grained Study of the Experience of Drought, Risk and Climate Change Among Australian Wheat Farming Households". *Annals of the Association of American Geographers*, **101**(5): 1089—1108.
97. Herschel W., 1801. "Observations Tending to Investigate the Nature of the Sun, in Order to Find the Causes and Symptoms of its Variable Emission of Light and Heat", *Philosophical Transactions of the Royal Society of London*, **91**, 261—331.
98. Hong P.K., H. Miyahara, Y. Yokoyama, Y. Takahashi, and M. Sato, 2011. "Implications for the low latitude cloud formations from solar activity and the quasi-biennial oscillation", *J. Atmospheric and Solar-Terrestrial Physics*, **73**, 587—591.
99. Hooker P.H., 1907. "Correlations of the weather and crops", *Journ. Roy. Statistical Society*, **70**(1).
100. Hruska J. and Shea M.A., 1993, *Adv. Space Res*. **13**, 451.
101. International Institute of Social History, 2005. Available online http://www.iisg.nl/index.php.
102. Iucci N., L.I. Dorman, A.E. Levitin, A.V. Belov, E.A. Eroshenko, N.G. Ptitsyna, G. Villoresi, G.V. Chizhenkov, L.I. Gromova, M. Parisi, M.I. Tyasto, and V.G. Yanke, 2006. "Spacecraft operational anomalies and space weather impact hazards", *Adv. Space Res*., **37**, No. 1, 184—190.
103. Jevons W.S., 1878. "Commercial Crises and Sun-Spots 1", *Nature*, **19**, No. 472, 33—37.
104. Jevons W.S., 1879. "Sun-Spots and Commercial Crises", *Nature*, **19**, No. 495, 588—590.
105. Jevons W.S., 1882. "The solar commercial cycle", *Nature*, **26**, No. 662, 226—228.
106. Jones P.D., K.R. Briffa, T.P. Barnett, and S.F.B. Tett, 1998. "High resolution palaeoclimatic records for the last millennium: interpretation, integration and comparison with general circulation model control run temperatures", *The Holocene*, **8**, 455—471.
107. Kappenman J.G. and V.D. Albertson, 1990. "Bracing for the geomagnetic storms", *IEEE Spectrum*, **27**, No. 3, 27—33.

108. Kasatkina E.A., O.I. Shumilov, and M. Krapiec, 2007a. "On periodicities in long term climatic variations near 68° N, 30° E", *Adv. Geosci*., **13**, 25—29.
109. Kasatkina E.A., O.I. Shumilov, N.V. Lukina, M. Krapiec, and G. Jacoby, 2007b. "Stardust component in tree rings", *Dendrochronologia*, **24**, 131—135.
110. King J.W., 1975. "Sun-weather relationships", *Astronautics and Aeronautics*, **13**, No. 4, 10—19.
111. Kirkby J. and CLOUD collaboration, 2011, "Role of sulphuric acid, ammonia and galactic cosmic rays in atmospheric aerosol formation", *Nature*, **476**, No. 10343, 429—433.
112. Kishcha P.V., Dmitrieva I.V., and Obridko V.N., 1999, "Long-term variations of the solar-geomagnetic correlation, total solar irradiance, and northern hemispheric temperature (1868□1997)", *Journal of Atmospheric and Solar-Terrestrial Physics*, **61**, 799—808.
113. Koenig, H., & Ankermueller, F. 1982, *Naturwissenscahften,* **17**, 47.
114. Kristjánsson J.E., A. Staple, and J. Kristiansen, 2002. "A new look at possible connections between solar activity, clouds and climate", *Geophys. Res. Lett*., **23**, 2107—2110.
115. Kristjánsson J.E., J. Kristiansen and E. Kaas, 2004. "Solar activity, cosmic rays, clouds and climate - an update", *Adv. Space Res*., **34**, No. 2, 407—415.
116. Kudela K. and P. Bobik, 2004. "Long-term variations of geomagnetic rigidity cutoffs", *Solar Physics*, **224**, 423—431.
117. Labitzke K. and H. van Loon, 1993. "Some recent studies of probable connections between solar and atmospheric variability", *Ann. Geophys*., **11**, 1084—-1094.
118. Laken B.A. and D.R. Kniveton, 2011. "Forbush decreases and Antarctic cloud anomalies in the upper troposphere", *J. Atmospheric and Solar-Terrestrial Physics*, **73**, 371—376.
119. Lassen K. and E. Friis-Christiansen, 1995. "Variability of the solar cycle length during the past five centuries and the apparent association with terrestrial climate", *J. Atmos. Solar-Terr. Phys*., **57**, 835—845.
120. Lean J., A. Skumanich, and O. White, 1992. "Estimating the Sun's radiative output during the Maunder minimum", *Geophys. Res. Lett*., **19**, 1591—1594.
121. Lean J., J. Beer, and R. Breadley, 1995. "Reconstruction of solar irradiance since 1610: implications for climate change", *Geophys. Res. Lett*., **22**, 3195—3198.
122. Lockwood M., R. Stamper, and M.N. Wild, 1999. "A doubling of the Sun's coronal magnetic field during the past 100 years", *Nature*, **399**, No. 6735, 437—439.
123. Lukianova R. and Alekseev G., 2004. "Long-Term Correlation between the NAO and Solar Activity". *Solar Physics,* **224**(1-2), 445—454.
124. Mann M.E., R.S. Bradley, and M.K. Hughes, 1998. "Global-scale temperature patterns and climate forcing over the past six centuries", *Nature*, **392**, 779—787.
125. Mansilla G.A., 2011. "Response of the lower atmosphere to intense geomagnetic storms", *Advances in Space Research*, **48**, 806–810.
126. Markson R., 1978. "Solar modulation of atmospheric electrification and possible implications for the Sun-weather relationship", *Nature*, **273**, 103—109.
127. Marsh N.D. and H. Swensmark, 2000a. "Low cloud properties influenced by cosmic rays", *Phys. Rev. Lett*., **85**, 5004—5007.
128. Marsh N. and H. Swensmark, 2000b. "Cosmic rays, clouds, and climate", *Space Sci. Rev*., **94**, No. 1-2, 215—230.
129. Martin I.M., A.A. Gusev, G.I. Pugacheva, A. Turtelli, and Y.V. Mineev, 1995. "About the origin of high-energy electrons in the inner radiation belt", *J. Atmos. and Terr. Phys*., **57**, No. 2, 201—204.
130. Maseeva O.A., 2004. "Role of huge molecular clouds in the evolution of Oort's cloud," *Astronomichesky vestnik*, **38**, No. 4, 372—382.
131. McCracken K.G. and N.R. Parsons, 1958. "Unusual Cosmic-Ray Intensity Fluctuations Observed at Southern Stations during October 21—24, 1957", *Phys. Rev.,Ser. 2,* **112**, No. 5, 1798—1801.
132. Mendoza B. and M. Pazos, 2009. "A 22 yr hurricane cycle and its relation with geomagnetic activity", *J. Atmospheric and Solar-Terrestrial Physics*, **71**, 2047—2054.
133. Munakata K., J.W. Bieber, S.-I. Yasue, C. Kato, M. Koyama, S. Akahane, K. Fujimoto, Z. Fujii, J.E. Humble, and M.L. Duldig, 2000. "Precursors of geomagnetic storms observed by the muon detector network", *J. Geophys. Res.*, **105**, No. A12, 27,457—27,468.
134. Nagashima K., S. Sakakibara, K. Fujimoto, R. Tatsuoka, and I. Morishita, 1990. "Localized pits and peaks in Forbush decrease, associated with stratified structure of disturbed and undisturbed magnetic fields", *IL Nuovo Cimento C,* **13C**, Ser. 1, No. 3, 551—587.
135. Nagovitsyn Yu.A., 2007. "Solar cycles during the Maunder minimum", *Astronomy Letters*, **33**, 5, 385—391.
136. Ney E.R., 1959. "Cosmic radiation and weather", *Nature*, **183**, 451—452.
137. Ogurtsov M.G. and O.M. Raspopov, 2011. "Possible impact of interplanetary and interstellar dust fluxes on the Earth's climate", *Geomagnetism and Aeronomy*, **51**, No. 2, 275—283.
138. Ogurtsov M.G., Kocharov G.E., and Nagovitsyn Yu.A., 2003, "Solar Cyclicity during the Maunder Minimum", *Astron. Reports*., **47**, Issue 6, 517—-524.
139. Ogurtsov M.G., O.M. Raspopov, M. Oinonen, H. Jungner, and M. Lindholm, 2010. "Possible manifestation of nonlinear effects when solar activity affects climate changes", *Geomagnetism and Aeronomy*, **50**, No. 1, 15—20.
140. Ohring G. and P.F. Clapp, 1980. "The effect of changes in cloud amount on the net radiation on the top of the atmosphere", *J. Atmospheric Sci*., **37**, 447—454.
141. Parker E.N., M1963. *Interplanetary Dynamical Processes*, John Wiley and Suns, New York-London.
142. Parker E.N., M1965. *Interplanetary Dynamical Processes*, Inostrannaja Literatura, Moscow (In Russian, Translation by L.I. Miroshnichenko, Editor L.I. Dorman).
143. Petit J.R., J. Jouzel, D. Raunaud, at.al., 1999. "Climate and atmospheric history of the past 420,000 years from Vostok ice core, Antarctica", *Nature*, **399**, 429—436.
144. Price C., 2000. "Evidence for a link between global lightning activity and upper tropospheric water vapour", *Nature*, **406**, 290—293.
145. Ptitsyna N.G., G. Villoresi, L.I. Dorman, N. Iucci, and M.I. Tyasto. 1998. "Natural and man-made low-frequency magnetic fields as a potential health hazard", *UFN (Uspekhi Physicheskikh Nauk*), 168, No 7, pp. 767—791.
146. Pudovkin M. and S. Veretenenko, 1995. "Cloudiness decreases associated with Forbush-decreases of galactic cosmic rays", *J. Atmos. Solar-Terr. Phys*., **57**, 1349—1355.
147. Pudovkin M. and S. Veretenenko, 1996. "Variations of the cosmic rays as one of the possible links between the solar activity and the lower atmosphere". *Adv. Space Res*., **17**, No. 11, 161—164.

148. Pudovkin M.I. and O.M. Raspopov, 1992. "The mechanism of action of solar activity on the state of the lower atmosphere and meteorological parameters (a review)", *Geomagn. and Aeronomy*, **32**, 593—608.
149. Pudovkin M.I. and O.M. Raspopov, 1993. "Physical mechanism of the action of solar activity and other geophysical factors on the state of the lower atmosphere, meteorological parameters, and climate", *Phys. Usp*., **36**, No.7, 644—647.
150. Pugacheva G.I., A.A. Gusev, I.M. Martin et al., 1995. "The influence of geomagnetic disturbances on the meteorological parameters in the BMA region", *Proc. 24th Intern. Cosmic Ray Conf*., Rome, **4**, 1110—1113.
151. Pulkkinen T.I., H. Nevanlinna, P.J. Pulkkinen, and M. Lockwood, 2001. "The Sun-Earth connection in time scales from years to decades and centuries", *Space Sci. Rev*., **95**, 625—637.
152. Pustil'nik L., G. Yom Din, and L. Dorman, 2003. "Manifestations of Influence of Solar Activity and Cosmic Ray Intensity on the Wheat Price in the Medieval England (1259–1703 Years)", *Proc. 28th Intern. Cosmic Ray Conf*., Tsukuba, **7**, 4131—4134.
153. Pustil'nik L. and G. Yom Din, 2004a. "Influence of solar activity on the state of the wheat market in medieval England", *Solar Physics*, **223**, 335—356.
154. Pustil'nik L. and G. Yom Din, 2004b. "Space climate manifestation in earth prices – from medieval England up to modern U.S.A.", *Solar Physics*, **224**, 473—481.
155. Quante M., 2004. "The role of clouds in the climate system", *J. Phys. IV France*, **121**, 61—86.
156. Ramanathan V., R.D. Cess, E.F. Harrison, P. Minnis, B.R. Barkstrom, E. Ahmad, and D. Hartmann, 1989. "Cloud-radiative forcing and climate: results from the Earth Radiation Budget Experiment", *Science*, **243**, No. 4887, 57—63.
157. Reiter R., 1954. "The importance of the atmospheric long radiation disturbances for the statistical biometeorology", *Archiv fur Physikalische Therapie*, **6**, No. 3, 210—216.
158. Reiter R., 1955. "Bio-meteorologie auf physikalisher Basis", *Phys. Blaetter*, **11**, 453—464.
159. Renaker D., 1979. Swift's Laputians as a Caricature of the Cartesians. *PMLA*, **94**(5): 936-944. Published by Modern Language Association.
160. Richter G.M. and Semenov M.A., 2005, "Modeling impacts of climate change on wheat yields in England and Wales—assessing drought risks", *Agric. Syst*., **84** (1), 77—97.
161. Rogers J.E.T., M1887. *Agriculture and Prices in England*, Vol. 1-8, Oxford, Clarendon Press; Reprinted by Kraus Reprint Ltd, Vaduz in 1963.
162. Rossow W.B. and B. Cairns, 1995. "Monitoring changes of clouds", *J. Climate*, **31**, 305—347.
163. Rossow W.B. and R. Shiffer, 1991. "ISCCP cloud data products", *Bull. Am. Met. Soc*., **72**, 2—20.
164. Ruzmaikin A., 1999, "Can El Nino amplify the solar forcing of climate", *Geophysical Research Letters*, **26**, 15, 2255—2258
165. Ruzmaikin A., 2007, "Effect of solar variability on the Earth's climate pattern", *Advances in Space Research*, **40**, 1146—1151.
166. Sakurai K., 2003. "The Long-Term Variation of Galactic Cosmic Ray Flux and Its Possible Connection with the Current Trend of the Global Warming", *Proc. 28th Intern. Cosmic Ray Conf*., Tsukuba, **7**, 4209—4212.
167. Schlegel K., G. Diendorfer, S. Them, and M. Schmidt, 2001. "Thunderstorms, lightning and solar activity – Middle Europe", *J. Atmos. Solar-Terr. Phys*., **63**, 1705—1713.
168. Shapiro A.I., W. Schmutz, E. Rozanov, M. Schoell, M. Haberreiter, A.V. Shapiro, and S. Nyeki, 2011. "A new approach to the long-term reconstruction of the solar irradiance leads to large historical solar forcing", *Astronomy & Astrophysics*, **529**, A67 (1—8), DOI: 10.1051/0004-6361/201016173.
169. Shaviv N.J., 2005, "On Climate Response to Changes in the Cosmic Ray Flux and Radiative Budget", *J. Geophys. Res.–Space Phys*., **110** (A8): A08105.
170. Shea M.A. and Smart D.F., 1992, "Recent and Historical Solar Proton Events", *Radiocarbon*, **34**, No. 2,. 255—262.
171. Shea M.A. and D.F. Smart, 2003. "Preliminary Study of the 400-Year Geomagnetic Cutoff Rigidity Changes, Cosmic Rays and Possible Climate Changes", *Proc. 28th Intern. Cosmic Ray Conf*., Tsukuba, **7**, 4205—4208.
172. Shiller R.J., 1990. "Speculative Prices and Popular Models". *The Journal of Economic Perspectives*, **4** (2), 55—65.
173. Shindell D., D. Rind, N. Balabhandran, J. Lean, and P. Lonengran, 1999. "Solar cycle variability, ozone, and climate", *Science*, **284**, 305—308.
174. Smith A., M1776. *An Inquiry into the Nature and Causes of the Wealth of Nations*. London, W. Strahan & T. Cadell.
175. Smith G.L., K.J. Priestley, N.G. Loeb, B.A. Wielicki, T.P. Charlock, P. Minnis, D.R. Doelling, and D.A. Rutan, 2011. "Clouds and Earth Radiant Energy System (CERES), a review: Past, present and future", *Advances in Space Research*, **48**, 254—263.
176. Soon W. and Yaskell S., M2003. *The Maunder Minimum and the Variable Sun-Earth Connection*, World Scientific Publishing Company.
177. Stowe L.L., C.G. Wellemayer, T.F. Eck, H.Y.M. Yeh, and the Nimbus-7 Team, 1988. "Nimbus-7 global cloud climatology, Part 1: Algorithms and validation", *J. Climate*, **1**, 445—470.
178. Stozhkov Yu.I., 2002. "The role of cosmic rays in atmospheric processes", *J. Phys. G: Nucl. Part. Phys*., **28**, 1—11.
179. Stozhkov Yu.I., J. Zullo, I.M. Martin et al., 1995a. "Rainfalls during great Forbush-decreases", *Nuovo Cimento*, **C18**, 335—341.
180. Stozhkov Yu.I., P.E. Pokrevsky, I.M. Martin et al., 1995b. "Cosmic ray fluxes and precipitations", *Proc. 24th Intern. Cosmic Ray Conf*., Rome, **4**, 1122—1125.
181. Stozhkov Yu.I., P.E. Pokrevsky, J. Jr. Zullo et al., 1996. "Influence of charged particle fluxes on precipitation", *Geomagn. and Aeronomy*, **36**, 211—216.
182. Stozhkov Yu.I., P.E. Pokrevsky, and V.P. Okhlopkov, 2000. "Long-term negative trend in cosmic ray flux", *J. Geophys. Res*., **105**, No. A1, 9—17.
183. Stozhkov Yu.I., V.I. Ermakov, and P.E. Pokrevsky, 2001. "Cosmic rays and atmospheric processes", *Izvestia Russian Academy of Sci*. , Ser. Phys., **65**, No. 3, 406—410.
184. Suits D.B., 1957. "Use of Dummy Variables in Regression Equations". *Journal of the American Statistical Association*, **52**(280), 548—551.
185. Swensmark H., 1998. "Influence of cosmic rays on the Earth's climate", *Phys. Rev. Lett*., **81**, 5027—5030.
186. Svensmark H., 2000. "Cosmic rays and Earth's climate", *Space Sci. Rev*., **93**, 175—185.
187. Swensmark H. and E. Friis-Christiansen, 1997. "Variation of cosmic ray flux and global cloud coverage – a missing link in solar-climate relationships", *J. Atmos. Solar-Terr. Phys*., **59**, 1225—1232.
188. Swift J., M1726. *Gulliver's Travels, Part III. A Voyage to Laputa, Balnibarbi, Luggnagg, Glubbdubdrib, and Japan*.
189. Thomas W.B., 1995. "Orbital anomalies in Goddard Spacecraft for Calendar Year 1994", *NASA Technical Paper 9636*, pp. 1—53.
190. Thornton P.K., Jones P.G., Alagarswamy G., and Andresen J., 2009. "The temporal dynamics of crop yield responses to climate change in East Africa". *Global Environmental Change*, **19**, 54—65.
191. Tinsley B.A., 1996. "Solar wind modulation of the global electric circuit and the apparent effects of cloud microphysics, latent heat release, and tropospheric dynamics", *J. Geomagn. Geoelectr*., **48**, 165-175.

192. Tinsley B.A., 2000. "Influence of solar wind on the global electric circuit, and inferred effects on cloud microphysics, temperature, and dynamics in the troposphere", *Space Sci. Rev.*, **94**, No. 1-2, 231—258.
193. Tinsley B.A. and G.W. Deen, 1991. "Apparent tropospheric response to MeV-GeV particle flux variations: a connection via electrofreezing of supercooled water in high-level clouds?", *J. Geophys. Res.*, **96**, No. D12, 22283—22296.
194. Todd M.C. and D.R. Kniveton, 2001. "Changes in cloud cover associated with Forbush decreases of galactic cosmic rays", *J. Geophys. Res.*, **106**, No. D23, 32031—32042.
195. Todd M.C. and D.R. Kniveton, 2004. "Short-term variability in satellite-derived cloud cover and galactic cosmic rays: an update" *J. .Atmosph. and Solar-Terrestrial Physics*, **66**, 1205—1211.
196. USDA, 2004. "Prices Received by Farmers: Historic Prices & Indexes 1908-1992 (92152)". *National Agricultural Statistics Service*. http://usda.mannlib.cornell.edu/, accessed 23 July 2004.
197. Usoskin I.G., O.G. Gladysheva, and G.A. Kovaltsov, 2004. "Cosmic ray induced ionization in the atmosphere: spatial and temporal changes", *J. Atmosph. Solar-Terr. Phys.*, **66**, No. 18, 1791—1796.
198. Vasey D.A., 2001. "A quantative assessment of buffer among temperature variations, livestock, and Human Population of Iceland, 1784 to 1900", *Climatic Change*, **48**, 243—263.
199. Veizer J., Y. Godderis, and I.M. Francois, 2000. "Evidence for decoupling of atmospheric CO_2 and global climate during the Phanerozoiceon," *Nature*, **408**, 698—701.
200. Velinov P., Nestorov G., and Dorman L., M1974. *Cosmic Ray Influence on Ionosphere and Radio Wave Propagation*. Bulgaria Academy of Sciences Press, Sofia.
201. Veretenenko S.V. and M.I. Pudovkin, 1994. "Effects of Forbush-decreases in cloudiness variations", *Geomagnetism and Aeronomy*, **34**, 38—44.
202. Villoresi G., Breus T.K., Dorman L.I., Iucci N., Rapoport S.I., 1994. "The influence of geophysical and social effects on the incidences of clinically important pathologies (Moscow 1979-1981)". *Physica Medica*, **10**, No 3, 79—91.
203. Villoresi G., Dorman L.I., Ptitsyna N.G., Iucci N., Tyasto M.I., 1995. "Forbush-decreases as indicators of health-hazardous geomagnetic storms". *Proc. 24-th Intern. Cosmic Ray Conf.*, Rome, **4**, 1106—1109.
204. Waliser D.E., J.-L.F. Li, T.S. L'Ecuyer, and W.-T. Chen, 2011. "The impact of precipitating ice and snow on the radiation balance in global climate models", *Geophys. Res. Lett.*, **38**, L06802, doi:10.1029/2010GL046478.
205. Weng F. and N.C. Grody, 1994. "Retrieval of cloud liquid water using the special sensor microwave imager (SSM/I)", *J. Geophys. Res.*, **99**, 25535—25551.
206. Zecca A. and L. Chiari, 2009. "Comets and climate", *J. Atm. and Solar-Terr. Physics*, **71**, 1766—1770.

УДК 524.1: 58.057:57.045:551.581.1:504.4:338.5(631.165)

КОСМИЧЕСКИЕ ЛУЧИ И ПРОЧИЕ ФАКТОРЫ КОСМИЧЕСКОЙ ПОГОДЫ, ВЛИЯЮЩИЕ НА РАБОТУ СПУТНИКОВ И ТЕХНИКИ, НА ЗДОРОВЬЕ ЛЮДЕЙ, НА ИЗМЕНЕНИЕ КЛИМАТА И НА СЕЛЬСКОХОЗЯЙСТВЕННОЕ ПРОИЗВОДСТВО

Профессор Лев И. Дорман, руководитель Израильского центра по изучению космических лучей и космической погоды (Тель-Авивский университет и Израильское Космическое Агентство), главный научный сотрудник отдела космических лучей ИЗМИРАН, Российская Академия Наук (г. Троицк)
E-mail: lid@physics.technion.ac.il

Лев А. Пустыльник, Израильский центр по изучению космических лучей и космической погоды (Тель-Авивский университет и Израильское Космическое Агентство)
E-mail: levpust2149@gmail.com

Григорий Йом Дин, Открытый Университет, Раанана, Израиль

Давид Ш. Апплбаум, Израильский центр по изучению космических лучей и космической погоды (Тель-Авивский университет и Израильское Космическое Агентство), Тель-Авивский Университет, Израиль

Настоящая статья представляет собой пример использования результатов фундаментальных исследований в области физики космических лучей (КЛ) для решения весьма важных и актуальных практических задач, таких, как наблюдения за космической погодой и прогноз степени опасности космических лучей для электронного оборудования космических летательных аппаратов и для здоровья астронавтов при полётах в космос, для здоровья экипажей и пассажиров гражданской авиации при полётах в атмосфере, и – в некоторых редких случаях – на технику и на людей на земле; исследования роли и влияния КЛ и других факторов космической погоды, как на изменения климата Земли, так и на сельскохозяйственное производство.

Хорошо известно, что в периоды крупных солнечных вспышек потоки Солнечных космических лучей (СКЛ) могут быть настолько мощными, что память компьютеров и электронное оборудование космических летательных аппаратов могут быть выведены из строя, а спутники и космические корабли погибнут (каждый год страховые компании выплачивают свыше 500 млн. долларов из-за подобных аварий. Если произойдёт событие, подобное тому, что имело место 23-го февраля 1956 года, то в таком случае всего за 1—2 часа будут выведены из строя почти все искусственные спутники Земли (ИСЗ), одна только потеря которых оценивается более чем в 10—20 миллиардов долларов, не говоря уже о полном нарушении спутниковой связи и множестве других проблем). В такие периоды необходимо на короткий срок выключать некоторую часть электроники, чтобы защитить память компьютеров. Такие периоды опасны

также как для астронавтов на борту космических кораблей, так и для пассажиров и экипажей самолётов гражданской авиации (особенно во время радиационных бурь категории S5—S7). Задача состоит в том, чтобы дать точный прогноз этих опасных явлений. Нами показано, что точный прогноз может быть выполнен посредством использования частиц высокой энергии (около 2—10 ГэВ/нуклон и выше) перенос которых от Солнца характеризуется гораздо более высокими значениями коэффициента диффузии, чем для частиц, обладающих меньшей энергией. Поэтому частицы высокой энергии достигают Земли от Солнца гораздо раньше (за 8-20 минут после разгона и выброса в солнечный ветер), чем основная часть частиц с меньшей энергией (достигающих Земли почти на 30—60 минут позже), представляющих опасность для электроники и здоровья людей.

В предлагаемой статье описываются основы и опыт применения автоматически работающих программ «SEP-Search-1 min», «SEP-Search-2 min», «SEP-Search-5 min», созданных и испытанных в Обсерватории имени Эмилио Сегре Израильского центра по изучению космических лучей и космической погоды (на горе Хермон, на высоте 2050 м над уровнем моря). Следующий шаг — это автоматическое определение энергетического спектра частиц в солнечной вспышке, и затем автоматическое определение коэффициента диффузии в межпланетном пространстве, времени выброса и энергетического спектра Солнечных космических лучей (СКЛ) в источнике, и, после этого, прогноз предполагаемого потока СКЛ и радиационной угрозы для находящихся в космическом пространстве зондов, искусственных спутников Земли, а также самолетов и различных иных объектов в земной атмосфере и на земле.

Мы описываем также теорию и практику использования данных о космических лучах высокой энергии для прогноза сильных геомагнитных бурь, сопровождаемых Форбуш-эффектами[1] (которые очень сильно влияют как на здоровье людей, так и на работу спутников, средств связи, систем навигации и высокотехнологических систем в космосе, в атмосфере и на земле).

Также мы обсуждаем вопрос о влиянии космических лучей на рынок сельскохозяйственной продукции и возможные социальные эффекты такого влияния.

[1] Эффект Форбуша, или Форбуш-эффект, — кратковременное и резкое понижение интенсивности галактических космических лучей в Солнечной системе, обусловленное выбросом вещества из Солнца

Ключевые слова: космические лучи, космическая погода, земной климат, Солнце, солнечный ветер, Форбуш-эффект, сельскохозяйственная продукция, цены на пшеницу.

DORMAN L.I., PUSTIL'NIK L.A., YOM DIN G., APPLBAUM D.SH. COSMIC RAYS AND OTHER SPACE WEATHER FACTORS
INFLUENCED ON SATELLITE OPERATION AND TECHNOLOGY, PEOPLE HEALTH, CLIMATE CHANGE, AND AGRICULTURE PRODUCTION